STATE OF CALIFORNIA • DEPARTMENT OF TRANSPORTATION

TECHNICAL REPORT DOCUMENTATION PAGE

TR-0003 (REV 04/2024)

1. REPORT NUMBER	2. GOVERNMENT ASSOCIATION NUMBER	3. RECIPIENT'S CATALOG NUMBER
CA25-3237		

4. TITLE AND SUBTITLE	5. REPORT DATE
Soil Amendment Guidance for Infiltration and Stormwater Treatment	October 2025
	6. PERFORMING ORGANIZATION CODE N/A
7. AUTHOR	8. PERFORMING ORGANIZATION REPORT NO.
Sanjay Mohanty, Michael K. Stenstrom, Tonoy Das, Chandra M. Tummala	N/A
9. PERFORMING ORGANIZATION NAME AND ADDRESS UCLA Samueli School of Engineering 420 Westwood Plaza, 5732-C Boelter Hall Los Angeles, CA 90095-1600	10. WORK UNIT NUMBER N/A
	11. CONTRACT OR GRANT NUMBER
12. SPONSORING AGENCY AND ADDRESS California Department of Transportation (Caltrans) Division of Research, Innovation and System Information, MS-83 1727 30th Street Sacramento, CA 95816	13. TYPE OF REPORT AND PERIOD COVERED Final Report
	14. SPONSORING AGENCY CODE N/A

15. SUPPLEMENTARY NOTES

16. ABSTRACT

Pollutants from roadway runoff are the leading cause of surface water impairments. Thus, treatment of road runoff by building roadside stormwater best management practices (BMPs) could prevent pollution. However, limited infiltration in compacted roadside soil poses a significant challenge to designing roadside BMPs. This study investigated the properties of various soil amendments to maximize the stormwater treatment performance of soils mixtures used in the California Department of Transportation (Caltrans) right of way (ROW) and clear recovery zone (CRZ) across the four hydrologic soil groups (HSGs) A, B, C, and D with all soils exhibiting limited infiltration capacity under compaction and contained low organic carbon. To improve their infiltration capacity, four types of bulking agents were tested: coarse sand, vermiculite, perlite, and expanding shale clay silt aggregate (ESCS). The results reveal that sand and ESCS could achieve a minimum infiltration capacity (6 in h-1) under compaction, whereas vermiculite and perlite failed to meet the infiltration criteria because they became compressed and restricted the free flow of stormwater. A pilot-scale field study was then conducted to evaluate the performance of an engineered filter media composed of ESCS, biochar, and topsoil, relative to a standard sand–compost–soil blend. The engineered media demonstrated a 3.3-fold higher infiltration or drainage capacity (5.9 cm h^{-1} vs. 1.8 cm h^{-1}) compared to the conventional system. During initial monitoring effort without appropriate conditioning of media, conventional media amendment with compost and sand showed net leaching of metals (negative removal), whereas the engineered media (biochar and ESCS) showed a net removal for heavy metals, including Pb (55%), Co (47%), Ni (59%), Cu (61%), and Cd (54%), and Zn (27%). These improvements are attributed to the high porosity, chemical reactivity, and structural stability of ESCS and biochar under compaction, which together maintain permeability and enhance pollutant retention. In contrast, the compost-rich media exhibited low capacity for infiltration after being compacted and potential for initial metal leaching. A long-term monitoring of effluent could provide realistic removal rates for both media. These findings affirm the potential of biochar–ESCS-amended media as a viable, field-validated alternative to conventional amendments for curbside infiltration and treatment of road runoff.

17. KEY WORDS	18. DISTRIBUTION STATEMENT	
Stormwater treatment, roadway runoff, biochar, expanding shale clay silt aggregate, sand, compost, soil amendments, engineered filter media		
19. SECURITY CLASSIFICATION *(of this report)*	20. NUMBER OF PAGES	21. COST OF REPORT CHARGED
Unclassified	247	

Soil Amendment Guidance for Infiltration and Stormwater Treatment

California Department of Transportation

Contract No. 65A0715

Final Report

By

Sanjay K. Mohanty, Ph.D. (Principal Investigator)
Michael K. Stenstrom, Ph.D., P.E. (Key Personnel)
Tonoy K Das, Ph.D., (Postdoctoral Researcher)
Chandra Tummala, Ph.D., (Postdoctoral Researcher)

Department of Civil and Environmental Engineering

The University of California, Los Angeles

October, 2025

Executive Summary

Pollutants from roadway runoff are the leading cause of surface water impairments. Thus, treatment of road runoff by building roadside stormwater best management practices (BMPs) could prevent pollution and turn the road infrastructure into a sustainable water solution. However, limited infiltration in compacted roadside soil poses a significant challenge to designing roadside BMPs. To overcome this challenge, roadside or curbside soil where compaction is required could be mixed with amendments to alleviate the negative impact of compaction and increase infiltration and stormwater treatment. Compaction could decrease the amendment's particle size if it crumbles under pressure. Furthermore, the amendment amount could vary based on soil hydraulic properties. This study aims to provide selection guidance for amendments and their quantity to achieve stormwater treatment goals in curbside soil where compaction is required for road design.

To create a study that is representative of all California soil types, soils were collected within Caltrans Right of Way (ROW) from 8 sites, with two soil sites from each of the four hydrologic soil groups (HSG) A, B, C, and D. The selected physical, geotechnical, and chemical properties of all soils were measured to verify their HSG type. All soils exhibited a limited infiltration capacity under compaction and contained low organic carbon, indicating amendments were needed to improve their capacity to infiltrate stormwater and remove pollutants. To improve their infiltration capacity, four types of bulking agents were tested: coarse sand, vermiculite, perlite, and expanding shale clay silt aggregate (ESCS). Testing the infiltration capacity of compacted bulking agents reveals that sand and ESCS could achieve a minimum infiltration capacity (6 in h^{-1}) under compaction, whereas vermiculite and perlite failed to meet

the infiltration criteria because they became compressed and restricted the free flow of stormwater. The amount of sand needed to achieve the minimum infiltration rate varied between 70 to 95% based on hydrological soil groups. Four empirical models were tested to predict the infiltration capacity of compacted soil and sand mixture. The result reveals that all existing models underestimated the hydraulic conductivity of the compacted soil-sand mixture. An empirical model was suggested to predict the infiltration capacity of compacted soil and amendment mixture that incorporates compaction effects on porosity, particle size, and, consequently, infiltration.

As bulking agents such as sand have a limited pollutant removal capacity, a fraction of the sand content in the sand-soil mixture was replaced with amendments such as biochar and compost to enhance the contaminants removal performance, and the performance of the media mixture was tested under compaction. To select the best biochar for roadside application, four different biochars from local suppliers were tested for their *E. coli* removal. Fecal indicator bacteria are the leading cause of surface water impairment and the most difficult type of pollutant to remove, and therefore present the worst-case scenario to test the performance of biochar or amendments for stormwater treatment. To select the best biochar in the future from other vendors, a predictive model was developed using the known biochar properties such as surface area, organic carbon content, ash content, and volatile matter. The selected biochar was further tested to evaluate its performance under compaction. The result showed that compaction reduced the infiltration rate of biochar-augmented media, but adding moisture during packing would partially alleviate the negative impact of compaction. Compaction could break biochar particles, but adding large-sized biochar (1180-2000 μm) relative to sand minimized the negative impact of compaction on infiltration capacity or clogging in the compacted media filters. An

empirical model was developed to predict the clogging rate of biochar-amended biofilter based on suspended sediment loading and D_{10} of the biochar-media mixture. Sand and biochar fractions were optimized for all soil types to achieve the required infiltration rate.

To address the critical limitations of conventional stormwater biofiltration systems under compacted roadside conditions, a pilot-scale field study was conducted to evaluate the performance of an engineered filter media composed of expanded shale, clay, and slate (ESCS), biochar, and topsoil, relative to a standard sand–compost–soil blend. The engineered media demonstrated a 3.3-fold higher infiltration or drainage capacity (5.9 cm h^{-1} vs. 1.8 cm h^{-1}) compared to the conventional system. During initial monitoring effort without appropriate conditioning of media, conventional media amendment with compost and sand showed net leaching of metals (negative removal), whereas the engineered media (biochar and ESCS) showed a net removal for heavy metals, including Pb (55%), Co (47%), Ni (59%), Cu (61%), and Cd (54%), and Zn (27%). These improvements are attributed to the high porosity, chemical reactivity, and structural stability of ESCS and biochar under compaction, which together maintain permeability and enhance pollutant retention. In contrast, the compost-rich media exhibited low capacity for infiltration after being compacted and potential for initial metal leaching. A long-term monitoring of effluent could provide realistic removal rates for both media. These findings affirm the potential of biochar–ESCS-amended media as a viable, field-validated alternative to conventional amendments for curbside infiltration and treatment of road runoff. This method does not require additional space and could provide water quantity and quality benefits despite compaction. However, underdrains could be required in most places where a low hydraulic conductivity soil layer beneath the compacted media would limit infiltration and treatment of road runoff.

Table of Contents

List of Tables

Table of Figures

1 Task 1: Selection of 8 sites and collection of soil samples

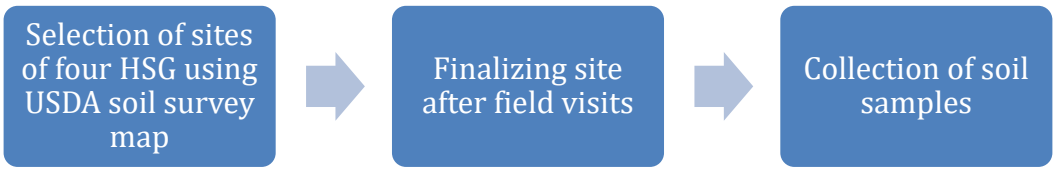

1.1 Motivation

The motivation behind this task is to collect enough soils with distinct hydraulic conductivity ranges so that the effect of soil properties on the quantity of amendments needed to achieve a desired BMP performance goal can be evaluated with statistical confidence. Four Hydrologic Soil Group (HSG): A, B, C, D were selected for this work. The soil groups, A, B, C, and D are defined based on runoff potential in completely wet conditions. Group A soils typically consist of sand (>90 %) with a low amount of clay (< 10%). It has the lowest runoff potential, with high hydraulic conductivity (> 5.7 in/h). Group B soils consist of 10-20% clays and 50-90% sand and have moderately low runoff potential. Group C soils typically have between 20-40% clay and less than 50% sand and have moderately high runoff potential. Group D soils typically have more than 40% clay and less than 50% sand and have high runoff potential.

Objective: Select 8 sites and collect soil samples for characterization and laboratory experiment.

Deliverable: A short document including GPS coordinates of all sites or sample locations, and choice of eight sites for sample collection.

1.2 Method

1.3 Results and discussion

We found all 4 soil group types near Los Angeles: three locations with type A soil, two locations with type B soil, 3 locations with type C soil, and two locations with type D soils (Table 1.2). The majority of the study locations within Caltrans ROW around Los Angeles are of group B, C, or type B/C. Only a few study locations near coastal areas were of type D, the soil group with the lowest infiltration capacity. Thus, the installation of roadside BMP in this area would not reduce overland flow, and the treated stormwater from BMP needs to be directed into the nearest storm drainage. We assumed that the soil type recorded by the USDA Soil Survey database accurately reflects the properties of soil collected between 10-45 cm soil layer below the ground. However, urban soils are often disturbed or replaced during construction, the USDA Soil Survey data may not represent the actual soil conditions at our sites. Nevertheless, the 8 soils are expected (as the true nature of soil type can not be known until we test due to the heterogeneity of urban soil) to provide a wide range of scenarios to estimate the amount of bulking agent needed to achieve the required infiltration capacity.

Table 1.2. Soil data of selected locations retrieved from NRCS database.

Site	A1	A2	A3	B1	B2	C1	C2	C3	C4	D1	D2
Location	San Perdo	Santa Paula	Ventura	Ventura	Ventura	Ventura	Long beach	Long beach	Cal Poly Pomona	Santa Barbara	San Dimas
Site Unit Symbol	1174	CrC	CoC	MoA	Cd	SxA	125	123	1141	HuC2*	1146
Site Unit Name	Calcic Haploxerepts (40%)-Longshore (25%)-Urban land complex(20 %), 10 to 35 percent slopes	Cortina stony sandy loam, 2 to 9 percent slopes	CoC-Corralitos loamy sand, 0 to 2 percent slopes	Mocho loam, 0 to 2 percent slopes, warm MAAT, MLRA 19	Camarillo loam, 0 to 2 percent slopes	Sorrento silty clay loam, 0 to 2 percent slopes, warm MAAT, MLRA	Bolsa silty clay loam, drained	Bolsa silt loam, drained	Zaca(50%)-Apollo warm complex(35 %) , 20 to 55 percent slopes	Huerhuero very fine sandy loam, 5 to 9 percent slopes, eroded	
Parent Material	Colluvium and/or residuum weathered from sandstone	Alluvium derived from Sedimentary rock	Stratified alluvium derived from Sedimentary rock	Alluvium derived from sedimentary rock	Alluvium derived from sedimentary rock	Alluvium derived from sedimentary rock	Mixed alluvium derived from igneous, metamorphic and sedimentary rock	Mixed alluvium derived from igneous, metamorphic and sedimentary rock	Colluvium and/or residuum weathered from sandstone and siltstone	Alluvium derived from sedimentary rock	
Unified Soil Classification of surface (0-18 in)	CL-ML, SC-SM	GM,SM	SM & SM	CL	CL-ML	CL	CL	CL	CH, CL	CL-ML,ML	
AASHTO Soil Classification of Surface Soil (0-18 in)	A-4	A-2	A-1, A-2	A-6	A-4	A-7-6	A-6	A-6	A-7-6	A-4	
Surface Texture (0-18 in)	Fine sandy loam; Loam	Stony sandy loam	Loamy sand	Loam	Loam & Stratified sandy loam to sandy clay loam	Silty clay loam	Silty clay loam; Silty clay loam, silt loam; Silt loam,	Silt loam; Silt loam, silty clay loam	Clay; Clay loam	Very fine sandy loam & Clay	
Hydrologic Soil Group	A	A	A	B	B	C	C	C	C	D	D
Surface Runoff	Medium	Low	Very low	Low	Low	Medium	Low	Low	Very high	Low	Low
Natural Drainage Class	Well-drained	Somewhat excessively	Excessively drained	well-drained	Poorly drained	Well-drained	Somewhat poorly drained	Somewhat poorly drained	Well-drained	Moderately well-drained	

Depth to restrictive feature	> 80 in	> 80 in	> 80 in	> 80 in	> 80 in	> 80 in	> 80 in	> 80 in	37-69 inches to paralithic bedrock	> 80 in	
Depth to Water Table	> 80 in	> 80 in	> 80 in	> 80 in	24-60 in	> 80 in	> 80 in	> 80 in	> 80 in	> 80 in	
Liquid Limit (0-18 in)	22-25	25	0	39-36	25	47	40-33	33	64-42	30-51	
Plasticity Index (0-18 in)	5-7	3	NP	15-16	5	22	21-16	16	35-21	8-20	
Bulk Density under water tension of 1/3 bar (Representative value at 0-18 in)	1.52 g/cc	1.53 g/cc	1.65 g/cc	1.5 g/cc	1.45 g/cc	1.5 g/cc	1.46-1.36 g/cc	1.44 - 1.36 g/cc	1.27-1.46 g/cc	1.4 g/cc	
Organic Matter (Representative value at 0-18 in)	0.5-1.3%	0.80%	0.80%	3.0-1.5%	2.50%	3%	0.30%	0.30%	2.5-1.0%	1.5-0.8%	
Percent Clay (0-18 in)	10-12	18	3	23	19	31	30-22	22	50-31	20-40	
Percent Sand (0-18 in)	60	67	81	40	43	18	7-8	7-8	13- 36	58-30	
Percent silt (0-18 in)	28-47	15	17	37	39	51	63-70	71-70	37-33	23-30	
Saturated Hydraulic Conductivity (Ksat) (Representative value at 0-18 in)	28.00 µm/sec	28.00 µm/sec	92 µm/sec	9 µm/sec	9 µm/sec	2.8 µm/sec	2.84-9.17 µm/sec	9.17 µm/sec	9-0.22 µm/sec	9-0.22 µm/sec	0 - 0.01 in/h

2 Task 2a: Characterization of soils

2.1 Motivation

The overarching goal of this project is to select amendments that could increase the infiltration of stormwater on the roadside despite compaction. However, the amount of amendments required for a specific soil could vary with the soil properties and amendment size and properties. Therefore, it is important to characterize all soils and amendments so that the amount of amendments needed for a specific soil can be predicted based on their properties by validating the data obtained in this study.

Objective: Characterization of soil samples for physical and chemical properties with protocol details and selection of the right bulking agent with an appropriate amount for high hydraulic conductivity.

Deliverable: A summary of physical and chemical properties of soils and selection of suitable bulking agents with the right amount.

2.2 Methods

The tests were conducted at Mohanty's laboratory and Scott's geotechnical laboratory at UCLA to characterize eight soil samples above for physical, geotechnical, and chemical properties. The tests included particle size distribution, hydraulic conductivity, water retention, plastic and liquid limit, pH, and organic carbon content.

2.2.1 Particle Size Distribution: Sieve Analysis (CTM 202)

Approximately 500 grams of each soil were oven-dried at 110^{o}C, and lumps were broken into smaller particles. The soil sample was placed into the sieves stack and shaken by a

mechanical shaker for 10 minutes. Portions retained on each sieve were collected separately, and mass was measured. The sieve analysis results are expressed in terms of the percentages of the weight of soil passed through different sieves and presented by particle-size distribution curves. The particle size distributions of the mixtures at finer resolution were determined using a laser diffraction particle size analyzer (model LS 13 320, Beckman Coulter, CA).

2.2.2 Unsaturated Hydraulic Conductivity and Water-Retention: HYPROP

The HYPROP is a fully automated measuring and evaluation system based on Schindlers evaporation method to measure hydraulic conductivity and soil water retention (METER 2015) in this study (Figure 2.1). Soil from each soil type was compacted into a sample ring and covered by a nonwoven cloth on the top. After compaction, the soil sample was placed into a filling bowl, then put into a tray filled with 2 cm of degassed water. Degassed water was continued to fill in the tray up to the surface of the soil sample. After the sample was saturated, the cloth was removed. The filling bowl was mounted into the sensor unit and balanced to measure unsaturated hydraulic conductivity and water retention curve.

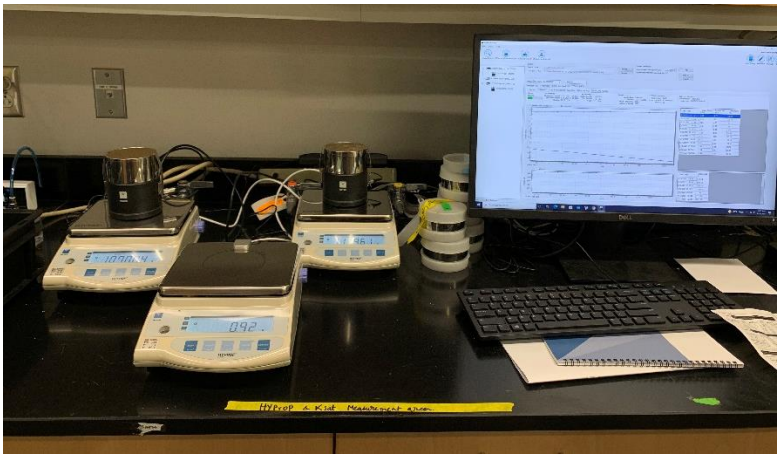

Figure 2.1. Hyprop setup for measurement of soil-water retention sample analysis of compacted soil, relevant for vegetation survival in dry conditions.

2.2.3 Saturated hydraulic conductivity

Saturated hydraulic conductivity was measured using KSAT (Meter 2015), which is an automated instrument. This method was selected over ASTM because: i) it requires a smaller sample volume, which facilitates achieving a fully saturated condition faster, and ii) the high accuracy sensor can capture a very small drop in pressure head to measure low hydraulic conductivity (as small as 0.01 cm/day). In this method, each soil was uniformly compacted into a ring with 8 cm diameter and 5 cm height. The filter paper was placed on the top and bottom of the soil. The soil sample was put into a pan of DI water to become saturated under capillarity. The height of water in the pan was about three-quarters of the height of the sample. Before weighing, the outer surface of the sample was dried using a paper towel. After the saturation, the sample was placed into the falling head permeability measurement device. For each soil, three different amounts of soil were compacted into the ring to measure the hydraulic conductivity at three different relative compactions.

2.2.4 Soil Compaction: California compaction test (CTM 216)

CTM 216 was followed to determine the compaction behavior. First, approximately 2400 g of each soil was obtained. Water was gradually added to the soil to reach the minimum water content. Then, 2300 g of the wet soil with a known water content was prepared for measurement. The sample was divided into five equal portions stored in zip-lock bags. Each portion was placed into the Caltrans compaction test mold (Figure 2.2), compacted with 20 blows of the tamper dropping free from a height of 18 inches above the surface of the material in the mold. This operation was repeated for each of the remaining four portions. After the compaction of the fifth portion, the piston was placed in the mold, and the top of the compacted specimen was leveled with 5 blows. The tamper was placed resting on the piston atop the compacted specimen, and the

reading was taken from the graduated tamper shaft to the nearest graduation at a point level with the top of the mold. As this reading represents the height of the compacted, density of the specimen was calculated by knowing the mass of soil and volume of the mold based on height and diameter. There was no need for correction for oversize material as the soils did not contain particles passing the 3/4 inch sieve. At the end of the test, the mold was dismantled, and about 100 g of the compacted specimen was sampled from different locations along with the specimen for water content measurement.

Figure 2.2. Caltrans compaction test device.

2.2.5 Plastic and Liquid Limit: Atterberg Limits (CTM 204)

Approximately, 200 g of soil passing No. 4 sieve was used in this study. The soil was air-dried and sieved over the No. 40 sieve, mixed thoroughly, and transferred into a container.

Liquid limit: 100 g of soil from the container was placed in the mixing dish and mixed with 15 mL DI water (addition in increments of 1 mL to 3 mL) by repeatedly stirring, kneading, and chopping with a spatula until a uniform mass was obtained. Then soil was placed into the

cup up to 2/3 full with spreading motion to avoid entrapping the air pocket and divided into two separated sides using a grooving tool. The cup was subjected to blows to close the groove. A slice of soil from the cup was removed with the spatula extending from edge to edge and oven-dried at 110 ^{o}C overnight to determine the moisture content. The test was repeated with the same sample to obtain one determination in each of the following ranges: 25 – 35 blows, 20 – 30 blows, and 15 – 25 blows. The flow curve was plotted to present the relation between moisture content and the corresponding number of blows. The liquid limit was determined at the intersection of the flow curve with 25 blows ordinates.

Plastic limit: 20 g of soil from the container was placed in the mixing dish and mixed with DI water until the mass became plastic enough to shape into a ball easily. A portion of 8 g was taken from the ball, and 2 g of the 8g soil ball was rolled by hand into a thread about 3 mm in diameter. When the thread got crumbled into segments 6-10 mm in length, the samples were collected into a container and oven-dried at 110 ^{o}C overnight to determine the moisture content of the soil. The test was repeated until 8 grams of soil was completely tested. The plastic limit was the average of the moisture content range.

2.2.6 Specific Gravity: Water Pycnometer (CTM 209)

25 g of soil, which was oven-dried at 110 ^{o}C for at least 12 h, was placed into a 100 mL volumetric flask, and DI water was added to the flask up to ¾ full. The flask was boiled gently for 10 min with occasionally rolling to remove entrapped air and then cooled down the mixture to approximately 20 ^{o}C. After cooling, DI water was added to the volumetric flask up to the full mark. The volumetric flask was weighted, and the specific gravity of the soil was calculated.

2.2.7 pH

20 g of air-dried soil was placed into an Erlenmeyer flask, and 100 mL of DI water was added. The flask was sealed with a rubber stopper, placed into a mechanical shaker (end-over-end one), and shaken for 10 min at 25 ºC. The pH of the soil slurry was measured using an electrometric pH probe.

2.2.8 Soil Salinity: 1:5 Soil/Water Extract ($EC_{1:5}$)

20 g of air-dried soil was mixed with 100 mL DI water in an Erlenmeyer flask. The flask was sealed with a rubber stopper, placed into a mechanical shaker (end-over-end one), and shaken for 30 min at 25 ºC to dissolve soluble salts. After shaking, the flask was allowed for 15 min for the soil to settle to the bottom. Calibrated conductivity cells were dipped into the supernatant with up and down motion without disturbing the settled soil until the system was stabilized, and $EC_{1:5}$ ($\mu S\ cm^{-1}$) at 25 ºC was recorded.

2.2.9 Organic Carbon Content: Loss on Ignition (ASTM D297/ AASHTO T267)

The loss-on-ignition (LOI) organic matter method was used to measure the number of organics in each soil. In this method, 100 g of oven-dried soil was combusted at 450 °C for 6 h in an oven. The difference between the soil masses before and after combustion over the initial dry mass of soil was measured as the percentage of organic matter.

2.3 Results and Discussion

The soils were characterized for selected physical, geotechnical, and chemical properties and reported in Table 2.1. Among these properties, physical properties such as grain size distribution play a critical role in determining the hydraulic conductivity of the soil. It is expected that soils from group A would have a higher sand fraction and lower clay fraction than

soils from group D. However, our soil analysis shows that sand or clay fraction fractions did not vary as expected based on the soil group type. The result indicates that soil group type is not an accurate predictor of soil characteristics in a location, and particle size distribution should be measured irrespective of the soil group type. The discrepancy is attributed to soil heterogeneity within sites. Our findings show that measured soil properties should be used instead of relying on USDA Soil Survey data, as urban soils are highly engineered and heterogeneous. For the same reason, we obtained particle size distribution curves for all soils so that particle size corresponding to 10, 50, and 90% passing (D_{10}, D_{50}, and D_{90}, respectively) can be estimated (Figure 2.3). The result will feed into the model (Task 4) to predict the hydraulic conductivity of the mixture containing the soil and amendment, where the particle size distribution is expected to change due to the addition of amendments.

Table 2.1. Physical, geochemical, and chemical properties of collected soils.

Parameter	A1	A4	B1	B2	C2	C5	D1	D2
Actual Soil Type	B	A	B	B	A	B	B	A
Sand (%)	45.4	67.5	23.7	26.9	56.9	18.6	39.4	54.6
Silt (%)	47.3	28.1	63	61.9	37.1	67.7	51	39.7
Clay (%)	7.3	4.4	13.2	11.2	6	13.8	9.5	5.7
K_{sat} of compacted soil (inch/h)	0.13	0.29	0.1	0.07	0.14	—	—	0.2
Plasticity index (%)	21	20	20	19	22	20	—	—
Liquid Limit (%)	26	24	35	31.43	25.69	36.09	—	—
Specific gravity	2.04	2.35	2.08	2.11	2.25	2.06	2	1.96
EC (µs/cm)	198.4	93.4	151.3	1349.3	120.6	153.9	147.1	144.4
pH	7.58	7.65	7.37	7.5	7.6	7.4	7.3	7.3
Organic Carbon Content (%)	0.39	0.27	0.53	0.46	0.27	0.47	0.53	0.33

"—" The dash means we do not have data for these soil types.

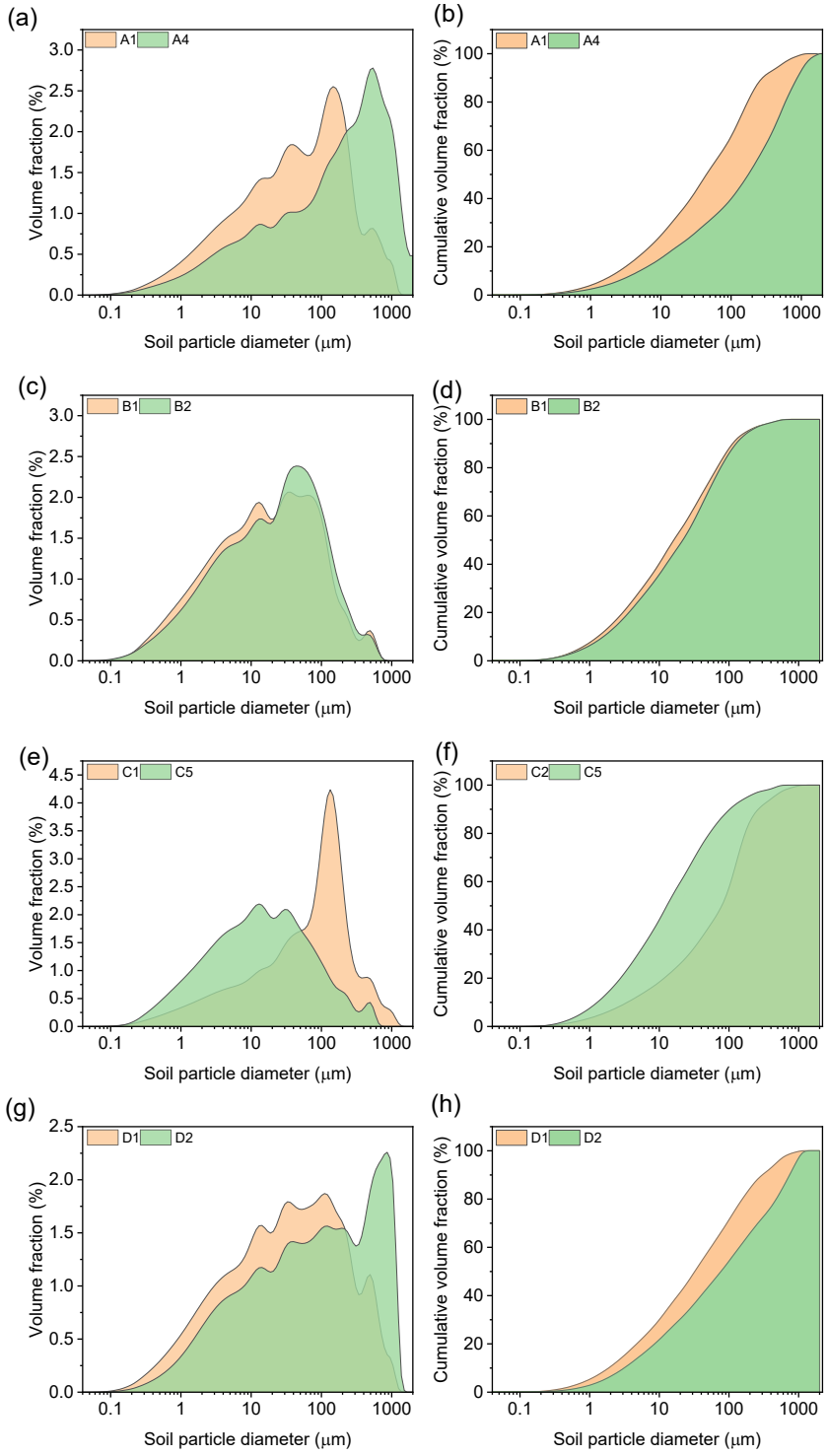

Figure 2.3. Particles size distribution of four hydrologic group soils. We showed % volume distribution (a,c,e,g) and % volume cumulative distribution (b,d,f,h). The legends in each graph denote the hydrologic group.

2.4 Summary

Physical, chemical, and geotechnical characterization of all 8 soils reveals that all soils have a range (A &B) of characteristics. Our C and D soil types from the USDA database did not match our lab results. So, our results represent A and B. The sand content varied from 19% to 57% in soil, indicating the amount of bulking agent needed for the collected soils could vary widely. Saturated hydraulic conductivities of all soils under compaction were below 0.3 in/h, indicating they failed to meet the infiltration requirement. Thus, bulking agents are needed for all soil. Organic carbon contents in all soils were below 0.5%, indicating they all require amendments such as biochar or compost to remove pollutants.

2.5 References

ASTM D698. "Standard test methods for laboratory compaction characteristics of soil using standard effort."

ASTM D4972-01 Standard test method for pH of soils

ASTM D 2974–14 Standard Test Methods for Moisture, Ash, and Organic Matter of Peat and Other Organic Soils.

California Test 202- Method of test for sieve analysis of fine and coarse aggregates.

California Test 209- Method of test for specific gravity of soils.

California Test 201- Method of tests for liquid limit, plastic limit, and plasticity index of soils.

California Test 216- Method of test for relative compaction of untreated and treated soils and aggregates

METER, 2015. Operation Manual HYPROP 2, METER Group AG, Munich, Germany.

METER, 2015. Operation Manual KSAT, METER Group AG, Munich, Germany.

3 Task 2b: Selection of best bulking agent to alleviate compaction

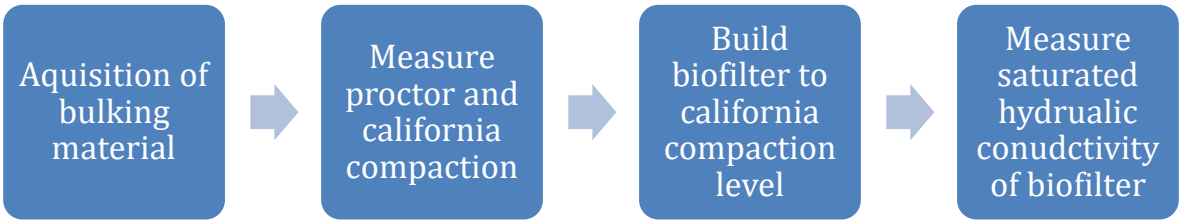

3.1 Motivation

One of the primary challenges for installing soil-based BMPs on the roadside is that the compaction of amended soil by roadside activities would adversely affect the infiltration and treatment of stormwater (Yang and Zhang, 2011). As native roadside soil has limited infiltration capacity, various types of amendments or bulking agents such as sand, gravel, wood chips, compost, perlite, and vermiculite have been suggested to use in BMPs to enhance infiltration capacity. However, the best bulking agent that could be most effective in maintaining the infiltration rate despite compaction is unclear. In this work, we tested bulking agents such as sand, vermiculite, perlite, and expanded shale, clay, and slate (ESCS) to identify the best amendment to restore hydraulic conductivity of soil under compaction. These amendments are selected as they are widely used in literature in different stormwater BMP structures or roadside structures constrictions.

Objective: Selection of the best bulking agent to alleviate the negative effect of compaction on infiltration capacity of roadside soil.

Deliverable: Identification of the best two choices for bulking agent to be used in roadside stormwater BMP.

3.1. Methods

Inorganic amendments such as sand, vermiculite, perlite, and ESCS were tested to maintain the high hydraulic conductivity of the soil. Bench-top columns filled with compacted bulking agents including sand, vermiculite, ESCS, and perlite were tested to measure their saturated hydraulic conductivity. Four amendments selected after the prescreening procedure were tested for changes in hydraulic conductivities as a compaction function.

3.1.1. Acquisition of material

The four bulking agents are sand, vermiculite, ESCS, and perlite (Figure 3.1). They were acquired from the marketplace, and vendor details are given in Table 3.1.

Table 3.1. Product and vendor details of bulking materials

Material	Vendor name	Product link
Sand	Humboldt manufacturing company	https://www.humboldtmfg.com/test-sand-astm.html
Perlite	Home Depot	https://www.homedepot.com/p/Vigoro-2-cu-ft-Organic-Perlite-Soil-Amendment-100521091/205655210
Vermiculite	Garnera in Amazon	https://www.amazon.com/Horticultural-Organic-Vermiculite-GARDENERA-Hydroponics/dp/B094GP256S
ESCS	Expanded Shale, Clay and Slate Institute	https://www.escsi.org/escs-lwa/

Figure 3.1. Four bulking agents' sand, perlite, vermiculite, ESCS.

3.1.2. Preparation of media

The soil was sieved to remove particles greater than 2 mm (mesh #10). The bulking agents were also sieved through mesh number 10 to remove particles greater than 2 mm. The sieved soil and bulking agent were mixed 30% to 70% by volume. The moisture content of the soil was maintained at 10%.

3.1.3. Standard proctor compaction

The soil and bulking agents mix was compacted with the standard proctor method (ASTM D698) to achieve maximum compaction level, and their bulk density was measured in the Proctor device. Briefly, the standard proctor test was done as follows; soil and bulking media were sieved using the number 4 sieve. First, we recorded the empty mold's weight (4-inch diameter) with its base (but no collar) and then placed the collar back on the mold. The compaction was done in three layers, and the mold height was marked into three layers. After that, the soil-media mix was spooned into the mold at approximately ⅓ of the height of the mold (not counting the collar height). The mold was placed on the concrete floor, and the soil was compacted with the rammer for 25 blows per layer, following this pattern in Figure 3.2. The process was repeated three times to reach the top of the base mold collar. After compaction, the collar was removed, and the excess compacted layer above the mold was trimmed. Finally, the weight of the compacted mold was recorded to calculate the bulk density.

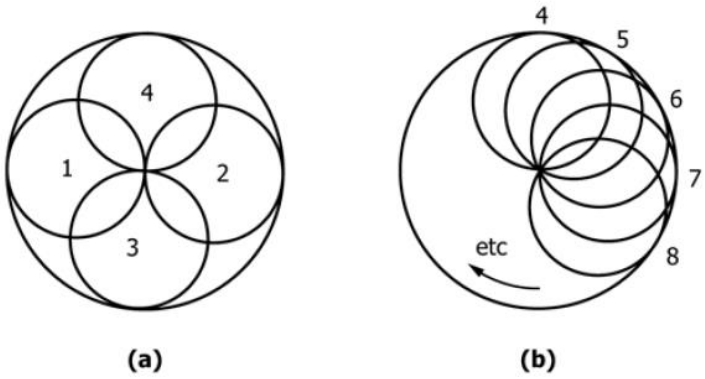

Figure 3.2. Rammer pattern for compaction in 4-inch mold.

3.1.4. Biofilter media design

To design a laboratory column set-up, a transparent PVC tube (2.54 cm ID and 30 cm length) was glued with PVC fittings and connected to a control valve to regulate the effluent flow. The columns were packed with the prepared media mixture (soil and bulking agents) under different compaction conditions. Before packing the filter media in each column, a nylon mesh (100 µm pores) was inserted at the bottom to prevent the filter media from falling into the outlet tube. Pea gravels were poured over the mesh up to 6 cm in height, and a second mesh was placed over the gravel layer to prevent the filter media top from falling into the pore space between gravels. The media mixture was added incrementally and compacted to a comparable bulk density from the standard proctor test at a 5 cm layer height using a metal rod to ensure compaction. The single-layer height of filter media was calculated by dividing the column area by the column volume, and it equaled 3.8 cm. The procedure was repeated until the filter media depth reached 15.2 cm with a total of 3 layers. The bulk density was estimated after compaction of the entire filter layer. An additional 2 cm layer of pea gravels was added on the top of filter media to prevent the floating of bulking media particles in case of ponding. After packing, DI water was injected from the bottom to fill the space until the top of the top gravel layer to measure the pore volume of the compacted media.

3.1.5. Measurement of hydraulic conductivity

After pore volume measurement, a hydraulic conductivity test was immediately conducted on each column. The hydraulic conductivity (K, $in.h^{-1}$) of each column was measured using the falling head method: $K = L/t\ \ln(h_1/h_2)$, where L is the depth of filter media, t is the duration to drain water from the initial height h1 to the final height is the initial height h_2, both heights were above the filter media (Figure 3.3). Tap water was poured gently from the top of the column to prevent disturbance of filter media until the water level reached a 10 cm level above the bulking media-soil mixture. The initial height of water (h_1) was marked at 10 cm above the sand-biochar mixture, and a second mark (h_2) was made 5 cm below the first mark. The bottom outlet of the column was opened, and water was collected until the water level dropped from the h_1 to h_2 marks. The hydraulic conductivity was determined by measuring the volume of water released and the time required to drain the water from h_1 to h_2. The experiment was repeated five times per column in order to estimate the average hydraulic conductivity.

Figure 3.3. Experimental set-up for hydraulic conductivity test using the falling head method.

3.2. Results and discussion

Compaction decreased the hydraulic conductivity in all types of soil-bulking media biofilter configurations. The infiltration rate through compacted vermiculite and perlite was extremely low compared to sand (Figure 3.4). In the absence of compaction, a high infiltration rate was recorded in the sand biofilter, followed by perlite and vermiculite. The existing literature does not evaluate the performances of these bulking materials under compaction for roadside BMP designs. This is the first time such evaluation has been done.

The low infiltration rate of vermiculite and perlite-augmented biofilters was attributed to the low mechanical strength of vermiculite and perlite compared to sand (Belhouideg et al., 2015; Kormanek et al., 2021). Under compaction stress, vermiculite and perlite could break or compress and produce fine particles, which can further clog the constricted flow paths (Jamei et al., 2011). This concludes that sand is the only viable bulking agent to not deform under compaction and maintain the infiltration efficiency of stormwater treatment systems. However, despite adding 70% sand by volume, the soil and sand mixture did not maintain the required hydraulic conductivity under compaction. This indicates that further optimization of sand dosing is needed, and the sand fraction could vary with soil type.

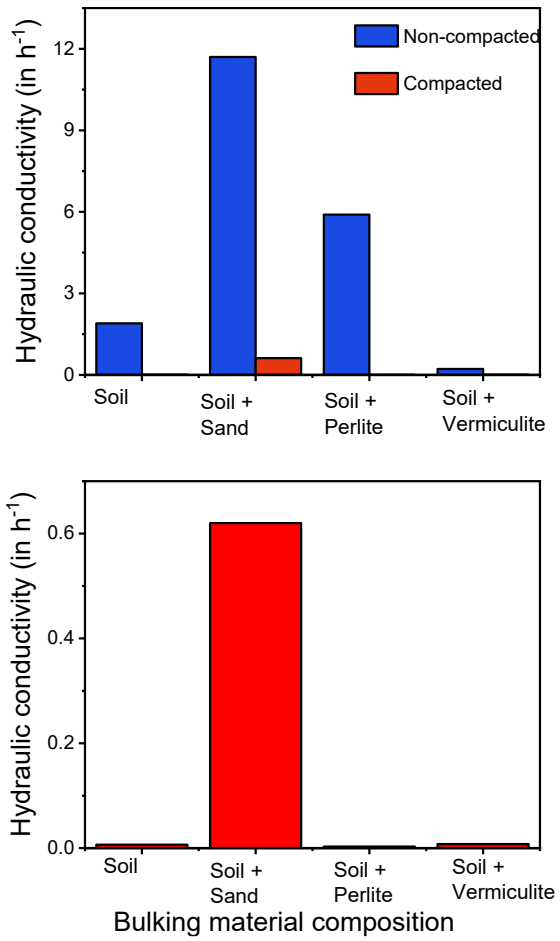

Figure 3.4. Effects of compaction on saturated hydraulic conductivity of vermiculite, sand, perlite, amended biofilter. The lower panel enlarges the compaction data to improve visibility of the data points, while the upper panel compares compaction and non-compaction conditions

We tested expanded shale, clay, and slate (ESCS) aggregates, a novel lightweight amendment as an alternative bulking material to sand, as the other two proposed bulking agents (perlite and vermiculite) failed to meet the minimum infiltration requirement. Compacted ESCS amended biofilter recorded a reasonable infiltration rate (Figure 3.5).

ESCS is a ceramic material produced by expanding and vitrifying select shales, clays, and slates in a rotary kiln that is structurally strong, stable, durable, low in density, and non-toxic. They are similar to cinders, which are also used as a bulking agent in road construction.

However, ESCS is a lighter material with the added advantage of its capacity to remove some pollutants. Similar to sand, ESCS aggregates could maintain their structural integrity under compaction, leading to better infiltration. Further, ESCS have larger particle sizes than sand, which contribute to a higher infiltration rate. This indicates that ESCS could replace part of sand as bulking media. Further, results of batch experiments and column studies revealed that biofilters amended with ESCS aggregates could adsorb significant amounts of metals such as Pb, Cu, and Zn from stormwater and organic contaminants, which is added benefit of any other bulking agent such as sand that does not remove many pollutants (Dordio and Carvalho, 2013, Kalhori et al., 2013, Nkansah et al., 2012).

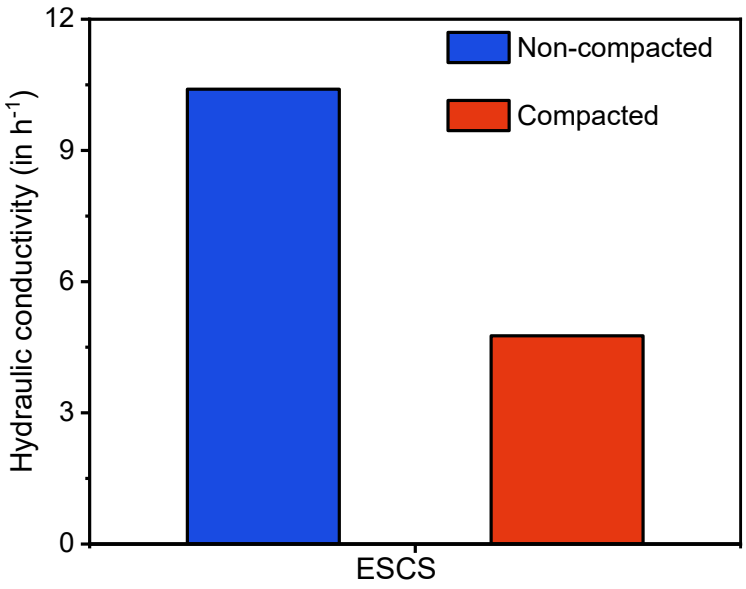

Figure 3.5. Effects of compaction on saturated hydraulic ESCS amended biofilter.

3.3. Summary and Implications

We evaluated the infiltration rate of compacted biofilter augmented with various bulking agents such as sand, vermiculite, perlite, and ESCS. We found that only sand and ESCS were two viable bulking agents to maintain the required infiltration rate under compaction. The addition of sand and ESCS improved the infiltration rate of compacted stormwater biofilter media. Other bulk agents were compressed under compaction and blocked the flow. However, the amount of bulking agent needed for each soil could vary and needs to be determined.

3.4 References

ASTM D698. "Standard test methods for laboratory compaction characteristics of soil using standard effort."

Belhouideg, S. and Lagache, M., 2015. Experimental determination of the mechanical behaviour of compacted exfoliated vermiculite. Strain, 51(2), pp.101-109.

Dordio, A. and Carvalho, A.J.P., 2013. Constructed wetlands with light expanded clay aggregates for agricultural wastewater treatment. Science of the total environment, 463, pp.454-461.

Jamei, M., Guiras, H., Chtourou, Y., Kallel, A., Romero, E. and Georgopoulos, I., 2011. Water retention properties of perlite as a material with crushable soft particles. Engineering Geology, 122(3-4), pp.261-271.

Kalhori, E.M., Yetilmezsoy, K., Uygur, N., Zarrabi, M. and Shmeis, R.M.A., 2013. Modeling of adsorption of toxic chromium on natural and surface modified lightweight expanded clay aggregate (LECA). Applied Surface Science, 287, pp.428-442.

Kormanek, M., Małek, S., Banach, J., Durło, G., Jagiełło-Leńczuk, K. and Dudek, K., 2021. Seasonal changes of perlite–peat substrate properties in seedlings grown in different sized container trays. New Forests, 52(2), pp.271-283.

Nkansah, M.A., Christy, A.A., Barth, T. and Francis, G.W., 2012. The use of lightweight expanded clay aggregate (LECA) as sorbent for PAHs removal from water. Journal of Hazardous Materials, 217, pp.360-365.

Yang, J.-L., Zhang, G.-L., 2011. Water infiltration in urban soils and its effects on the quantity and quality of runoff. J Soils Sediments 11, 751–761.

4 Task 2c: Selection of the best biochar for stormwater treatment

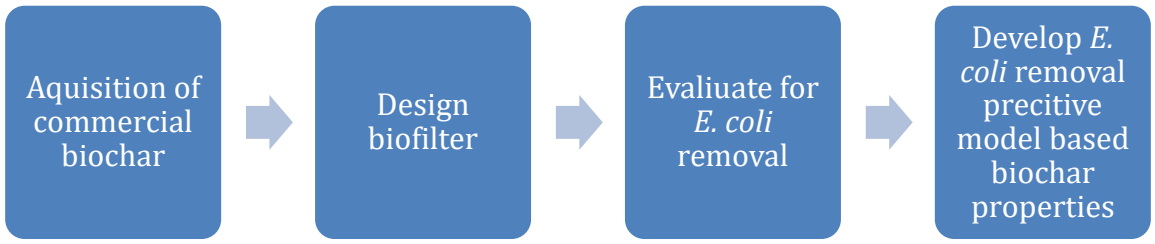

4.1 Motivation

Biochar, a carbon amendment produced by pyrolysis of waste biomass, has been shown to improve contaminant removal (Lau et al. 2017, Mohanty et al. 2018, Sun et al. 2020). Biochar can be produced at any location, thereby making it widely available for use by stormwater managers (Xie et al. 2015). However, biochar properties can vary widely based on preparation conditions and feedstock types (Xiao et al. 2018). This makes it challenging for the stormwater manager to select specific biochar from suppliers. It is generally recommended to use wood-based biochar prepared at high pyrolysis temperature (Abit et al. 2012, Bolster and Abit 2012) without removing fine biochar (Guan et al. 2020, Mohanty and Boehm 2014, Sasidharan et al. 2016). Pathogens and fecal indicator bacteria (FIB) are one of the most difficult pollutants to remove from stormwater, making them the leading cause of TMDL violations in many urban areas (EPA 2002). Bacterial removal by biochar could vary widely (Boehm et al. 2020),

indicating the competing effects of different properties, including carbon content, ash content, volatile carbon content, and surface area (Manya 2012).

4.1.1 Objective

This study aims to select the most effective biochar from the suppliers for stormwater treatment by using *E. coli* removal as an indicator parameter.

4.1.2 Hypothesis

We hypothesized that commonly reported bulk biochar properties can be used to develop an empirical model to predict E. coli removal capacity. The model can be used by stormwater managers to select biochar from the suppliers for the treatment of stormwater.

4.2 Experimental design and operation

4.2.1 Stormwater preparation

Synthetic stormwater was created in deionized water mixed with the following salts: 0.75 mM of $CaCl_2$, 0.075 mM of $MgCl_2$, 0.33 mM of Na_2SO_4, 1 mM of $NaHCO_3$, 0.072 mM of $NaNO_3$, 0.072 mM of NH_4Cl, and 0.016 mM of Na_2HPO_4 (Mohanty and Boehm 2014). This limits the influence of the fluctuating composition of natural stormwater on the measurement and comparison of the removal capacity of four types of biochar.

4.2.2 Biofilter design

Biofilter media for each biofilter consisted of a mixture of coarse Ottawa sand (0.6 – 0.85 mm) and one of the biochar from the following suppliers: Terra Char (BioEnergy Innovations Global, Inc.), Agricultural Carbon (National Carbon Technologies, LLC), Naked Char (American BioChar Company), and Rogue Biochar (Oregon Biochar Solutions, LLC). Our previous work shows that biochar capacity to remove biological pollutants can vary by orders of magnitude based on feedstock types, pyrolysis temperature, and biochar size. Biochar made from

wood biomass and produced at high pyrolysis temperature tends to have high removal capacity for bacterial. We selected these biochars based on these criteria and also their availability in large scale and readiness to supply to California market. Each biochar was characterized for surface area, carbon content, ash content, volatile carbon, and elemental composition (Table 4.1). Prior to packing, large biochar particles (> 2.0 mm) were removed by sieving to minimize preferential flow through the filters. Sand and biochar (30% v/v) were mixed manually and packed in triplicate polypropylene columns of 2.54 cm in diameter and 30 cm in height (Mohanty and Boehm 2014).

Table 4.1. Preparation condition and properties of four types of biochar used

Parameters	**Terra Char**	**Agricultural Carbon**	**Naked Char**	**Rogue Biochar**
Vendor	BioEnergy Innovations Global, Inc., MO	National Carbon Technologies, LLC, MN	American BioChar Co., MI	Oregon Biochar Solutions, LLC, OR
Feedstock	Oak Hardwood Sawdust	Wood-based	Southern Yellow Pine Species	80% Softwood, 15% Hardwood, and 5% Nutshells
Pyrolysis Temperature (ºC)	540	>550	550 – 990	>900
Surface Area (m^2 g^{-1})	207	339	283	475
S, %	0.003	0.002	0.005	0.041
C, %	70.16	85.03	80.96	84.66
H, %	1.89	2.77	0.59	0.83
N, %	0.62	0.31	0.53	0.81
O, %	9.36	7.78	5.67	5.43
Polarity Index, (O+N)/C	0.142	0.095	0.077	0.074
Ash, %	17.97	4.11	12.24	8.23
Volatile Matter, %	18.55	12.19	6.66	7.86
Fixed Carbon, %	63.48	83.7	81.1	83.91

4.2.3 E-coli experiment

After packing the biofilters, synthetic stormwater without *E. coli* was injected for 24 hours at 2 mL min^{-1} (e.g. hydraulic loading rate of 139.9 GPD ft^{-2}) using a peristaltic pump (Masterflex L/S Digital Drive, Cole Parmer) to condition the filter media. To maintain an upward flow direction, stormwater was injected at the bottom of the biofilter, and samples were collected on top. Upward direction ensured a complete saturation of the columns, which enables the comparison of the maximum removal capacity of the biochar without interferences of preferential flow (Mohanty et al. 2013). To measure the biofilter's pore volume (PV), e.g. the volume of the empty space in the filter media, the weight difference between wet-biofilter and dry-biofilter was measured. The average PV of all biofilters was 50.3 ± 2.8 mL, and it is not statistically different (*p-value* > 0.05) between biofilters.

4.2.4 Estimation of removal capacity of biochar

Stormwater containing *E. coli* was injected through the columns in an upward direction at 2.0 mL min^{-1} using a peristaltic pump, and effluent sample fractions were collected using 15-mL centrifuge tubes. Stormwater containing *E. coli* was created by growing *E. coli* in LB broth solution for 16-24 hours at 37 ºC and 120 rpm, followed by a triple wash procedure with phosphate buffer solution to remove the LB broth solution. The washed *E. coli* solution was used to spike the synthetic stormwater to achieve a concentration of nearly 10^5 CFU mL^{-1}. This concentration is much higher than the bacterial concentration expected in road runoff, where low concentration is measured as MPN/100 mL. However, the use of high concentrations in the laboratory was necessary to measure effluent concentration accurately and quantify a high removal capacity of biochar. Upward flow is necessary to compare the maximum removal capacity of biochar without preferential flow. The removal capacity of the biofilter was

calculated as, $-log_{10}(C_e/C_i)$ where C_e and C_i represents the concentration of *E. coli* in the effluent and influent, respectively. The clean-bed removal capacity (triplicated columns) was estimated by comparing the effluent concentration after the injection of ~5 PV of *E. coli*-contaminated stormwater. The long-term removal capacity of the biofilters can be significantly different from the clean bed removal capacity due to the exhaustion of the attachment sites by *E. coli* and other competing agents in stormwater. The long-term removal capacity of biofilters (duplicated columns) was estimated after the injection of 57PV of contaminated stormwater in 10 intermittent rainfall events. In each infiltration event, 8±1 PV of E. coli-contaminated stormwater was injected for 4 h followed by 24–96 hours of flow interruption. 57 PV was chosen as an indicator of long-term removal capacity because this rainfall quantity is equivalent to 9.1 years of *E. coli* loading to a biofilter located in Los Angeles (38.1 cm of rainfall per year), assuming a catchment area of 10 acres and an average *E. coli* concentration of 10 CFU mL^{-1} in the stormwater. It should be noted that this method of extrapolating laboratory study to field performance assumed that the aging of biochar during that 10 years would not have any effect on bacterial removal capacity. The long-term removal capacity was calculated as the average of the last three rainfall events which occurred at 57, 66, and 75 PV.

In between infiltration events, *E. coli* trapped in the pore water inside the biofilter can grow or die, thereby increasing or decreasing the effluent concentration. We introduced the growth-die off index (GDI), which is the negative log of the ratio of *E. coli* concentration before and after the flow interruption, to quantitatively determine the fate of *E. coli* trapped in biofilters during the pause between infiltration events. Positive and negative GDI, respectively, indicates a net-growth and die-off of *E. coli* in between infiltration events. It should be noted that *E. coli* removed by biochar can grow and become the source of contamination in subsequent storm

events unless they die or lose viability after adsorption on biochar. The GDI parameter calculated in this study provides information about the long-term fate of bacteria removed by biochar.

Analysis of Pearson correlations was used to verify the correlation between biochar properties and *E. coli* removal capacities. Analysis of variance, principal component analysis (PCA) and partial linear squares (PLS) regression models were used to interpret the results and rank the properties that predict biochar capacity to remove fecal indicator bacteria.

4.3 Results and discussion

4.3.1 E-coli removal capacity by biochar

The clean-bed removal of *E. coli* depended on biochar types (Figure 4.1) and varied by more than one order of magnitude between different biochar. For instance, the clean-bed removal capacity of biofilters packed with Rogue Biochar (log removal of 3.36±0.70) or Agricultural Carbon (3.67±0.72) was greater than biofilters packed with Terra Char (1.98±0.38) or Naked Char (1.90±0.50). The long-term removal capacity was different from their clean-bed removal capacities based on biochar type. After the exposure to 57+ pore volume of contaminated stormwater, which is equivalent to 9.1 years of *E. coli* loading in biofilters in Los Angeles, the removal capacities of Rogue Biochar and Terra Char increased ($p < 0.05$) by 71% and 62%, respectively, whereas the removal capacity of Agricultural Carbon decreased ($p < 0.05$) by 20%. No significant difference ($p > 0.05$) between the clean-bed and the long-term removal was observed for the biofilters packed with Naked Char.

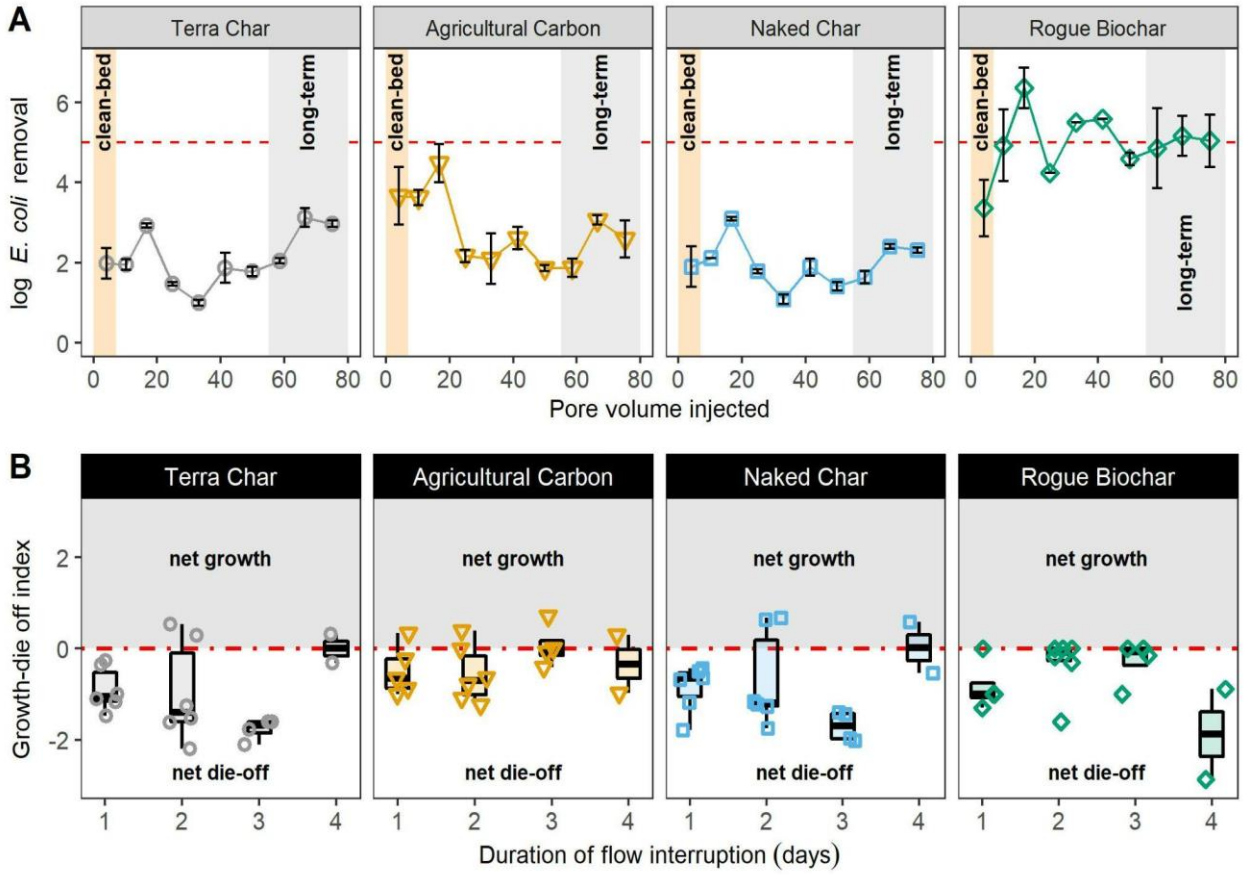

Figure 4.1. (A) Removal capacity of biochar-augmented filters during 10 infiltration events. Yellow and grey shaded areas represent clean-bed and long-term removal, respectively. (B) Growth-die off Index (GDI) between two consecutive infiltration events as a function of drying duration between the infiltration events. GDI was calculated as $-\log_{10}(C_b - C_c)$, where C_b and C_a represent the concentration of *E. coli* in the effluent before and after flow interruption, respectively. Positive GDI values (grey shaded area) represents net-growth of bacteria during flow interruption, while negative GDI values represents net die-off (or decay) or bacteria. Positive GDI values (grey shaded area) represents net-growth of bacteria during flow interruption, while negative GDI values represents net die-off (or decay) or bacteria.

The *E. coli* concentration in pore water of sand-biochar filters mostly decreased (with few exceptions) during intervals between infiltration events, resulting in the growth-die off index (GDI) below zero (Figure 4.1B). The log GDI values appear to be independent of the duration between infiltration events, indicating a lack of growth of *E. coli*. The result indicates that despite the presence of nutrients in pore water, *E. coli* did not grow in pore water or on biochar in between infiltration events. Thus, biochar could continue to remove or inactivate *E. coli* from pore water in between infiltration events, thereby replenishing filter media for the removal of more contaminants in the following infiltration events. It should be noted that previous study with sand without biochar showed less than 0.15 log removal and the E. coli grew on biochar when dissolved organic carbon or nutrient was high.

We showed that the removal in clean-bed biofilters could be different from long-term exposure. Compared to other studies that examined long-term *E. coli* removal by biochar, our study used stormwater without native bacteria and dissolved organic carbon (DOC) that may exhaust biochar faster. Thus, our results could overestimate the capacity of biochar in removing *E. coli*. Another possible overestimation of our results is related to flow direction. Although we used an upward injection in the current study, actual field application usually experiences several complexities such as downward injections, presence of dissolved organic carbon and other bacteria, and aging of biochar, all of which may affect the removal capacity of the filter. Here, the objective is to select the best biochar and not to measure the actual removal capacities. Nonetheless, the best biochar in this controlled study will likely be the best biochar in field conditions.

4.3.2 Correlation of Removal with Biochar Properties

Removal was positively correlated with surface area and fixed carbon but negatively correlated with polarity, volatile matter, and ash content (Figure 4.2). The ash content is found to be the most important indicator of bacterial removal in biochar. The vendors could lower ash content in biochar by optimizing the production condition such as feedstock type and pyrolysis temperature (Ahmed et al. 2016), or they can also be washed with strong acids to dissolve and remove the ash (Sun et al. 2013).

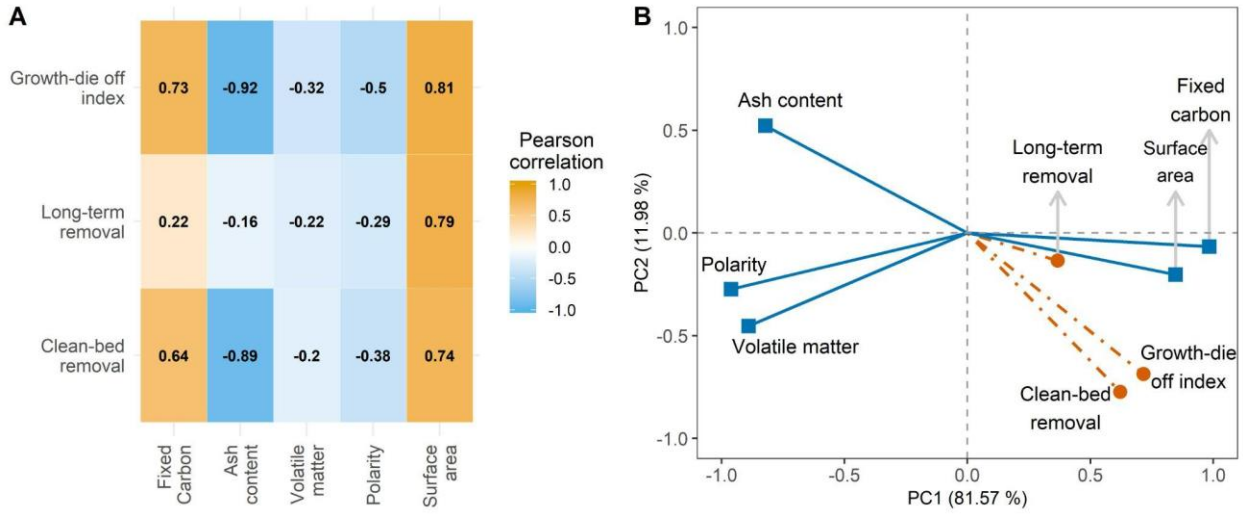

Figure 4.2. **(A)** Correlation of clean-bed removal capacity, long-term removal capacity, and growth-die off index (GDI) with specific biochar properties including fixed carbon, ash, volatile matter, polarity, and surface area. **(B)** Principal Component Analysis (PCA) between biochar properties, removal capacities, and growth-die off index (GDI).

Growth-die off index was negatively correlated with the biochar polarity (r = -0.5) and ash content (r = -0.92), but positively correlated with biochar surface area (r = 0.81). We attribute these results to the biochar's ability to continue to remove bacteria by inactivation (Gurtler et al. 2014) and adsorption (Mohanty et al. 2014) or to reduce the availability of growth metabolites (Hill et al. 2019).

Principal component analysis (PCA) showed that while surface area and fixed carbon positively affect the growth-die off index and the clean-bed removal, polarity and ash content negatively affect the growth-die off index and the clean-bed removal capacity. Long-term removal appears to be uncorrelated or weakly correlated to most variables.

4.3.3 Predictive model based on biochar properties

Based on the partial least squares (PLS) regression, an empirical model was developed to predict clean-bed removal (R_S, equation 1) and growth-die off index (GDI, equation 2) based on surface area (SA), fixed carbon (FC), ash content (AC), and volatile matter (VM). The model was optimized to predict the removal capacity of biochar with high confidence (variation above 5% is considered failure). Our model was able to predict the removal capacity of another commercially available biochar (Sonoma Biochar) used in a previously published study (Mohanty et al. 2014). Our model predicted that Sonoma Biochar would remove 99.90% of *E. coli*, while the reported data showed the removal of 99.52% (Table 4.2). We analyzed the interaction between variables and found that the interactive effect between the variables is either statistically insignificant for the prediction of GDI or yields an unrealistic outcome for the prediction of the clean bed removal capacity. This result indicates that the interaction effect between variables is minimal. Overall, our results show that the model could be used to indicate

the *E. coli* removal capacity of biochar's from different suppliers, although validating the model with more biochar's can improve the model.

$$R_s = 0.0045\,SA + 0.0097\,FC - 0.113\,AC + 0.104\,VM + 0.531 \quad \text{(Eq 4.1)}$$

$$GDI = 0.0008\,SA + 0.0023\,FC - 0.019\,AC + 0.015\,VM - 0.157 \quad \text{(Eq 4.2)}$$

Table 4.2. Clean-bed log removal results for the prediction models generated through partial least squares regression analysis with and without the interaction between variables.

Biochar type	**Model validation results**		
	Model without interaction[1]	**Model with interaction[2]**	**Laboratory exp.**
Terra Char	1.98	123.70	1.98 ± 0.38
Agricultural Carbon	3.67	269.23	3.64 ± 0.74
Naked Char	1.90	210.17	1.90 ± 0.50
Rogue Biochar	3.37	369.31	3.20 ± 0.48

[1]Model without interaction: $R_s = 0.0045\,SA + 0.0097\,FC - 0.113\,AC + 0.104\,VM + 0.531$

[2]Model with interaction: $R_s = 0.0045\,SA + 0.0097\,FC - 0.113\,AC + 0.104\,VM - 0.0016\,SA\,AC + 0.0092\,SA\,FC + 0.0019\,SA\,VM + 0.531$

where SA = surface area, FC = fixed carbon, AC = ash content, and VM = volatile matter.

4.4 Summary and implications

- *E. coli* removal capacity of fresh biochar and used biochar varied with biochar types.
- Rogue biochar worked better than other biochar for *E. coli* removal, both in clean bed biofilters and long-term exposure.
- The *E. coli* removal capacities of sand-biochar filters were positively correlated with the surface area and organic carbon content of biochar and negatively correlated with ash content and volatile matter.
- A model relating biochar removal capacity with these commonly measured biochar properties was developed based on partial least squares regression, which has the potential to predict the *E. coli* removal capacity of commercially available biochar.
- This model could not only help stormwater managers to select biochar for biofilters but also inform the biochar production company to tailor the production method to produce biochar with specific properties.

4.5 Reference

Abit, S.M., Bolster, C.H., Cai, P. and Walker, S.L. (2012) Influence of feedstock and pyrolysis temperature of biochar amendments on transport of Escherichia coli in saturated and unsaturated soil. Environmental Science and Technology 46(15), 8097-8105.

Ahmed, M.B., Zhou, J.L., Ngo, H.H. and Guo, W.S. (2016) Insight into biochar properties and its cost analysis. Biomass & Bioenergy 84, 76-86.

Boehm, A.B., Bell, C.D., Fitzgerald, N.J.M., Gallo, E., Higgins, C.P., Hogue, T.S., Luthy, R.G., Portmann, A.C., Ulrich, B.A. and Wolfand, J.M. (2020) Biochar-augmented biofilters to improve pollutant removal from stormwater – can they improve receiving water quality? Environmental Science: Water Research & Technology, https://doi.org/10.1039/d1030ew00027b

Bolster, C.H. and Abit, S.M. (2012) Biochar Pyrolyzed at Two Temperatures Affects Escherichia coli Transport through a Sandy Soil. Journal of Environmental Quality 41(1), 124-133.

EPA, U. (2002) National water quality inventory 2000 report.

Guan, P., Prasher, S.O., Afzal, M.T., George, S., Ronholm, J., Dhiman, J. and Patel, R.M. (2020) Removal of Escherichia coli from lake water in a biochar-amended biosand filtering system. Ecological Engineering 150, https://doi.org/10.1016/j.ecoleng.2020.105819.

Gurtler, J.B., Boateng, A.A., Han, Y.X. and Douds, D.D. (2014) Inactivation of E. coli O157:H7 in Cultivable Soil by Fast and Slow Pyrolysis-Generated Biochar. Foodborne Pathog Dis 11(3), 215-223.

Hathaway, J.M., Hunt, W.F., Wright, J.D. and Jadlocki, S.J. (2009) World Environmental and Water Resources Congress 2009, pp. 1-10.

Hill, R.A., Hunt, J., Sanders, E., Tran, M., Burk, G.A., Mlsna, T.E. and Fitzkee, N.C. (2019) Effect of Biochar on Microbial Growth: A Metabolomics and Bacteriological Investigation in E. coli. Environmental Science & Technology 53(5), 2635-2646.

Lau, A.Y.T., Tsang, D.C.W., Graham, N.J.D., Ok, Y.S., Yang, X. and Li, X.-d. (2017) Surface-modified biochar in a bioretention system for Escherichia coli removal from stormwater. Chemosphere 169, 89-98.

Manya, J.J. (2012) Pyrolysis for Biochar Purposes: A Review to Establish Current Knowledge Gaps and Research Needs. Environmental Science and Technology 46(15), 7939-7954.

Mohanty, S.K. and Boehm, A.B. (2014) Escherichia coli Removal in Biochar-Augmented Biofilter: Effect of Infiltration Rate, Initial Bacterial Concentration, Biochar Particle Size, and Presence of Compost. Environmental Science & Technology 48(19), 11535-11542.

Mohanty, S.K., Cantrell, K.B., Nelson, K.L. and Boehm, A.B. (2014) Efficacy of biochar to remove Escherichia coli from stormwater under steady and intermittent flow. Water Research 61, 288-296.

Mohanty, S.K., Torkelson, A.A., Dodd, H., Nelson, K.L. and Boehm, A.B. (2013) Engineering Solutions to Improve the Removal of Fecal Indicator Bacteria by Bioinfiltration Systems during Intermittent Flow of Stormwater. Environmental Science & Technology 47(19), 10791-10798.

Mohanty, S.K., Valenca, R., Berger, A.W., Yu, I.K.M., Xiong, X.N., Saunders, T.M. and Tsang, D.C.W. (2018) Plenty of room for carbon on the ground: Potential applications of biochar for stormwater treatment. Science of the Total Environment 625, 1644-1658.

Sasidharan, S., Torkzaban, S., Bradford, S.A., Kookana, R., Page, D. and Cook, P.G. (2016) Transport and retention of bacteria and viruses in biochar-amended sand. Science of the Total Environment 548, 100-109.

Sun, K., Kang, M., Zhang, Z., Jin, J., Wang, Z., Pan, Z., Xu, D., Wu, F. and Xing, B. (2013) Impact of Deashing Treatment on Biochar Structural Properties and Potential Sorption Mechanisms of Phenanthrene. Environmental Science and Technology 47(20), 11473-11481.

Sun, Y., Chen, S.S., Lau, A.Y.T., Tsang, D.C.W., Mohanty, S.K., Bhatnagar, A., Rinklebe, J., Lin, K.-Y.A. and Ok, Y.S. (2020) Waste-derived compost and biochar amendments for

stormwater treatment in bioretention column: Co-transport of metals and colloids. Journal of Hazardous Materials 383, 121243.

Valenca, R., Ramnath, K., Dittrich, T.M., Taylor, R.E. and Mohanty, S.K. (2020) Microbial quality of surface water and subsurface soil after wildfire. Water Research, https://doi.org/10.1016/j.watres.2020.115672

Xiao, X., Chen, B., Chen, Z., Zhu, L. and Schnoor, J.L. (2018) Insight into Multiple and Multilevel Structures of Biochars and Their Potential Environmental Applications: A Critical Review. Environmental Science & Technology 52(9), 5027-5047.

Xie, T., Reddy, K.R., Wang, C., Yargicoglu, E. and Spokas, K. (2015) Characteristics and Applications of Biochar for Environmental Remediation: A Review. Critical Reviews in Environmental Science and Technology 45(9), 939-969.

5 Task 3a: Amount of sand needed for optimum infiltration capacity

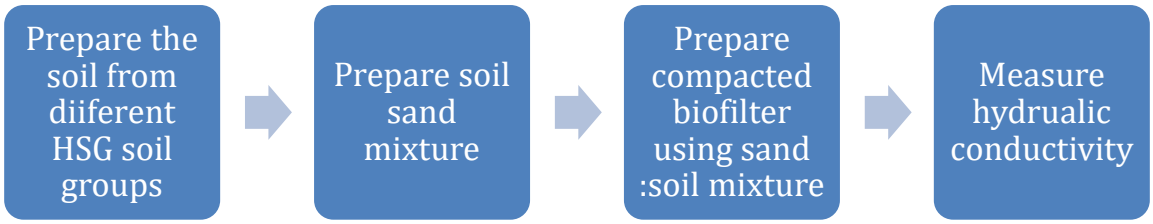

5.1 Background

5.1.1 Motivation

Transportation infrastructures such as road surfaces accumulate contaminants resulting from traffic activities, and compaction of the roadside stormwater best management practices (BMPs) minimize natural infiltration of stormwater structures (Pereira et al., 2017; Sax et al., 2017). Our work from section 3 task 2b shows that the negative impact of compaction on hydraulic permeability can be reduced by adding sand as bulking material. Sand-based media also have greater resiliency and consistency with respect to the compaction effect, but the net increase of soil permeability depends on the particle size of sand and the mixing ratio with soil. Thus, the mixing ratio is expected to change based on soil types. Currently, no specific guideline is available to determine the amount of sand needed for biofilter under compaction based on soil properties.

5.1.2 Objective

The objective of the work is to estimate the fraction and amount of coarse sand needed in the mixture of soil and sand to maintain minimum hydraulic conductivity (at least 6 inch.h^{-1}) after compaction.

5.1.3 Hypothesis

We hypothesized that adding coarse sand will increase the infiltration capacity of compacted soil, but the fraction of sand needed to achieve the desired infiltration will increase with a higher clay or silt content of the soil. We will test these hypotheses in the laboratory using four different soil groups (duplicate from each group) collected from 8 sites.

5.2 Experimental design and methods

5.2.1 Collection of soils:

Soil from four hydrologic soil groups as per USDA soil survey map, A, B, C, D, was collected from multiple Right-of-Way locations in Los Angeles County. However, our lab analysis shows C and D are not available. So, these results are valid only for A &B. The location, GPS coordinates, and details of the soil group are provided in the previous section (Table 1.1). A coarse sand (ASTM 20 – 30, Humboldt Mfg company) was used.

5.2.2 Preparation of filter media

Sand (0.6 – 0.85 mm) was washed with tap water and dried at 100 ºC overnight. The soil was air-dried at room temperature until the soil moisture was below 10% and then sieved to remove particles greater than 2 mm (mesh #10). The sieved soil was mixed with sand with the ratio 50% - 90% by volume, respectively and one mixture only soil (no sand added, 0% sand). DI water was added incrementally and mixed manually for up to 10 minutes to create a homogeneous mixture with 10% moisture content. The wet mixture was immediately covered with aluminum foil to prevent moisture loss before packing.

5.2.3 Compacting sand-soil filter media into columns

To design a laboratory column set-up, a transparent PVC tube (5.1 cm I.D. and 61.0 cm length) was glued with PVC fittings and connected to a control valve to regulate the effluent flow. A total of 18 columns with three replicates per treatment were packed with the following media mixture with sand under different compaction conditions. Before packing the filter media in each column, a nylon mesh (100 μm pores) was inserted at the bottom to prevent the filter media from falling into the outlet tube. Pea gravels were poured over the mesh to a height of 9 cm, and a second mesh was placed over the gravel layer to prevent the filter media top from falling into the pore space between gravels. The media mixture was added incrementally and compacted to a height of 3.8 cm layer using a standard Proctor hammer (2.5 kg). To ensure that comparable energy of a standard Proctor test was applied on the filter media, the hammer was dropped seven times from 30.5 cm height per layer following the equation: $Number\ of\ blow\ per\ layer = (E \times V)/(W \times N \times H)$, where energy per unit volume (E), hammer weight (W), number of total layers (N), and drop height (H) were kept constant as 593 kN-mm^{-3}, 2.5 kg, four layers, and 15.2 cm, respectively. The single-layer height of filter media was calculated by dividing the column area by the column volume, and it equaled 3.8 cm. The procedure was repeated until the filter media depth reached 15.2 cm with a total of 4 layers. The bulk density was estimated after compaction of the entire filter layer. An additional 2.5 cm layer of pea gravel was added on the top of the filter media to prevent the floating of soil particles in the case of ponding. After packing, DI water was injected from the bottom to fill the space until the top of the pea gravel layer on the top column.

5.2.4 Hydraulic conductivity measurement

After pore volume measurement, a hydraulic conductivity test was immediately conducted on each column. The hydraulic conductivity (K, inch.h^{-1}) of each column was

measured using the falling head method: $K_s = L/t \ \ln(h_1/h_2)$, where L is the depth of filter media, t is the duration to drain water from the initial height h_1 to the final height is the initial height h_2, both heights were above the filter media. Tap water was poured gently from the top of the column to prevent disturbance of filter media until the water level reached a 10 cm level above the sand-soil mixture. The initial height of water (h_1) was marked at 10 cm level above the sand-soil mixture, and a second mark (h_2) was made 5 cm below the first mark. The bottom outlet of the column was opened, and water was collected until the water level dropped from h_1 to h_2 marks. The hydraulic conductivity was determined by measuring the volume of water released and the time required to drain the water from h_1 to h_2. The experiment was repeated five times per column in order to estimate the average hydraulic conductivity for each hydrologic soil type.

5.3 Result and discussion

5.3.1 Hydraulic conductivity as a function of added sand

The hydraulic conductivity increases with an increase in the sand fraction in all four hydrologic soil group biofilters (Figure 5.1). The amount of sand needed to achieve the desired infiltration rate of 6 inches h^{-1} varied from 70-95 %. The soil from hydrologic group D (D2) required minimum sand of ~70%, whereas group C required a maximum of sand of ~95%. Soil group A (Soil A1 and A4) required >80% of sand, and group B (Soil B1 and B2) required ~90% of sand. We plotted the amount of sand needed vs. hydraulic conductivity of all soil groups and fitted data with a nonlinear model (Figure 5.2). Our model predicted data indicates that overall soil needs greater than 85% of sand to meet the minimum infiltration rate of 6 inch.h^{-1}. However, the exact amount of individual soil group needs to be optimized based on inherent soil properties and infiltration rate.

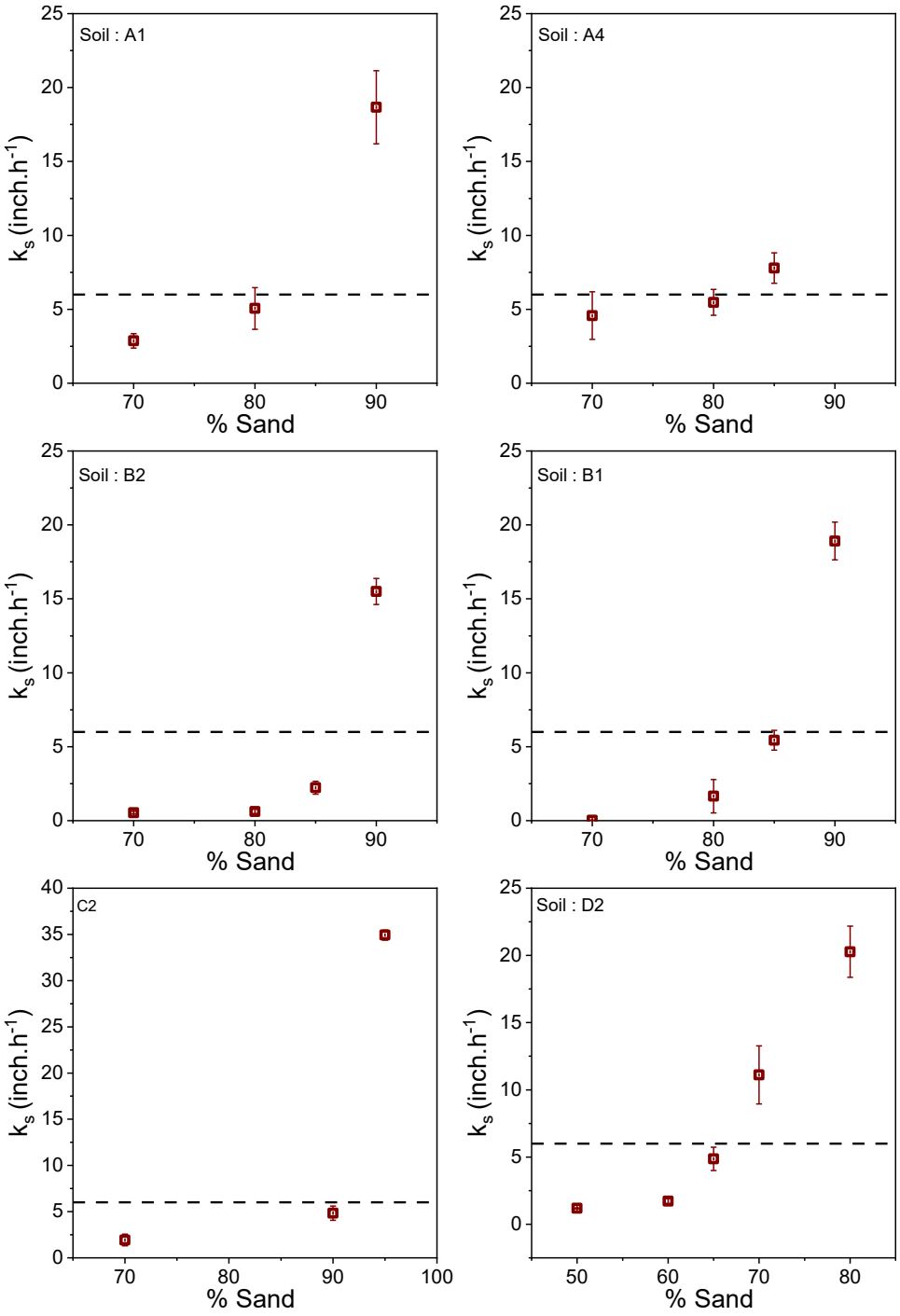

Figure 5.1. Saturated hydraulic conductivity (k_s) of four (A, B, C, D) hydrologic group soil with varying amounts of sand under compaction. The dotted horizontal line at 6 inch.h^{-1} is the desirable k_s for designed stormwater biofilters.

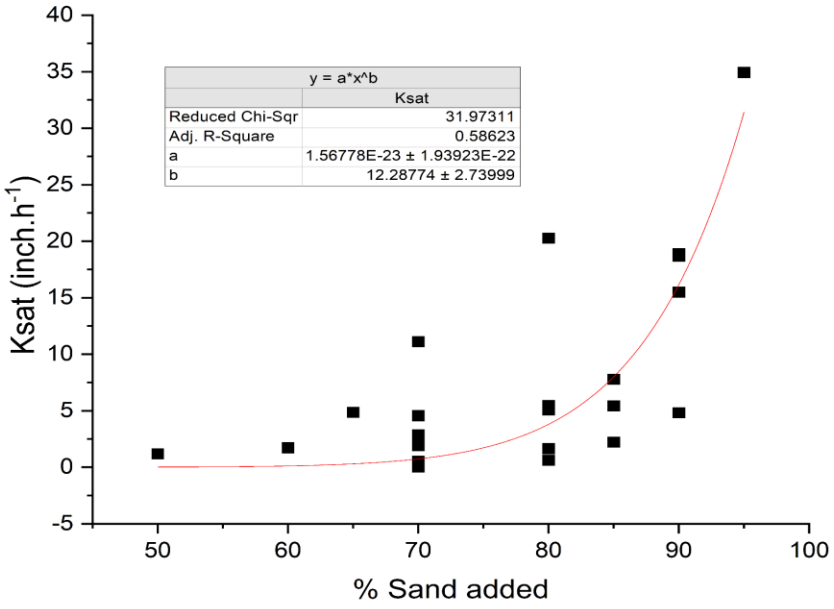

Figure 5.2. Measured hydraulic conductivity values as a function of the sand added.

The addition of optimum sand to different hydrologic groups of urban soil (groups A, B, C, and D) enhanced its infiltration rate despite compaction. Heavily compacted soils contain few large pores, thereby lowering infiltration rates (Itsukushima et al., 2021). In contrast, sand restricts compression of some of these pore paths, thereby alleviating the negative impact of compaction.

5.4 Summary and implications

Compactions reduced the infiltration capacity of biofilters, but the addition of sand alleviated the negative impact of compaction by increasing the infiltration capacity. The amount of sand required to achieve a desired infiltration rate of biofilter varied with soil hydrologic groups class and inherent soil physical properties. While the addition of sand can restore the infiltration capacity of compacted biofilter, it has a limited capacity to remove pollutants. Therefore, it is necessary to replace part of sand with other types of bulking agents or amendments like biochar which have higher pollutant removal capacity.

5.5 References

Itsukushima, R., Ideta, K., Takata, H., 2021. Relationship between compaction and infiltration capacity of amended soil for urban flood damage mitigation. Soil Use and Management n/a.

Pereira, R.S., Emmert, F., Miguel, E.P., Mota, F.C.M., Rezende, A.V. and Leal, F.A. (2017) Mechanical stabilization of soils as alternative for construction of low cost forest road. Nativa 5(3), 212-217.

Sax, M.S., Bassuk, N., van Es, H. and Rakow, D. (2017) Long-term remediation of compacted urban soils by physical fracturing and incorporation of compost. Urban Forestry & Urban Greening 24, 149-156.

6 Task 3a: Potential effects of compactions on stormwater treatments on roadsides - A review

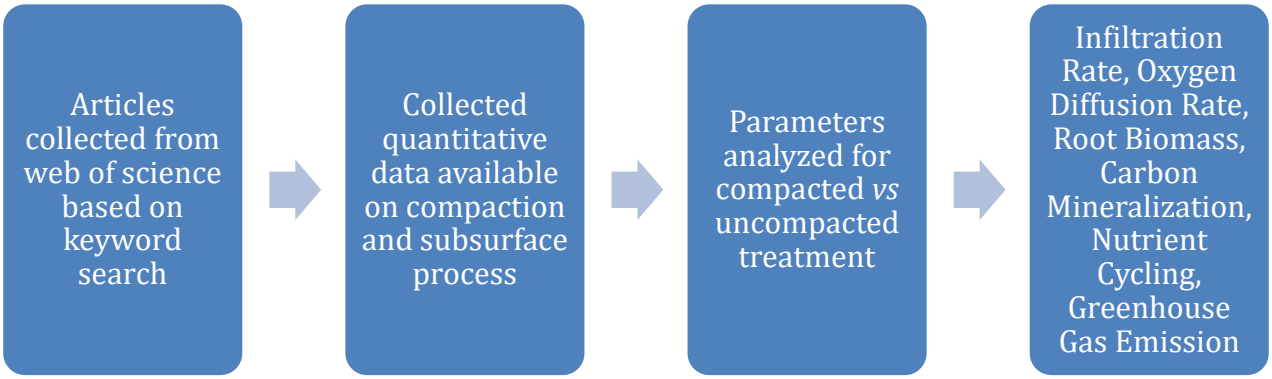

6.1 Introduction

Nearly 70% of the world's population is going to live in urban areas, which are severely water-stressed in many regions (He et al., 2021; United Nations, 2018). Impervious cover and compaction of the soils during urban development not only limit natural infiltration and recharge of groundwater (Pitt et al., 2008; Edmondson et al., 2011, Jefferson et al., 2017; LeFevre et al., 2015; McGrane, 2016; Müller et al., 2020). Road surfaces accumulate contaminants resulting from traffic activities (Gilbert and Clausen, 2006; Krein and Schorer, 2000; Lau et al., 2009; Zhao et al., 2011). Furthermore, compaction of the roadside soil, which is required for bank stability, minimizes the natural infiltration of stormwater (Yang and Zhang, 2011). Both these factors increase stormwater runoff that conveys the accumulated contaminants to water bodies. Thus, the installation of stormwater control measures on the roadside could enhance the infiltration and treatment of stormwater (Rivers et al., 2021; Sileshi et al., 2012; Winston et al.,

2012). Example of SCM includes detention ponds, bioswales, dry well, biofilters, bioinfiltration systems, vegetated filter strip, constructed wetlands, infiltration trenches, and permeable pavements. These roadside SCM could also provide multiple benefits including groundwater recharge, carbon sequestration, and ecological habitat restoration (Alam et al., 2021; Kavehei et al., 2018; Prudencio and Null, 2018; Säumel et al., 2016). Treatment and reuse of contaminated road runoff can potentially transform the nation's road infrastructure from a leading cause of water pollution to a network of water solutions to solve water scarcity issues in urban areas.

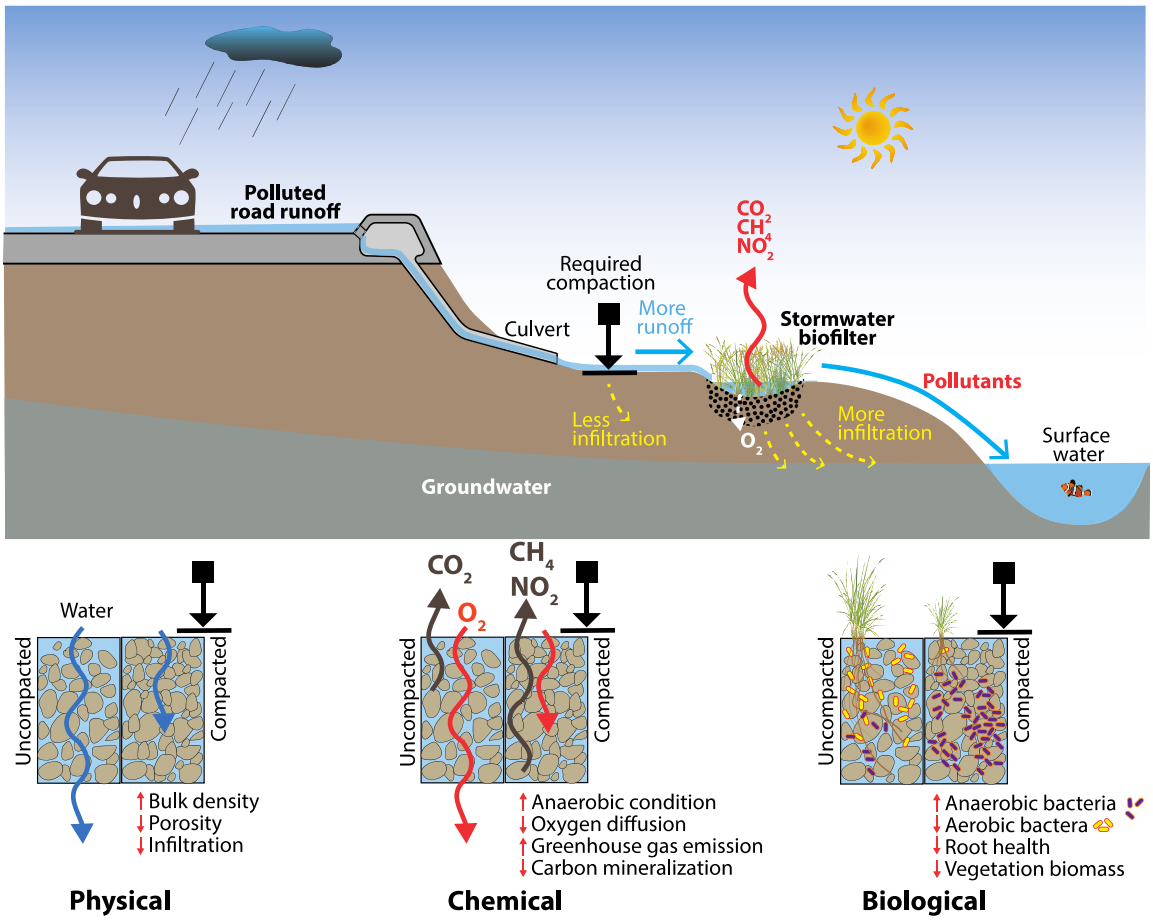

Figure 6.1. Potential Impacts of compaction on the performance of roadside stormwater control measures. Compaction could affect physical, chemical, and biological processes in subsurface soil. Compaction could increase bulk density, reduce infiltration rate, and decrease aeration. Compaction could induce an anaerobic environment and alter microbial communities in a way that could increase greenhouse gas emissions. Compaction could also affect vegetation health in SCM by blocking root growth and reducing nutrient uptake. All these processes could affect the water quantity and quality of stormwater discharged into surface waters originating from road surfaces during rainfall events.

The review aims to estimate the extent to which compaction could affect different processes in the subsurface soil and use the data to understand how compaction could affect functions of SCM including infiltration capacity, root health, and microbial processes. Despite the importance of compaction, no review to date has analyzed the potential impacts of compaction on SCM functions. A few review articles described the effect of compaction on the agriculture (Hamza and Anderson, 2005; Nawaz et al., 2013; Shah et al., 2017) and forest ecosystems (Cambi et al., 2015; Mariotti et al., 2020), where understanding the impact of compaction on plant health was the primary objective. In contrast, the main functions of SCM are infiltration and pollutant removal. Furthermore, the composition of filter media in SCM is a mixture of sand, soil, and other amendments (Tirpak et al., 2021), which may respond to compaction to a different extent than soil in forest or agricultural land. Thus, the analysis could inform the design guidelines for stormwater treatment systems where compaction is unavoidable.

6.2 Data collection and analysis

We collected data from stormwater systems, agricultural soil, and forest ecosystem to understand the impact of compaction on different biochemical processes as limited data is available on stormwater systems. However, the subsurface processes in agricultural soil and forest ecosystem are relevant to understanding the impact of compaction on SCM functions. We searched the Web of Science using keywords including compaction, stormwater control measures, biofiltration, bulk density, infiltration rate, oxygen diffusion rate, root biomass, carbon mineralization, nutrient cycling, greenhouse gas emission, nitrous oxide, methane, pasture, and agriculture. All studies cataloged in the database before December 24, 2021, were included in the analysis. The search resulted in a total of 1248 articles, of which 136 articles were selected after reading the titles and abstract. After further analysis of reported data in those articles, a total of

34 articles were selected, where data was available to link compaction with the subsurface functions. The complete dataset used in the analysis is provided in a separate data file.

6.3 Compaction impacts on subsurface processes

6.3.1 Infiltration rate

Soil compaction can decrease the infiltration rate, which is the primary function of SCM. Compaction could reduce the pore spaces, thereby decreasing natural infiltration rates (Gregory et al., 2006; Nawaz et al., 2013; Yang and Zhang, 2011). Analyzing data from both laboratory and field compaction studies, we found that compaction reduced the infiltration rate in soil by two orders of magnitude (Figure 6.2**a**), whereas compaction of sand or sandy soil did not significantly ($p = 0.089$) affect the infiltration rate. Based on the median value, compaction increased soil's average bulk density by 18 % (Figure 6.2b) and decreased infiltration rate by 91% (Figure 6.2**a**). The result indicates that the addition of sand to the urban soil could maintain its infiltration rate despite compaction. As the filter media used in SCM is typically sandy soil or a mixture of sand and soil (Tirpak et al., 2021), the compaction effect could be less detrimental than that observed in soil. Heavily compacted soils contain few large pores, thereby lowering infiltration rates (Itsukushima et al., 2021). In contrast, the presence of sand restricts compression of some of these pore paths, thereby alleviating the negative impact of compaction. Thus, sand should be used as an effective bulking agent in stormwater infrastructure. The reported infiltration rates through both compacted soil and sand are highly variable, possibly because of the degree of compaction and soil types varied between the studies. The infiltration rate in compacted soil could vary with the degree of compaction, soil textural class, soil moisture content, and ponded water depth (Pearson et al., 2013; Pitt et al., 2002; Sileshi et al., 2015).

Collectively, these results indicate that amount of sand may determine the negative impact of compaction on the infiltration capacity of roadside SCM.

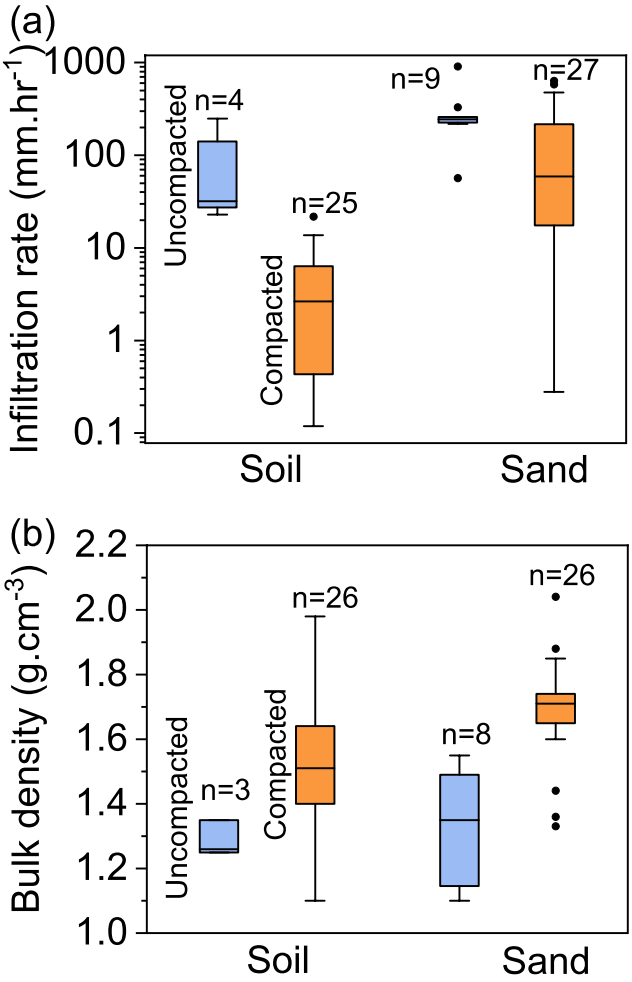

Figure 6.2. (a) Effect of compaction on infiltration rate of soil and sand. Infiltration rate is in log scale; (b) Effect of compaction on bulk density. For our data set, soil bulk densities ranged from 1.1 to 1.98 g.cm^{-3} where 53% of the data had a bulk density greater than 1.5 g.cm^{-3}. Sand bulk densities ranged from 1.3 to 2.04 g.cm^{-3}, where 80% of the data had a bulk density larger than 1.5 g.cm^{-3}. Here clayey and silty soils are classified as soils and all sandy soils are classified as sand. Data was collected from 8 peer-reviewed articles. n is the number of data points reviewed.

Opportunities: The degree of compaction that occurred in the filter media after SCM installation is rarely reported. A decrease in infiltration rate in SCM can be attributed to both compaction and clogging with sediments, but both relative importance of either is rarely studied. Compaction could also accelerate the clogging rate. Future studies should measure compaction and examine their contribution to decreasing infiltration in SCM. The analysis also reveals that sand can be an effective amendment to alleviate the negative impact of compaction. While the addition of sand can restore the infiltration capacity of compacted soil, it has a limited capacity to remove pollutants. Therefore, future studies should explore other types of bulking agents or amendments with higher pollutant removal capacity, their optimum size, and amounts needed to improve infiltration, and how compaction affects the physical integrity and pollutant removal capacity of the amendment.

6.3.2 Aeration or oxygen diffusion

Analyzing oxygen diffusion rate and soil bulk density data reported from a series of field experiments that quantified the effect of different vehicle passes on soil aeration conditions on different soils (Czyż, 2004; Czyz et al., 2001; Lipiec et al., 2012), we show that compaction could decrease oxygen diffusion rate by 36.8% and increased the bulk density by 33.3% based on median values (Figure 6.3). When the diffusion rate decreased below 35 μg O_2 $m^{-2} \cdot s^{-1}$, aeration can be considered a limiting factor in subsurface (Szafranek-Nakonieczna and Stępniewska, 2015). The result indicates that compaction could reduce the diffusion rate to near this threshold in soil. Compaction can limit oxygen supply in the vadose zone, which could limit root growth and alter microbial communities (Watson and Kelsey, 2006). Thus, compaction of the subsurface soil could affect the amount of oxygen the root zone has access to either directly by the exchange of gas from the atmosphere or via dissolved oxygen in stormwater. Both

processes require oxygen diffusion, which is often used as an indicator of the aeration capacity (Czyż, 2004). Compaction reduces macropore spaces, which could restrict oxygen diffusion and limit the exchange of oxygenated stormwater with anoxic pore water. However, sand is typically added to filter media used in SCM, which can lower the negative impact of compaction on oxygen diffusivity. However, no study to date has examined the oxygen diffusion rate in SCM filter media. Our analysis also revealed that there is a wide variation in the measured oxygen diffusion rate in compacted soils compared to uncompacted soil, possibly due to different degrees of compaction and soil types that determine the porosity around the soil root system (Neira et al., 2015). The results, however, did not account for the change in the concentration gradient that can also affect diffusion rate. Diffusion rate can be higher when a large oxygen concentration gradient is created between macropores with fresh stormwater and anoxic zones in the submerged organic layer, where microbial activity could deplete oxygen. Higher moisture content could reduce aeration as diffusion of oxygen through water is much slower than the supply of gaseous oxygen through dry pores (Kechavarzi et al., 2010). Thus, a combination of compaction and saturation could limit oxygen supply and impair root growth in biofilters. Oxygen concentration can affect many biochemical processes in the root zone including nitrogen and phosphorus cycling (Moreau et al., 2019).

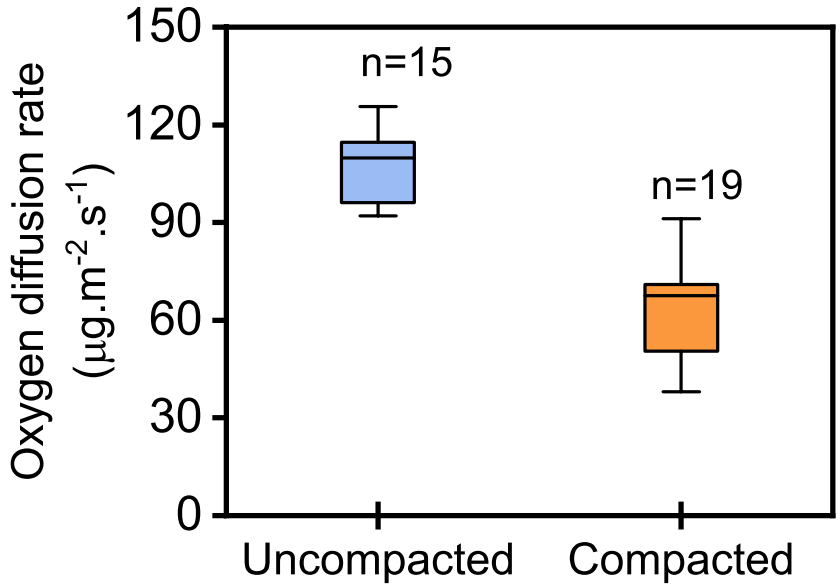

Figure 6.3. Effects of compaction on oxygen diffusion rate in soil under field experiments, the bulk density of uncompacted soil: 1.23-1.54 g.cm^{-3} and compacted soil 1.58-1.71 g.cm^{-3}. Compaction reduced the oxygen diffusion rate by 36.2%. Data were collected from 3 peer-reviewed articles (Czyż, 2004; Czyz et al., 2001; Lipiec et al., 2012). n is the number of data points used.

Opportunities: Oxygen concentration is measured in-situ in different systems reported in this study (Bittig et al., 2018; Elberling et al., 2011; Reiser et al., 2020; Song et al., 2019). Most of these studies did not have appropriate controls; that is, oxygen diffusion before compaction was not reported. Thus, future studies should use appropriate control in the same setup to estimate the effect of compaction. The degree of compaction could also affect oxygen diffusion. Thus, future studies should examine systematically the long-term oxygen level using in-situ probes before and after compaction. The anoxic condition created by compaction can increase the dissolution of iron, which typically releases nutrients such as phosphate (Herndon et al., 2019). Anoxic conditions could also promote denitrification (Subramaniam et al., 2016). Thus, future studies should examine whether compaction of filter media in SCM can result in net release or removal of nutrients such as nitrogen.

6.3.3 Plant functions

Analyzing the limited available dataset, we found no significant difference between compacted and non-compacted dry root biomass (Figure 6.4a). The result reveals that compaction increased the bulk density from 1 to 2 $g.cm^{-3}$, resulting in the root biomass change from -75% to +97% (Figure 6.4b). Nearly 70% of the data shows a negative effect of compaction. We attributed this unexpected outcome to smaller data sets and a wide variation in experimental conditions with many confounding factors such as plant types, soil type, and compaction level. For instance, a moderate level of compaction resulted in a net root biomass growth compared to no-compaction control in *Acer Cappadocium*, whereas severe compaction level (80-90%) decreased the root growth (Jourgholami, 2018).

As plants in SCM play a critical role in transforming contaminants accumulated in the biofilters (Mehmood et al., 2021; Muerdter et al., 2018; Payne et al., 2018), compaction could negatively affect SCM function by influencing the vegetation establishment (Correa et al., 2019; Picchio et al., 2019; Tracy et al., 2011). Compaction could hinder the plant functions such as nutrient uptake and transpiration by affecting root traits and root microbiome (Longepierre et al., 2021; Mariotti et al., 2020). Poor gas diffusion in compacted soil enhanced root secreted volatile ethylene hormone concentration in the rhizosphere, triggering plant hormone response and restricting root growth (Pandey et al., 2021). Rhizosphere microorganisms can degrade contaminants accumulated in the filter media (Chaudhry et al., 2005; Hoang et al., 2021; Read et al., 2009), thereby recharging the adsorption capacity of filter media. Plant roots can also enhance stormwater infiltration by maintaining high hydraulic conductivity through the pore paths created after root death (Bartens et al., 2008; Hatt et al., 2009). Plants with extensive root systems improve contaminants removal performance (Hermawan et al., 2019; Palacios et al.,

2021). Thus, any changes in root health by compaction could affect all these functions. Poor root growth means less access to plant-available water and nutrients, which could significantly reduce above-ground plant growth such as the growth of leaf and stem and plant height (Colombi et al., 2018; Mariotti et al., 2020). Poor aeration and reduced root growth, which are typical symptoms of compacted soil, can disrupt the rhizosphere biochemical environment, which further reduces the nutrient uptakes and alters the microbial degradation of pollutants (LeFevre et al., 2012; Mehmood et al., 2021; Muerdter et al., 2018).

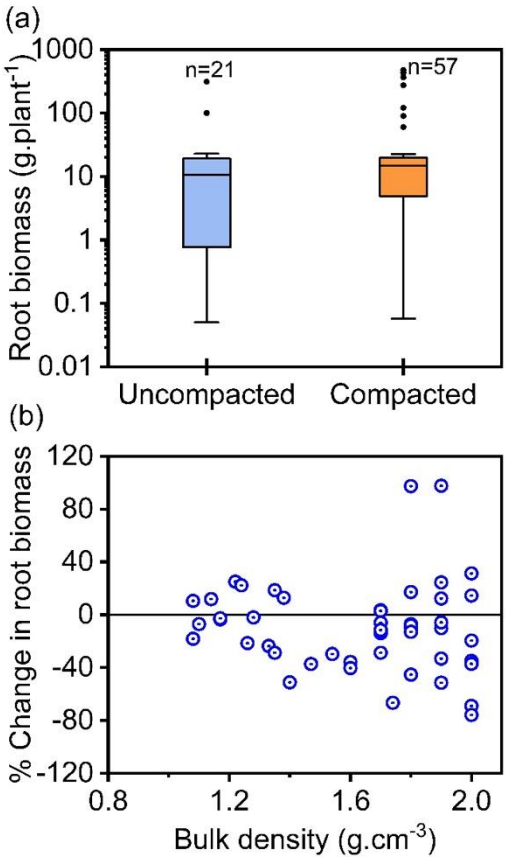

Figure 6.4. (a) Effects of compaction on root biomass. Based on a limited dataset, the root biomass did not significantly change after compaction ($p>0.05$). The bulk density of soils in the reported studies ranged between 0.9-2.1 g.cm $^{-3}$; (b) Changes in root biomass because of compaction. 70% of data points show a negative effect of compaction on biomass production. Data were collected from 11 peer-reviewed articles, and n is the number of data points reviewed.

Opportunities: Unlike soil, biofilter media could be composed of materials of different densities (Tirpak et al., 2021). For example, sand or soil is often mixed with amendments such as compost or biochar, which are lighter materials. The addition of these amendments can decrease the bulk density of soil (Ghavanloughajar et al., 2020). Thus, changes in bulk density in biofilter media due to compaction can be different from changes in bulk density in soil. Consequently, bulk density may not explain the degree of compaction in SCM media when compared with other studies that used soil without amendment. Thus, studies examining the extent of compaction should not use changes in bulk density as an indicator of the degree of compaction that occurred in SCM after their installation. The effect of compaction on other functions of plants relevant for SCM has not been studied. In particular, the effect of compaction on plants' ability to remove pollutants in SCM is understudied. Compaction can also trigger plant biochemical metabolic processes such as the release of root exudates (Badri and Vivanco, 2009). Change in rhizosphere biochemistry can influence pollutants degradation (LeFevre et al., 2013; Muerdter and LeFevre, 2019). Mechanistic studies linking compaction level and changes in root rhizosphere chemistry are needed. For instance, certain plant species with deep rooting systems can tolerate high compaction levels and low oxygen concentrations and alleviate compaction (Ampoorter et al., 2011; Colombi and Walter, 2017). The suitability of such plant species in SCM needs to be explored further. Compaction tolerant plant species are developed through genetic manipulation for better crop growth (Colombi and Keller, 2019). This type of work can be extended to improve SCM vegetation physiological traits to alleviate the negative impacts of the compaction (Correa et al., 2019).

6.3.4 Carbon mineralization

To examine carbon mineralization in the field, researchers measure CO_2 emission in the field or lab incubation studies where the soil is typically repacked to field density (Chen et al., 2016). Thus, compaction can be integrated into laboratory studies to understand its impact on carbon mineralization rate. Based on limited available data, compaction increased bulk density by 11.5-17.7% and altered carbon mineralization rate between -36.2 to 91.9% compared to uncompacted soil (Figure 6.5). The carbon mineralization rates in compacted and uncompacted soils were not significantly different, potentially due to the high variability of the limited data set. The wide variation in carbon mineralization has been attributed to the degree of compaction, pore size distribution, soil type difference, and variability in the microbial community. As compaction increases bulk density and decreases macropores, they can be used as indicators to determine when compaction could negatively affect carbon mineralization rate. Based on our data, when the bulk density value exceeds 1.6 g cm^{-3}, the carbon mineralization process is significantly reduced (Chen et al., 2016; Taboada et al., 1998). Compaction reduces the large macropores (>150 μm) and increases the small macropores (15-150 μm) fraction and this small macropore is desirable for microbial activities (Chen et al., 2016; Yoo et al., 2006) and increased carbon mineralization rate. However, the further reduction of small macropores can hinder the soil microbial activities (Chen et al., 2016; Strong et al., 2004; Taboada et al., 1998) and eventually the mineralization rate. Thus, pore size distribution should be monitored in all compaction studies to better understand to link between compaction and mineralization of carbon in SCM.

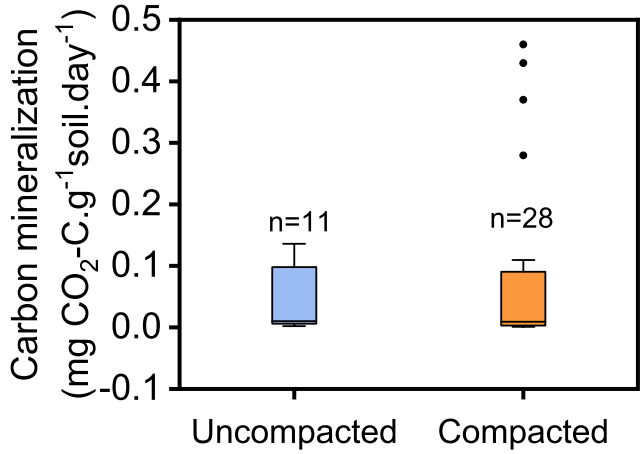

Figure 6.5. Effects of soil compaction on the rate of carbon mineralization. The bulk density of non-compacted soil ranges between 1.01-1.46 g.cm^{-3} and compacted soil between 1.11-1.65 g.cm^{-3}. The carbon mineralization rate is not significantly ($p>0.05$) different between compacted and non-compacted soils. Data were collected from 6 peer-reviewed articles. n is the number of data points reviewed.

Opportunities: The second most important function of SCM is to remove pollutants from stormwater, and biodegradation is a critical pathway to transform and degrade the accumulated pollutants (Biswal et al., 2021; LeFevre et al., 2015; Mehmood et al., 2021). Some soil microorganisms typically may use certain organic pollutants as electron acceptors or donors, thereby eventually transforming them to CO_2 in an aerobic environment (Ghattas et al., 2017; Li et al., 2021). This carbon mineralization process is often sensitive to microbial activities and redox environments (Gougoulias et al., 2014; Keiluweit et al., 2017), and compaction could alter the carbon mineralization process by limiting oxygen supply in the rhizosphere (Beylich et al., 2010). The degree of compaction can affect these processes. Yet, most of the reported studies did not systematically implement different compaction levels. Furthermore, the fate of the group of microorganisms that serves a specific function or mineralization of other elements such as N, P, and S was rarely monitored in those studies. For instance, nitrification and denitrification processes are carried out by a specific group of microorganisms in SCM (Chen et al., 2013; Gold

et al., 2019). However, the effect of compaction on these processes in SCM has not been studied. Most studies measured carbon mineralization, enzymatic activities, and microbial populations, whereas they rarely reported the effect of compaction on microbial community structure. Understanding the evolution of microbial community structure in SCM that undergo compaction will help improve the design to ensure the desirable microbial communities strive in SCM.

6.3.5 Nutrient uptake

Compaction could negatively influence nutrient removal by affecting the root health (Wang et al., 2019) and rhizosphere microorganisms (Ahmad et al., 2009). Analyzing available data (Figure 6.6), we showed that compaction significantly reduced plant N concentrations by 36.1% and P concentrations by 43.8%. As SCM typically uses sand to increase infiltration rate, compaction could increase the water retention in sandy or sandy loam through pore structure reorganization (Le et al., 2020). Increased water availability for vegetation positively affects plant growth and nutrient uptakes (Zhang et al., 2017).

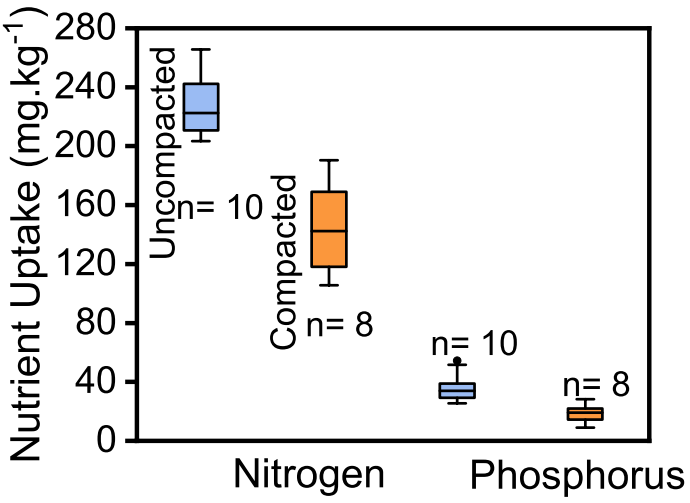

Figure 6.6. Effects of compaction on nitrogen and phosphorus uptake by plants. Compaction reduces nitrogen uptake by 36.1% and phosphorus by 43.8%. n is the number of data points reviewed.

In SCM, nutrient removal is sensitive to hydraulic retention time, redox conditions, plant health, and soil microorganisms (Valenca et al., 2021). Compaction can affect all these factors for nutrient removal to various degrees. For instance, compaction can increase water retention time and help develop anaerobic patches in SCM (Fassman-Beck et al., 2015; Schnurr-Putz et al., 2006), which are beneficial for the denitrification (Payne et al., 2017). On the other hand, compaction can negatively affect plant roots and root microbiomes, thereby lowering the nutrient uptake (Hartmann et al., 2014; Lucas and Greenway, 2008; Mariotti et al., 2020). Therefore, moderate compaction could positively affect plant growth and nutrient uptakes, whereas high compaction could inhibit plant growth and nutrient uptake (Botta et al., 2007; Wang et al., 2019; Zhang et al., 2017).

Opportunities: Compaction alters soil pore size distribution, root architecture, and root microbiome, which could affect nutrient uptakes. Future studies should systematically investigate changes in these factors with different degrees of compaction, and examine the relative importance of these compaction-induced changes on nutrient uptake. Compaction can change redox conditions in the filter layer from aerobic to anaerobic conditions. To what extent that shifts the soil microbiome and nutrient cycles require more detailed investigation.

6.3.6 Greenhouse gas emission

Subsurface soil can act both as a source and sink for greenhouse gas emissions (Kavehei et al., 2021). In soil, N_2O can be produced by nitrification and denitrification whereas CH_4 can be produced by methanogenesis under anaerobic conditions (Payne et al., 2017). Compaction could disrupt oxygen diffusion, redox condition, nutrient cycling, and microbial health, which in turn affect these greenhouse gas emissions. In particular, compaction can enhance anaerobic conditions (Bessou et al., 2010), which is necessary for greenhouse gas production in soil (Beare

et al., 2009). However, a qualitative estimate of the compaction effect on greenhouse gas emission in the subsurface is lacking. Analyzing limited available data, we show that compaction could significantly ($P < 0.05$) influence both fluxes of N_2O and CH_4 (Figure 6.7). Mean N_2O emission fluxes increased two-fold as a result of compaction, potentially because compaction created favorable conditions for denitrification pathways. Compaction could increase water retention and restrict oxygen diffusion (Nawaz et al., 2013; Richard et al., 2001). Reduced aeration and low oxygen diffusion create anaerobic conditions that promote denitrification by reduction of NO_3^- to N_2O and N_2 and increasing net N_2O emissions. Compaction could also restrict carbon mineralization and plant root activities, leading to lower plant uptake of nutrients (Shah et al., 2017). Therefore, a temporary accumulation of mineral nitrogen in SCM is expected, which can increase net N_2O production and emission potential (Wang et al., 2019). The anaerobic soil conditions caused by compaction also create favorable conditions for methane production by methanogens. Our data also show that mean CH_4 consumption decreased from -2.1 g CH_4-C $ha^{-1}.d^{-1}$ to -0.75 g CH_4-C $ha^{-1}.d^{-1}$ (64.3%) due to compaction. For example, cultivable methanogens in the compacted soil were found to increase nearly 100-fold compared to uncompacted soils (Schnurr-Putz et al., 2006).

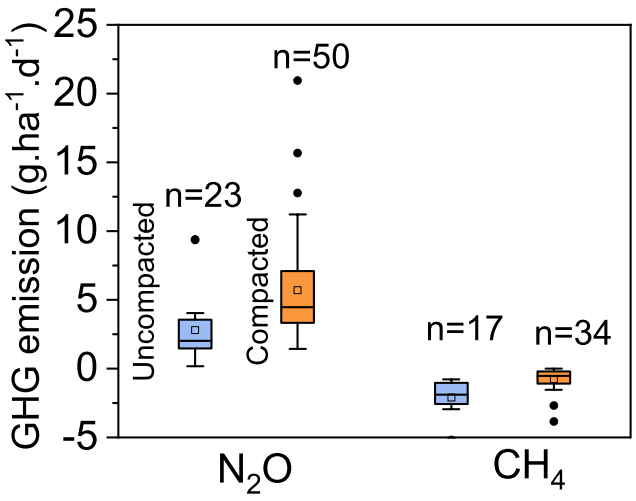

Figure 6.7. Effect of compaction on mean N_2O emission fluxes and mean CH_4 emission fluxes. Both emissions are significantly affected by compaction ($p < 0.05$). Data were collected from five studies (Hargreaves et al., 2021; Hynšt et al., 2007; Teepe et al., 2004; Tullberg et al., 2018; Yamulki and Jarvis, 2002). n is the number of data points for each category.

Opportunities: SCM are implemented to improve resilience to the negative impacts of climate changes such as flooding, contamination, water scarcity, and heatwaves. However, rarely they are examined for their contribution to greenhouse gas emission. Our analysis indicates that the compaction of SCM filter media could increase N_2O and CH_4 emission. However, limited studies have examined greenhouse gas emissions from SCM (Elberling et al., 2011; Kavehei et al., 2021; Payne et al., 2017, 2014). A comprehensive account of compaction effects on greenhouse gas emissions in SCM will give insights into the designs that could make them a net sink for greenhouse gases. Systematic studies are needed to understand the long-term greenhouse gas emission in SCM due to compaction. In particular, the effects of compaction on community structure and functions of methanogens and denitrifying microorganisms need further investigation.

6.4 SCM Design implications to alleviate the impacts of compaction

Controlled anthropogenic activity*:* Compaction can be minimized by limiting traffic or human activities after biofilter construction. This can be done by controlling traffic paths or foot traffic in the designated area (Gasso et al., 2013). Monitoring the health and maintenance often requires access to SCM. Providing designated paths or adding stepping stones can minimize the compaction of the entire area.

Designs to enhance natural regenerative processes*:* Natural processes such as earthworm activities through burrow creation, freeze-thaw, and tap-rooted plant growth can create preferential flow paths and reduce the negative impact of compaction on the infiltration rate (Jabro et al., 2014; Yvan et al., 2012; Colombi and Keller, 2019). Colonization of earthworms in compacted soil enhanced the macropores and infiltration rate through extensive burrowing activities of earthworms (Yvan et al., 2012). Repeated freeze-thaw cycles could alter soil structure, increase porosity, and improve plant root health in soil ecosystems and thus reduce the negative impact of compaction (Jabro et al., 2014). However, freezing can expand the pore only if the pores are large enough to freeze the water against negative capillary force (Watanabe and Flury, 2008). For instance, water trapped in clay is less susceptible to freezing due to high negative pressures. Thus, adding more sand or sandy loam soil could increase the freezing depth and alleviate the compaction effect. Future studies should examine the effect of freezing on restoring hydraulic conductivity of different soil types to link freezing with soil structure or texture. Improving soil structure and reducing compaction with the help of extensive tap-root systems is a prolonged process and restricted to a few feet of the surface (Bartens et al., 2008). Bio-drilling can accelerate this process. In the bio-drilling process, the root system grows within the compacted biofilter layer and once the plant dies, the root leaves a channel in the soil for

water to drain away. Deep tap-rooted plants create vertical drainage channels, whereas fine-rooted species like grass make horizontal channels in compacted soil. For instance, bio-drilling using Dakinson Radish alleviated 40% of overall compaction with a 44% increase in soil porosity (Raut and Dick, 2020). Growing annual or biennial plants with a long taproot system and quick growth is recommended for bio drilling.

Amendments to resist compaction: Soils are susceptible to compaction, but the addition of amendments such as compost, fly ash, biochar, and sand could alleviate the media compaction by improving the hydraulic conductivities (Schwartz and Smith, 2021; Tirpak et al., 2021). The addition of amendments with large aggregate or grain sizes such as sand and biochar could increase porosity and infiltration capacity. Many other amendments were used in SCM including coconut coir, manure, straw, zeolite, vermiculite, peat, hydro-absorbent polymer, sphagnum moss (Pitt et al., 2021; Tirpak et al., 2021). However, they are rarely tested for their capacity to alleviate compaction. Recently, biochar was tested for its ability to resist compaction and found that moisture content and particle size of biochar are critical in preventing breakage of biochar during the compaction (Ghavanloughajar et al., 2020; Le et al., 2020).

6.5 Conclusions

The data analysis reveals the extent to which compaction can affect subsurface processes and informs potential implications of compaction on SCM to infiltrate stormwater, remove pollutants by biochemical processes, and provide other ecosystem functions. Compaction could reduce infiltration capacity in SCM, but the addition of sand could alleviate the negative impact of compaction by increasing the infiltration capacity by 22 folds on average. The efficacy of amendment depends on size fraction, amount and inherent moisture level, and degree compaction. Compaction could reduce oxygen diffusion rate. Low oxygen availability could

induce poor root growth and reduced microbial activities. Effects of compaction on root biomass were found to be insignificant due to a large variation in the reported data. Root biomass is positively correlated with compaction in moderate to low compaction levels, whereas severe compaction levels significantly reduced root biomass. Reduced root growth could lead to poor vegetation establishment and reduce the pollutants processing capacity of the biofilter. Compaction had a mixed impact on the carbon mineralization rate. The mineralization rate reduced significantly at a high degree of compaction (bulk density>1.6 g cm^{-3}) due to a reduction in macropore size (<15 μm) and aeration status. Compaction could reduce phytoextraction of nutrients such as nitrogen by 36.1% and phosphorus by 43.8%. Reduced root growth and oxygen level could increase nitrogen uptake rate in SCM. Compaction could trigger the emission of N_2O and CH_4, respectively, by altering denitrifying and methanogenic microbial communities under anoxic microenvironments. The analysis estimates that N_2O emission could increase by 103.2%, and CH_4 emission could increase by 64.2% because of compaction. The detrimental effect of compaction can be minimized by adding soil amendments, natural attenuation, and reducing unintentional compaction. While natural attenuation could take a longer time to alleviate compaction, soil amendment could provide some immediate improvement. The result will inform the design of roadside stormwater control measures and predict their long-term performance.

6.6 References

Ahmad, N., Hassan, F.U., Belford, R.K., 2009. Effect of soil compaction in the sub-humid cropping environment in Pakistan on uptake of NPK and grain yield in wheat (Triticum aestivum). Field Crops Research 110, 54–60. https://doi.org/10.1016/j.fcr.2008.07.001

Alam, S., Borthakur, A., Ravi, S., Gebremichael, M., Mohanty, S.K., 2021. Managed aquifer recharge implementation criteria to achieve water sustainability. Science of The Total Environment 768, 144992. https://doi.org/10.1016/j.scitotenv.2021.144992

Ampoorter, E., De Frenne, P., Hermy, M., Verheyen, K., 2011. Effects of soil compaction on growth and survival of tree saplings: A meta-analysis. Basic and Applied Ecology 12, 394–402. https://doi.org/10.1016/j.baae.2011.06.003

Antille, D.L., Chamen, W.C.T., Tullberg, J.N., Lal, R., 2015. The Potential of Controlled Traffic Farming to Mitigate Greenhouse Gas Emissions and Enhance Carbon Sequestration in Arable Land: A Critical Review. Transactions of the ASABE 58(3), 707–731.

Badri, D.V., Vivanco, J.M., 2009. Regulation and function of root exudates. Plant, Cell & Environment 32, 666–681. https://doi.org/10.1111/j.1365-3040.2009.01926.x

Bartens, J., Day, S.D., Harris, J.R., Dove, J.E., Wynn, T.M., 2008. Can Urban Tree Roots Improve Infiltration through Compacted Subsoils for Stormwater Management? J. environ. qual. 37, 2048–2057. https://doi.org/10.2134/jeq2008.0117

Beare, M.H., Gregorich, E.G., St-Georges, P., 2009. Compaction effects on CO2 and N2O production during drying and rewetting of soil. Soil Biology and Biochemistry 41, 611–621. https://doi.org/10.1016/j.soilbio.2008.12.024

Bessou, C., Mary, B., Léonard, J., Roussel, M., Gréhan, E., Gabrielle, B., 2010. Modelling soil compaction impacts on nitrous oxide emissions in arable fields. European Journal of Soil Science 61, 348–363. https://doi.org/10.1111/j.1365-2389.2010.01243.x

Beylich, A., Oberholzer, H.-R., Schrader, S., Höper, H., Wilke, B.-M., 2010. Evaluation of soil compaction effects on soil biota and soil biological processes in soils. Soil and Tillage Research 109, 133–143. https://doi.org/10.1016/j.still.2010.05.010

Biswal, B.K., Vijayaraghavan, K., Adam, M.G., Lee Tsen-Tieng, D., Davis, A.P., Balasubramanian, R., 2021. Biological nitrogen removal from stormwater in bioretention cells: a critical review. Critical Reviews in Biotechnology 1–23. https://doi.org/10.1080/07388551.2021.1969888

Bittig, H.C., Körtzinger, A., Neill, C., van Ooijen, E., Plant, J.N., Hahn, J., Johnson, K.S., Yang, B., Emerson, S.R., 2018. Oxygen Optode Sensors: Principle, Characterization, Calibration, and Application in the Ocean. Frontiers in Marine Science 4, 429. https://doi.org/10.3389/fmars.2017.00429

Botta, G.F., Pozzolo, O., Bomben, M., Rosatto, H., Rivero, D., Ressia, M., Tourn, M., Soza, E., Vazquez, J., 2007. Traffic alternatives for harvesting soybean (Glycine max L.): Effect on yields and soil under a direct sowing system. Soil and Tillage Research 96, 145–154. https://doi.org/10.1016/j.still.2007.05.003

Cambi, M., Certini, G., Neri, F., Marchi, E., 2015. The impact of heavy traffic on forest soils: A review. Forest Ecology and Management 338, 124–138. https://doi.org/10.1016/j.foreco.2014.11.022

Chaudhry, Q., Blom-Zandstra, M., Gupta, S.K., Joner, E., 2005. Utilising the Synergy between Plants and Rhizosphere Microorganisms to Enhance Breakdown of Organic Pollutants in the Environment (15 pp). Env Sci Poll Res Int 12, 34–48. https://doi.org/10.1065/espr2004.08.213

Chen, X., Peltier, E., Sturm, B.S.M., Young, C.B., 2013. Nitrogen removal and nitrifying and denitrifying bacteria quantification in a stormwater bioretention system. Water Research 47, 1691–1700. https://doi.org/10.1016/j.watres.2012.12.033

Chen, X., Yang, J., Liang, A., Zhang, X., 2016. Effects of Soil Compaction and Tillage Practices on Carbon Dioxide Efflux in Northeast China: Evidence from an Incubation Study. Pol. J. Environ. Stud. 25, 1769–1776. https://doi.org/10.15244/pjoes/62344

Colombi, T., Keller, T., 2019. Developing strategies to recover crop productivity after soil compaction—A plant eco-physiological perspective. Soil and Tillage Research 191, 156–161. https://doi.org/10.1016/j.still.2019.04.008

Colombi, T., Torres, L.C., Walter, A., Keller, T., 2018. Feedbacks between soil penetration resistance, root architecture and water uptake limit water accessibility and crop growth – A vicious circle. Science of The Total Environment 626, 1026–1035. https://doi.org/10.1016/j.scitotenv.2018.01.129

Colombi, T., Walter, A., 2017. Genetic Diversity under Soil Compaction in Wheat: Root Number as a Promising Trait for Early Plant Vigor. Frontiers in Plant Science 8, 420. https://doi.org/10.3389/fpls.2017.00420

Correa, J., Postma, J.A., Watt, M., Wojciechowski, T., 2019. Soil compaction and the architectural plasticity of root systems. Journal of Experimental Botany 70, 6019–6034. https://doi.org/10.1093/jxb/erz383

Czyż, E.A., 2004. Effects of traffic on soil aeration, bulk density and growth of spring barley. Soil and Tillage Research 79, 153–166. https://doi.org/10.1016/j.still.2004.07.004

Czyz, E.A., Tomaszewska, J., Dexter, A.R., 2001. Response of spring barley to changes of compaction and aeration of sandy soil under model conditions 15, 9–12.

Danfoura, M., Gurdak, J., 2016. Redox Dynamics and Oxygen Reduction Rates of Infiltrating Urban Stormwater beneath Low Impact Development (LID). Water 8, 435. https://doi.org/10.3390/w8100435

Das, T.K., Kabir, A., Zhao, W., Stenstrom, M.K., Mohanty, S.K., 2022. Supporting material - A review of compaction effects on subsurface processes: Implications on the design of roadside stormwater control measures. https://doi.org/10.6084/m9.figshare.18129395.v1

Davis, A.P., Hunt, W.F., Traver, R.G., Clar, M., 2009. Bioretention Technology: Overview of Current Practice and Future Needs. J. Environ. Eng. 135, 109–117. https://doi.org/10.1061/(ASCE)0733-9372(2009)135:3(109)

Ebrahimian, A., Sample-Lord, K., Wadzuk, B., Traver, R., 2020. Temporal and spatial variation of infiltration in urban green infrastructure. Hydrological Processes 34, 1016–1034. https://doi.org/10.1002/hyp.13641

Edmondson, J.L., Davies, Z.G., McCormack, S.A., Gaston, K.J., Leake, J.R., 2011. Are soils in urban ecosystems compacted? A citywide analysis. Biology Letters 7, 771–774. https://doi.org/10.1098/rsbl.2011.0260

Elberling, B., Askaer, L., Jørgensen, C.J., Joensen, H.P., Kühl, M., Glud, R.N., Lauritsen, F.R., 2011. Linking Soil O2, CO2, and CH4 Concentrations in a Wetland Soil: Implications for CO2 and CH4 Fluxes. Environ. Sci. Technol. 45, 3393–3399. https://doi.org/10.1021/es103540k

Fassman-Beck, E., Wang, S., Simcock, R., Liu, R., 2015. Assessing the Effects of Bioretention's Engineered Media Composition and Compaction on Hydraulic Conductivity and Water Holding Capacity. J. Sustainable Water Built Environ. 1, 04015003. https://doi.org/10.1061/JSWBAY.0000799

Feng, W., Liu, Y., Gao, L., 2022. Stormwater treatment for reuse: Current practice and future development – A review. Journal of Environmental Management 301, 113830. https://doi.org/10.1016/j.jenvman.2021.113830

Galli, A., Peruzzi, C., Beltrame, L., Cislaghi, A., Masseroni, D., 2021. Evaluating the infiltration capacity of degraded vs. rehabilitated urban greenspaces: Lessons learnt from a real-world Italian case study. Science of The Total Environment 787, 147612. https://doi.org/10.1016/j.scitotenv.2021.147612

Gasso, V., Sørensen, C.A.G., Oudshoorn, F.W., Green, O., 2013. Controlled traffic farming: A review of the environmental impacts. European Journal of Agronomy 48, 66–73. https://doi.org/10.1016/j.eja.2013.02.002

Ghattas, A.-K., Fischer, F., Wick, A., Ternes, T.A., 2017. Anaerobic biodegradation of (emerging) organic contaminants in the aquatic environment. Water Research 116, 268–295. https://doi.org/10.1016/j.watres.2017.02.001

Ghavanloughajar, M., Valenca, R., Le, H., Rahman, M., Borthakur, A., Ravi, S., Stenstrom, M.K., Mohanty, S.K., 2020. Compaction conditions affect the capacity of biochar-amended sand filters to treat road runoff. Science of The Total Environment 735, 139180. https://doi.org/10.1016/j.scitotenv.2020.139180

Gilbert, J.K., Clausen, J.C., 2006. Stormwater runoff quality and quantity from asphalt, paver, and crushed stone driveways in Connecticut. Water Research 40, 826–832. https://doi.org/10.1016/j.watres.2005.12.006

Gold, A.C., Thompson, S.P., Piehler, M.F., 2019. Nitrogen cycling processes within stormwater control measures: A review and call for research. Water Research 149, 578–587. https://doi.org/10.1016/j.watres.2018.10.036

Gougoulias, C., Clark, J.M., Shaw, L.J., 2014. The role of soil microbes in the global carbon cycle: tracking the below-ground microbial processing of plant-derived carbon for manipulating carbon dynamics in agricultural systems. Journal of the Science of Food and Agriculture 94, 2362–2371. https://doi.org/10.1002/jsfa.6577

Grebel, J.E., Mohanty, S.K., Torkelson, A.A., Boehm, A.B., Higgins, C.P., Maxwell, R.M., Nelson, K.L., Sedlak, D.L., 2013. Engineered Infiltration Systems for Urban Stormwater Reclamation. Environmental Engineering Science 30, 437–454. https://doi.org/10.1089/ees.2012.0312

Gregory, J.H., Dukes, M.D., Jones, P.H., Miller, G.L., 2006. Effect of urban soil compaction on infiltration rate. Journal of Soil and Water Conservation 61, 117–124.

Grover, S.P.P., Cohan, A., Chan, H.S., Livesley, S.J., Beringer, J., Daly, E., 2013. Occasional large emissions of nitrous oxide and methane observed in stormwater biofiltration systems. Science of The Total Environment 465, 64–71. https://doi.org/10.1016/j.scitotenv.2013.01.035

Hamza, M.A., Anderson, W.K., 2005. Soil compaction in cropping systems: A review of the nature, causes and possible solutions. Soil and Tillage Research 82, 121–145. https://doi.org/10.1016/j.still.2004.08.009

Hargreaves, P.R., Baker, K.L., Graceson, A., Bonnett, S.A.F., Ball, B.C., Cloy, J.M., 2021. Use of a nitrification inhibitor reduces nitrous oxide (N2O) emissions from compacted grassland with different soil textures and climatic conditions. Agriculture, Ecosystems & Environment 310, 107307. https://doi.org/10.1016/j.agee.2021.107307

Hartmann, M., Niklaus, P.A., Zimmermann, S., Schmutz, S., Kremer, J., Abarenkov, K., Lüscher, P., Widmer, F., Frey, B., 2014. Resistance and resilience of the forest soil microbiome to logging-associated compaction. ISME J 8, 226–244. https://doi.org/10.1038/ismej.2013.141

Hatt, B.E., Fletcher, T.D., Deletic, A., 2009. Hydrologic and pollutant removal performance of stormwater biofiltration systems at the field scale. Journal of Hydrology 365, 310–321. https://doi.org/10.1016/j.jhydrol.2008.12.001

He, C., Liu, Z., Wu, J., Pan, X., Fang, Z., Li, J., Bryan, B.A., 2021. Future global urban water scarcity and potential solutions. Nat Commun 12, 4667. https://doi.org/10.1038/s41467-021-25026-3

Hermawan, A., Talei, A., Leong, J., Jayatharan, M., Goh, H., Alaghmand, S., 2019. Performance Assessment of a Laboratory Scale Prototype Biofiltration System in Tropical Region. Sustainability 11, 1947. https://doi.org/10.3390/su11071947

Herndon, E.M., Kinsman-Costello, L., Duroe, K.A., Mills, J., Kane, E.S., Sebestyen, S.D., Thompson, A.A., Wullschleger, S.D., 2019. Iron (Oxyhydr)Oxides Serve as Phosphate Traps in Tundra and Boreal Peat Soils. J. Geophys. Res. Biogeosci. 124, 227–246. https://doi.org/10.1029/2018JG004776

Hoang, S.A., Lamb, D., Seshadri, B., Sarkar, B., Choppala, G., Kirkham, M.B., Bolan, N.S., 2021. Rhizoremediation as a green technology for the remediation of petroleum hydrocarbon-contaminated soils. Journal of Hazardous Materials 401, 123282. https://doi.org/10.1016/j.jhazmat.2020.123282

Hynšt, J., Šimek, M., Brůček, P., Petersen, S.O., 2007. High fluxes but different patterns of nitrous oxide and carbon dioxide emissions from soil in a cattle overwintering area. Agriculture, Ecosystems & Environment 120, 269–279. https://doi.org/10.1016/j.agee.2006.10.003

Itsukushima, R., Ideta, K., Takata, H., 2021. Relationship between compaction and infiltration capacity of amended soil for urban flood damage mitigation. Soil Use and Management n/a. https://doi.org/10.1111/sum.12705

Jabro, J.D., Iversen, W.M., Evans, R.G., Allen, B.L., Stevens, W.B., 2014. Repeated Freeze-Thaw Cycle Effects on Soil Compaction in a Clay Loam in Northeastern Montana. Soil Science Society of America Journal 78, 737–744. https://doi.org/10.2136/sssaj2013.07.0280

Jefferson, A.J., Bhaskar, A.S., Hopkins, K.G., Fanelli, R., Avellaneda, P.M., McMillan, S.K., 2017. Stormwater management network effectiveness and implications for urban watershed function: A critical review. Hydrological Processes 31, 4056–4080. https://doi.org/10.1002/hyp.11347

Jonasson, S., Michelsen, A., Schmidt, I.K., 1999. Coupling of nutrient cycling and carbon dynamics in the Arctic, integration of soil microbial and plant processes. Applied Soil Ecology 11, 135–146. https://doi.org/10.1016/S0929-1393(98)00145-0

Jourgholami, M., 2018. Effects of soil compaction on growth variables in Cappadocian maple (Acer cappadocicum) seedlings. J. For. Res. 29, 601–610. https://doi.org/10.1007/s11676-017-0491-7

Kavehei, E., Iram, N., Rezaei Rashti, M., Jenkins, G.A., Lemckert, C., Adame, M.F., 2021. Greenhouse gas emissions from stormwater bioretention basins. Ecological Engineering 159, 106120. https://doi.org/10.1016/j.ecoleng.2020.106120

Kavehei, E., Jenkins, G.A., Adame, M.F., Lemckert, C., 2018. Carbon sequestration potential for mitigating the carbon footprint of green stormwater infrastructure. Renewable and Sustainable Energy Reviews 94, 1179–1191. https://doi.org/10.1016/j.rser.2018.07.002

Kechavarzi, C., Dawson, Q., Bartlett, M., Leeds-Harrison, P.B., 2010. The role of soil moisture, temperature and nutrient amendment on CO2 efflux from agricultural peat soil microcosms. Geoderma 154, 203–210. https://doi.org/10.1016/j.geoderma.2009.02.018

Keiluweit, M., Wanzek, T., Kleber, M., Nico, P., Fendorf, S., 2017. Anaerobic microsites have an unaccounted role in soil carbon stabilization. Nat Commun 8, 1771. https://doi.org/10.1038/s41467-017-01406-6

Krein, A., Schorer, M., 2000. Road runoff pollution by polycyclic aromatic hydrocarbons and its contribution to river sediments. Water Research 34, 4110–4115. https://doi.org/10.1016/S0043-1354(00)00156-1

Lau, S.-L., Han, Y., Kang, J.-H., Kayhanian, M., Stenstrom, M.K., 2009. Characteristics of Highway Stormwater Runoff in Los Angeles: Metals and Polycyclic Aromatic Hydrocarbons. Water Environment Research 81, 308–318. https://doi.org/10.2175/106143008X357237

Le, H., Valenca, R., Ravi, S., Stenstrom, M.K., Mohanty, S.K., 2020. Size-dependent biochar breaking under compaction: Implications on clogging and pathogen removal in biofilters. Environmental Pollution 266, 115195. https://doi.org/10.1016/j.envpol.2020.115195

LeFevre, G.H., Hozalski, R.M., Novak, P.J., 2013. Root Exudate Enhanced Contaminant Desorption: An Abiotic Contribution to the Rhizosphere Effect. Environ. Sci. Technol. 47, 11545–11553. https://doi.org/10.1021/es402446v

LeFevre, G.H., Hozalski, R.M., Novak, P.J., 2012. The role of biodegradation in limiting the accumulation of petroleum hydrocarbons in raingarden soils. Water Research 46, 6753–6762. https://doi.org/10.1016/j.watres.2011.12.040

LeFevre, G.H., Paus, K.H., Natarajan, P., Gulliver, J.S., Novak, P.J., Hozalski, R.M., 2015. Review of Dissolved Pollutants in Urban Storm Water and Their Removal and Fate in Bioretention Cells. Journal of Environmental Engineering 141, 04014050. https://doi.org/10.1061/(ASCE)EE.1943-7870.0000876

Li, Y., Wu, S., Wang, S., Zhao, S., Zhuang, X., 2021. Anaerobic degradation of xenobiotic organic contaminants (XOCs): The role of electron flow and potential enhancing strategies. Journal of Environmental Sciences 101, 397–412. https://doi.org/10.1016/j.jes.2020.08.030

Lipiec, J., Horn, R., Pietrusiewicz, J., Siczek, A., 2012. Effects of soil compaction on root elongation and anatomy of different cereal plant species. Soil and Tillage Research 121, 74–81. https://doi.org/10.1016/j.still.2012.01.013

Longepierre, M., Widmer, F., Keller, T., Weisskopf, P., Colombi, T., Six, J., Hartmann, M., 2021. Limited resilience of the soil microbiome to mechanical compaction within four growing seasons of agricultural management. ISME COMMUN. 1, 44. https://doi.org/10.1038/s43705-021-00046-8

Lucas, W.C., Greenway, M., 2008. Nutrient Retention in Vegetated and Nonvegetated Bioretention Mesocosms. J. Irrig. Drain Eng. 134, 613–623. https://doi.org/10.1061/(ASCE)0733-9437(2008)134:5(613)

Mariotti, B., Hoshika, Y., Cambi, M., Marra, E., Feng, Z., Paoletti, E., Marchi, E., 2020. Vehicle-induced compaction of forest soil affects plant morphological and physiological attributes: A meta-analysis. Forest Ecology and Management 462, 118004. https://doi.org/10.1016/j.foreco.2020.118004

McGrane, S.J., 2016. Impacts of urbanisation on hydrological and water quality dynamics, and urban water management: a review. Hydrological Sciences Journal 61, 2295–2311. https://doi.org/10.1080/02626667.2015.1128084

Mehmood, T., Gaurav, G.K., Cheng, L., Klemeš, J.J., Usman, M., Bokhari, A., Lu, J., 2021. A review on plant-microbial interactions, functions, mechanisms and emerging trends in bioretention system to improve multi-contaminated stormwater treatment. Journal of Environmental Management 294, 113108. https://doi.org/10.1016/j.jenvman.2021.113108

Minett, D.A., Cook, P.L.M., Kessler, A.J., Cavagnaro, T.R., 2013. Root effects on the spatial and temporal dynamics of oxygen in sand-based laboratory-scale constructed biofilters. Ecological Engineering 58, 414–422. https://doi.org/10.1016/j.ecoleng.2013.06.028

Moore, J.R., 2008. Effect of compaction on removal efficiency of lead, copper, zinc, nitrate, and phosphate in a bioretention system: a column study. https://doi.org/10.7282/T3P26ZFP

Moreau, D., Bardgett, R.D., Finlay, R.D., Jones, D.L., Philippot, L., 2019. A plant perspective on nitrogen cycling in the rhizosphere. Funct Ecol 33, 540–552. https://doi.org/10.1111/1365-2435.13303

Mossadeghi-Björklund, M., Jarvis, N., Larsbo, M., Forkman, J., Keller, T., 2019. Effects of compaction on soil hydraulic properties, penetration resistance and water flow patterns at the soil profile scale. Soil Use Manage 35, 367–377. https://doi.org/10.1111/sum.12481

Muerdter, C.P., LeFevre, G.H., 2019. Synergistic Lemna Duckweed and Microbial Transformation of Imidacloprid and Thiacloprid Neonicotinoids. Environ. Sci. Technol. Lett. 6, 761–767. https://doi.org/10.1021/acs.estlett.9b00638

Muerdter, C.P., Wong, C.K., LeFevre, G.H., 2018. Emerging investigator series: the role of vegetation in bioretention for stormwater treatment in the built environment: pollutant removal, hydrologic function, and ancillary benefits. Environ. Sci.: Water Res. Technol. 4, 592–612. https://doi.org/10.1039/C7EW00511C

Müller, A., Österlund, H., Marsalek, J., Viklander, M., 2020. The pollution conveyed by urban runoff: A review of sources. Science of The Total Environment 709, 136125. https://doi.org/10.1016/j.scitotenv.2019.136125

Nawaz, M.F., Bourrié, G., Trolard, F., 2013. Soil compaction impact and modelling. A review. Agron. Sustain. Dev. 33, 291–309. https://doi.org/10.1007/s13593-011-0071-8

Neira, J., Ortiz, M., Morales, L., Acevedo, E., 2015. Oxygen diffusion in soils: Understanding the factors and processes needed for modeling. Chilean J. Agric. Res. 75, 35–44. https://doi.org/10.4067/S0718-58392015000300005

Palacios, Y.M., Gleadow, R., Davidson, C., Gan, W., Winfrey, B., 2021. Do mycorrhizae increase plant growth and pollutant removal in stormwater biofilters? Water Research 202, 117381. https://doi.org/10.1016/j.watres.2021.117381

Pandey, B.K., Huang, G., Bhosale, R., Hartman, S., Sturrock, C.J., Jose, L., Martin, O.C., Karady, M., Voesenek, L.A.C.J., Ljung, K., Lynch, J.P., Brown, K.M., Whalley, W.R., Mooney, S.J., Zhang, D., Bennett, M.J., 2021. Plant roots sense soil compaction through restricted ethylene diffusion. Science 371, 276–280. https://doi.org/10.1126/science.abf3013

Payne, E.G.I., Fletcher, T.D., Russell, D.G., Grace, M.R., Cavagnaro, T.R., Evrard, V., Deletic, A., Hatt, B.E., Cook, P.L.M., 2014. Temporary Storage or Permanent Removal? The Division of Nitrogen between Biotic Assimilation and Denitrification in Stormwater Biofiltration Systems. PLoS ONE 9, e90890. https://doi.org/10.1371/journal.pone.0090890

Payne, E.G.I., Pham, T., Cook, P.L.M., Deletic, A., Hatt, B.E., Fletcher, T.D., 2017. Inside Story of Gas Processes within Stormwater Biofilters: Does Greenhouse Gas Production Tarnish the Benefits of Nitrogen Removal? Environ. Sci. Technol. 51, 3703–3713. https://doi.org/10.1021/acs.est.6b05653

Payne, E.G.I., Pham, T., Deletic, A., Hatt, B.E., Cook, P.L.M., Fletcher, T.D., 2018. Which species? A decision-support tool to guide plant selection in stormwater biofilters. Advances in Water Resources 113, 86–99. https://doi.org/10.1016/j.advwatres.2017.12.022

Pearson, B., Beeson, R., Reinhart-Adams, C., Olexa, M., Shober, A., 2013. Determining Variability in Characteristics of Residential Landscape Soils that Influences Infiltration Rates. AUF 39. https://doi.org/10.48044/jauf.2013.032

Picchio, R., Tavankar, F., Nikooy, M., Pignatti, G., Venanzi, R., Lo Monaco, A., 2019. Morphology, Growth and Architecture Response of Beech (Fagus orientalis Lipsky) and Maple Tree (Acer velutinum Boiss.) Seedlings to Soil Compaction Stress Caused by Mechanized Logging Operations. Forests 10, 771. https://doi.org/10.3390/f10090771

Pitt, R., Chen, S.-E., Clark, S., 2002. Compacted Urban Soils Effects on Infiltration and Bioretention Stormwater Control Designs, in: Global Solutions for Urban Drainage. Presented at the Ninth International Conference on Urban Drainage (9ICUD), American Society of Civil Engineers, Lloyd Center Doubletree Hotel, Portland, Oregon, United States, pp. 1–21. https://doi.org/10.1061/40644(2002)14

Pitt, R., Chen, S.-E., Clark, S.E., Swenson, J., Ong, C.K., 2008. Compaction's Impacts on Urban Storm-Water Infiltration. Journal of Irrigation and Drainage Engineering 134, 652–658. https://doi.org/10.1061/(ASCE)0733-9437(2008)134:5(652)

Pitt, R., Otto, M., Questad, A., Isaac, S., Colyar, M., Steets, B., Gearheart, R., Jones, J., Josselyn, M., Stenstrom, M.K., Clark, S., Wokurka, J., 2021. Laboratory Media Test Comparisons to Long-Term Performance of Biofilter and Media Filter Treatment-Train Stormwater Controls. J. Sustainable Water Built Environ. 7, 04021015. https://doi.org/10.1061/JSWBAY.0000956

Pitt, R., Otto, M., Questad, A., Isaac, S., Colyar, M., Steets, B., Gearheart, R., Jones, J., Josselyn, M., Stenstrom, M.K., Costa, P., Wokurka, J., 2022. Performance Changes during Long-Term Monitoring of Full-Scale Media Filter Stormwater Controls at an Industrial Site. J. Sustainable Water Built Environ. 8, 04021019. https://doi.org/10.1061/JSWBAY.0000965

Prudencio, L., Null, S.E., 2018. Stormwater management and ecosystem services: a review. Environ. Res. Lett. 13, 033002. https://doi.org/10.1088/1748-9326/aaa81a

Raut, Y.Y., Dick, W.A., 2020. Bio-drilling, Compaction Alleviation, and Fate of Storm-Water Management. JCEA 14. https://doi.org/10.17265/1934-7359/2020.10.001

Read, J., Fletcher, T.D., Wevill, T., Deletic, A., 2009. Plant Traits that Enhance Pollutant Removal from Stormwater in Biofiltration Systems. International Journal of Phytoremediation 12, 34–53. https://doi.org/10.1080/15226510902767114

Reiser, R., Stadelmann, V., Weisskopf, P., Grahm, L., Keller, T., 2020. System for quasi-continuous simultaneous measurement of oxygen diffusion rate and redox potential in soil. Journal of Plant Nutrition and Soil Science 183, 316–326. https://doi.org/10.1002/jpln.201900518

Richard, G., Cousin, I., Sillon, J.F., Bruand, A., Guérif, J., 2001. Effect of compaction on the porosity of a silty soil: influence on unsaturated hydraulic properties: Soil compaction, pore geometry and hydraulic properties. European Journal of Soil Science 52, 49–58. https://doi.org/10.1046/j.1365-2389.2001.00357.x

Rivers, E.N., Heitman, J.L., McLaughlin, R.A., Howard, A.M., 2021. Reducing roadside runoff: Tillage and compost improve stormwater mitigation in urban soils. Journal of Environmental Management 280, 111732. https://doi.org/10.1016/j.jenvman.2020.111732

Roy-Poirier, A., Champagne, P., Filion, Y., 2010. Review of Bioretention System Research and Design: Past, Present, and Future. Journal of Environmental Engineering 136, 878–889. https://doi.org/10.1061/(ASCE)EE.1943-7870.0000227

Säumel, I., Weber, F., Kowarik, I., 2016. Toward livable and healthy urban streets: Roadside vegetation provides ecosystem services where people live and move. Environmental Science & Policy 62, 24–33. https://doi.org/10.1016/j.envsci.2015.11.012

Schnurr-Putz, S., Baath, E., Guggenberger, G., Drake, H.L., Kusel, K., 2006. Compaction of forest soil by logging machinery favours occurrence of prokaryotes: Compaction of soil by logging machinery favours prokaryotes. FEMS Microbiology Ecology 58, 503–516. https://doi.org/10.1111/j.1574-6941.2006.00175.x

Schwartz, S.S., Smith, B., 2021. Cultivating Stormwater Services with Soil Decompaction and Amendment. J. Hydrol. Eng. 26, 04020059. https://doi.org/10.1061/(ASCE)HE.1943-5584.0002031

Shah, A.N., Tanveer, M., Shahzad, B., Yang, G., Fahad, S., Ali, S., Bukhari, M.A., Tung, S.A., Hafeez, A., Souliyanonh, B., 2017. Soil compaction effects on soil health and cropproductivity: an overview. Environ Sci Pollut Res 24, 10056–10067. https://doi.org/10.1007/s11356-017-8421-y

Sileshi, R., Pitt, R., Clark, S., 2015. Impacts of Soil Texture, Structure, and Compaction on Bioinfiltration Device Performance: Results of Lab and Field Investigations, in: Low Impact Development Technology: Design Methods and Case Studies. Presented at the 2011 Low Impact Development Conference, American Society of Civil Engineers, Philadelphia, Pennsylvania, pp. 4–15. https://doi.org/10.1061/9780784413883.002

Sileshi, R., Pitt, R., Clark, S., 2012. Assessing the Impact of Soil Media Characteristics on Stormwater Bioinfiltration Device Performance: Lab and Field Studies, in: World Environmental and Water Resources Congress 2012. Presented at the World Environmental And Water Resources Congress 2012, American Society of Civil Engineers, Albuquerque, New Mexico, United States, pp. 3505–3516. https://doi.org/10.1061/9780784412312.353

Song, X., Ju, X., Topp, C.F.E., Rees, R.M., 2019. Oxygen Regulates Nitrous Oxide Production Directly in Agricultural Soils. Environ. Sci. Technol. 53, 12539–12547. https://doi.org/10.1021/acs.est.9b03089

Strong, D.T., Wever, H.D., Merckx, R., Recous, S., 2004. Spatial location of carbon decomposition in the soil pore system: Spatial location of carbon decomposition. European Journal of Soil Science 55, 739–750. https://doi.org/10.1111/j.1365-2389.2004.00639.x

Subramaniam, D., Mather, P., Russell, S., Rajapakse, J., 2016. Dynamics of Nitrate-Nitrogen Removal in Experimental Stormwater Biofilters under Intermittent Wetting and Drying. J. Environ. Eng. 142, 04015090. https://doi.org/10.1061/(ASCE)EE.1943-7870.0001043

Szafranek-Nakonieczna, A., Stępniewska, Z., 2015. The influence of the aeration status (ODR, Eh) of peat soils on their ability to produce methane. Wetlands Ecol Manage 23, 665–676. https://doi.org/10.1007/s11273-015-9410-x

Taboada, M.A., Micucci, F.G., Cosentino, D.J., Lavado, R.S., 1998. Comparison of compaction induced by conventional and zero tillage in two soils of the Rolling Pampa of Argentina. Soil and Tillage Research 49, 57–63. https://doi.org/10.1016/S0167-1987(98)00132-9

Teepe, R., Brumme, R., Beese, F., Ludwig, B., 2004. Nitrous Oxide Emission and Methane Consumption Following Compaction of Forest Soils. Soil Science Society of America Journal 68, 605–611. https://doi.org/10.2136/sssaj2004.6050

Tirpak, R.A., Afrooz, A.N., Winston, R.J., Valenca, R., Schiff, K., Mohanty, S.K., 2021. Conventional and amended bioretention soil media for targeted pollutant treatment: A critical review to guide the state of the practice. Water Research 189, 116648. https://doi.org/10.1016/j.watres.2020.116648

Tracy, S.R., Black, C.R., Roberts, J.A., Mooney, S.J., 2011. Soil compaction: a review of past and present techniques for investigating effects on root growth. Journal of the Science of Food and Agriculture 91, 1528–1537. https://doi.org/10.1002/jsfa.4424

Tullberg, J., Antille, D.L., Bluett, C., Eberhard, J., Scheer, C., 2018. Controlled traffic farming effects on soil emissions of nitrous oxide and methane. Soil and Tillage Research 176, 18–25. https://doi.org/10.1016/j.still.2017.09.014

United Nations, 2018. World Urbanization Prospects - Population Division [WWW Document]. URL https://population.un.org/wup/ (accessed 12.30.21).

Valenca, R., Le, H., Zu, Y., Dittrich, T.M., Tsang, D.C.W., Datta, R., Sarkar, D., Mohanty, S.K., 2021. Nitrate removal uncertainty in stormwater control measures: Is the design or climate a culprit? Water Research 190, 116781. https://doi.org/10.1016/j.watres.2020.116781

Wang, M., He, D., Shen, F., Huang, J., Zhang, R., Liu, W., Zhu, M., Zhou, L., Wang, L., Zhou, Q., 2019. Effects of soil compaction on plant growth, nutrient absorption, and root respiration in soybean seedlings. Environ Sci Pollut Res 26, 22835–22845. https://doi.org/10.1007/s11356-019-05606-z

Watanabe, K., Flury, M., 2008. Capillary bundle model of hydraulic conductivity for frozen soil: CAPILLARY BUNDLE MODEL FOR FROZEN SOIL. Water Resour. Res. 44. https://doi.org/10.1029/2008WR007012

Watson, G.W., Kelsey, P., 2006. The impact of soil compaction on soil aeration and fine root density of Quercus palustris. Urban Forestry & Urban Greening 4, 69–74. https://doi.org/10.1016/j.ufug.2005.08.001

Wen, D., Ordonez, D., McKenna, A., Chang, N.-B., 2020. Fate and transport processes of nitrogen in biosorption activated media for stormwater treatment at varying field conditions of a roadside linear ditch. Environmental Research 181, 108915. https://doi.org/10.1016/j.envres.2019.108915

Winston, R.J., Hunt, W.F., Kennedy, S.G., Wright, J.D., Lauffer, M.S., 2012. Field Evaluation of Storm-Water Control Measures for Highway Runoff Treatment. J. Environ. Eng. 138, 101–111. https://doi.org/10.1061/(ASCE)EE.1943-7870.0000454

Yamulki, S., Jarvis, S., 2002. Short-term effects of tillage and compaction on nitrous oxide, nitric oxide, nitrogen dioxide, methane and carbon dioxide fluxes from grassland. Biol Fertil Soils 36, 224–231. https://doi.org/10.1007/s00374-002-0530-0

Yang, J.-L., Zhang, G.-L., 2011. Water infiltration in urban soils and its effects on the quantity and quality of runoff. J Soils Sediments 11, 751–761. https://doi.org/10.1007/s11368-011-0356-1

Yoo, G., Nissen, T.M., Wander, M.M., 2006. Use of Physical Properties to Predict the Effects of Tillage Practices on Organic Matter Dynamics in Three Illinois Soils. J. Environ. Qual. 35, 1576–1583. https://doi.org/10.2134/jeq2005.0225

Yvan, C., Stéphane, S., Stéphane, C., Pierre, B., Guy, R., Hubert, B., 2012. Role of earthworms in regenerating soil structure after compaction in reduced tillage systems. Soil Biology and Biochemistry 55, 93–103. https://doi.org/10.1016/j.soilbio.2012.06.013

Zhang, J., Busse, M.D., Young, D.H., Fiddler, G.O., Sherlock, J.W., TenPas, J.D., 2017. Aboveground biomass responses to organic matter removal, soil compaction, and competing vegetation control on 20-year mixed conifer plantations in California. Forest Ecology and Management 401, 341–353. https://doi.org/10.1016/j.foreco.2017.07.023

Zhao, H., Li, X., Wang, X., 2011. Heavy Metal Contents of Road-Deposited Sediment along the Urban–Rural Gradient around Beijing and its Potential Contribution to Runoff Pollution. Environ. Sci. Technol. 45, 7120–7127. https://doi.org/10.1021/es2003233

7 Task 3b: Comparison of biochar and compost to alleviate compaction effects

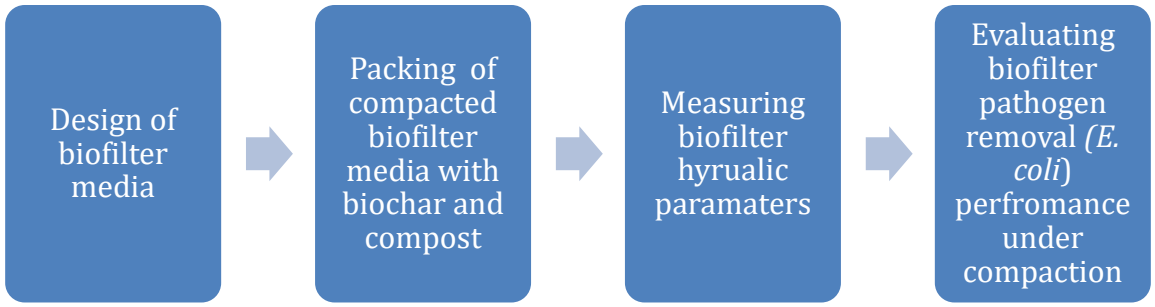

7.1 Background

To minimize the pollution from road runoff, roadside green infrastructures can be implemented to remove pollutants from road runoff as it infiltrates through roadside soil mixed with amendments. Thus, it is critical to examine whether or how compaction may affect the performance of infiltration-based green infrastructure, so that a design guideline for roadside green infrastructure with compaction can be developed (Pereira et al., 2017; Sax et al., 2017). Amendments such as compost and biochar have been used to improve the contaminant removal capacity of stormwater biofilters (Boehm et al., 2020; Sun et al., 2020). Treatment capacity biochar subjected to compaction has not been evaluated, partly because compaction may not be recommended in most cases. In some cases, however, compaction of biochar-amended media may naturally occur or is required (e.g., road bank or permeable pavement). The extent to which compaction may affect the physical integrity of biochar and their ability to treat stormwater is unknown (Mohanty et al., 2018).

7.1.1 Objective

This work aims to quantify the effect of compaction on the performance of biochar and compost augmented biofilters, which includes changes in hydraulic conductivity, flow-path heterogeneity, leaching of biochar particles, and removal of pathogen-indicator bacteria.

7.1.2 Hypothesis

We hypothesized that the effect of compaction on the net loss of biochar particles is dependent on media type and moisture content during compaction. Furthermore, we evaluated the utility of engineering controls such as compost and initial moisture content to test their role in minimizing the detrimental effect of compaction on biochar-augmented biofilter.

7.2 Experimental design

7.2.1 Biofilter media

Commercially available biochar (Black Owl BiocharTM, Biochar Supreme, WA), sand (20-30 Ottawa Sand, Certified Material Testing Products, FL), and garden compost (Whitter Fertilizer, CA) were used in this study. This biochar was purchased from the same vendor that supplied Rouge biochar (same biochar) in Section 4 and was selected because of high removal capacity and availability for large scale application in California. The biochar, produced by gasification of softwood at high temperature (900-1000 ºC), exhibits a high BET surface area (800 m^2 g^{-1}) and low ash content (5.8%) (Table 7.1). Typically, biomass pyrolysis can alter its physical properties and decrease its mechanical strength (Reza et al., 2012). Thus, it is expected biochar would be more susceptible to breakage under compaction than the biomass used for biochar production. Sand was used as the main bulking material to increase stormwater infiltration, whereas compost was used to increase pollutant removal with the added benefit of its ability to alleviate the effect of compaction (Sax et al., 2017). To remove silica colloids from sand, sand was washed in deionized (DI) water and dried in an oven. Biochar and compost were

sieved to remove particles smaller than 833 μm, the mean size of sand particles, to ensure that any fine particles released in the effluent were generated during the packing of media under compaction in the columns. Particles larger than 2 mm were also removed to minimize preferential flow.

The typical biofilter media may contain 10-30% amendment to increase pollutant removal. We mixed sand (85% by volume) with biochar or compost (15% by volume) in a sterile 4 L bucket to compare the effect of compaction on biochar and compost, the widely used soil amendment to alleviate the compaction effect. The media was mixed manually for 5 minutes to ensure a uniform mixture. We mixed the same volume of compost and biochar (15% of each) with sand (70% by volume) to examine whether the addition of biochar would affect the treatment capacity of compost-biofilter after compaction. We compacted biochar-sand mixture without and with water (15% by weight) to examine the presence of moisture during compaction affects the treatment capacity of compacted biochar. We chose 15% moisture content because it is the optimum moisture content for maximum dry density after compaction of poorly graded sand (Deb, K. 2010), although the critical moisture content for biochar-sand mixture could be different. The mixtures were immediately used to pack the columns after preparation. It should be noted that we did not include a sand-only column because, unlike biochar or compost, or soil, sand is not affected by compaction. The physical properties of compacted mixtures are described in Table 7.1. Additionally, the particle size distributions of the mixtures were determined using a laser diffraction particle size analyzer (model LS 13 320, Beckman Coulter, CA).

Table 7.1. Physical and chemical properties of the Black Owl Biochar™ provided by the company.

Black Owl Biochar™		
Property	**Value**	**Unit**
Water Holding Capacity	874	g H_2O/100
Surface area	800	$m^2\ g^{-1}$
Organic Carbon	80.1	%
Inorganic Carbon	0.39	%
H-$C_{organic}$ (molar Ratio)	0.56	%
Hydrogen	3.7	%
Nitrogen	0.4	%
Oxygen	9.6	%
Ash	5.8	%
Calcium	1.28	%
Magnesium	0.1	%
Sulfur	0.01	%
Iron	0.05	%
Manganese	0.03	%
Ammonia NH_4-N Mineral	6.7	$mg\ kg^{-1}$
Nitrate NO_3-N	6.3	$mg\ kg^{-1}$
Phosphorous Total*	0.086	$mg\ kg^{-1}$
Phosphorous Available**	14	$mg\ kg^{-1}$
K-Potassium Total & Available	1.17	%
Bulk Density	4.94	$lb\ ft^{-3}$

*Total phosphorus (TP) is all the forms of phosphorus, dissolved or particulate, ** Phosphorous Available is fraction of TP readily available

7.2.2 Packing of filter media in columns

76 A total of 15 columns were packed with the following media mixture with sand under different compaction conditions: uncompacted biochar, compacted biochar under dry condition, compacted biochar under wet condition, compacted compost, compacted biochar + compost. Each mixture was packed in triplicate columns (Figure 7.1). Wet biochar refers to biochar moistened during compaction; both biochar and compost were pre-sieved to remove fines, so any observed fines result from compaction rather than pre-existing material

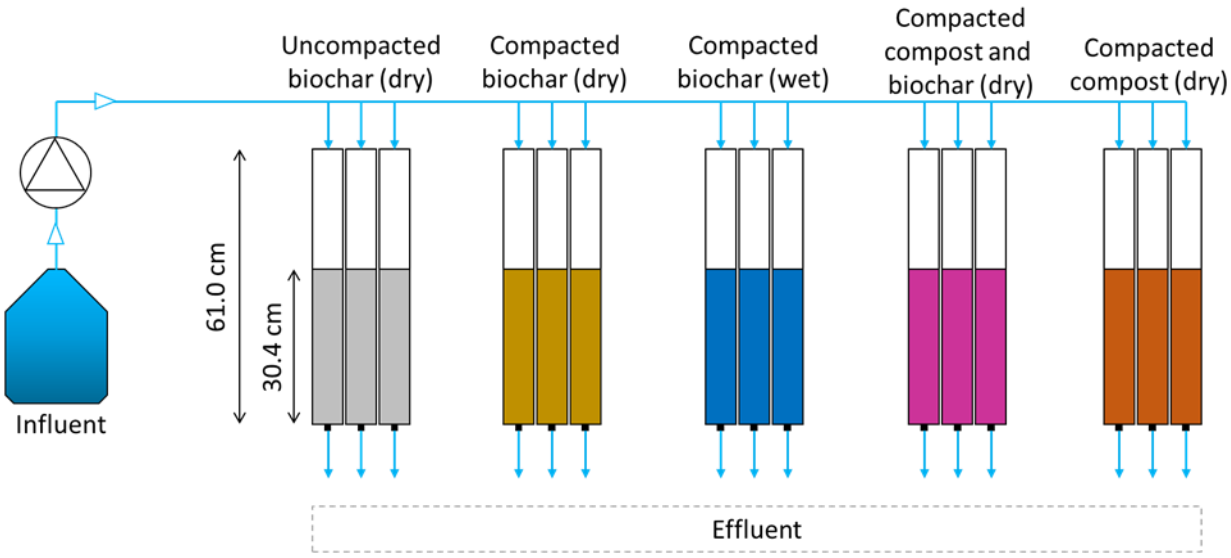

Figure 7.1. Schematic of five different types of laboratory biofilters

Before packing the filter media in each column, a 6 cm drainage layer was created in the bottom of the column using nylon membranes (100 µm pores) and pea gravels. The media mixture was added incrementally and compacted to a height of a 3.8 cm layer using a standard Proctor hammer (2.5 kg). To ensure that comparable energy of a standard Proctor test was applied on the filter media, the hammer was dropped 7 times from 30.2 cm height per layer. The procedure was repeated for 8 layers so that the total height of the filter layer became 30.4 cm. The bulk density was estimated after compaction of each layer to ensure uniform distribution of

filter media by depth (Figure 7.2.). A 2.5-cm layer of pea gravel was added on the top of filter media to prevent biochar or compost particles from floating in the event of ponding.

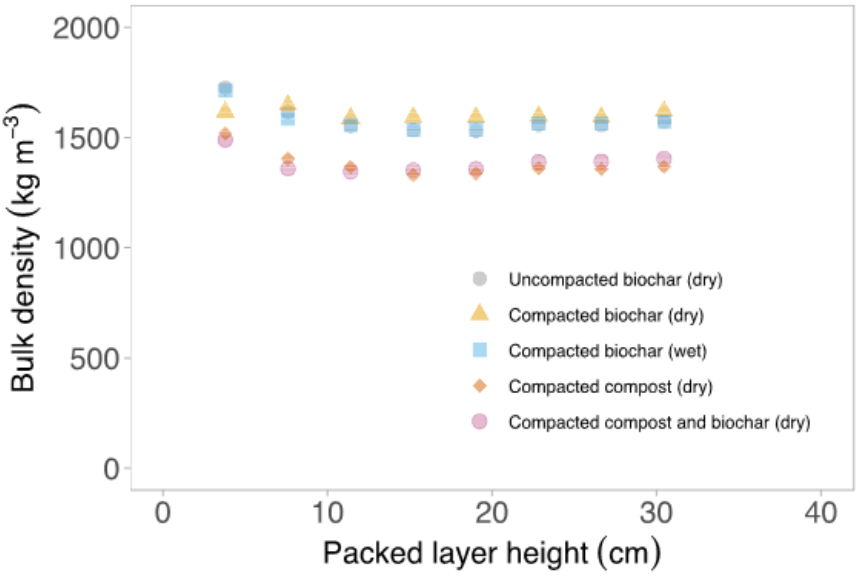

Figure 7.2. Bulk density of different layers of media during packing. The similar bulk density of each layer during packing indicates that uniform level of compaction of each layer.

Experiments were conducted using the same columns in the following order to determine the effects of compaction on (1) initial release of particles, (2) hydraulic conductivity of packed media, (3) flow-path connectivity via tracer study, and (4) *E. coli* removal capacity of the columns. The particle release experiment was conducted at the beginning in order to examine the immediate effect of compaction on particle release. The next two experiments helped determine the change in hydraulic properties of filter media following compaction. The *E. coli* experiment was conducted at the end to correlate any change in removal capacity to changes in hydraulic properties of columns after compaction. Between each experiment, the columns were drained by gravity and kept for 2-3 days.

7.2.3 Release of particles during the infiltration of stormwater

To examine the release of biochar particles during the application of stormwater, synthetic stormwater (10 mM NaCl) was used so that the influent water would be particulate-free. Synthetic stormwater was applied on the top of the filter media at a flow rate of 5 mL min^{-1} or flux of 14.8 cm h^{-1} for 2 pore volume, following which the filter media was drained by gravity. We expect that increases in flow rate can increase particle release (Shang et al., 2008) and decrease bacterial removal (Mohanty and Boehm, 2014b). We used a fixed velocity to rule out the effect of flow fluctuation on the results. Effluents were collected in 250 mL amber bottles at 0.5 PV fractions and analyzed for particle concentration and volume. The experiment was repeated for five consecutive days, beyond which particle release did not change with successive infiltration events. Particle concentration in the effluent samples was estimated by measuring the absorbance at 890 nm and the wavelength used to determine turbidity using a UV-Vis Spectrophotometer (Lambda 365, PerkinElmer) and correlating the absorbance with concentration using a calibration curve. The particle size distribution of the effluent was measured using a single-particle optical sensor instrument (AccuSizer 780, Entegris Company).

7.2.4 Measurement of hydraulic conductivity

Hydraulic conductivity (K) of each column was measured using a falling head method using the equation: $K = L/t\ \ln(h_1/h_2)$, where L is the depth of filter media, t is the time to drain water from initial height h_1 to final height h_2 after drainage of a specific volume of water. Briefly, 2 PV of synthetic stormwater (without particulates) was applied on the top of packed media to permit free drainage of stormwater at the bottom valve. The effective hydraulic conductivity of biofilters was estimated by recording the time required to drain a specific volume of stormwater. The procedure was repeated 6 times to estimate the average hydraulic conductivity of each column.

7.2.5 Measurement of effective pore volume and flow path heterogeneity

We measured effective pore volume, the fraction of total pore space filled with stormwater during an infiltration event, by estimating the volume of stormwater injected to achieve 50% of the concentration of bromide (a conservative tracer) in the feed solution i.e. effluent (Ptak et al., 2004). Briefly, synthetic stormwater containing bromide (9 mM NaCl + 1 mM KBr) was applied on the top of each column at 5 mL min^{-1} for 2 h before applying 10 mM NaCl for an additional 2 h at 5 mL min^{-1} to flush bromide from pore water. The flow was interrupted for 12 h, followed by an injection of 10 mM NaCl for an additional 0.7 h to compare the extent of diffusion-limited regions in different media mixture (Brusseau et al., 1997). We used the ratio of bromide concentration before and after flow interruption as an indicator of the presence of diffusion-limited zones in the biochar-augmented sand filters, as compaction is expected to create low-permeable zones or flow-stagnant zones, where diffusion would be significant for the transport of solute in between rainfall events.

7.2.6 E. coli removal

Stormwater contains a wide range of pollutants. However, we chose *E. coli* to test the removal of particulate pollutants as the removal process based on physical filtration is most likely to be affected by changes in pore structure under compaction. Furthermore, the presence of pathogens or indicator bacteria is the lead cause of water quality violations in the Los Angeles area. Pathogens can be removed in biofilters by a combination of processes, including Physico-chemical filtration, inactivation, gazing, and natural die-off via starvation or drying (Rippy, 2015). We hypothesize that compaction could increase bacterial removal via physico-chemical filtration by decreasing pore size. To investigate the effect of compaction on removal of E. coli, 5 PV of natural stormwater spiked with *E. coli* (concentration ~ 10^5 CFU mL^{-1}) was applied at 5 mL min^{-1} on the top of each column, and samples were collected at the bottom. The

concentration of *E. coli* was measured in the last 0.5 PV fraction of the samples, which serves as an indicator for the steady-state removal capacity of the filter. We did not measure *E. coli* concentration during first-flush because the previous study with biochar (Mohanty et al., 2014) showed that the concentration of *E. coli* in the first flush (old water in the column) were lower than that of pore water collected in the last part of infiltration events, due to inactivation or increased adsorption of *E. coli* trapped in pore water during period between rainfall events. *E. coli* concentration in stormwater was quantified by a spread plate technique and reported as colony-forming units (CFU) per mL of effluent. The experiment was repeated 3 times at 2 days interval to estimate a change in the bacterial removal capacity of biofilters with an increase in exposure to contaminated stormwater.

7.3 Results and discussion

7.3.1 Compaction conditions affected hydraulic conductivity

Compaction decreased the hydraulic conductivity of biofilter, but the extent to which the hydraulic conductivity decreased depended on media type and the presence of water (Figure 7.3). All compacted columns had significantly ($p < 0.005$) lower hydraulic conductivity than uncompacted biochar columns. Compaction of biochar under dry condition lowered the hydraulic conductivity by 44% than the uncompacted dry biochar. Compaction of biochar in wet condition (15% moisture) decreased the hydraulic conductivity by only 12% of the uncompacted wet biochar. Compaction decreased the hydraulic conductivity of biochar columns to a greater extent than compost columns. An addition of biochar to compost columns did not significantly ($p = 0.99$) change their hydraulic conductivity.

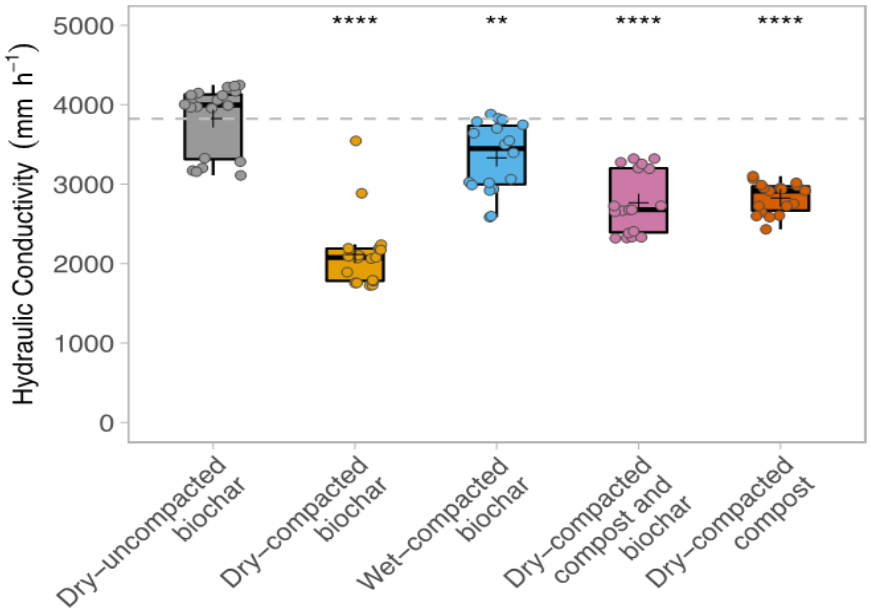

Figure 7.3. Effect of compaction on saturated hydraulic conductivity of biofilter packed with a mixture of sand and adsorbent (15% by volume), including biochar and compost. The horizontal dashed line indicates the mean hydraulic conductivity of uncompacted biochar columns. Plus (+) signs indicate mean hydraulic conductivity of total 18 measurements between triplicate columns of each type. Hydraulic conductivities of compacted columns were significantly lower than that of the uncompacted columns. A p-value of 0.01 and 0 correspond to notation "**" and "****," respectively.

A decrease in saturated hydraulic conductivity of biofilters after compaction confirmed that compaction reduced the flow path permeability. The negative effect of compaction on the hydraulic conductivity of biochar and sand mixture was more severe when the media was packed dry. This result confirmed that the presence of water in the filter media during compaction could reduce the negative impact of compaction on hydraulic conductivity. It should be noted that water content (15% by weight) used in this study can be nearly the field capacity of the mixture. At lower water contents, the presence of water could decrease friction between soil grains and increase compaction (Rollins et al., 1998). Thus, optimum moisture content for compaction could vary with filter media types and particle size distribution of filter media (Henderson et al.,

2005). Our results showed the extent to which flow paths could change after the compaction of biofilter media, which in turn could affect the transport and removal of contaminants through biofilters (Hatt et al., 2008). Comparing the hydraulic conductivity of columns containing compacted biochar and compost, we showed that the hydraulic conductivity of biochar decreased to a greater extent than that of compost after compaction. We attribute this to the low mechanical strength of biochar compared with compost. While the hydraulic conductivity for dry compacted biochar is indeed lower than that for dry compacted compost, the hydraulic conductivity of the dry compacted compost/biochar mixture is not. The compost acts as a cushion during compaction, reducing biochar breakage and fines release, which helps maintain higher hydraulic conductivity in the mixture. Under stress, biochar could break and produce fine particles, which can further clog the constricted flow paths under compaction. Thus, biochar is less effective compared to compost in mitigating the impact of compaction on hydraulic conductivity. However, biochar offers a better contaminant removal capacity than compost. Thus, when high hydraulic conductivity of biofilter is desired, biochar should be mixed with compost to withstand the impact of compaction and to maintain both high infiltration and contaminant removal capacity.

7.3.2 Compaction increased water-holding capacity and macropore-matrix interaction

Effective pore volume, estimated from bromide breakthrough curves in unsaturated biofilters, provides a quantitative estimate of the fraction of total biofilter media exposed to contaminated stormwater during infiltration events (Figure 7.4 -A). The effective pore volume of uncompacted biochar and wet-compacted biochar were similar, which was significantly ($p < 0.05$) lower than that of dry-compacted biochar columns (Figure 7.4-B). It should be noted that the effective pore volume estimated from bromide breakthrough curves includes the volume of

water in the drainage layer. Flow interruption during the breakthrough tail increased the bromide concentration by a factor of 3 to 15 depending on the compaction conditions or media type (Figure 7.4-B). The increase in bromide concentration was more apparent in compacted columns than the uncompacted columns.

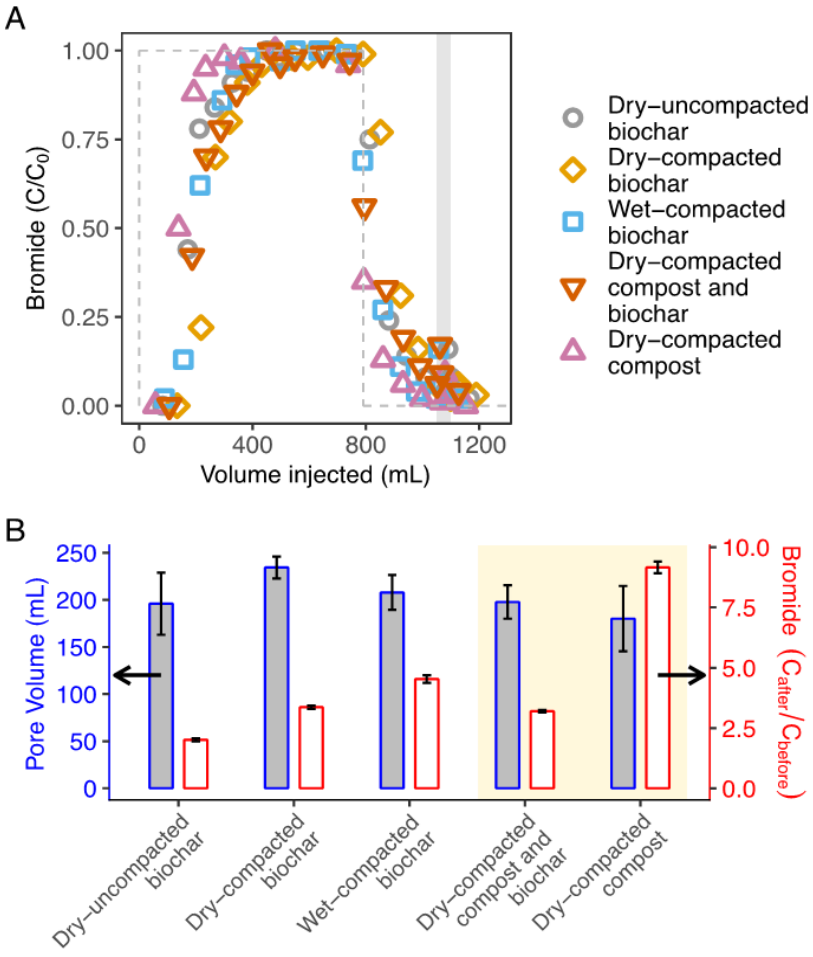

Figure 7.4. (A) Breakthrough curves of bromide through columns packed with uncompacted biochar, compacted biochar under dry condition, compacted biochar under wet condition, compacted compost, and compacted compost and biochar mixture. The vertical shaded line indicates flow interruption for 12 h. (B) Effective pore volume, which is estimated based on the volume of stormwater injected to achieve 50% of bromide breakthrough ($C/C_0 = 0.5$) and increase in bromide concentration as a result of a flow interruption, an indicator of diffusion dominated region in all columns. Error bars indicate one standard deviation over the mean between triplicate columns.

Although biofilters are designed to infiltrate stormwater quickly, a high infiltration rate provides limited opportunity for contaminants to interact with the filter media, which consequently lowers the overall contaminant removal capacity of biofilters (Mohanty and Boehm, 2014a). Thus, conditions that could increase the interaction time without decreasing the infiltration capacity of biofilters could serve both purposes: reducing the quantity of runoff over land and contaminants in the effluent. Based on the bromide breakthrough time and exchange of bromide between macropores and micropores during flow interruption, we showed that compaction could increase the interaction of stormwater with filter media. Effective pore volume, a measure of the fraction of filter media exposed to stormwater during an infiltration event, was slightly lower in compacted biochar columns than that of uncompacted biochar columns (Figure 7.4). Compaction increased the retention time of water in biofilters, which could help improve contaminant removal from stormwater (Figure 7.3). Sands were used in this study, which cannot be compacted to the extent that it would block water entirely. Because sand has higher hydraulic conductivity than the rainfall application rate, stormwater is expected to move through preferential flow paths in unsaturated columns. Adding biochar and compaction could minimize the preferential flow paths by blocking the large pores.

7.3.3 Compaction conditions affected the quantity of particles released

During the infiltration of stormwater after compaction, particles were released in the effluent, but the concentration and total quantity of released particles depended on the media type and compaction conditions (Figure 7.5). One of the concerns of compacting biochar is that biochar may break into smaller particles, which can be flushed out of the biofilter, thereby decreasing the concentration of biochar that remains in the biofilter for the intended application. However, we found that the total amount of particles released from each column was

insignificant compared to the total amount of amendment (biochar or compost) added to the column. During each infiltration event, particle concentration peaked initially, but the particle concentration rapidly decreased with the passage of more stormwater. The peak in particle concentration decreased with successive rainfall events. The cumulative mass of particles released varied with column types. Among columns without compost, dry-compacted biochar columns released the least amount of biochar particles. The particle release potential in biochar columns increased with the following design conditions: dry compaction < no compaction < wet compaction. After dry compaction, compacted compost released more particles than compacted biochar.

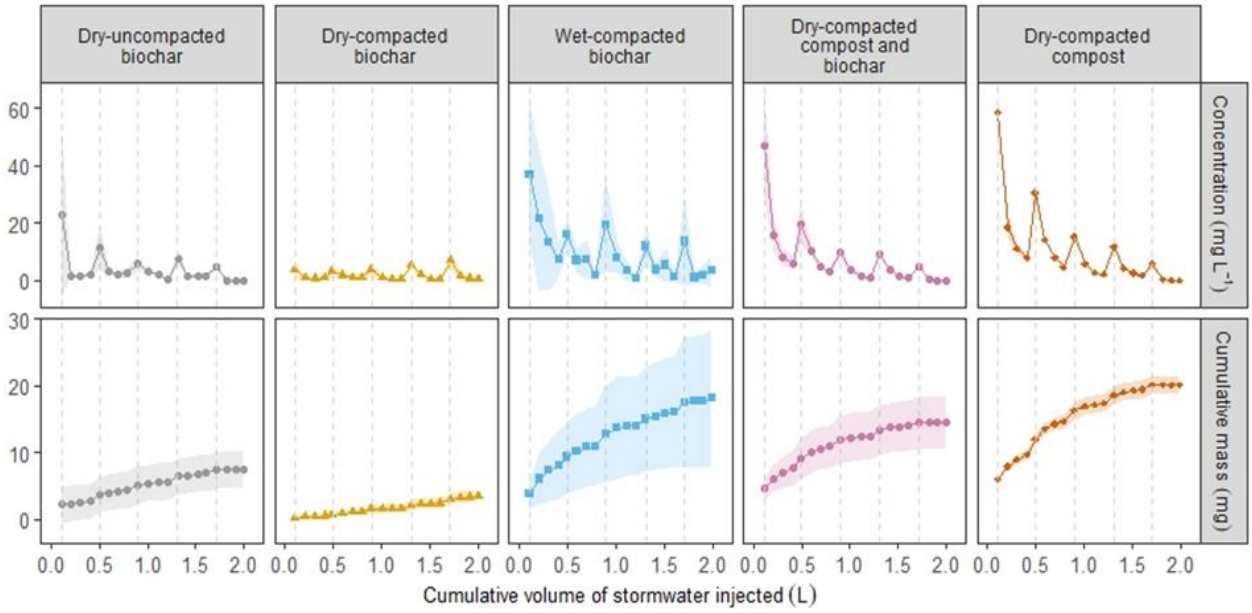

Figure 7.5. Concentration (top) and cumulative mass (bottom) of particles released from biofilters packed with biochar or compost under different compaction conditions. Dashed lines indicate the start of rainfall infiltration events. Shaded area indicates one standard deviation over the mean value from triplicate columns.

Millions of particles (> 99% are smaller than 3 μm) were present in the effluent, and the number of particles was higher in the columns with compost than in the columns with biochar (Figure 7.6-A). The size distribution of particles in the effluent was slightly different based on the compaction conditions and types of filter media used (Figure 7.6-B). The particle size corresponding to peak distribution was smaller for biochar columns than compost columns. The compaction conditions did not significantly ($p = 0.13$) affect the concentration of biochar particles released, but it affected the particle size distribution: the wet compacted biochar columns released a greater number of large particles than dry compacted columns. Columns with biochar released significantly fewer particles than the column with compost, indicating biochar is less susceptible to physical loss than compost under compaction. An addition of 15% (by volume) of biochar to compost-only columns significantly ($p < 0.05$) decreased the number of particles released and shifted the peak of the particle size distribution towards a smaller particle size, indicating that biochar can lower the loss of compost particles and block large particles.

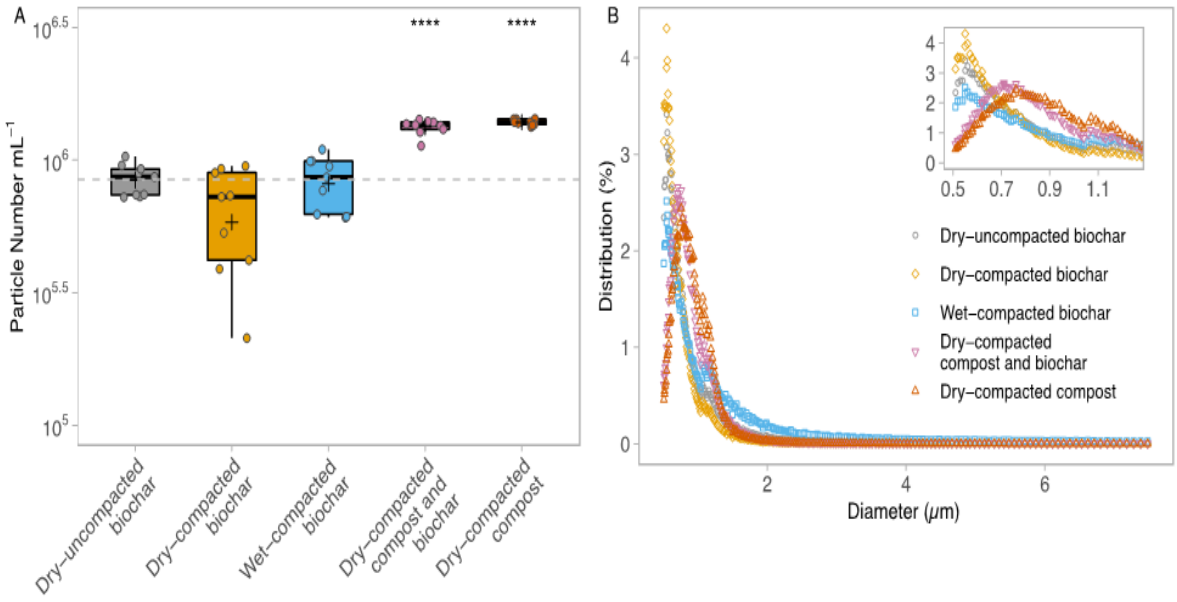

Figure 7.6. (A) Concentration of particles (number per mL) in the first sample during the infiltration event, and (B) the size distribution of the particles. The insert shows the peak in particle size distribution curves. The **** they are statistically different from others' means. This comparison of means.

We used hydraulic conductivity as a proxy measurement for flow path permeability or connectivity. Higher hydraulic conductivity of wet-compacted biochar columns than that of dry-compacted biochar columns suggests that wet compacted biochar columns were more conducive to transport biochar particles. Consequently, a decrease in flow-path permeability in dry-compacted biochar columns resulted in a decrease in particle leaching. For the same reason, columns with compost leached more particles than biochar-only columns. These results confirmed that particle release processes after compaction is dominated by a transport-limited process, not a source-limited condition. This means particle movement or leaching from biofilter more depend on factors that control the transport rather than the source of particulates. The transport of particles was dependent on the diffusion of particles from grain walls to bulk water in flow paths and physical filtration of particles when flow path width is smaller than particle

size. The addition of water would also minimize the dust emission (Ravi et al., 2016) during installation.

7.3.4 Compaction conditions affected E. coli removal

Compaction increased *E. coli* removal in biochar columns, but the increase in removal depended on compaction conditions and the volume of contaminated stormwater injected (Figure 7.7). During the first infiltration event, compacted biochar columns removed more *E. coli* than uncompacted biochar columns, and wet-compacted biochar columns removed more *E. coli* than dry-compacted biochar columns. However, increases in the exposure to contaminated water during the successive rainfall events reduced the *E. coli* removal capacity of all columns. After the exposure to 20 pore volumes of contaminated stormwater, the *E. coli* removal capacity of wet-compacted biochar columns (95%) remained significantly ($p < 0.05$) greater than the removal capacity of dry-compacted (75%) or uncompacted biochar columns (70%), indicating wet compaction favors *E. coli* removal. The *E. coli* removal by dry-compacted compost columns was similar to the removal by dry-compacted biochar columns, and the addition of biochar to compost did not improve bacterial removal under the tested conditions. It should be noted that sand has a significantly lower removal capacity than biochar (Mohanty and Boehm, 2014b; Mohanty et al., 2014); thus, the amount of sand is not expected to influence the overall capacity of biochar-augmented columns.

Removal in wet-compacted biochar was more than that in dry-compacted biochar, which indicates that *E. coli* interaction with biochar was greater in the wet-compacted column than in the dry-compacted columns. Based on bromide breakthrough data, pore-water connectivity was higher in wet-compacted biochar columns compared with dry-compacted biochar columns, indicating a greater fraction of wet-compacted biochar columns was in contact with *E. coli* in

infiltrating stormwater. Overall, these results indicate that compacting biochar in the presence of water may increase *E. coli* removal in biofilters.

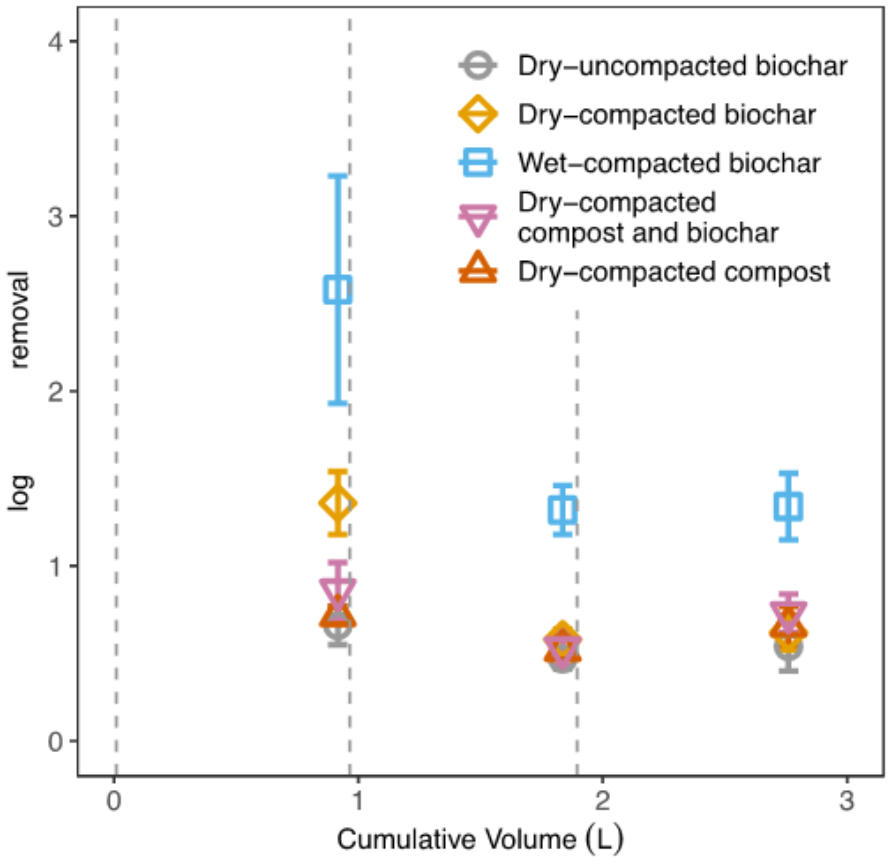

Figure 7.7. Average *E. coli* removal by columns packed with a mixture of biochar or compost under different compaction conditions. Dashed lines indicate the start of a rainfall event, where more than 5 pore volume of contaminated stormwater was injected through the columns. Error bars indicate one standard deviation over mean log *E. coli* removal by triplicate columns of each type.

7.3.5 Mechanism of biochar release

Filter media serves a critical role in removing the contaminants from stormwater. However, intermittent infiltration of stormwater can release particles from filter media (Mohanty and Boehm, 2015), which has consequences on the loss of filter media and particle-facilitated leaching of contaminants in biofilter (Mohanty et al., 2013). Our results revealed that compaction could affect the quantity of particles available for mobilization during infiltration of stormwater, although pools of particles available depletes with successive infiltration events due to exhaustion of particles generated during compaction. A fewer amount of biochar particles were released from dry-compacted columns than from the wet-compacted columns.

Based on the results, biochar release after compaction can be explained by a three-step process: (1) generation of particles by compaction, (2) diffusion of particles from grain wall to bulk liquid inflow paths, (3) transport in flow paths by advection and removal of large particles by filtration (Figure 7.8). First, compaction can generate a high concentration of biochar particles due to the disintegration of biochar under pressure exerted during compaction. Increases in the percentage of particles smaller than 100 μm after compaction confirmed that compaction disintegrated biochar particles and produced smaller particles, and increased the pool of particles in the biofilter (Figure 7.9). Thus, the source is not a limiting factor for the release of particles. Second, during infiltration events, the suspended particles in pore paths were quickly eluted, which contributes to the initial peak. A rapid decrease in particle concentration indicates a limited supply of particles to pore paths during infiltration. A linear relationship between cumulative particles released during a rainfall event as a function of the square root of time (Jacobsen et al., 1997) suggested that diffusion is a limiting step in the mobilization of biochar particles from grain walls to bulk liquid inflow paths (Figure 7.10). A difference in leaching of particles in dry- and wet-compacted biochar columns indicates that the presence of water during

compaction could help mobilization and transport of biochar particles. As the extent of diffusive transport would increase with the increase in water-filled pores, more biochar particles were mobilized in wet-compacted biochar, thereby increasing the availability of biochar particles for transport in flow paths. Third, the filtration of large biochar particles in narrow flow paths, which may be constricted during compaction, can limit the leaching of biochar particles.

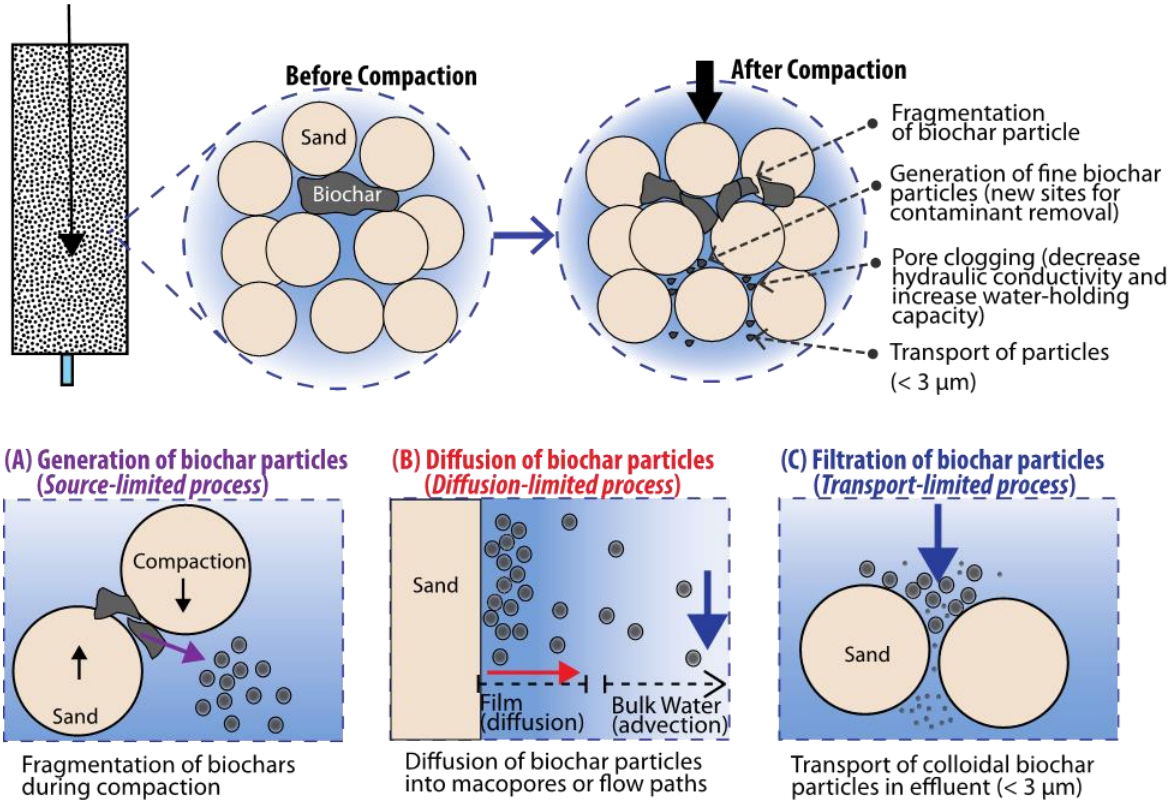

Figure 7.8. Suggested mechanisms of biochar particle release due to compaction. First, compaction causes the disintegration of biochar particles, which generates fine biochar particles and decreases the average biochar particle size in the sand filter. Second, fine biochar particles deposited on grain surfaces diffuse from the film surrounding particles to bulk water inflow paths, which limits the amount of biochar particles available for transport during an infiltration event. Third, only a fraction of total available biochar particles based on size (< 3 µm) could transport as the pore path width, which may become constricted during compaction, can limit the transport or leaching of biochar particles during infiltration events.

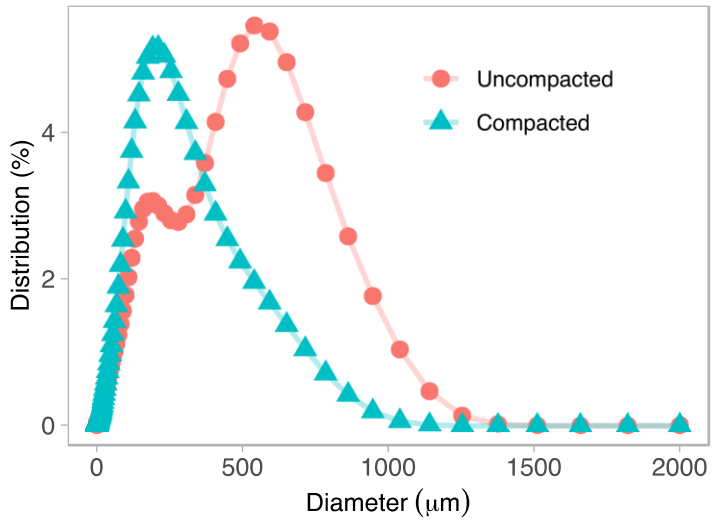

Figure 7.9. A decrease in the mean particle size of biochar in biofilter after compaction.

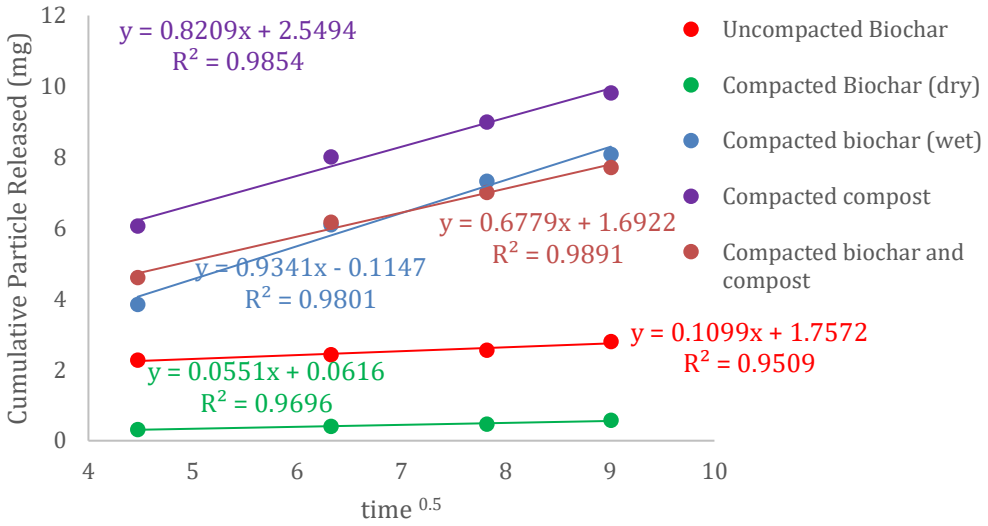

Figure 7.10. A linear relationship between cumulative particles released during a rainfall event as a function of the square root of time suggested that diffusion is a limiting step in the mobilization of particle.

7.4 Summary and implications

We examined the effect of compaction on physical processes of stormwater treatment, including stormwater infiltration, particle release, and removal of particulate pollutants such as *E. coli*, and provide a mechanistic understanding of how compaction conditions such as the presence of moisture could affect the performance of roadside soil augmented with biochar. The results can inform the design guideline for the construction of roadside biofilters with biochar as an amendment.

- Compaction decreased the hydraulic conductivity of biochar-augmented biofilter, but the detrimental effect of compaction can be minimized by adding compost and water.
- Compaction disintegrated biochar particles, which can be released during intermittent infiltration of stormwater. Although compactions generated fine biochar particles, the net release of these particles was controlled by the flow-path permeability after compaction.
- Irrespective of the initial release of biochar particles after compaction, the total biochar amount released is insignificant compared to the total biochar that remained in the system, and the extent of biochar release was less than that observed in compost columns.
- Compaction increased water holding capacity and interaction time of stormwater with filter media.
- Compaction increased *E. coli* removal in a short term, but the benefit was short-lived in dry-compacted biofilters augmented with biochar. Wet-compacted biofilter consistently removes more *E. coli* than dry-compacted or uncompacted biofilter with biochar.

7.5 References

Ahmed, A., Gariepy, Y. and Raghavan, V. (2017) Influence of wood-derived biochar on the compactibility and strength of silt loam soil. International Agrophysics 31(2), 149-155.

Ahmed, A.S.F. and Raghavan, V. (2018) Influence of wood-derived biochar on the physico-mechanical and chemical characteristics of agricultural soils. International Agrophysics 32(1), 1-10.

Boehm, A.B., Bell, C.D., Fitzgerald, N.J., Gallo, E., Higgins, C.P., Hogue, T.S., Luthy, R.G., Portmann, A.C., Ulrich, B.A. and Wolfand, J.M. (2020) Biochar-augmented biofilters to improve pollutant removal from stormwater–can they improve receiving water quality? Environmental Science: Water Research & Technology. doi: https://doi.org/10.1039/D0EW00027B

Brown, J.S., Stein, E.D., Ackerman, D., Dorsey, J.H., Lyon, J. and Carter, P.M. (2013) Metals and bacteria partitioning to various size particles in Ballona creek storm water runoff. Environmental Toxicology and Chemistry 32(2), 320-328.

Brusseau, M.L., Hu, Q. and Srivastava, R. (1997) Using flow interruption to identify factors causing nonideal contaminant transport. Journal of Contaminant Hydrology 24(3-4), 205-219.

Cambi, M., Certini, G., Neri, F. and Marchi, E. (2015) The impact of heavy traffic on forest soils: A review. Forest Ecology and Management 338, 124-138.

Etana, A., Larsbo, M., Keller, T., Arvidsson, J., Schjønning, P., Forkman, J. and Jarvis, N. (2013) Persistent subsoil compaction and its effects on preferential flow patterns in a loamy till soil. Geoderma 192, 430-436.

Gold, M., Hogue, T., Pincetl, S., Mika, K. and Radavich, K. (2015) Los Angeles Sustainable Water Project: Ballona Creek Watershed. https://escholarship.org/uc/item/0kv1z03v (accessed, April 12, 2020)

Gregory, J.H., Dukes, M.D., Jones, P.H. and Miller, G.L. (2006) Effect of urban soil compaction on infiltration rate. Journal of Soil and Water Conservation 61(3), 117-124.

Hatt, B.E., Fletcher, T.D. and Deletic, A. (2008) Hydraulic and pollutant removal performance of fine media stormwater filtration systems. Environmental Science and Technology 42(7), 2535-2541.

Henderson, J.J., Crum, J.R., Wolff, T.F. and Rogers, J.N.I. (2005) Effects of particle size distribution and water content at compaction on saturated hydraulic conductivity and strength of high sand content root zone materials. Soil Science 170(5), 315-324.

Jacobsen, O.H., Moldrup, P., Larsen, C., Konnerup, L. and Petersen, L.W. (1997) Particle transport in macropores of undisturbed soil columns. Journal of Hydrology 196(1-4), 185-203.

Kranner, B.P., Afrooz, A.R.M.N., Fitzgerald, N.J.M. and Boehm, A.B. (2019) Fecal indicator bacteria and virus removal in stormwater biofilters: Effects of biochar, media saturation, and field conditioning. PLOS ONE 14(9), e0222719.

Kumar, H., Ganesan, S.P., Bordoloi, S., Sreedeep, S., Lin, P., Mei, G.X., Garg, A. and Sarmah, A.K. (2019) Erodibility assessment of compacted biochar amended soil for geo-environmental applications. Science of The Total Environment 672, 698-707.

Kumari, K.G.I.D., Moldrup, P., Paradelo, M., Elsgaard, L., Hauggaard-Nielsen, H. and de Jonge, L.W. (2014) Effects of Biochar on Air and Water Permeability and Colloid and Phosphorus Leaching in Soils from a Natural Calcium Carbonate Gradient. Journal of Environmental Quality 43(2), 647-657.

Lau, A.Y.T., Tsang, D.C.W., Graham, N.J.D., Ok, Y.S., Yang, X. and Li, X.-d. (2017) Surface-modified biochar in a bioretention system for Escherichia coli removal from stormwater. Chemosphere 169, 89-98.

Liu, Q., Liu, B.J., Zhang, Y.H., Lin, Z.B., Zhu, T.B., Sun, R.B., Wang, X.J., Ma, J., Bei, Q.C., Liu, G., Lin, X.W. and Xie, Z.B. (2017) Can biochar alleviate soil

compaction stress on wheat growth and mitigate soil N2O emissions? Soil Biology & Biochemistry 104, 8-17.

McPherson, T.N., Burian, S.J., Turin, H.J., Stenstrom, M.K. and Suffet, I.H. (2002) Comparison of the pollutant loads in dry and wet weather runoff in a southern California urban watershed. Water Science and Technology 45(9), 255-261.

Menon, M., Tatari, A. and Smith, C.C. (2018) Mechanical properties of soil freshly amended with Miscanthus biochar. Soil Use and Management 34(4), 563-574.

Mohanty, S.K. and Boehm, A.B. (2014a) Escherichia coli Removal in Biochar-Augmented Biofilter: Effect of Infiltration Rate, Initial Bacterial Concentration, Biochar Particle Size, and Presence of Compost. Environmental Science & Technology 48(19), 11535-11542.

Mohanty, S.K. and Boehm, A.B. (2014b) Escherichia coli removal in biochar-augmented biofilter: Effect of infiltration rate, initial bacterial concentration, biochar particle size, and presence of compost. Environmental Science and Technology 48(19), 11535-11542.

Mohanty, S.K. and Boehm, A.B. (2015) Effect of weathering on mobilization of biochar particles and bacterial removal in a stormwater biofilter. water research 85, 208-215.

Mohanty, S.K., Cantrell, K.B., Nelson, K.L. and Boehm, A.B. (2014) Efficacy of biochar to remove Escherichia coli from stormwater under steady and intermittent flow. water research 61, 288-296.

Mohanty, S.K., Torkelson, A.A., Dodd, H., Nelson, K.L. and Boehm, A.B. (2013) Engineering solutions to improve the removal of fecal indicator bacteria by bioinfiltration systems during intermittent flow of stormwater. Environmental Science and Technology 47(19), 10791-10798.

Mohanty, S.K., Valenca, R., Berger, A.W., Iris, K., Xiong, X., Saunders, T.M. and Tsang, D.C. (2018) Plenty of room for carbon on the ground: Potential applications of biochar for stormwater treatment. Science of The Total Environment 625, 1644-1658.

Mossadeghi-Bjorklund, M., Arvidsson, J., Keller, T., Koestel, J., Lamande, M., Larsbo, M. and Jarvis, N. (2016) Effects of subsoil compaction on hydraulic properties and preferential flow in a Swedish clay soil. Soil & Tillage Research 156, 91-98.

Peake, L.R., Reid, B.J. and Tang, X.Y. (2014) Quantifying the influence of biochar on the physical and hydrological properties of dissimilar soils. Geoderma 235, 182-190.

Pereira, R.S., Emmert, F., Miguel, E.P., Mota, F.C.M., Rezende, A.V. and Leal, F.A. (2017) Mechanical stabilization of soils as alternative for construction of low cost forest road. Nativa 5(3), 212-217.

Pitt, R., Chen, S.E., Clark, S.E., Swenson, J. and Ong, C.K. (2008) Compaction's impacts on urban storm-water infiltration. Journal of Irrigation and Drainage Engineering 134(5), 652-658.

Ptak, T., Piepenbrink, M. and Martac, E. (2004) Tracer tests for the investigation of heterogeneous porous media and stochastic modelling of flow and transport - a review of some recent developments. Journal of Hydrology 294(1-3), 122-163.

Ravi, S., Sharratt, B.S., Li, J., Olshevski, S., Meng, Z. and Zhang, J. (2016) Particulate matter emissions from biochar-amended soils as a potential tradeoff to the negative emission potential. Scientific Reports 6, 35984.

Reza, M.T., Lynam, J.G., Vasquez, V.R. and Coronella, C.J. (2012) Pelletization of Biochar from Hydrothermally Carbonized Wood. Environmental Progress & Sustainable Energy 31(2), 225-234.

Rippy, M.A. (2015) Meeting the criteria: linking biofilter design to fecal indicator bacteria removal. Wiley Interdisciplinary Reviews: Water 2(5), 577-592.

Rollins, K.M., Jorgensen, S.J. and Ross, T.E. (1998) Optimum moisture content for dynamic compaction of collapsible soils. Journal of Geotechnical and Geoenvironmental Engineering 124(8), 699-708.

Sasidharan, S., Torkzaban, S., Bradford, S.A., Kookana, R., Page, D. and Cook, P.G. (2016) Transport and retention of bacteria and viruses in biochar-amended sand. Science of the Total Environment 548, 100-109.

Sax, M.S., Bassuk, N., van Es, H. and Rakow, D. (2017) Long-term remediation of compacted urban soils by physical fracturing and incorporation of compost. Urban Forestry & Urban Greening 24, 149-156.

Shang, J., Flury, M., Chen, G. and Zhuang, J. (2008) Impact of flow rate, water content, and capillary forces on in situ colloid mobilization during infiltration in unsaturated sediments. Water Resources Research 44(6). https://doi.org/10.1029/2007WR006516

Sileshi, R., Pitt, R. and Clark, S. (2016) Prediction of Flow Rates through Various Stormwater Biofilter Media Mixtures. World Environmental and Water Resources Congress. doi: 10.1061/9780784479889.021.

Sun, Y., Chen, S.S., Lau, A.Y.T., Tsang, D.C.W., Mohanty, S.K., Bhatnagar, A., Rinklebe, J., Lin, K.-Y.A. and Ok, Y.S. (2020) Waste-derived compost and biochar amendments for stormwater treatment in bioretention column: Co-transport of metals and colloids. Journal of Hazardous Materials 383, 121243.

Ulrich, B.A., Im, E.A., Werner, D. and Higgins, C.P. (2015) Biochar and activated carbon for enhanced trace organic contaminant retention in stormwater infiltration systems. Environmental Science and Technology 49(10), 6222-6230.

Wong, T., Breen, P.F. and Lloyd, S.D. (2000) Water sensitive road design: design options for improving stormwater quality of road runoff, CRC for Catchment Hydrology Melburne, Australia.

8 Task 3c: Optimum size of biochar to minimize compaction effects

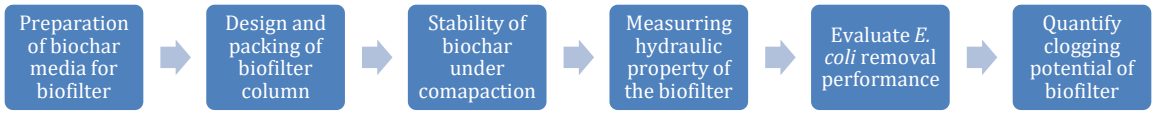

8.1 Background

Biochar can be added as an amendment to compacted biofilter that has been shown to remove a wide range of pollutants (Boehm et al., 2020; Mohanty et al., 2018). Under compaction, biochar particles could break by splitting or disintegration and surface abrasion because it has a lower load-bearing capacity than other soil amendments, including sand (Reza et al., 2012). Production and deposition of broken biochar particles can alter the flow path in compacted biofilters, which could lead to clogging of pores and change in contaminant removal. To reduce the negative impact of compaction, initial biochar size can be controlled as biochar size has been shown to affect the hydraulic conductivity of uncompacted sand or soil (Liu et al., 2016; Herath et al., 2013). Biofilters can be clogged due to the accumulation of suspended sediments with a size predominantly smaller than 6 µm (Siriwardene et al., 2007) in the top of 20% of the filter media (Hatt et al. 2008). Although several studies have examined the design parameters to minimize clogging risk (Kandra et al.,2014; Le Coustumer et al., 2009), it is

unclear how the clogging rate is related to suspended sediment loading. Developing a model that predicts the clogging of compacted biofilters could help develop maintenance guidelines for roadside biofilters (Hatt et al., 2008; Le Coustumer and Barraud, 2007).

8.1.1 Objective

We aim to examine the effect of biochar size on the extent of biochar breaking under compaction, clogging rate, and *E. coli* removal in compacted biochar-sand filters.

8.1.1. Hypothesis

We hypothesize that the breaking of biochar particles would be sensitive to their initial size, which will also determine the clogging rate and *E. coli* removal in the compacted biofilters. To test the hypothesis, we packed mixtures of sand and biochar of different sizes under compaction in columns, applied contaminated stormwater, and compared the number of broken biochar particles released, the clogging rate, and *E. coli* removal.

8.2. Experimental methods

8.2.1. Stormwater preparation

Natural stormwater was collected from the Ballona Creek in Los Angeles, CA (34° 00'32" N, 118° 23'3" W), which receives dry-weather irrigation runoff from 318 km^2 urban area with 82% developed and 61% impervious surface. The detailed characteristics of stormwater were reported in the previous studies (Brown et al., 2013). Immediately after the collection, the stormwater was characterized for pH (Ion-Selective Electrode, model #9107BN, Fisher Scientific), conductivity (Two-Cell Accumet Probe, Fisher Scientific), and particle concentration, and stored at 4ºC until further use. To quantify initial particle release from biofilters after compaction, synthetic stormwater was used so that there were no particles in the influent. Synthetic stormwater was prepared by adding 10 mM NaCl to deionized (DI) water and adjusting the pH to 7.8 ± 0.2 using a small volume of concentrated HCl or NaOH. This step

ensured that the ionic strength and pH, the geochemical driver for particle release or deposition, were consistent during particle release experiments.

Our preliminary study revealed that it would take years to clog the columns due to the low concentration (< 30 mg L^{-1}) of suspended sediments in the natural stormwater. To accelerate the clogging during this study, turbid stormwater with a suspended solid concentration of 3 g L^{-1} was prepared by spiking fine (< 75 μm) sediments collected from a wetland that receives Ballona Creek stormwater (Valenca et al., 2020).

To examine removal of *E. coli*, the stormwater was spiked with kanamycin-resistant *E. coli* suspension following the method described earlier (Mohanty et al., 2014). Briefly, *E. coli* were cultured to a stationary phase, centrifuged and washed with phosphate buffer solution to remove the growth medium, and suspended in the collected stormwater to achieve an initial concentration of nearly 10^6 colony forming units (CFU) mL^{-1}.

8.2.2. Preparation of biofilter media

Commercially available biochar (Black Owl Biochar ™, Biochar Supreme, WA) and sand (20 - 30 Standard sand, Certified Material Testing Products, FL) were used. We selected based on performance and availability. We expect the result can vary with biochar types. Therefore, we recommended using the regression model developed in this study (Chapter 4) based on the properties of biochar to identify biochar for better performance. The coarse sand (0.6 - 0.85 mm) was washed in DI water to remove silica colloids and dried at 100 ºC overnight. The biochar, produced by gasification of softwood at high temperature (900 - 1000 ºC), was characterized for surface area, particle size distribution, elemental analysis, and ultimate and proximate analysis. Biochar was sieved to remove particles smaller than 150 μm (mesh #100), to ensure fine particles released from biofilters originated from the broken biochar produced during

compaction. Biochar with a size greater than 2000 μm (mesh #10) was also removed to minimize preferential flow. The sieved biochar was further separated into three size fractions relative to the sand size: small (150 μm < d < 833 μm), medium (833 μm < d < 1180 μm), and large (1180 μm < d < 2000 μm). The sand was mixed with each biochar size fraction (5% biochar by weight, which is 15% by volume roughly) to prepare homogeneous geo-media mixtures.

To examine the biochar breaking mechanisms under compaction, a portion of small and large biochar size fractions was coated with acridine orange dye (Fisher Scientific, MA) following the method described in the Supplementary Materials. The biochar-sand mixture was packed up to a 11.4 cm height (3 compacted layers) and subjected to stormwater infiltration to monitor the release of broken biochar particles with different amounts of dye based on the breaking mechanism.

8.2.3. Packing of filter media in model biofilter columns

To design a laboratory column setup, a transparent PVC tube (5.1 cm I.D. and 61.0 cm length) was glued with PVC fittings and connected to a control valve to regulate the effluent flow. A total of 9 columns with three replicates per treatment were packed with the following media mixture with sand under different compaction conditions (**Error! Reference source not found.**): small biochar (150 μm < d < 833 μm), medium biochar (833 μm < d < 1180 μm), and large (1180 μm < d < 2000 μm). A peristaltic pump (Masterflex L/S, Cole-Parmer) was used to deliver stormwater at the top of the filter media, and effluents were collected at the bottom using 250 mL plastic amber bottles. Before packing the filter media in each column, a nylon membrane (100 μm pores) was inserted at the bottom to prevent the filter media from falling into the outlet tube. Pea gravels were poured over the membrane to a height of 9 cm, and a second membrane was placed over the gravel layer to prevent the filter media atop from falling into the pore space

between gravels. The media mixture was added incrementally and compacted to a height of 3.8 cm layer using a standard Proctor hammer (2.5 kg). To ensure that comparable energy of a standard Proctor test was applied on the filter media, the hammer was dropped 7 times from 30.5 cm height per layer following the equation: $\text{Number of blow per layer} = (\text{E} \times \text{V})/(\text{W} \times \text{N} \times \text{H})$, where energy per unit volume (E), hammer weight (W), number of total layers (N), and drop height (H) were kept constant as 593 kN-m m^{-3}, 2.5 kg, 3 layers, and 30.5 cm. The single-layer height of filter media was calculated by dividing the column area by the column volume, and it equaled 3.8 cm. The procedure was repeated until the filter media depth reached 30.5 cm with a total of 8 layers. The bulk density was estimated after compaction of each layer to ensure uniform distribution of filter media by depth (Figure 8.2). A 2.5 cm layer of pea gravel was added on the top of the filter media to prevent the floating of biochar or compost particles in case of ponding. After packing, DI water was injected from the bottom to fill the space until the top of the gravel layer, and the volume of water required to fill the drainage layer was estimated to be 75.4 ± 11.3 mL.

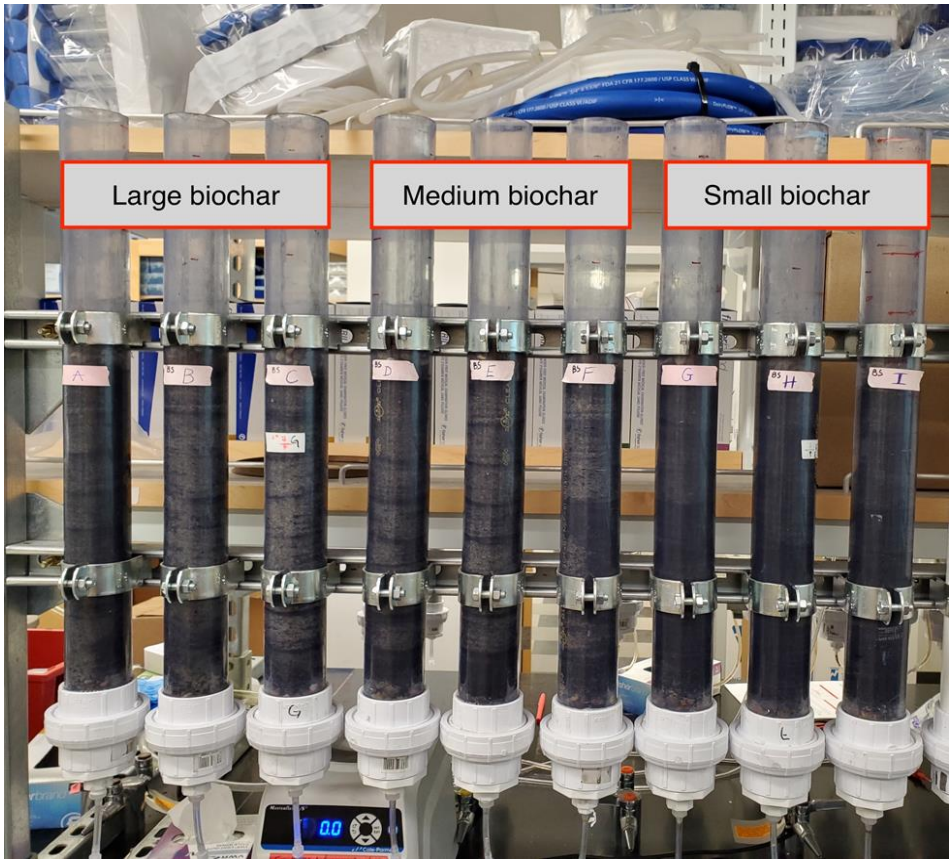

Figure 8.1. Triplicates columns for each biochar size fraction (total 9 columns) were used to quantify the effect of biochar particle size on their performance in biofilters subjected to compaction.

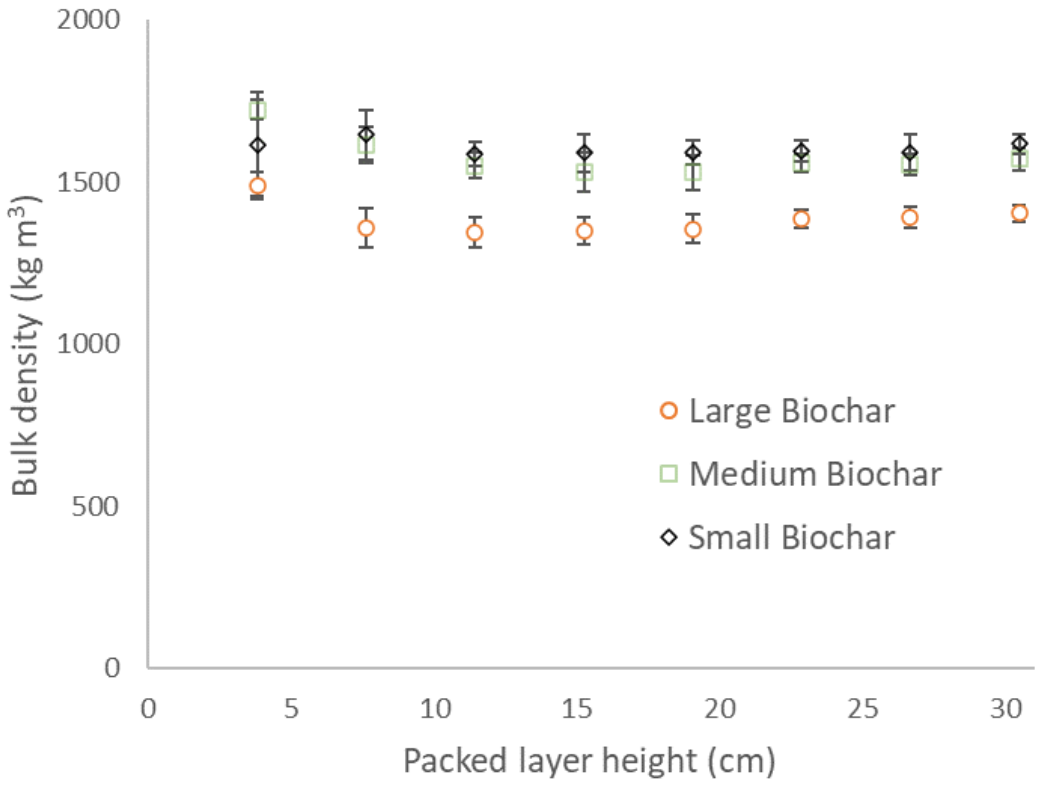

Figure 8.2. Bulk density of filter media with the increase in packing layer. Measurements were conducted in triplicated columns. Error bars represent one standard deviation over the mean.

After packing, the columns were subjected to different tests in the following order: (1) quantification of initial biochar particle release from compacted columns, (2) measurement of effective pore volume and flow-path heterogeneity by bromide tracer study, (3) estimation of *E. coli* removal capacity, and (4) quantification of clogging potential by measuring changes in hydraulic conductivity of the compacted biofilters with increases in suspended sediment loading. Separate columns were used to examine the breaking mechanism.

8.2.4. Release of biochar particles from compacted biofilters

To examine the initial release of biochar particles from the biofilters following compaction, 2 PV of synthetic stormwater (10 mM NaCl) was intermittently applied on the top of filter media at a flow rate of 8.5 mL min^{-1} using a peristaltic pump (Masterflex L/S Digital Drive, Cole Parmer). The flow rate was kept consistent to rule out the effect of flow fluctuation on particle release, as the increase in the flow is expected to increase particle mobilization (Shang et al., 2008). Effluents from the bottom of columns were collected at 0.5 PV fractions and analyzed for particle concentration and volume. The experiment was repeated every day for 5 consecutive days to examine if the quantity of particles released varied with successive rainfall events. Particle concentration was estimated based on the light (890 nm) absorbance of water samples.

8.2.5. Characterization of flow path heterogeneity in compacted biofilters

We conducted a bromide tracer study to estimate the effective pore volume of biofilters, which corresponds to the volume of stormwater injected to achieve half of the highest bromide concentration in the inflow. Synthetic stormwater containing bromide (1 mM KBr) and 9 mM NaCl was applied at 8.5 mL min^{-1} on the top of each column for 1.2 h, followed by the application of bromide-free synthetic stormwater (10 mM NaCl) for 0.8 h to flush bromide

solution from the pore water. After this step flow was interrupted, during which the bottom valve was closed, and the top of the column was sealed to prevent evaporation of stormwater. After 12 h of a flow interruption, the flow was resumed for 0.5 h. The effluents were collected at 5-10 min intervals and analyzed for bromide using ion chromatography (Dionex^{TM} Integrion^{TM} HPIC^{TM} System, ThermoFisher). A change in bromide concentration during flow interruption was used as an indicator to qualitatively compare the extent of back-diffusion of solutes from immobile water trapped in compacted regions to bulk pore water in the flow paths (Brusseau et al., 1997).

8.2.6. E. coli removal in compacted biofilters

We chose *E. coli* to test the removal of particulate pollutants as their removal is more sensitive to change in pore size distribution under compaction than other dissolved pollutants. The *E. coli* removal capacity of compacted columns was tested following the method described in our previous study (Section 7.2.6). Stormwater contaminated with *E. coli* at 10^6 CFU mL^{-1} was applied (8.5 mL min^{-1}) on the top of each column, and samples were collected at the bottom. The concentration of *E. coli* in the final 0.5 PV fraction, measured using an agar-plate technique, provides the steady-state removal capacity of the biofilter. It is expected that the *E. coli* concentration in the first flush would be lower due to adsorption or die-off of *E. coli* in the trapped pore water that contributes to the first flush (Mohanty et al., 2014). The experiment was repeated for five consecutive days to determine if the bacterial removal capacity of compacted biofilters changes with an increase in exposure to contaminated stormwater.

8.2.7. Quantification of clogging potential of compacted biofilters

The hydraulic conductivity of each column was measured using a falling-head method. The clogging potential of each column was estimated by tracking the changes in hydraulic conductivity with increases in the loading of suspended sediments. The experiment was repeated

until the hydraulic conductivity decreased to less than $1/10^{th}$ of its initial value. The suspended sediment loading was estimated by multiplying the concentration of suspended sediments in the stormwater suspension with the cumulative volume of stormwater applied.

The deposition of suspended sediment is expected to decrease the effective porosity of filter media, which consequently affects their hydraulic conductivity. We used several models that have used the change in the filter media porosity to predict their hydraulic conductivity (Table 8.1). These models assume that the deposition of particles decreases the porosity of the column uniformly throughout the depths. Because clogging may occur by the formation of the cake layer without complete penetration of suspended sediments into the columns, we used an exponential empirical model (Phipps, 2007) that correlates hydraulic conductivity with sediment loading: $\ln(K/K_0) = -rL$, where r is the sediment interaction coefficient related to properties of the filter media and sediments; L ($kg.m^{-2}$) is the total sediment loading per unit coverage area of biofilter; K_0 is the initial hydraulic conductivity before sediment loading; K is the final hydraulic conductivity of biofilter after sediment loading L.

Table 8.1. Overview of commonly established modeling equations for hydraulic conductivity.

Methodology	Expression	Effective grain size diameter (mm)
Hazen	$K = \frac{g}{v} \times 6 \times 10^{-4}[1 + 10(n - 0.26)] \times d_{10}^2$	0.1 – 3
Kozeny- Carman	$K = \frac{g}{v} \times 8.3 \times 10^{-3}[\frac{n^3}{(1-n)^2}] \times d_{10}^2$	≤ 3
Slitcher	$K = \frac{g}{v} \times 1 \times 10^{-2} n^{3.287} d_{10}^2$	0.01 – 5
Terzaghi	$K = \frac{g}{v} \times C_t \times (\frac{n - 0.13}{\sqrt[3]{1-n}})^2 \times d_{10}^2$	0.01 – 5
Clement et al (1996)	$K_{rel} = (1 - n_{rel})^p, p > 0$	N/A

Hydraulic conductivity equations are described elsewhere (Cabalar and Akbulut, 2016; Clement et al; 1996), with g is the acceleration due to gravity (m/s^2), n is the effective porosity (-), v is the kinematic viscosity of water, d_{10} is the effective particle diameter at which 10% of the sample is finer than this size, C_t is the sorting coefficient raging from $6.1 \times 10^{-3} < 10.7 \times 10^{-3}$; in this study, an average of C_t is used. $C_t = 8.4 \times 10^{-3}$; g = 9.8 m/s^2; $v = 10^{-6}$ m^2/s. Clement et al (1996) described the degree of clogging as the funcion of power relationship. The relative hydraulic conductivity, $K_{rel} = \frac{K}{K_0}$ is strongly related to the reduction of the relative porosity, $n_{rel} = \frac{n}{n_0}$. The subscript 0 represents the value of clean media before turbid water was injected.

8.3. Result and discussion

8.3.1. Quantity of particles released by the biofilter did not depend on biochar size

Stormwater infiltration released fine biochar particles from biofilters, but the total quantity of particles released was independent of the biochar size packed in the biofilters (Figure 8.3). Although the concentration of particles released by medium and large biochar columns was initially high (> 10 mg L^{-1}) due to the first-flush effect, the volume of the first sample was low compared to the total volume injected. Consequently, the total mass of biochar released initially has a significant effect on the total cumulative mass of biochar released. Thus, the cumulative mass released by the columns was not statistically different ($p > 0.05$). The columns with large, medium, and small biochar respectively released nearly 5.4±2.3, 4.6±1.3, and 4.4±0.6 mg of fine biochar particles after 5 consecutive rainfall events. The amount released was negligible compared to the amount of biochar that remained in the biofilters.

The particle released from compacted biofilters is a function of the total particle pool created during compaction due to the breaking of biochar. The fraction of the generated particle pool is available for transport based on the width of the pore path or hydraulic conductivity. Although the columns with large biochar had higher initial hydraulic conductivity (or high transport potential of broken particles), the pool of broken particles created during compaction could be low because of their limited fragmentation, as explained earlier. Similarly, the columns with small biochar would have a larger pool of broken particles created by fragmentation during compaction, but most of them could be trapped in the columns due to low hydraulic conductivity (or low transport potential). As the biochar size in the filter media had the opposite effect on the generation of biochar particles during compaction, and their transportation after compaction, the net amount of biochar particles mobilized became independent of biochar size in the filter media.

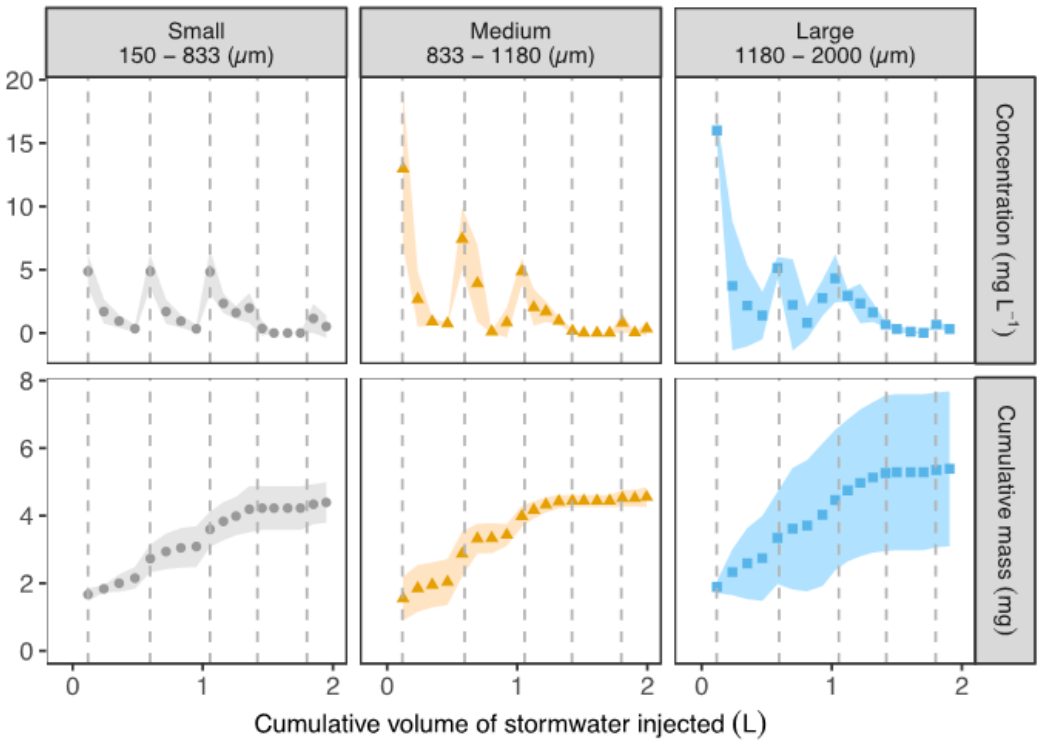

Figure 8.3. Release of particles from compacted biochar-sand biofilters during intermittent infiltration of stormwater. Points represent the mean value obtained from triplicated columns, and the shaded area represents one standard deviation over the mean.

8.3.2. Stormwater interaction with compacted biochar was affected by biochar size

Biochar size in compacted biofilters affected the biofilter's pore volume, but this effect was more apparent in columns with small biochar particles (Figure 8.4). The effective pore volume of the compacted biochar biofilters decreased with increases in biochar sizes (Figure 8.4-B). Compaction is expected to create a low permeable zone, where solute diffusion can become the dominant transport process. Flow interruption resulted in the highest relative bromide concentration in the effluent of the large biochar column, which confirms the presence of back diffusion of bromide from micropores in the low-permeable compacted zone to macropores. However, biochar size has no significant effect ($p > 0.05$) on the extent to which back diffusion of bromide occurred during flow interruption, indicating the amount of capillary pore space in internal pores of biochar particles or between particles did not change as a result of compaction.

While compaction breaks particles and decreases capillary pore space in internal pores, compaction also creates smaller particles and provides additional capillary space between adjacent broken particles. Thus, the net effect is no significant change in the volume of diffused region.

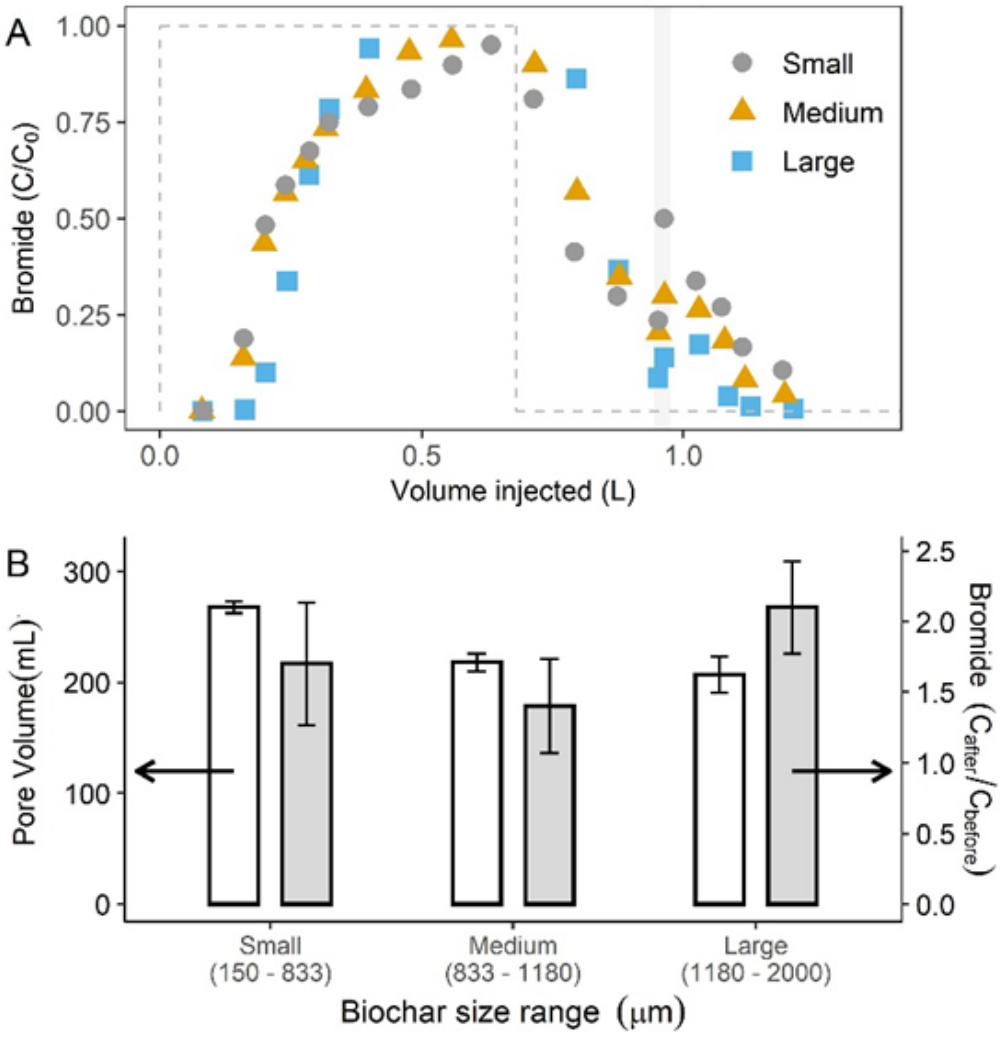

Figure 8.4. (A) Breakthrough curves of bromide (a conservative tracer) in columns packed with compacted sand and biochar of three size ranges: small, medium, and large biochar. The dashed line indicates the bromide concentration in the influent. Shaded vertical area indicates a flow interruption event. (B) White bar (left y-axis) indicates the effective pore volume of compacted columns, and grey filled bars (right y-axis) indicate the extent of bromide diffusion during flow interruption.

8.3.3. Biochar size affected the initial hydraulic conductivity clogging potential of compacted biofilters

The initial hydraulic conductivity of compacted biofilters was the lowest for columns with small biochar, although the hydraulic conductivities of columns with medium and large biochar were not significantly different (Figure 8.5). The hydraulic conductivity of all biofilters decreased with the increases in suspended sediment loading due to clogging (Figure 8.6-A), but the clogging rate was the highest for biofilters with small biochar particles. The sediment interaction coefficient (r) increased with decreases in biochar size, particularly D_{10} diameter where 10% of the distribution has a smaller particle size (Figure 8.6B (insert)).

Columns with small biochar had the lowest initial hydraulic conductivity, although an increase in biochar size from medium to large did not significantly increase the hydraulic conductivity. In columns with medium and large biochar particles, sand is the dominant fraction and smaller than biochar. Thus, their hydraulic conductivity is dominated by sand size, which does not change as a result of compaction. In contrast, the columns with biochar smaller than the size of sand were significantly affected by compaction because compaction lowered the biochar particle size and potentially displaced them into the pores between sand particles. A decrease in pore space and blockage of flow paths can effectively decrease the hydraulic conductivity of the columns. In our study, compaction coupled with pore blockage by broken biochar particles produced during compaction synergistically lowered the hydraulic conductivity. The extent to which inter-particle pores can be filled with broken particles depends on the relative size of broken biochar particles with respect to pore size. As small biochar has small gap between particles, they are more susceptible to clogging. Our result confirmed this hypothesis.

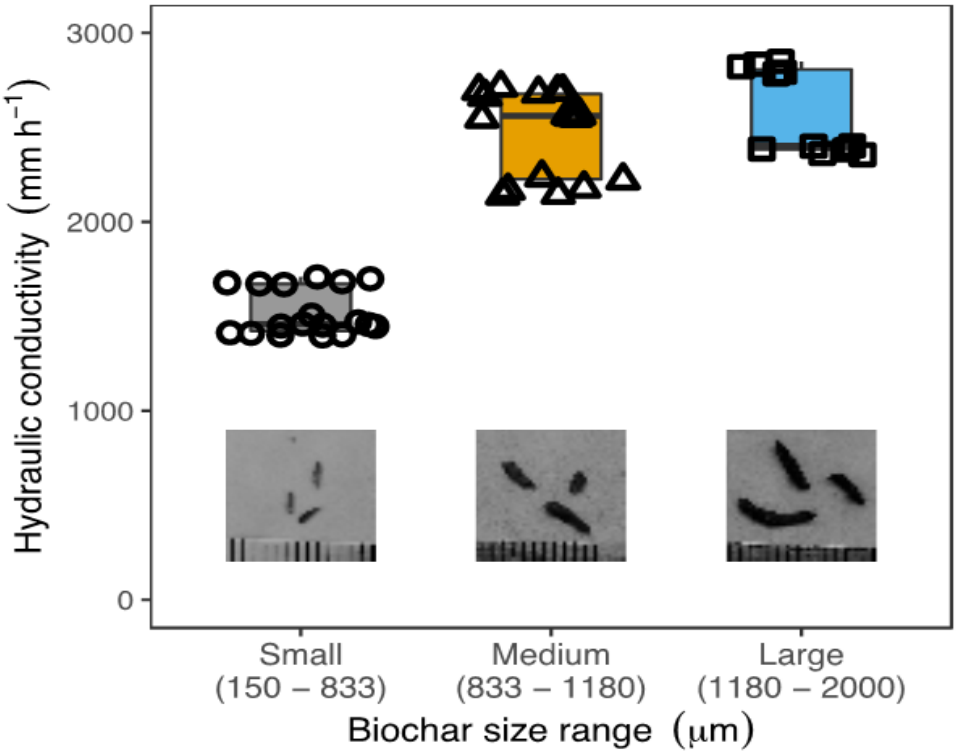

Figure 8.5. Hydraulic conductivity of columns packed with sand and biochar (5% by weight) of different size ranges. The picture in bottom show the sizes of different size biochar. Measurements were conducted in triplicated columns and repeated 6 times per column (n = 18).

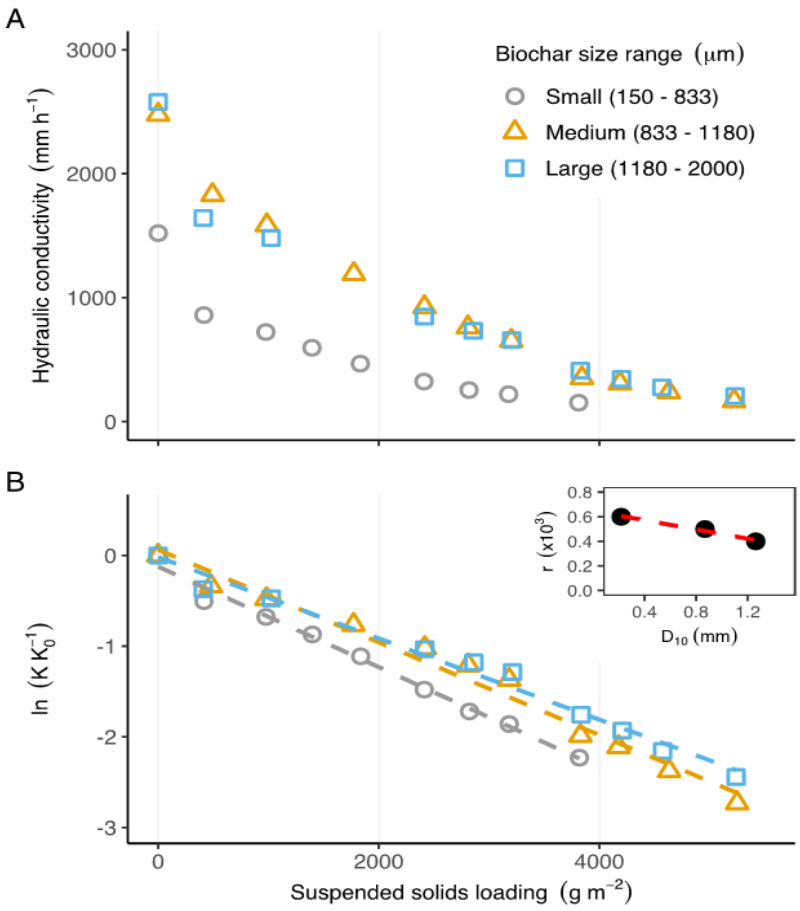

Figure 8.6. (A) Suspended solid loading exponentially decreased the saturated hydraulic conductivity of the compacted sand-biochar mixture. (B) Exponential model predicts relative changes in hydraulic rate (K/K_0) with an increase in the suspended solid loading, with slopes ® for columns with small, medium, and large biochar were 0.0006, 0.0005, and 0.0004, respectively. The insert in B shows the sediment interaction coefficient (r) increased with decreases in biochar size (D_{10}).

Fitting the hydraulic conductivity with changes in porosity of biofilters using previous models listed in Table 8.1, we showed that porosity change because of the deposition of suspended sediments could not predict the clogging of biofilters (Figure 8.7). The exponential empirical model predicted how fast a compacted column would clog based on the suspended sediment loading at the site. We showed that sediment interaction coefficient (r) increased with decreases in biochar size in the compacted biofilters. We also demonstrated that other traditional models that link saturated hydraulic conductivity with the porosity of filter media did not predict the changes in hydraulic conductivity with suspended sediment loading (Figure 8.7 and Figure 8.8). These models assume that the changes in porosity of biofilter should be uniform across the layers, which is unlikely in the stormwater biofilters. Compaction could particularly prevent penetration of suspended sediment beyond the top layer. The porosity of the top layer is expected to decrease rapidly compared to the rest of the filter media layers (Siriwardene et al. 2007; Hatt et al., 2008), and the change in the porosity in the top layer could dictate the overall hydraulic conductivity of the biofilters. Therefore, a minor alteration in the column's overall porosity due to the deposition of suspended sediment resulted in a severe change in hydraulic conductivity. We provided empirical parameters linking particle size (D_{10}) with the clogging rate. The model enabled the use of the filter media size to predict the hydraulic conductivity of biofilters receiving runoff containing suspended sediments. The suspended sediment loading on a biofilter is a function of annual rainfall and characteristic of the catchment. Thus, the clogging rate in a biofilter can be estimated using the mean concentration of suspended sediments in stormwater, annual runoff volume passing through the biofilters, and particle size (D_{10}) of the biofilter media.

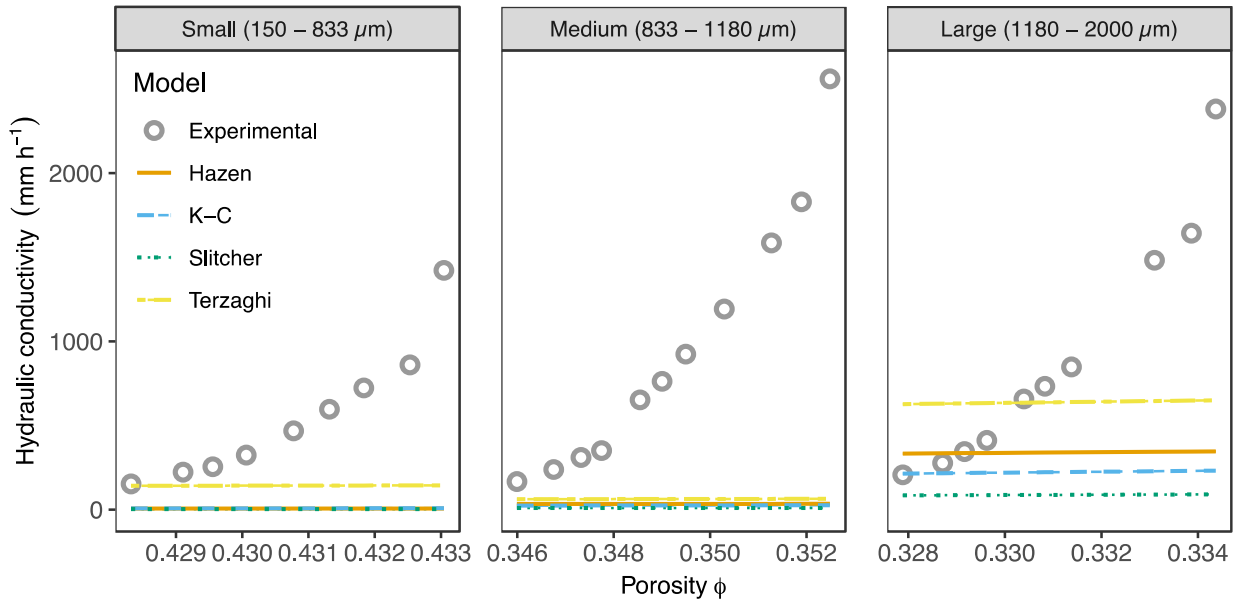

Figure 8.7. Change of hydraulic conductivity over the effective porosity because of deposition of suspended sediment predicted from analytic models compared to actual data from compaction experiment.

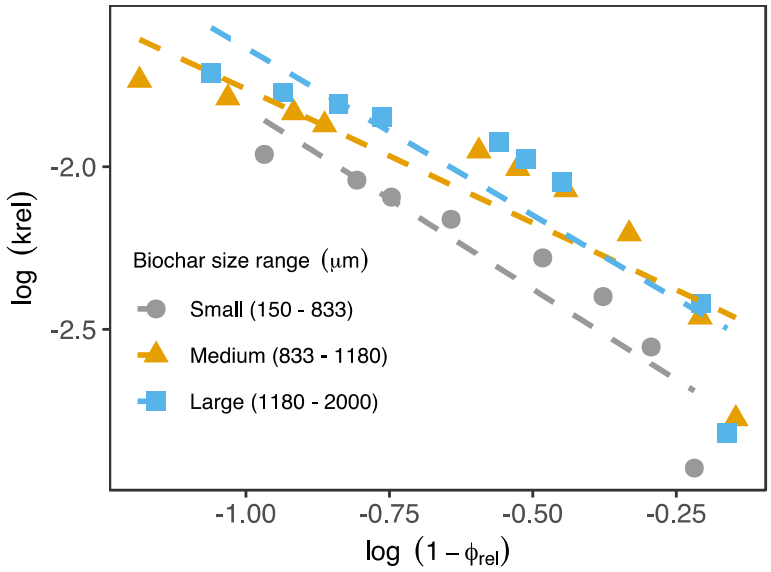

Figure 8.8. Power relationship between relative change in hydraulic conductivity and porosity, following models described elsewhere (Clement et al.,1996). Slope for small, medium and large biochar is -0.07743, -0.9751, -0.7793 respectively.

8.3.4. Mechanism of biochar breaking during compaction depended on biochar size

We compared the specific fluorescent intensity of the mobilized biochar particles with that of the packed biochar as a function of the relative size of biochar to examine the relative importance of biochar breaking mechanisms fragmentation vs. abrasion (Figure 8.9). In both columns, the specific fluorescent intensity of mobilized biochar was never more than that of packed biochar. A low dye concentration in mobilized biochar compared with packed column indicates abrasion is not the dominant biochar mechanism, and biochar predominantly breaks by fragmentation or splitting during compaction. In small biochar columns, the specific fluorescent intensity of mobilized biochar was significantly lower ($p < 0.05$) than that of packed biochar. In large biochar columns, the specific fluorescent intensity for both packed and mobilized biochar was not significantly different ($p > 0.05$). The result indicates that the extent of fragmentation depended on the relative size of biochar with sand.

The relative concentration of dye in mobilized biochar was significantly less than dye concentration on packed biochar. The result indicates that fragmentation by splitting, not abrasion, was the dominant mechanism of the breaking of small biochar particles under compaction. The fragmentation by splitting was less prominent for large biochar. Typically, abrasion occurs when particles slide against each other under compressive force. Biochar could slide into empty pores if the size of pores between sand or biochar particles was bigger than the sliding biochar. As a significant fraction of small biochar particles (150 – 833 μm) was still larger than the mean inter-particle pore size (373 μm) of sand (Trifunovic et al., 2018), abrasion was not found to be the dominant mechanism in our study. The lesser likelihood of "peeling" compared with "fracturing" during compaction suggests that compaction would expose new internal surface sites for contaminant adsorption, and the release of surface coating and any associate contaminants is less of a concern after compaction.

The fragmentation by splitting was less prominent for large biochar. We attributed the increased likelihood of biochar breaking by fragmentation in small biochar to a lower number of contact points between the biochar particles of interest and the adjacent particles that exert pressure on the biochar particle during compaction (Figure 8.9). The contact points transmit compaction energy into the biochar particles; thus, a lower number of contact points would result in higher tensile stress at each contact point (McDowell and Bono, 2013). As large biochar particles have a larger surface area than the small biochar particles, the number of contact points on large biochar particles would be greater than that of small biochar particles. Consequently, large biochar particles would experience less tensile stress at the points and be highly protected by numerous neighbors. In contrast, small particles could carry higher tensile stress at each contact point, leading to the formation of fractures through the biochar. This result is in agreement with the outcome of a previous study (Suescun-Florez et al., 2020) that showed that smaller sand particles break more than large sand particles. In summary, our result proved that the small particles are more likely to experience large tensile stress leading to their breaking under compaction primarily by fragmentation.

The mechanical properties of a biochar particle are dependent on temperature and residence time during pyrolysis, not particle size (Das et al., 2015). However, the mechanical properties of bulk biochar and sand mixture may vary with particle size based on the dissipation of compaction force due to either displacement of biochar particles into the pore space or breaking of biochar particles. Direct evidence using an optical microscope is not feasible because biochar and sand are opaque, and possible disturbance of biochar and sand grains during compaction and during sample preparation for optical imaging. Future studies should use a transparent column packed with transparent glass beads and biochar to observe the breaking

mechanism under compaction.Understanding biochar breakage under compaction helps Caltrans choose materials and practices that maintain biofilter performance and prevent clogging over time.

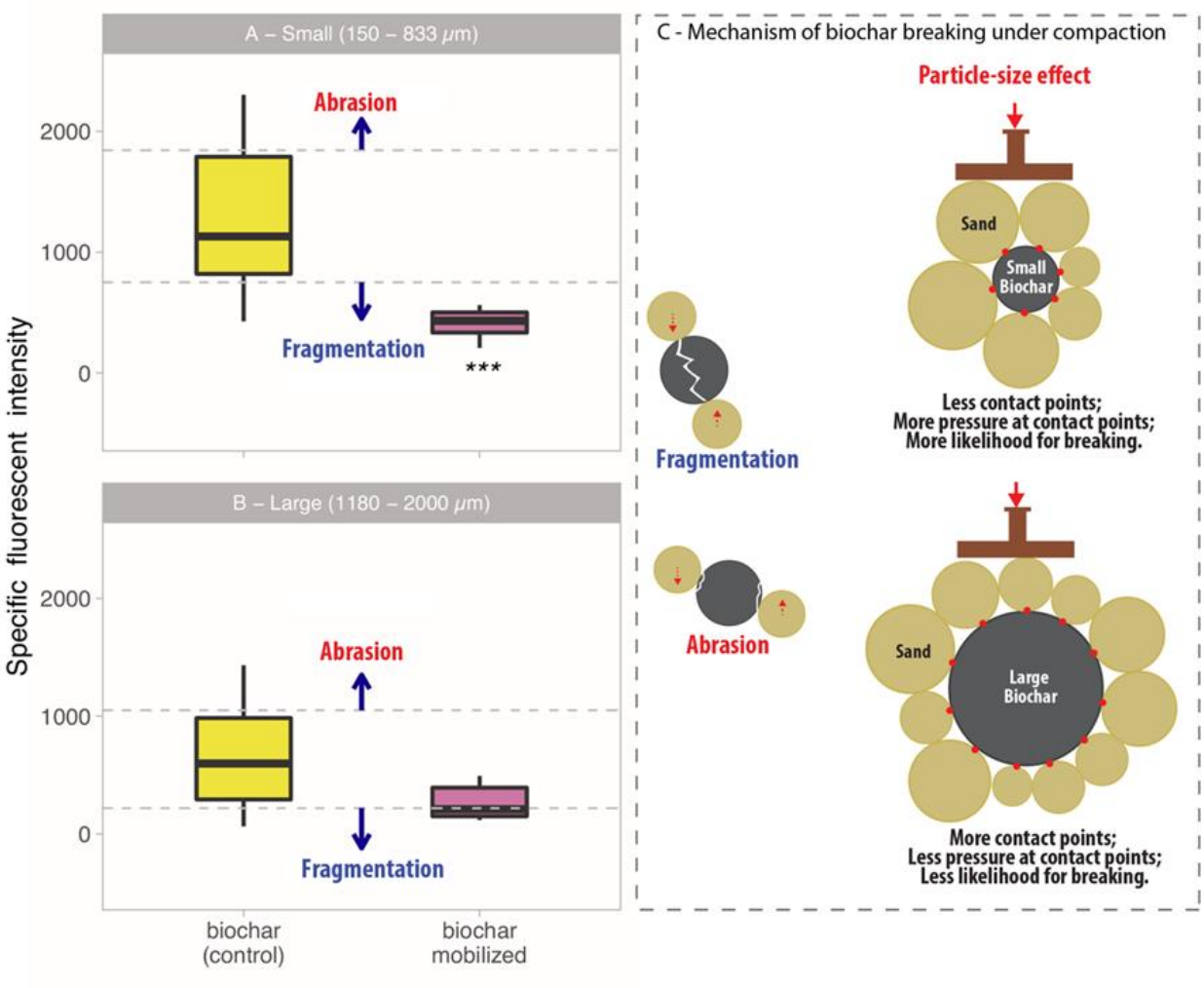

Figure 8.9. Specific fluorescent intensity of packed biochar (control) and mobilized biochar for (A) small biochar column and (B) large biochar column. The specific fluorescent intensity of packed biochar is higher than the mobilized biochar. *** indicates a p-value < 0.05. (C) The illustration shows the difference in compaction mechanisms (abrasion vs. fragmentation or splitting) and dissipation of compaction energy based on biochar size.

8.3.5. Removal of E. coli in compacted biofilters depended on initial biochar size.

E. coli removal capacity of compacted biofilters with different biochar sizes was similar initially, but the removal capacity of biofilters with medium and large biochar decreased with increases in exposure to contaminated stormwater (Figure 8.10). The removal in biofilters with small biochar particles mostly remained high: the effluent concentration was near the detection limit.

E. coli removal capacity of compacted biofilters decreased with increases in exposure to contaminated stormwater if the biochar size was similar to or greater than the size of sand. The removal remained consistently high in biofilters packed with biochar smaller than the size of sand, indicating an increase in overall surface sites by breaking of biochar particles lowered the exhaustion rate of biochar adsorption capacity. Hence, the creation of fine particles by compaction is expected to increase bacteria removal. Our results show that smaller biochar is more likely to break under compaction, thereby exposing more surfaces for adsorption. The biochar fragments can clog the pore paths and increase the removal of bacteria by straining. However, mobilization of fine biochar carrying *E. coli* from biofilters due to disturbance during compaction could increase the *E. coli* concentration in the effluent (Mohanty and Boehm, 2015). However, our study shows that the initial release of biochar particles is insignificant, and they are irrelevant after the initial first flush. Thus, the initial biochar particle size should be selected to optimize the effect of compaction on both infiltration and *E. coli* removal in biofilters.

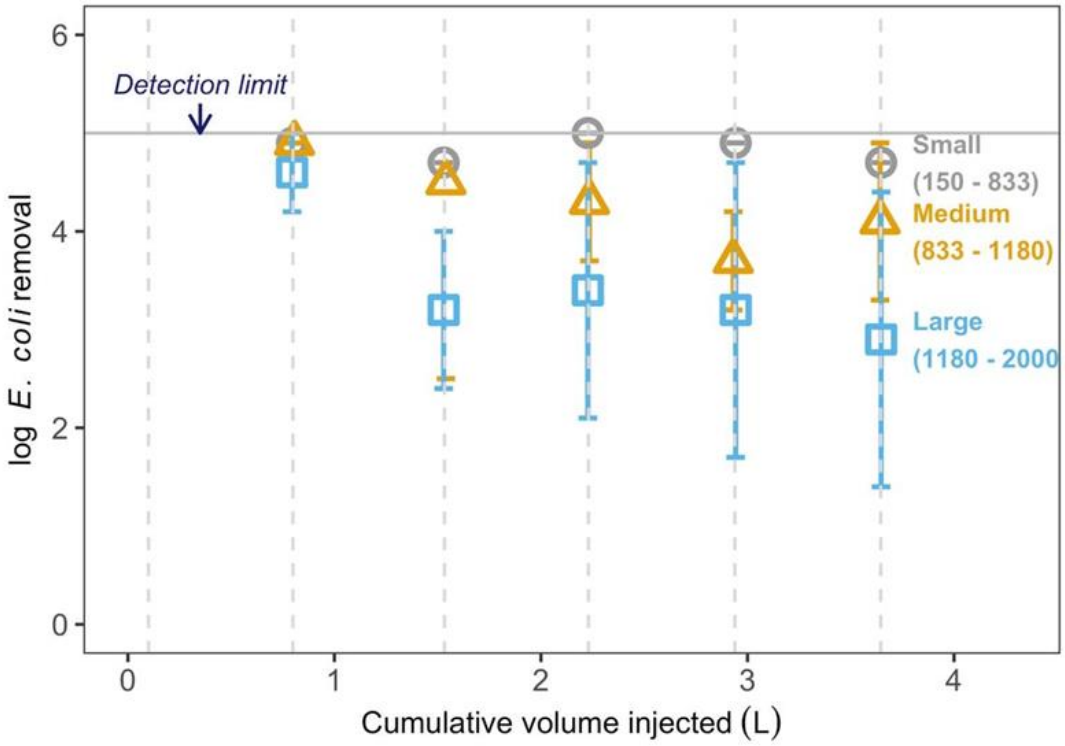

Figure 8.10. Removal of *E. coli* during rainfall events. The error bars indicate one standard deviation over the mean from triplicate columns with duplicate measurements per column (n = 6). The vertical dashed lines indicate the start of a rainfall event.

8.4. Summary and implications

The results revealed the importance of biochar size on their breaking by compaction, clogging rate, and bacterial removal in compacted biofilters.

- Under compaction, biochar is predominantly broken by fragmentation, not abrasion. The initial loss of biochar particles with infiltrating water was negligible, indicating the broken biochar particles were trapped in the packed columns.
- The hydraulic conductivity of compacted biochar columns exponentially decreased with increases in suspended sediment loading. The clogging rate was higher in the columns with small biochar. The empirical model based on suspended sediment loading and

particle size (D_{10}) of packed media could predict the clogging rate of compacted biochar-amended sand.

- The change in *E. coli* removal with an increase in stormwater loading was sensitive to biochar size in the compacted columns. The removal capacity of columns packed with biochar smaller than sand was consistently high, whereas the removal capacity of columns packed with biochar of the same size or larger than sand decreased with an increase in stormwater loading.

The results showed that the use of large-sized biochar could minimize the negative impact of compaction on infiltration capacity or clogging of biofilters, but their capacity to remove *E. coli* may decrease with time. Thus, the size of biochar should be optimized to limit clogging and increase pathogen removal.

8.5. References

Batey, T., & McKenzie, D. C. (2006). Soil compaction: Identification directly in the field. Soil Use and Management, 22(2), 123–131. https://doi.org/10.1111/j.1475-2743.2006.00017.x

Boehm, A. B., Bell, C. D., Fitzgerald, N. J. M., Gallo, E., Higgins, C. P., Hogue, T. S., Luthy, R. G., Portmann, A. C., Ulrich, B. A., & Wolfand, J. M. (2020). Biochar-augmented biofilters to improve pollutant removal from stormwater – can they improve receiving water quality? Environmental Science: Water Research & Technology. https://doi.org/10.1039/D0EW00027B

Brown, J. S., Stein, E. D., Ackerman, D., Dorsey, J. H., Lyon, J., & Carter, P. M. (2013). Metals and bacteria partitioning to various size particles in Ballona creek storm water runoff. Environmental Toxicology and Chemistry, 32(2), 320–328. https://doi.org/10.1002/etc.2065

Brusseau, M. L., Hu, Q., & Srivastava, R. (1997). Using flow interruption to identify factors causing nonideal contaminant transport. Journal of Contaminant Hydrology, 24(3), 205–219. https://doi.org /10.1016/S0169-7722(96)00009-5

California Department of Transportation. (2017). Highway Design Manual Sixth Edition. Retrieved from: https://dot.ca.gov/-/media/dot-media/programs/design/documents/hdm-complete-14dec2018.pdf

Das, O., Sarmah, A. K., & Bhattacharyya, D. (2015). Structure–mechanics property relationship of waste derived biochars. Science of the Total Environment, 538, 611-620. https://doi.org/10.1016/j.scitotenv.2015.08.073

Davis, A. P. (2005). Green Engineering Principles Promote Low-impact Development. Environmental Science & Technology, 39(16), 338A-344A. https://doi.org/10.1021/es053327e

Ding, L., Tan, W., Xie, S., Mumford, K., Lv, J., Wang, H., Fang, Q., Zhang, X., Wu, X., & Li, M. (2018). Uranium adsorption and subsequent re-oxidation under aerobic conditions by

Leifsonia sp. - Coated biochar as green trapping agent. Environmental Pollution, 242, 778–787. https://doi.org/10.1016/j.envpol.2018.07.050

Ghavanloughajar, M., Valenca, R., Le, H., Rahman, M., Borthakur, A., Ravi, S., Stenstrom, M.K. and Mohanty, S. (2020) Compaction conditions affect the capacity of biochar-amended sand filters to treat road runoff. Science of the Total Environment, 139180. https://doi.org/10.1016/j.scitotenv.2020.139180.

Głąb, T., Palmowska, J., Zaleski, T., & Gondek, K. (2016). Effect of biochar application on soil hydrological properties and physical quality of sandy soil. Geoderma, 281, 11–20. https://doi.org /10.1016/j.geoderma.2016.06.028

Gregory, J. H., Dukes, M. D., Jones, P. H., & Miller, G. L. (2006). Effect of urban soil compaction on infiltration rate. Journal of Soil and Water Conservation, 61(3), 117–124. https://www.jswconline.org/content/61/3/117

Hameed, R., Cheng, L., Yang, K., Fang, J., & Lin, D. (2019). Endogenous release of metals with dissolved organic carbon from biochar: Effects of pyrolysis temperature, particle size, and solution chemistry. Environmental Pollution, 255, 113253. https://doi.org/10.1016/j.envpol.2019.113253

Hatt, B. E., Siriwardene, N., Deletic, A., & Fletcher, T. D. (2006). Filter media for stormwater treatment and recycling: The influence of hydraulic properties of flow on pollutant removal. Water Science and Technology, 54(6–7), 263–271. https://doi.org/10.2166/wst.2006.626

Hatt, Belinda E., Fletcher, T. D., & Deletic, A. (2008). Hydraulic and Pollutant Removal Performance of Fine Media Stormwater Filtration Systems. Environmental Science & Technology, 42(7), 2535–2541. https://doi.org/10.1021/es071264p

Herath, H. M. S. K., Camps-Arbestain, M., & Hedley, M. (2013). Effect of biochar on soil physical properties in two contrasting soils: An Alfisol and an Andisol. Geoderma, 209–210, 188–197. https://doi.org/10.1016/j.geoderma.2013.06.016

Kandra, Harpreet Singh, Deletic, A., & McCarthy, D. (2014). Assessment of Impact of Filter Design Variables on Clogging in Stormwater Filters. Water Resources Management, 28(7), 1873–1885. https://doi.org/10.1007/s11269-014-0573-7

Kumar, H., Ganesan, S. P., Bordoloi, S., Sreedeep, S., Lin, P., Mei, G., Garg, A., & Sarmah, A. K. (2019). Erodibility assessment of compacted biochar amended soil for geo-environmental applications. Science of The Total Environment, 672, 698–707. https://doi.org/10.1016/j.scitotenv.2019.03.417

Lau, A. Y. T., Tsang, D. C. W., Graham, N. J. D., Ok, Y. S., Yang, X., & Li, X. (2017). Surface-modified biochar in a bioretention system for Escherichia coli removal from stormwater. Chemosphere, 169, 89–98. https://doi.org/10.1016/j.chemosphere.2016.11.048

Le Coustumer, S., & Barraud, S. (2007). Long-term hydraulic and pollution retention performance of infiltration systems. Water Science and Technology, 55(4), 235–243. https://doi.org/10.2166 /wst.2007.114

Le Coustumer, Sébastien, Fletcher, T. D., Deletic, A., Barraud, S., & Lewis, J. F. (2009). Hydraulic performance of biofilter systems for stormwater management: Influences of design and operation. Journal of Hydrology, 376(1), 16–23. https://doi.org/10.1016/j.jhydrol.2009.07.012

Liu, Z., Dugan, B., Masiello, C. A., Barnes, R. T., Gallagher, M. E., & Gonnermann, H. (2016). Impacts of biochar concentration and particle size on hydraulic conductivity and DOC leaching of biochar– sand mixtures. Journal of Hydrology, 533, 461–472. https://doi.org/10.1016/j.jhydrol.2015.12.007

Liu, Z., Dugan, B., Masiello, C. A., & Gonnermann, H. M. (2017). Biochar particle size, shape, and porosity act together to influence soil water properties. PLOS ONE, 12(6), e0179079. https://doi.org /10.1371/journal.pone.0179079

Lu, L., & Chen, B. (2018). Enhanced bisphenol A removal from stormwater in biochar-amended biofilters: Combined with batch sorption and fixed-bed column studies. Environmental Pollution, 243, 1539–1549. https://doi.org/10.1016/j.envpol.2018.09.097

McDowell, G. R., & de Bono, J. P. (2013). On the micro mechanics of one-dimensional normal compression. Géotechnique, 63(11), https://doi:10.1680/geot.12.P.041

Mohanty, S.K. and Boehm, A.B. (2014). Escherichia coli Removal in Biochar-Augmented Biofilter: Effect of Infiltration Rate, Initial Bacterial Concentration, Biochar Particle Size, and Presence of Compost. Environmental Science & Technology 48(19), 11535-11542. https://doi.org/10.1021/es5033162.

Mohanty, S.K. and Boehm, A.B. (2015). Effect of weathering on mobilization of biochar particles and bacterial removal in a stormwater biofilter. Water research, 85, pp.208-215. https://doi.org/10.1016/j.watres.2015.08.026.

Mohanty, S. K., Cantrell, K. B., Nelson, K. L., & Boehm, A. B. (2014). Efficacy of biochar to remove Escherichia coli from stormwater under steady and intermittent flow. Water Research, 61, 288–296. https://doi.org/10.1016/j.watres.2014.05.026.

Mohanty, S. K., Valenca, R., Berger, A. W., Yu, I. K. M., Xiong, X., Saunders, T. M., & Tsang, D. C. W. (2018). Plenty of room for carbon on the ground: Potential applications of biochar for stormwater treatment. Science of The Total Environment, 625, 1644–1658. https://doi.org/10.1016 /j.scitotenv.2018.01.037

Phipps, D. W., Jr., Lyon, S., & Hutchinson, A. S. (2007). Development of a Percolation Decay Model to Guide Future Optimization of Surface Water Recharge Basins. In P. Fox (Ed.), Management of aquifer recharge for sustainability, Proceedings of 6th International Symposium on Managed Aquifer Recharge of Groundwater (pp. 433-466). Phoenix: Acacia Publishing.

Pitt, R. E., Chen, S.-E., Clark, S., Lantrip, J., Ong, C. K., & Voorhees, J. (2003). Infiltration Through Compacted Urban Soils and Effects on Biofiltration Design. Journal of Water Management Modeling. https://doi.org/10.14796/JWMM.R215-12

Reddy Krishna R., Xie Tao, & Dastgheibi Sara. (2014). Evaluation of Biochar as a Potential Filter Media for the Removal of Mixed Contaminants from Urban Storm Water Runoff.

Journal of Environmental Engineering, 140(12), 04014043. https://doi.org/10.1061/(ASCE)EE.1943-7870.0000872

Reza, M. T., Lynam, J. G., Vasquez, V. R., & Coronella, C. J. (2012). Pelletization of biochar from hydrothermally carbonized wood. Environmental Progress & Sustainable Energy, 31(2), 225–234. https://doi.org/10.1002/ep.11615

Sasidharan, S., Torkzaban, S., Bradford, S. A., Kookana, R., Page, D., & Cook, P. G. (2016). Transport and retention of bacteria and viruses in biochar-amended sand. The Science of the Total Environment, 548–549, 100–109. https://doi.org/10.1016/j.scitotenv.2015.12.126

Shang, J., Flury, M., Chen, G. and Zhuang, J. (2008) Impact of flow rate, water content, and capillary forces on in situ colloid mobilization during infiltration in unsaturated sediments. Water Resources Research 44(6). https://doi.org/10.1029/2007WR006516

Shaneyfelt, K. M., Anderson, A. R., Kumar, P., & Hunt, W. F. (2017). Air quality considerations for stormwater green street design. Environmental Pollution, 231, 768–778. https://doi.org/10.1016/j.envpol.2017.08.081

Shrestha, P., Hurley, S. E., & Wemple, B. C. (2018). Effects of different soil media, vegetation, and hydrologic treatments on nutrient and sediment removal in roadside bioretention systems. Ecological Engineering, 112, 116–131. https://doi.org/10.1016/j.ecoleng.2017.12.004

Siriwardene, N. R., Deletic, A., & Fletcher, T. D. (2007). Clogging of stormwater gravel infiltration systems and filters: Insights from a laboratory study. Water Research, 41(7), 1433–1440. https://doi.org/10.1016/j.watres.2006.12.040

Suescun-Florez, E., Iskander, M., & Bless, S. (2020). Evolution of particle damage of sand during axial compression via arrested tests. Acta Geotechnica, 15(1), 95–112. https://doi.org/10.1007 /s11440-019-00892-w

Sun, Y., Chen, S. S., Lau, A. Y. T., Tsang, D. C. W., Mohanty, S. K., Bhatnagar, A., Rinklebe, J., Lin, K.-Y. A., & Ok, Y. S. (2020). Waste-derived compost and biochar amendments

for stormwater treatment in bioretention column: Co-transport of metals and colloids. Journal of Hazardous Materials, 383, 121243. https://doi.org/10.1016/j.jhazmat.2019.121243

Trifunovic, B., Gonzales, H. B., Ravi, S., Sharratt, B. S., & Mohanty, S. K. (2018). Dynamic effects of biochar concentration and particle size on hydraulic properties of sand. Land Degradation & Development, 29(4), 884–893. https://doi.org/10.1002/ldr.2906

Valenca, R., Ramnath, K., Dittrich, T. M., Taylor, R. E., & Mohanty, S. K. (2020). Microbial quality of surface water and subsurface soil after wildfire. Water Research, 175, 115672. https://doi.org /10.1016/j.watres.2020.115672

Wang, H., Xin, J., Zheng, X., Li, M., Fang, Y., & Zheng, T. (2020). Clogging evolution in porous media under the coexistence of suspended particles and bacteria: Insights into the mechanisms and implications for groundwater recharge. Journal of Hydrology, 582, 124554. https://doi.org/10.1016 /j.jhydrol.2020.124554

Wang, L., Lyon, J., Kanehl, P., & Bannerman, R. (2001). Impacts of Urbanization on Stream Habitat and Fish Across Multiple Spatial Scales. Environmental Management, 28(2), 255–266. https://doi.org/10.1007/s0026702409

Williamson, R. B., & Water Quality Centre (1993). Urban runoff data book: A manual for the preliminary evaluation of urban stormwater impacts on water quality (2nd ed). Hamilton N.Z. : Water Quality Centre, Ecosystems Division, National Institute of Water and Atmospheric Research. https://trove.nla.gov.au/version/12761345

Wong, J. T. F., Chen, Z., Wong, A. Y. Y., Ng, C. W. W., & Wong, M. H. (2018). Effects of biochar on hydraulic conductivity of compacted kaolin clay. Environmental Pollution, 234, 468–472. https://doi.org/10.1016/j.envpol.2017.11.079

Yu, F. (2019). Particle breakage in granular soils: A review. Particulate Science and Technology, 0(0), 1–10. https://doi.org/10.1080/02726351.2019.1666946

Zhang, X., & Baudet, B. A. (2013). Particle breakage in gap-graded soil. Géotechnique Letters, 3(2), 72–77. https://doi.org/10.1680/geolett.13.00022

9 Task 3d: Testing the capacity of expanded shale, clay, and slate (ESCS) to remove heavy metals and bacterial pollutants.

9.1 Background

The bulking agent such as sand has limited capacity to remove metals and pathogens or pathogen indicators in urban stormwater, which is one of the leading causes of surface water and groundwater impairment (Alam et al., 2021; Galfi et al., 2016; McBride et al., 2013). To improve removals, stormwater treatment systems such as biofilters have been amended with adsorbents (Ghavanloughajar et al., 2021; Mohanty et al., 2014; Valenca et al., 2021b), but those adsorbents greatly reduced hydraulic conductivity under compaction. In contrast, expanded shale, clay, and slate (ESCS) aggregates, a novel light-weight amendment, has been used to as bulking agent in stormwater application. They could remove a wide range of stormwater pollutants due to their lightweight and high removal capacity of many stormwater pollutants (Dordio and Carvalho, 2013; Kalhori et al., 2013; Malakootian et al., 2009; Nkansah et al., 2012). The lightweight media, which can be produced at a wide grain size distribution, has the advantage over others to be used in green roofs or other stormwater infrastructure based on both infiltration and treatment needs. ESCS can replace sand, the most common amendment used for hydraulic control because the aggregate size can be chosen based on design need. They have additional advantages over sand because of lower freight and handling costs with much higher pollutant removal capacity. Thus, they can be used in rain gardens below the root zone to allow root growth, in a filter strip near the parking lot to permit rapid drainage of water and remove pollutants, and as filtering fills above the collection pipe in the infiltration basin. Different aggregate sizes can be used in permeable pavement. Yet, to what extent they can remove both metals and bacterial pollutants from road runoff, and whether the aging would affect their removal is unknown.

9.1.1 Objective

This study aims to test the bacterial removal capacity of ESCS aggregate under chemical aging condition, which is expected to occur in roadside environments.

9.1.2 Hypothesis

Aging of ESCS media with heavy metals naturally present in stormwater could improve their bacterial removal capacity with time. To test this hypothesis, biofilters amended with ESCS aggregates were aged by injecting stormwater contaminated with metals and compared their capacity to remove *E. coli* with unaged biofilters. The results will help improve the understanding of how the aging of biofilter media with co-contaminants could affect long-term pathogen removals.

9.2 Materials and Methods

9.2.1 Stormwater Preparation

Natural stormwater was used to simulate the aging of biofilter media. Natural stormwater was collected from Ballona Creek, Los Angeles, and autoclaved before use to remove any microorganisms to accurately estimate *E. coli* removal by biofilter media. Dry-weather flow was used as the base water matrix and spiked with pollutants to simulate roadway runoff, since stormwater was not available year-round. The stormwater naturally contained very low concentrations of Pb (below detection limit, 0.01 $\mu g\ L^{-1}$), Cu (1.8 $\mu g\ L^{-1}$), and Zn (8.3 $\mu g\ L^{-1}$) (Table 9.1**)**, which was not sufficient to simulate the long-term loading of metals within the experimental time scale. Therefore, stock solutions containing $CuCl_2$, $ZnCl_2$, and $Pb(NO_3)_2$ (Fisher Scientific) were spiked into the natural stormwater to raise the influent concentration to 500 $\mu g\ L^{-1}$ for all metals. The concentration was an order of magnitude higher than typically found in stormwater (Tirpak et al., 2021) to simulate total metal loading in a few years in the field during the laboratory experiments that had a short duration. Based on the International

Stormwater Best Management Practices (BMP) database, which aggregates data globally from different locations, these three metals were selected because they are typically found at higher concentrations than many other metals in stormwater and they exhibit a wide range of affinity to amendments (Tirpak et al., 2021). Among other metals that are present at high concentrations are Ni and Cr. While Ni exhibits similar adsorption characteristics as Zn (Tirpak et al., 2021), Cr exists as metals anions. Thus, the adsorption of negatively charged metalloids can have an opposite effect than positively charged metal ions on the surface charge of the amendment similar to other anions such as phosphate (Appenzeller et al., 2002). However, metal anion concentrations are present at a much lower concentration than metal cations (Tirpak et al., 2021), and can be outcompeted by other negatively charged species such as phosphate (Chowdhury and Yanful, 2010). Thus, we did not test the effect of metalloids on pathogen removal in this study.

Table 9.1. Properties of the stormwater

Properties	**Stormwater**
pH	8.52 ± 0.005
Electrical conductivity (μS cm^{-1})	1132.7 ± 2.05
Pb (ug L^{-1})	Below detection limit
Cu (ug L^{-1})	1.8
Zn (ug L^{-1})	8.3

To test the antibacterial effect of biofilter media with adsorbed metals, a kanamycin-resistant strain of *Escherichia coli K12*, a pathogen indicator was used (Ghavanloughajar et al., 2020; Mohanty et al., 2014). *E. coli* were grown in a Luria-Bertani broth solution to a stationary phase, extracted by centrifugation, washed twice using a phosphate buffer saline (PBS) solution to remove the broth. A small volume of stock E. coli concentrated was spiked into the natural stormwater and their concentration was measured by spread plate technique. The mean

concentration of *E. coli* in influent was measured to be $2.8 \pm 0.3 \times 10^5$ CFU mL^{-1}. The concentration is high enough to test the hypothesis and within the range found in the stormwater (Grebel et al., 2013).

9.2.2 Model biofilter design

In this study, model biofilters without vegetation were used to estimate the *E. coli* removal capacity of biofilter media without interferences from the confounding factors. Plants' effect on pathogen removal is limited, and any changes in pathogen removal in vegetated biofilters have been attributed to plants' ability to alter the hydraulic retention time (Peng et al., 2016) and moisture content in the filter media (Li et al., 2012). Nevertheless, this reductionist approach without using plants has been used in numerous previous studies to examine the mechanisms of pollutant removal in the biofilters (Hatt et al., 2008; Mohanty et al., 2014; Sun et al., 2020).

The model biofilters were designed by packing a mixture of quartz sand (ASTM 20-30, Humboldt Mfg Co.) and ESCS aggregate (Arcosa) at a ratio of 7:3 in PVC columns (2.54 cm ID x 30 cm length). Compost or soil was not used in the mixture and plants on top to distinguish the role of ESCS pathogen adsorption or removal. First, a drainage layer was created using pea gravel up to 6 cm height with a 100 μm nylon membrane on top to prevent biofilter media to get into the drainage layer. Then, sand and ESCS mixture was added in incremental layers to a total filter media depth of 15 cm. A 2-cm layer of pea gravel was added on top to prevent the resuspension or disturbance of the media particles during the stormwater application. Total six columns were packed. Of which, three columns were aged with metals and designated as aged biofilters, whereas the other three columns were exposed to stormwater without metals and designated as unaged biofilters (**Error! Reference source not found.**).

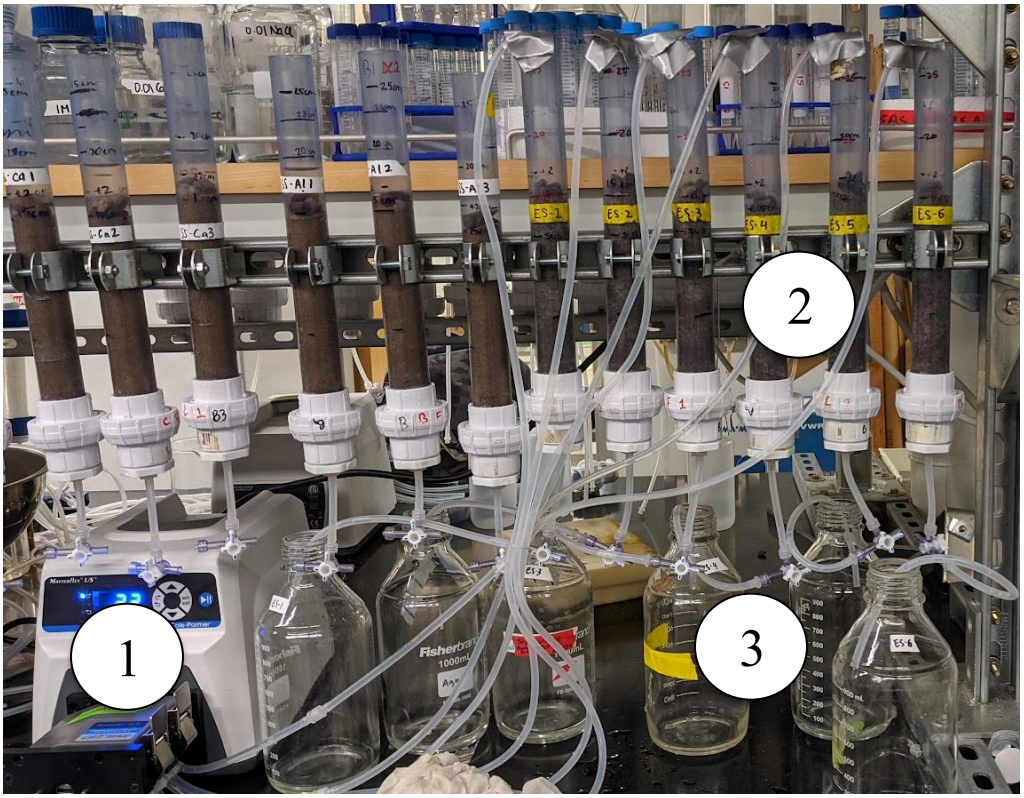

Figure 9.1. Experimental setup showing the pump (1) pumping stormwater into the columns (2), the effluent were then collected in the bottles (3).

To ensure consistent packing of all biofilters, the bulk density of the packed media was estimated by dividing the weight of the media with the inner volume of the column and comparing between biofilters (Table 9.2). The pore volume (PV) was measured by subtracting the weight of the dry media biofilters from the weight of the saturated media biofilters (Borthakur et al., 2021). The residual PV was calculated by draining the saturated biofilters under gravity and subtracting the weight of the dry media biofilters from the weight of the drained biofilters. The hydraulic conductivity of the media was measured using a falling head method (Ghavanloughajar et al., 2020).

Table 9.2. Properties of the ESCS media columns

Properties	Aged columns	Unaged columns
Bulk Density (g/cm^3)	1.54 ± 0.05	1.52 ± 0.03
Porosity (%)	29.8 ± 1.3	32.1 ± 0.3
Residual pore volume (mL)	7.3 ± 1.4	9.2 ± 0.4
Hydraulic conductivity (cm/sec)	0.02 ± 0.002	0.02 ± 0.002

9.2.3 Aging of ESCS media with heavy metals

The experiments were conducted in 5 phases: conditioning, aging, flushing, leaching, and *E. coli* injection. Experiments in the first four phases were designed to age biofilters by injecting stormwater with or without metals, whereas the last phase was designed to compare the *E. coli* removal capacities of aged and unaged biofilters. All six biofilters were first conditioned by injecting stormwater at a constant flow rate of 1 mL min^{-1} (11.8 cm h^{-1}) for 24 h to equilibrate the filter media with the stormwater until the effluent pH and ionic strength did not change (Borthakur et al., 2021). To age biofilter media with metals, 500 PV of stormwater spiked with metals was applied on the top of the biofilters at 11.8 cm h^{-1} for 10 days, and the effluent samples were collected at the bottom to measure for heavy metal concentration. It was estimated that the aging phase exposed 7.2 mg of each heavy metal to biofilter media. This amount is equivalent to 2.1 years of aging of biofilter receiving stormwater with similar metal constituents as Ballona Creek (19.9 ± 29.0 µg L^{-1} Cu, 4.4 ± 12.7 µg L^{-1} Pb, and 83.3 ± 241.2 µg L^{-1} Zn (Stein and Tiefenthaler, 2005) from an acre of catchment area in Los Angeles with an annual rainfall of 379.2 mm yr^{-1}. It should be noted that aging in field conditions can be more complex, and the speciation of adsorbed metals and metal oxides formed during aging could vary widely based on site conditions and time passed after the adsorption (Li et al., 2019; Meng et al., 2018).

Nevertheless, the experimental design tested the effect of adsorbed metal in the short term without accounting for changes that may occur in natural conditions.

After injection of metal-contaminated stormwater, the contaminated biofilters were then flushed with 50 PV of the natural stormwater without spiked metals, particularly to remove any unabsorbed heavy metals from the pore water. To estimate the leachability of the adsorbed metals, the flow was stopped for 24 h to allow time for loosely bound metal to desorb back into the pore water, and then 8 PV uncontaminated stormwater was injected to estimate the percentage of the adsorbed metals leached into pore water. To prepare the unaged biofilters or biofilters without adsorbed metals, the experiment was repeated by injecting natural stormwater without adding heavy metals into other triplicate biofilters. Effluent samples in all phases were analyzed for heavy metals by using Inductively Coupled Plasma- Optical Emission Spectroscopy (ICP-OES). The samples were centrifuged at 5000 rotation per minute (rpm) for 15 minutes to remove any particles, and the supernatant was acidified with nitric acid to lower pH below 1 before analysis.

9.2.4 Effect of aging on E. coli removal in biofilters

Aged and unaged biofilters were subjected to intermittent infiltration of stormwater contaminated with *E. coli*. Heavy metals were not added to influent when the experiments were carried out for testing of *E. coli* removal capacity of aged and unaged media because dissolved metals can inhibit or inactivate the *E. coli* in stormwater and may overestimate their removal of ESCS media. In each injection, 8 PV of stormwater with $2.8 \pm 0.3 \times 10^5$ CFU mL^{-1} of *E. coli* was applied on the top of the biofilters at 11.8 cm h^{-1} for 3.3 h, and the effluent samples were collected from the bottom at two fractions following the procedure described elsewhere (Ghavanloughajar et al., 2021). The “first flush” sample fraction consisted of the first 5-10 mL of

effluent sample collected, which contained the residual water from the previous infiltration event. The second fraction consisted of the stormwater injected during the infiltration events (179.9 ± 7.6 mL). Thus, the *E. coli* concentration in the first flush indicates the fate of *E. coli* in the pore water during the antecedent drying period, whereas the concentration in the second sample presents the overall bacterial removal capacity of the biofilter during the infiltration event. After each infiltration, the biofilters were drained by gravity and left at room temperature (22 °C) for a specific drying duration until the next infiltration event. The process was repeated twice to simulate removal at a specific drying duration. To simulate the effect of varying drying duration on *E. coli* removal or potential growth or inactivation of *E. coli* in biofilters, drying durations of 1, 2, 4, and 7 days were simulated, where two injection events were carried out corresponding to each drying duration. The *E. coli* concentration in the effluent samples was measured using a spread plate technique described elsewhere (Mohanty et al., 2013).

9.2.5 Heavy metal and E. coli removal by ESCS media

To examine the binding sites on ESCS media for the adsorption of heavy metals, ESCS media with and without adsorbed metals were characterized using Fourier Transform Infrared Spectroscopy (FTIR). 0.5 g of finely grounded ESCS media (size less than 75 μm) mixed with 40 mL of synthetic stormwater spiked with 25 g L^{-1} Cu, Pb, and Zn in separate 50 mL centrifuge tubes for 48 hours. An abnormally high concentration of heavy metals was used because the heavy metals need to constitute at least 5% of the total sample volume to be detectable in the FTIR spectra. 0.5 g of finely grounded ESCS media was also exposed to 40 mL synthetic stormwater without any heavy metals as a control. The ESCS media was then dried along with Potassium Bromide (KBr, Acros Organics) for 18 hours. The ESCS powders were then mixed with KBr and pelletized using a hydraulic press at 8000-10000 psi. These pellets were then

analyzed using a JASCO Model 420 FTIR instrument. To evaluate any change in surface charge of the ESCS media after heavy metal adsorption, the zeta potentials of ESCS media with and without adsorbed metals were measured at the pH (8.5) of stormwater. 0.5 g of finely ground ESCS media of size less than 45 μm were added to two sets of centrifuge tubes containing 40 mL synthetic stormwater. One set was spiked with 300 mg L^{-1} of Pb, Cu, and Zn, and both the sets were shaken in a wrist action shaker for 48 hours. The tubes were then centrifuged at 1000×g for 1 min to settle all particles larger than 1 μm. The supernatant from both the tubes was then extracted and the pH of the supernatant was adjusted to 8.5 using NaOH and HCl. The zeta potential of the supernatant was measured using a Brookhaven zetaPALS instrument. Note that only particles of size less than 1 μm were analyzed because particles of size greater than 1 μm gave erroneous results in the instrument.

E. coli can be removed by aged ESCS media through various mechanisms: adsorption to aged ESCS surface, inactivation of *E. coli* by dissolved metals leached from aged ESCS, and inactivation of *E. coli* by the adsorbed metals on aged ESCS media. To distinguish the role of each process, batch sorption studies were used. To estimate removal by ESCS media without metals, 4 g of ESCS media without metals (termed as unaged media) was mixed with 40 mL of stormwater with spiked *E. coli*, and the change in concentration in water samples was measured. To estimate the removal by aged ESCS, 4 g of ESCS was mixed in triplicated 50-mL centrifuge tubes for 48 hours using a wrist action shaker with 40 mL synthetic stormwater (10 mM NaCl) spiked with 300 mg L^{-1} of Pb, Cu, and Zn and adjusted to the same pH and electrical conductivity as the natural stormwater (Ghavanloughajar et al., 2020). This simulated exposure of 12 mg of each heavy metal to 4 g of ESCS media, which corresponded to about 20 days of heavy metal injection in the biofilter experiments. The tubes were centrifuged at 5000 RPM for

15 minutes, and the supernatants were analyzed for metal concentration to estimate the dissolved and adsorbed metal concentrations. The contaminated media settled in the tube were washed thrice with synthetic stormwater to remove heavy metals in the pore water. The washed media were designated as aged ESCS and were tested to examine their *E. coli* removal capacity by exposing them to stormwater containing *E. coli* for 7 h. In this case, *E. coli* in stormwater may be inactivated by the dissolved metals leached from the aged ESCS or inactivated by the adsorbed metals on the aged ESCS media. To distinguish the contribution of each process, the aged ESCS was mixed with 40 mL synthetic stormwater using an orbital shaker for 48 hours to leach any loosely bound metals and centrifuged at 5000 RPM for 15 minutes. The settled ESCS media contained strongly adsorbed metals that were retained after the leaching test and were exposed to *E. coli* contaminated stormwater to estimate the contribution of the strongly adsorbed metals on *E. coli* inactivation or removal. The supernatant containing the leached metals was exposed to *E. coli* to quantify the contribution of leached metals on the inactivation of *E. coli*. Live-dead analysis was performed using fluorescence microscopy to qualitatively examine the fate of the adsorbed *E. coli* on ESCS media with and without aging with metals. After exposing *E. coli* to ESCS media with and without adsorbed metals for 7 hours, *E. coli* sorbed on both media were exposed to specific dye and observed under a fluorescence microscope to distinguish live cells from the dead cells (Mandakhalikar et al., 2018; Polasko et al., 2021). 15 mL of 0.85% NaCl was added to both tubes. The tubes were then vortexed at full speed for 1 min, sonicated at 20 kHz, and 12 V amplitude for 50 s using a probe sonicator (QSonica, Newtown, CT), and vortexed again for 1 min to extract the adsorbed E. coli. The tubes were centrifuged again at 1000×g for 10 min to settle the ESCS media and supernatant was extracted. 0.5 mL of the supernatant was mixed with 0.5 mL sterile DI water mixed with propidium iodide (PI) and SYTO 9 dyes

(LIVE/DEAD BacLight Bacterial Viability Kit L13152, Invitrogen). Note that 0.85% NaCl was used to extract the *E. coli* instead of Phosphate buffer solution (PBS) as PBS solution reduces the staining efficiency of the dyes. The mixture was then allowed to equilibrate in the dark for 15 minutes. 400 µL of the mixture was then added to a 35 mm glass bottom petri dish and was observed under a Leica SP8 Confocal fluorescence microscope.

9.2.6 Data analysis

The amount of heavy metals adsorbed on the ESCS media during the injection of the stormwater spiked with metals was estimated using Eq 9.1:

$$\%\ adsorbed = \frac{\sum V_e C_e}{\sum V_i C_i} \times 100 \qquad \text{(Eq. 9.1)}$$

Where V_e and V_i are the volume of the effluent and influent samples, respectively, and C_e and C_i are the heavy metal concentration in the effluent and influent samples, respectively, during the injection and flushing stages. The amount of heavy metals leached during the leaching phase was determined using Eq. 9.2:

$$\%\ leached = \frac{\sum V_l C_l}{\sum V_i C_i - \sum V_e C_e} \times 100 \qquad \text{(Eq. 9.2)}$$

Where V_l is the volume of the effluent sample and C_l is the heavy metal concentration in the effluent samples during the leaching phase.

9.3 Results

9.3.1 Characterization of ESCS with adsorbed metal

The results reveal how the adsorbed metals change the surface properties of ESCS media. FTIR analysis shows adsorbed metals affect the characteristics of the peak 3500 cm^{-1} (Figure 9.2a), which corresponds to the hydroxyl groups ($R - OH$) in the media (Merlic et al., 2001). The peak completely disappeared in the Pb adsorbed ESCS media, while twin peaks were

observed in the Cu adsorbed ESCS sample. Adsorption of Zn also showed a sharp peak in that region. Zeta potential measurements showed that the adsorbed metals decreased the net negative surface charge of the ESCS media (Figure 9.2b). The zeta potential ESCS media without adsorbed metals at 8.5 pH was -31 ± 3.3 mV, but it decreased to -7.7 ± 2.6 mV after the exposure to 300 mg L^{-1} Cu, Pb, and Zn in the batch studies. Typically, ESCS media has a net negative surface charge similar to any other clay minerals. Adsorption of metal cations could lower the negative surface charge by neutralizing the surface charges on clay minerals (Yukselen-Aksoy and Kaya, 2011). These results confirmed that the interaction of metals on ESCS media changed their surface properties, but they did not confirm the mechanisms of metal interaction. It was assumed that the mechanism of metal adsorption on ESCS media is similar to metal adsorption mechanisms on the raw material used to produce ESCS such as clay minerals, which has been extensively studied (Altın et al., 1998; Bradl, 2004). Some other studies on ESCS also focused on ESCS adsorption (Kalhori et al., 2013; Malakootian et al., 2009). Therefore, the scope of the current study is to confirm metal adsorption so that the main hypothesis to understand the effect of adsorbed metal can be tested. The added metals (~ 7.2 mg), which is less than 0.0001% of the weight of filter media, would not change the surface area or porosity of filter media.

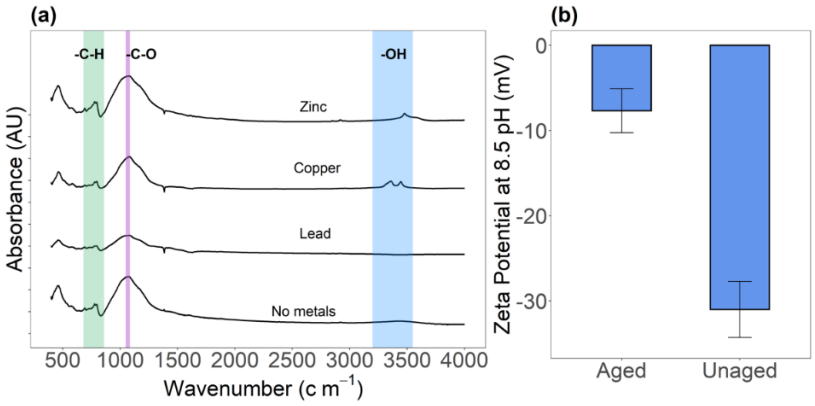

Figure 9.2. (a) FTIR analysis of unaged ESCS media (Control) and aged ESCS media with adsorbed metals. The green band refers to the wavenumber range for aromatic C-H bending , the pink band refers to the wavenumber range for C-O stretching bond of primary alcohols and the blue band refers to the wavenumber range for -OH stretch for alcohols/phenols. (b) Zeta potential of unaged ESCS (without metals) and aged ESCS media (with adsorbed metals) at a pH of 8.5 were statistically different ($p < 0.01$), where the error bars represent a standard deviation over the mean from triplicate samples.

9.3.2 ESCS has a high capacity to remove heavy metals

The goal of this study is to examine if the adsorbed metal has any effect on *E. coli* removal. Thus, metal adsorption is a precondition to test the hypothesis related to the aging effect on E. coli sorption. The results confirmed that the ESCS media had a high removal capacity for Pb and Zn (Figure 9.3), meaning they can be tested for their impact on E. coli removal. After injecting 500 PV of contaminated stormwater in the aging stage, the concentration of Pb and Zn remained below the detection limit ($C/C_0 = 0.1\%$), whereas the concentration of Cu in the effluent was 31.2% of the influent concentration (C_0).

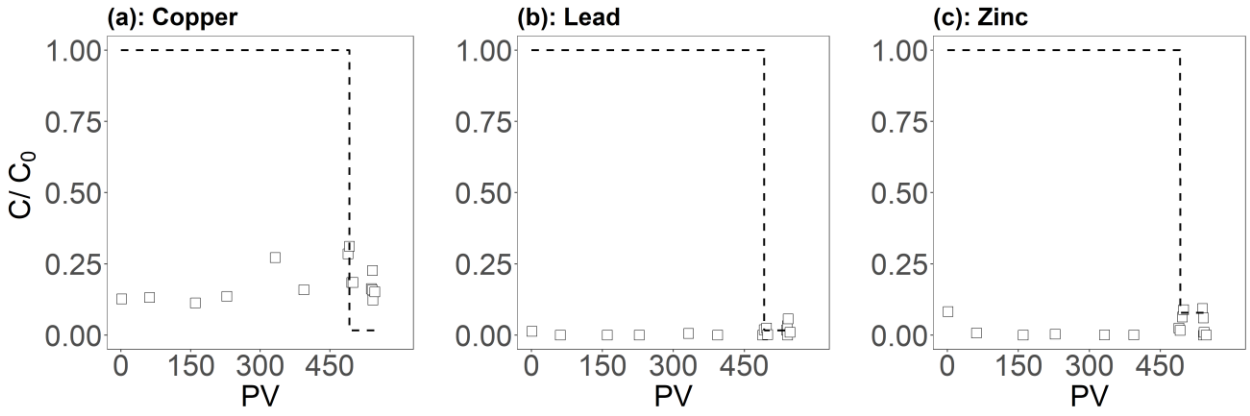

Figure 9.3. Breakthrough curves of (a) Cu, (b) Pb, and (c) Zn in the ESCS columns. The white squares denote the relative concentration of the respective heavy metal in the effluent samples while the dashed lines indicate the concentration of the heavy metal in the influent. The dash dropped `45- PV when the ESCS media reached breakthrough for all the metal ions.

Mass balance analysis (Figure 9.4) showed biofilters adsorbed 95.5 ± 3.9 % of the injected Zn, 86.5 ± 4.4% of injected Pb, and 80.5 ± 0.3% of injected Cu. The leaching potential of the adsorbed metals was found to be minimal. During the leaching phase, only 0.17 ± 0.02 % of adsorbed Cu and 0.02 ± 0.01% of adsorbed Pb were leached. The effluent concentration of Zn was below the influent concentration in natural stormwater, which resulted in additional retention of 0.09 ± 0.005% Zn during the injection of natural stormwater without added metals. It should be noted that metal adsorption to ESCS media was tested before in batch studies (Malakootian et al., 2009). This study confirmed that the removal is consistent with batch studies even though the hydraulic retention time (7.3-9.2 min) in the study is an order of magnitude lower than the contact time used in previous batch studies.

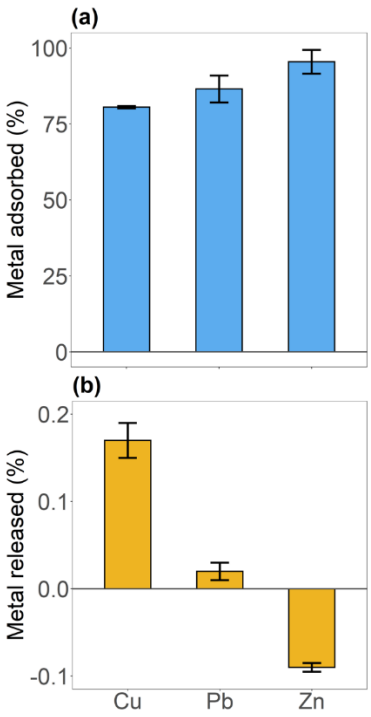

Figure 9.4. Mass balance analysis showing (a) percentage of injected metals adsorbed in biofilters after the aging and flushing stages and (b) the percentage of the adsorbed metals leached during the leaching stage. The error bars denote standard deviation over the mean values from triplicate biofilters. Negative % leaching for Zn indicates net adsorption, not leaching, because the Zn concentration in effluent was lower than the concentration in influent stormwater.

9.3.3 Aging of ESCS with heavy metals improved E. coli removal

Aged ESCS media removed more *E. coli* than unaged ECSC media (Figure 9.5). *E. coli* concentration in the second sample, which represents biofilter removal capacity during each rainfall event, increased with an increase in the drying duration in successive rainfall events, indicating that *E. coli* removal capacity of the biofilters had decreased with successive infiltration events. However, the loss in removal capacity in the unaged biofilters was higher than that of the aged biofilters.

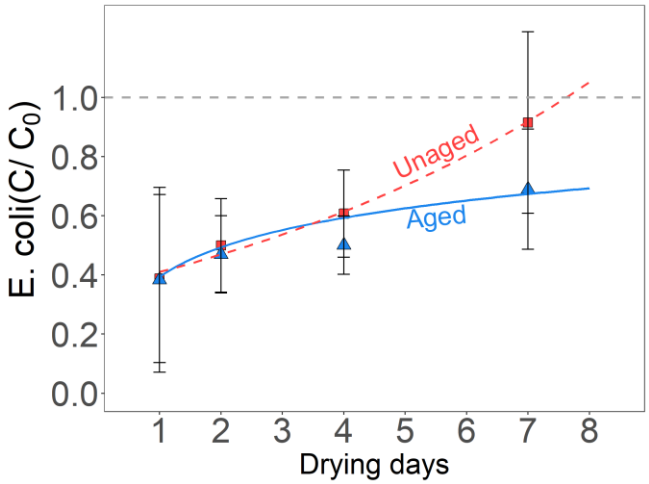

Figure 9.5. Change in mean effluent *E. coli* concentration in the effluent with an increase in drying duration for unaged biofilters and aged biofilters (with adsorbed metals). The error bars represent standard deviation over the mean value obtained from 18 samples from triplicate biofilters and duplicate experiments at a specific drying duration. The lines denote the best fits for the mean concentration in the effluents.

During infiltration events after the 4- and 7-days drying period, the effluent *E. coli* concentration in unaged biofilters without metals was significantly ($p < 0.05$) higher than the effluent concentration in aged biofilters (Figure 9.6). The effluent *E. coli* concentration in the unaged biofilters increased exponentially with the increase in drying duration ($R^2 = 0.99$): $C/Co = 0.36 \times e^{0.14 \times Drying\ days}$. However, the effluent *E. coli* concentration in aged biofilters increased logarithmically which appears to flatten out after 7 days of drying ($R^2 = 0.94$): $C/C0 = 0.14 \times \ln(Drying\ days) + 0.40$. The *E. coli* removal capacity of the aged biofilter was consistently higher than unaged biofilters, indicating faster exhaustion of unaged biofilters compared to aged biofilters.

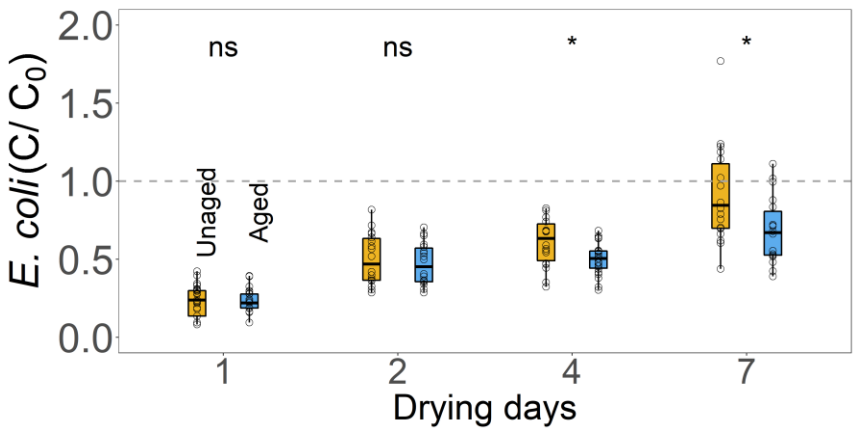

Figure 9.6. Effluent *E. coli* concentration (CFU mL^{-1}) in second samples from Unaged (No adsorbed metals) and aged biofilters (Adsorbed metals). The 'ns'notation denotes no significant difference in the *E. coli* concentration from the aged and unaged biofilters while * denotes a p value less than 0.05.

The remobilization of adsorbed *E. coli* from the biofilters during the first flush was lower in the aged biofilters than that in the unaged biofilters (Figure 9.7). While the difference (~5%) is small, it is meaningful because the results are normalized (C/C_0) and consistent across replicates. However, we recognize that the improvement is modest and should be interpreted within this context mind. The *E. coli* concentration in the first flush samples in aged biofilters decreased more rapidly than the unaged biofilters, indicating that the adsorbed metals reduced the leaching of *E. coli* from the biofilters during intermittent infiltration of stormwater.

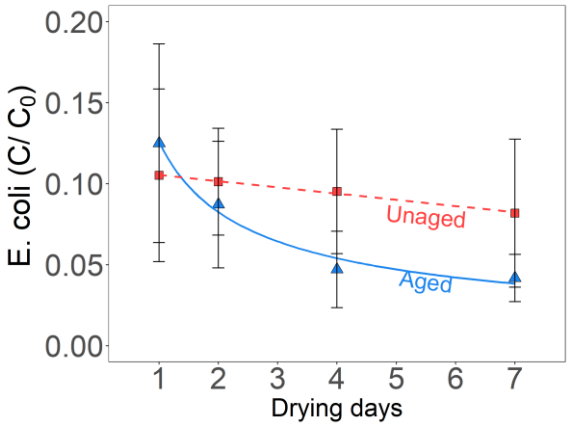

Figure 9.7. *E. coli* concentration in the first flush samples with an increase in drying duration in unaged (without adsorbed metals) and aged biofilters (with adsorbed metals). The error bars denote the standard deviation over the mean value obtained from triplicate biofilters and duplicate experiments at specific drying duration (total 18 samples per data point). The lines denote the best fits for the mean effluent concentration from biofilters.

The *E. coli* concentration in the unaged biofilters decreased linearly with the increase in drying duration ($R^2 = 0.99$): $C/Co = -0.0.004 \times Drying\ days + 0.109$. In contrast, the *E. coli* concentration in the aged biofilters decreased much faster by a power function ($R^2 = 0.98$): $C/Co = 0.125 \times (Drying\ days)^{-0.602}$. Due to this, the *E. coli* concentration in the effluent samples from the aged biofilters was significantly lower than the unaged biofilters after 4 and 7 days of drying (Figure 9.8).

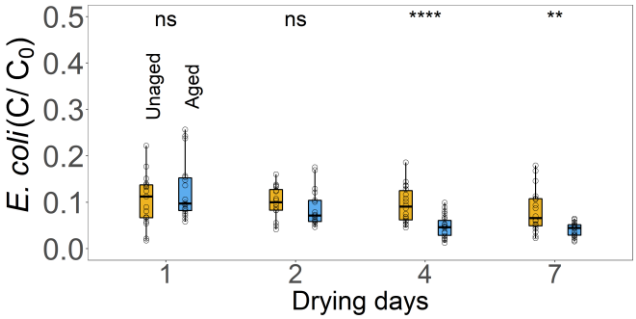

Figure 9.8. Effluent *E. coli* concentration (CFU mL^{-1}) in first flush samples from unaged (No adsorbed metals) and aged biofilters (Adsorbed metals). The 'ns'notation denotes no significant difference in the *E. coli* concentration from the aged and unaged biofilters while '**' and '****' denote a p value less than 0.01 and 0.0001.

9.3.4 Adsorbed metals, not desorbed metals, caused the inactivation of E. coli

Batch experiments validated the result of the column experiments: aged ESCS removed more *E. coli* than unaged ESCS. When *E. coli* was exposed to aged ESCS, all the injected *E. coli* were removed within 3 hours due to a combination of adsorption and inactivation. In contrast, *E. coli* concentration remained high in the entire 7 h of incubation study (See section 9.2.5 for experimental details) with unaged ESCS. By removing the readily leachable metals from aged column increased the time to remove all *E. coli* to 5 hours. The results from the batch experiments also revealed that removal due to leached metals was negligible compared to the removal by adsorbed metals on ESCS. Exposing the *E. coli* to the metal concentration that was leached from the aged ESCS due to the leaching test (68 μg L^{-1} Cu, 142.8 μg L^{-1} Pb, and 61.5 μg L^{-1} Zn) did not reduce the *E. coli* concentration after 7 hours of exposure.

The batch study also confirmed that removal of *E. coli* occurred via adsorption and inactivation, and adsorbed metals, not the leached metals, increased the inactivation of *E. coli*. Fluorescence microscopy confirmed that heavy metals adsorbed to the ESCS media or aged ESCS inactivated adsorbed *E. coli* (Figure 9.9a). A high number of green fluorescent cells were observed on unaged ESCS media (Figure 9.9b), indicating that most of the adsorbed cells were alive. In contrast, a high number of red fluorescent cells was observed in samples contacted with aged ESCS media (Figure 9.9c**)**, indicating heavy metals on ESCS media increased the inactivation of the *E. coli* after adsorption.

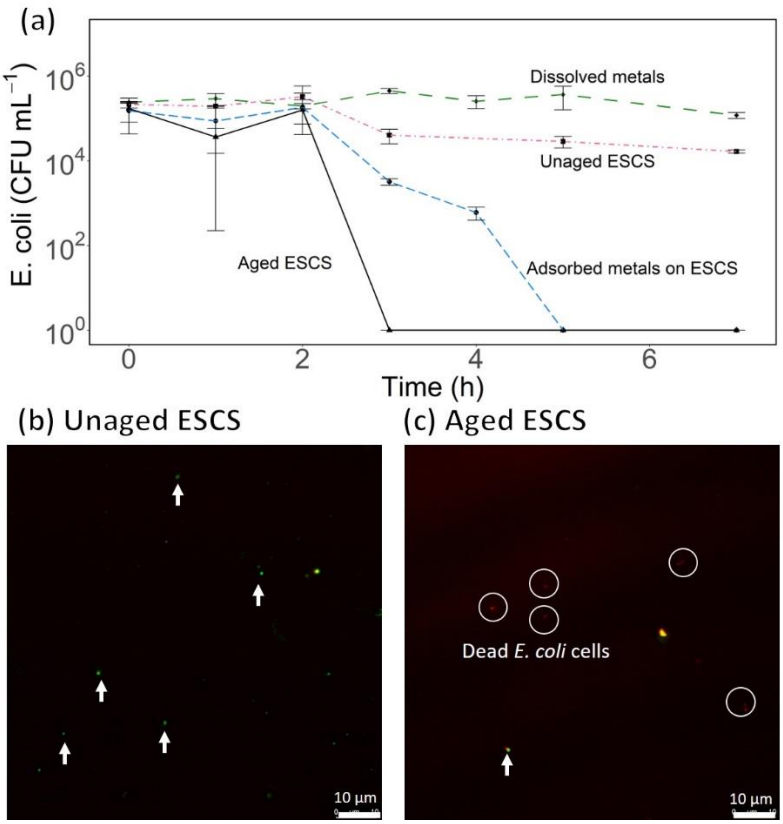

Figure 9.9. (a) Change in *E. coli* concentration batch studies after exposure to unaged ESCS (control), Dissolved metals (Metals leached from ESCS), Adsorbed metals on ESCS (ESCS with strongly adsorbed metals), and aged ESCS (ESCS media after metal adsorption). The error bars denote standard deviation over the mean value obtained from triplicate experiments. (b) Fluorescence microscopy images for *E. coli* adsorbed on unaged ESCS (no adsorbed metals). (c) Fluorescence microscopy images for *E. coli* extracted from aged ESCS (adsorbed metals). The white arrows point toward the green live cells whereas white circles enclose the red dead cells.

9.4 Discussion

9.4.1 Reasons for high metal adsorption capacity of ESCS

Heavy metals are typically found in high concentrations in urban stormwater, where their removal can be challenging, particularly when hydraulic retention time (HRT) in biofilters is low. Results in the study showed that ESCS aggregates could adsorb significant amounts of heavy metals without leaching them later. Despite the short HRT of 5-10 mins used in this study, concentrations of each metal in the effluent samples were very low, indicating the ESCS aggregates can quickly sorb heavy metals (Figure 9.2). The result is similar to a previous study

on copper-coated zeolite media, which also removed significant amounts of *E. coli* with a contact time of 4.5 minutes (Li et al., 2014a). However, copper-coated zeolite is cost-prohibitive to apply on a large scale. The average HRT in field-scale biofilters can range between 20 min to as high as 13 days (Hatt et al., 2009; Zhang et al., 2021a). Since an increase in HRT can increase the removal of pollutants from stormwater (Fang et al., 2021; Zhang et al., 2021b), the metal removal capacity of the ESCS amended biofilters could be much higher in the field setting with longer HRT used in this study. Compared to other amendments such as peat, compost, fly ash, or zeolite, ESCS exhibited a comparable or higher metal removal capacity (Lim et al., 2015; Tirpak et al., 2021). Thus, studies should adopt ESCS as an alternative amendment for biofilters to remove metals from stormwater.

Although two studies tested ESCS media for stormwater treatment, they did not examine the adsorption mechanisms of heavy metals (Malakootian et al., 2009; Shojaeimehr et al., 2014). The quick removal of metals by ESCS was attributed to the strong affinity of metal to specific sites and the porous structure of the ESCS media (Kalhori et al., 2013). Based on FTIR analysis, the heavy metals primarily sorb to the ESCS media by interacting with the hydroxyl ($R-OH$) groups on ESCS (Figure 9.2a), where the oxygen atom could act as a strong Lewis base and form complexes with the metal ions (Lim and Lee, 2015). Since the oxygen atom (O^{2-}) in the hydroxyl group is negatively charged, the adsorption of positively charged heavy metals could reduce the negative surface charge on the ESCS media. The zeta potential measurement of the ESCS media after heavy metal adsorption confirmed a net decrease in the negative surface charge of ESCS media (Figure 9.2b). Overall, these results indicate that metals bind strongly on specific sites on ESCS media, which limits the leaching of metals into clean stormwater. Metals ions adsorbing

on ESCS surface reduce the net negative surface charge and reverse to positive charge. , which increases the removal of negatively charged *E. coli*.

9.4.2 Antibacterial effect of adsorbed heavy metals in biofilters

Pathogen removal in stormwater biofilters is typically challenging because of the possibility of growth of previously removed pathogens and their release during intermittent flow (Mohanty et al., 2014, 2013). Amendments such as biochar or iron filings could improve removal, but the exhaustion of adsorption sites on those media because of bacterial growth limits their utility in long term, indicating aging of these media could lower pathogen removal (Chandrasena et al., 2014a; Valenca et al., 2021b). Using ESCS aggregate, it is shown that aging with metal-contaminated stormwater benefited bacterial removal. It was demonstrated that the aged biofilters were able to maintain their *E. coli* removal capacity when the unaged biofilters exhausted quickly. These findings should be through field studies for field validations. The results were attributed to the inactivation of adsorbed *E. coli* in aged biofilters. The ability of the heavy metals to limit *E. coli* growth or enhance inactivation increased with an increase in exposure time during the drying period between rainfall events. This result indicates that the growth of attached *E. coli* in between rainfall events is limited, and most adsorbed *E. coli* could be eventually inactivated during a long period between the rainfall events. Although the negative effect of aging is often highlighted in the literature (Valenca et al., 2021a), the positive effect of aging, particularly due to adsorption of metals, on pathogen removal has not been demonstrated before. We expect that other amendments that have high adsorption capacity as ESCS should also exhibit the positive effect of adsorbed metals on the pathogen removal (Tirpak et al., 2021) as long as the adsorbed metal is sufficiently high to alter surface charge and interaction with bacteria. Future studies should confirm the finding in field studies or other amendments. We

used zeta potential measurement to prove the changes in surface charge with aging, FTIR analysis to confirm possible changes in surface properties of clay minerals after metal adsorption, and live-dead analysis to confirm the inactivation of bacteria. Thus, media aged in field conditions should be measured for these changes in surface properties to confirm the finding and relevance in the actual field setting.

The remobilization of attached pathogens during intermittent infiltration of stormwater is a concern (Chandrasena et al., 2012; Li et al., 2012; Mohanty et al., 2013) because it would make the biofilter a source of pathogens. The results show that the adsorption of heavy metal on ESCS media also reduced the remobilization of adsorbed *E. coli* during intermittent infiltration of stormwater. Although unaged biofilters reduced the *E. coli* remobilization as well, the aged biofilters reduced the mobilization to a greater extent. This reduction in the remobilization of *E. coli* increased with exposure time drying periods between the rainfalls. In field, the drying duration between two rainfall could exceed 7 days, thereby enabling more inactivation of adsorbed *E. coli*. Thus, combination of aging with metals in road runoff and long duration between rainfalls could improve ESCS media capacity to remove bacterial pollutants. An increase in exposure time during drying did not improve the first flush leaching of *E. coli* in other studies with biochar (Valenca et al., 2021b) and iron filings (Ghavanloughajar et al., 2021), but those studies did not use amendments aged with heavy metals. Most media are inert to pathogens, where pathogens are adsorbed on the surface without resulting in an inactivation (Peng et al., 2016; Tirpak et al., 2021). To facilitate inactivation, silver or copper nanoparticles or other metals were mixed with media (Li et al., 2016, 2014a, 2014b; Matsumura et al., 2003; Zeng et al., 2015), but these media are cost-prohibitive for large scale applications and thus have low practical significance. In contrast, ESCS media, which is produced at an industrial scale, can

develop antibacterial coating by adsorbing metals naturally present in stormwater. Thus, with an increase in the age of biofilters, the ESCS media can become better at removing pathogens due to an increase in the concentration of metals on the media surface.

9.4.3 E. coli removal processes on metal-coated ESCS media

Metals in the biofilter media could mainly remove *E. coli* by two processes: inactivation and adsorption (Hrenovic et al., 2012; Li et al., 2014a; Nan et al., 2008). First, media could leach heavy metal into pore water, which could inactivate *E. coli* due to metal toxicity. Second, media could adsorb *E. coli* and inactivate them due to interaction with the adsorbed metals (Nan et al., 2008). Batch experiments showed that leached heavy metals did not remove *E. coli* from the stormwater (Figure 9.9), indicating the contribution of leached metals on *E. coli* removal in the biofilters was negligible. In contrast, adsorbed *E. coli* were inactivated as confirmed by live-dead analysis in the study (Figure 9.9c). The heavy metals could inactivate *E. coli* by damaging the cell walls and accumulating in the *E. coli* cells (Raffi et al., 2010; Siddiqi et al., 2018; Tian et al., 2012). Overall, the results confirmed that the inactivation of *E. coli* was caused by adsorbed metals, not the leached metals from the contaminated ESCS. It should be noted that this study compared inactivation processes by adsorbed and dissolved metals, which can be present in biofilters pre-contaminated with metals. The study did not confirm the mechanism of adsorption or inactivation by the metals. Future studies should examine the mechanism by probing the oxidative stress (Engel et al., 2018; Yang et al., 2021), and observing the changes in the cell wall characteristics (Glasauer et al., 2001). Knowing whether inactivation is due to adsorbed or leached metals helps Caltrans select media with durable adsorption capacity, improving long-term biofilter performance.

These results have practical significance in the performance lifetime of biofilters. Biofilters are constructed with a service life of at least 20 years. However, the media could become exhausted long before the design lifetime (Blecken et al., 2009; Mohanty and Boehm, 2015; Okaikue-Woodi et al., 2020; Zhang et al., 2014), particularly for bacterial pollutants due to their growth between rainfall events. For the same reason, unaged ESCS in the study became exhausted and lost the bacterial removal capacity after a few rainfall events. The exhaustion rate was much slower in aged ESCS with adsorbed metals, even with increasing in drying duration. Thus, the aging of ESCS could help the performance life of the biofilters amended with ESCS. However, the experiment should be repeated in the field settings to include additional complexities such as competitive adsorption by organic matter, nutrients, or ions (Charbonnet et al., 2020; Mohanty and Boehm, 2015; Okaikue-Woodi et al., 2020).

9.5 Conclusions and implications

The study shows that aging with co-contaminants such as heavy metals, which occur naturally, could have a net positive effect on the long-term removal of *E. coli* in biofilters. Results of batch experiments and column studies reveal that biofilters amended with aged ESCS aggregates could adsorb significant amounts of metals such as Pb, Cu, and Zn from stormwater and decrease net negative surface charge on ESCS media, and these changes increased *E. coli* removal. The metal coating developed with aging could help maintain the long-term *E. coli* removal capacity of the biofilter by inactivating *E. coli* or limiting their growth. This enhanced adsorption and inactivation of *E. coli* cells enabled the aged ESCS media to exhaust at a much slower rate than the unaged ESCS media. Thus, ESCS media should be used as bulking agent to remove stormwater pollutants such as heavy metals and pathogens from road runoff. However, further study is needed to examine their effectiveness under different degrees of compaction.

9.6 References

Alam, S., Borthakur, A., Ravi, S., Gebremichael, M., Mohanty, S.K., 2021. Managed aquifer recharge implementation criteria to achieve water sustainability. Science of The Total Environment 768, 144992. https://doi.org/10.1016/j.scitotenv.2021.144992

Altın, O., Özbelge, H.Ö., Doğu, T., 1998. Use of General Purpose Adsorption Isotherms for Heavy Metal–Clay Mineral Interactions. Journal of Colloid and Interface Science 198, 130–140. https://doi.org/10.1006/jcis.1997.5246

Appenzeller, B.M.R., Duval, Y.B., Thomas, F., Block, J.-C., 2002. Influence of Phosphate on Bacterial Adhesion onto Iron Oxyhydroxide in Drinking Water. Environ. Sci. Technol. 36, 646–652. https://doi.org/10.1021/es010155m

Blecken, G.-T., Zinger, Y., Deletić, A., Fletcher, T.D., Viklander, M., 2009. Influence of intermittent wetting and drying conditions on heavy metal removal by stormwater biofilters. Water Research 43, 4590–4598. https://doi.org/10.1016/j.watres.2009.07.008

Borthakur, A., Cranmer, B.K., Dooley, G.P., Blotevogel, J., Mahendra, S., Mohanty, S.K., 2021. Release of soil colloids during flow interruption increases the pore-water PFAS concentration in saturated soil. Environmental Pollution 117297. https://doi.org/10.1016/j.envpol.2021.117297

Bradl, H.B., 2004. Adsorption of heavy metal ions on soils and soils constituents. Journal of Colloid and Interface Science 277, 1–18. https://doi.org/10.1016/j.jcis.2004.04.005

Chandrasena, G.I., Deletic, A., Ellerton, J., McCarthy, D.T., 2012. Evaluating Escherichia coli removal performance in stormwater biofilters: a laboratory-scale study. Water Science and Technology 66, 1132–1138. https://doi.org/10.2166/wst.2012.283

Chowdhury, S.R., Yanful, E.K., 2010. Arsenic and chromium removal by mixed magnetite–maghemite nanoparticles and the effect of phosphate on removal. Journal of environmental management, 91(11), 2238-2247.

Charbonnet, J.A., Duan, Y., Sedlak, D.L., 2020. The use of manganese oxide-coated sand for the removal of trace metal ions from stormwater. Environ. Sci.: Water Res. Technol. 6, 593–603. https://doi.org/10.1039/C9EW00781D

Dordio, A., Carvalho, A.J.P., 2013. Constructed wetlands with light expanded clay aggregates for agricultural wastewater treatment. Science of The Total Environment 463–464, 454–461. https://doi.org/10.1016/j.scitotenv.2013.06.052

Engel, M., Hadar, Y., Belkin, S., Lu, X., Elimelech, M., Chefetz, B., 2018. Bacterial inactivation by a carbon nanotube–iron oxide nanocomposite: a mechanistic study using E. coli mutants. Environ. Sci.: Nano 5, 372–380. https://doi.org/10.1039/C7EN00865A

Fang, H., Jamali, B., Deletic, A., Zhang, K., 2021. Machine learning approaches for predicting the performance of stormwater biofilters in heavy metal removal and risk mitigation. Water Research 200, 117273. https://doi.org/10.1016/j.watres.2021.117273

Galfi, H., Österlund, H., Marsalek, J., Viklander, M., 2016. Indicator bacteria and associated water quality constituents in stormwater and snowmelt from four urban catchments. Journal of Hydrology 539, 125–140. https://doi.org/10.1016/j.jhydrol.2016.05.006

Ghavanloughajar, M., Borthakur, A., Valenca, R., McAdam, M., Khor, C.M., Dittrich, T.M., Stenstrom, M.K., Mohanty, S.K., 2021. Iron amendments minimize the first-flush release

of pathogens from stormwater biofilters. Environmental Pollution 281, 116989. https://doi.org/10.1016/j.envpol.2021.116989
Ghavanloughajar, M., Valenca, R., Le, H., Rahman, M., Borthakur, A., Ravi, S., Stenstrom, M.K., Mohanty, S.K., 2020. Compaction conditions affect the capacity of biochar-amended sand filters to treat road runoff. Science of The Total Environment 735, 139180. https://doi.org/10.1016/j.scitotenv.2020.139180
Glasauer, S., Langley, S., Beveridge, T.J., 2001. Sorption of Fe (Hydr)Oxides to the Surface of Shewanella putrefaciens: Cell-Bound Fine-Grained Minerals Are Not Always Formed De Novo. Applied and Environmental Microbiology. https://doi.org/10.1128/AEM.67.12.5544-5550.2001
Grebel, J.E., Mohanty, S.K., Torkelson, A.A., Boehm, A.B., Higgins, C.P., Maxwell, R.M., Nelson, K.L., Sedlak, D.L., 2013. Engineered Infiltration Systems for Urban Stormwater Reclamation. Environmental Engineering Science 30, 437–454. https://doi.org/10.1089/ees.2012.0312
Hatt, B.E., Fletcher, T.D., Deletic, A., 2009. Hydrologic and pollutant removal performance of stormwater biofiltration systems at the field scale. Journal of Hydrology 365, 310–321. https://doi.org/10.1016/j.jhydrol.2008.12.001
Hatt, B.E., Fletcher, T.D., Deletic, A., 2008. Hydraulic and Pollutant Removal Performance of Fine Media Stormwater Filtration Systems. Environ. Sci. Technol. 42, 2535–2541. https://doi.org/10.1021/es071264p
Hermawan, A.A., Teh, K.L., Talei, A., Chua, L.H.C., 2021. Accumulation of heavy metals in stormwater biofiltration systems augmented with zeolite and fly ash. Journal of Environmental Management 297, 113298. https://doi.org/10.1016/j.jenvman.2021.113298
Kalhori, E.M., Yetilmezsoy, K., Uygur, N., Zarrabi, M., Shmeis, R.M.A., 2013. Modeling of adsorption of toxic chromium on natural and surface modified lightweight expanded clay aggregate (LECA). Applied Surface Science 287, 428–442. https://doi.org/10.1016/j.apsusc.2013.09.175
Li, R., Tan, W., Wang, G., Zhao, X., Dang, Q., Yu, H., Xi, B., 2019. Nitrogen addition promotes the transformation of heavy metal speciation from bioavailable to organic bound by increasing the turnover time of organic matter: An analysis on soil aggregate level. Environmental Pollution 255, 113170. https://doi.org/10.1016/j.envpol.2019.113170
Li, Y., McCarthy, D.T., Deletic, A., 2016. Escherichia coli removal in copper-zeolite-integrated stormwater biofilters: Effect of vegetation, operational time, intermittent drying weather. Ecological Engineering 90, 234–243. https://doi.org/10.1016/j.ecoleng.2016.01.066
Lim, H.S., Lim, W., Hu, J.Y., Ziegler, A., Ong, S.L., 2015. Comparison of filter media materials for heavy metal removal from urban stormwater runoff using biofiltration systems. Journal of Environmental Management 147, 24–33. https://doi.org/10.1016/j.jenvman.2014.04.042
Lim, S.-F., Lee, A.Y.W., 2015. Kinetic study on removal of heavy metal ions from aqueous solution by using soil. Environ Sci Pollut Res 22, 10144–10158. https://doi.org/10.1007/s11356-015-4203-6
Malakootian, M., Nouri, J., Hossaini, H., 2009. Removal of heavy metals from paint industry's wastewater using Leca as an available adsorbent. Int. J. Environ. Sci. Technol. 6, 183–190. https://doi.org/10.1007/BF03327620

Mandakhalikar, K.D., Rahmat, J.N., Chiong, E., Neoh, K.G., Shen, L., Tambyah, P.A., 2018. Extraction and quantification of biofilm bacteria: Method optimized for urinary catheters. Sci Rep 8, 8069. https://doi.org/10.1038/s41598-018-26342-3

Matsumura, Y., Yoshikata, K., Kunisaki, S., Tsuchido, T., 2003. Mode of Bactericidal Action of Silver Zeolite and Its Comparison with That of Silver Nitrate. Applied and Environmental Microbiology 69, 4278–4281. https://doi.org/10.1128/AEM.69.7.4278-4281.2003

McBride, G.B., Stott, R., Miller, W., Bambic, D., Wuertz, S., 2013. Discharge-based QMRA for estimation of public health risks from exposure to stormwater-borne pathogens in recreational waters in the United States. Water Research 47, 5282–5297. https://doi.org/10.1016/j.watres.2013.06.001

Meng, J., Tao, M., Wang, L., Liu, X., Xu, J., 2018. Changes in heavy metal bioavailability and speciation from a Pb-Zn mining soil amended with biochars from co-pyrolysis of rice straw and swine manure. Science of The Total Environment 633, 300–307. https://doi.org/10.1016/j.scitotenv.2018.03.199

Merlic, C.A., Fam, B.C., Miller, M.M., 2001. WebSpectra: Online NMR and IR Spectra for Students. J. Chem. Educ. 78, 118. https://doi.org/10.1021/ed078p118

Mohanty, S.K., Boehm, A.B., 2015. Effect of weathering on mobilization of biochar particles and bacterial removal in a stormwater biofilter. Water Research 85, 208–215. https://doi.org/10.1016/j.watres.2015.08.026

Mohanty, S.K., Cantrell, K.B., Nelson, K.L., Boehm, A.B., 2014. Efficacy of biochar to remove Escherichia coli from stormwater under steady and intermittent flow. Water Research 61, 288–296. https://doi.org/10.1016/j.watres.2014.05.026

Mohanty, S.K., Torkelson, A.A., Dodd, H., Nelson, K.L., Boehm, A.B., 2013. Engineering Solutions to Improve the Removal of Fecal Indicator Bacteria by Bioinfiltration Systems during Intermittent Flow of Stormwater. Environ. Sci. Technol. 47, 10791–10798. https://doi.org/10.1021/es305136b

Nan, L., Liu, Y., Lü, M., Yang, K., 2008. Study on antibacterial mechanism of copper-bearing austenitic antibacterial stainless steel by atomic force microscopy. J Mater Sci: Mater Med 19, 3057–3062. https://doi.org/10.1007/s10856-008-3444-z

Nkansah, M.A., Christy, A.A., Barth, T., Francis, G.W., 2012. The use of lightweight expanded clay aggregate (LECA) as sorbent for PAHs removal from water. Journal of Hazardous Materials 217–218, 360–365. https://doi.org/10.1016/j.jhazmat.2012.03.038

Okaikue-Woodi, F.E.K., Cherukumilli, K., Ray, J.R., 2020. A critical review of contaminant removal by conventional and emerging media for urban stormwater treatment in the United States. Water Research 187, 116434. https://doi.org/10.1016/j.watres.2020.116434

Peng, J., Cao, Y., Rippy, M.A., Afrooz, A.R.M.N., Grant, S.B., 2016. Indicator and Pathogen Removal by Low Impact Development Best Management Practices. Water 8, 600. https://doi.org/10.3390/w8120600

Polasko, A.L., Ramos, P., Kaner, R.B., Mahendra, S., 2021. A multipronged approach for systematic in vitro quantification of catheter-associated biofilms. Journal of Hazardous Materials Letters 2, 100032. https://doi.org/10.1016/j.hazl.2021.100032

Raffi, M., Mehrwan, S., Bhatti, T.M., Akhter, J.I., Hameed, A., Yawar, W., ul Hasan, M.M., 2010. Investigations into the antibacterial behavior of copper nanoparticles against Escherichia coli. Ann Microbiol 60, 75–80. https://doi.org/10.1007/s13213-010-0015-6

Shojaeimehr, T., Rahimpour, F., Khadivi, M.A., Sadeghi, M., 2014. A modeling study by response surface methodology (RSM) and artificial neural network (ANN) on Cu2+ adsorption optimization using light expended clay aggregate (LECA). Journal of Industrial and Engineering Chemistry 20, 870–880. https://doi.org/10.1016/j.jiec.2013.06.017

Siddiqi, K.S., ur Rahman, A., Tajuddin, Husen, A., 2018. Properties of Zinc Oxide Nanoparticles and Their Activity Against Microbes. Nanoscale Research Letters 13, 141. https://doi.org/10.1186/s11671-018-2532-3

Sun, Y., Chen, S.S., Lau, A.Y.T., Tsang, D.C.W., Mohanty, S.K., Bhatnagar, A., Rinklebe, J., Lin, K.-Y.A., Ok, Y.S., 2020. Waste-derived compost and biochar amendments for stormwater treatment in bioretention column: Co-transport of metals and colloids. Journal of Hazardous Materials 383, 121243. https://doi.org/10.1016/j.jhazmat.2019.121243

Tian, W.-X., Yu, S., Ibrahim, M., Almonaofy, A.W., He, L., Hui, Q., Bo, Z., Li, B., Xie, G., 2012. Copper as an antimicrobial agent against opportunistic pathogenic and multidrug resistant Enterobacter bacteria. J Microbiol. 50, 586–593. https://doi.org/10.1007/s12275-012-2067-8

Tirpak, R.A., Afrooz, A.N., Winston, R.J., Valenca, R., Schiff, K., Mohanty, S.K., 2021. Conventional and amended bioretention soil media for targeted pollutant treatment: A critical review to guide the state of the practice. Water Research 189, 116648. https://doi.org/10.1016/j.watres.2020.116648

Valenca, R., Borthakur, A., Le, H., Mohanty, S.K., 2021a. Chapter Seven - Biochar role in improving pathogens removal capacity of stormwater biofilters, in: Sarmah, A.K. (Ed.), Advances in Chemical Pollution, Environmental Management and Protection, Biochar: Fundamentals and Applications in Environmental Science and Remediation Technologies. Elsevier, pp. 175–201. https://doi.org/10.1016/bs.apmp.2021.08.007

Valenca, R., Borthakur, A., Zu, Y., Matthiesen, E.A., Stenstrom, M.K., Mohanty, S.K., 2021b. Biochar Selection for *Escherichia coli* Removal in Stormwater Biofilters. Journal of Environmental Engineering 147, 06020005. https://doi.org/10.1061/(ASCE)EE.1943-7870.0001843

Yang, S., Qu, C., Mukherjee, M., Wu, Y., Huang, Q., Cai, P., 2021. Soil phyllosilicate and iron oxide inhibit the quorum sensing of Chromobacterium violaceum. Soil Ecol. Lett. 3, 22–31. https://doi.org/10.1007/s42832-020-0051-5

Yukselen-Aksoy, Y., Kaya, A., 2011. A study of factors affecting on the zeta potential of kaolinite and quartz powder. Environ Earth Sci 62, 697–705. https://doi.org/10.1007/s12665-010-0556-9

Zeng, X., McCarthy, D.T., Deletic, A., Zhang, X., 2015. Silver/Reduced Graphene Oxide Hydrogel as Novel Bactericidal Filter for Point-of-Use Water Disinfection. Advanced Functional Materials 25, 4344–4351. https://doi.org/10.1002/adfm.201501454

Zhang, K., Barron, N.J., Zinger, Y., Hatt, B., Prodanovic, V., Deletic, A., 2021a. Pollutant removal performance of field scale dual-mode biofilters for stormwater, greywater, and groundwater treatment. Ecological Engineering 163, 106192. https://doi.org/10.1016/j.ecoleng.2021.106192

Zhang, K., Liu, Y., Deletic, A., McCarthy, D.T., Hatt, B.E., Payne, E.G.I., Chandrasena, G., Li, Y., Pham, T., Jamali, B., Daly, E., Fletcher, T.D., Lintern, A., 2021b. The impact of stormwater biofilter design and operational variables on nutrient removal - a statistical

modelling approach. Water Research 188, 116486. https://doi.org/10.1016/j.watres.2020.116486
Zhang, K., Randelovic, A., Page, D., McCarthy, D.T., Deletic, A., 2014. The validation of stormwater biofilters for micropollutant removal using in situ challenge tests. Ecological Engineering 67, 1–10. https://doi.org/10.1016/j.ecoleng.2014.03.004

10 Task 3d: Comparing performance of expanded shale, clay, and slate (ESCS) media to sand in compacted roadside biofilter as bulking agent.

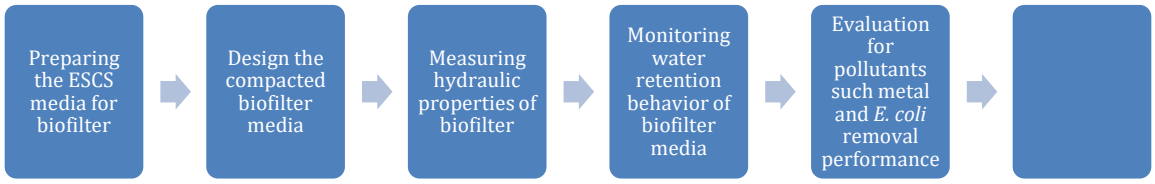

10.1 Background

Providing a sustainable supply of water for urban areas in the world, where nearly 70% of the world's population is projected to live by 2050, is a challenge (Ahmadi et al., 2020; He et al., 2021). Most urban areas are located in places that have been facing severe water scarcity (He et al., 2021). Ironically, urbanization also limits local water supply because the impervious surfaces or compacted soils created during land development increase runoff and limit ground infiltration or recharge of groundwater (Epps and Hathaway, 2021; McGrane, 2016). Hydrological events such as rainfall and drought are becoming more extreme during climate change, which will further limit surface and groundwater availability where they are needed the most (Wu et al., 2020). To increase the local water supply, city developers are using green infrastructures such as biofilters that are designed to capture surface runoff, treat them, and infiltrate into the ground to replenish groundwater for future use (Luthy et al., 2020; Vogel et al., 2015). For stormwater

management method to be effective, green infrastructures must be implemented on a large scale to soak water during heavy rainfall events (Fry and Maxwell, 2017; Tirpak et al., 2021b). However, space is a constraint in urban areas. During urban development, a large fraction of space is taken up for roads for transportation and compacted roadside soils for the use of heavy machinery for road maintenance. Thus, there is an opportunity to redevelop the roadside compacted soil for infiltration-based green infrastructures and transform them into multipurpose lands without compromising their original function.

Infiltration-based green infrastructures are typically designed by replacing native soil with a mixture of sand and soil with other optional amendments to increase the adsorption of pollutants (Tirpak et al., 2021a). In biofilters, 70% or more sand is typically used as a bulking agent to increase the infiltration capacity (Tirpak et al., 2021a). Sand is also an ideal bulking agent to alleviate the negative impact of compaction in roadside soil (Das et al., 2023). Despite the positive effect of sand on aiding infiltration, their use in high amounts in the roadside soil could pose two issues. First, sand has a limited capacity to remove pollutants, thereby requiring the use of other amendments, such as biochar, to remove pollutants (Mohanty et al., 2018). Road runoff particularly contains high concentrations of pollutants (Han et al., 2006), such as metals, pathogens, and organics, which can exhaust the adsorption capacity of soil containing high amounts of sand. Second, the sand has a low water-holding capacity for plants, thereby making it challenging to maintain vegetation during dry climates (Schaller et al., 2020). This issue will be severe during climate change when the drying duration is projected to increase (Grant et al., 2013; Weathers et al., 2023). Vegetation use is necessary on roadside soil because it serves many functions in addition to reducing roadside soil erosion or structure erosion (Muerdter et al., 2018). Therefore, it is critical to find an alternative bulking agent for roadside soil that could

meet three criteria: (1) it should infiltrate water despite compaction, (2) it should hold water longer after rainfall for plant use, (3) it should remove pollutants.

Expanded Shale, Clay, and Slate (ESCS) aggregates could be an alternative bulking agent that could meet these criteria and improve the desired hydraulic and pollutant removal functions of roadside soil. For instance, a recent study found that replacing sand with ESCS in rain gardens may increase plant life survival rates beyond rates currently observed in high sand-content rain gardens (Funai and Kupec, 2019). Another study found that ESCS could adsorb high amounts of metals as well as *E. coli* from polluted runoff, and their bacterial removal capacity could only increase with their aging (Borthakur et al., 2022). Other studies demonstrated ESCS capacity for a wide range of stormwater pollutants (Dordio and Carvalho, 2013; Kalhori et al., 2013a; Malakootian et al., 2009; Nkansah et al., 2012). However, the previous studies rarely tested ESCS infiltration capacity under compaction.

10.1.1 Objectives

The objective of this study is to compare the ability of ESCS aggregates with that of sand to infiltrate runoff during heavy rainfall, hold water for plants during drought, and remove *E. coli* and heavy metals from polluted runoff in compacted roadside biofilters amended with both types of the bulking agent.

10.1.2 Hypothesis

The use of ESCS in roadside stormwater infrastructure design could result in improved performance compared to the use of sand due to its higher aggregate strength under compaction pressure, better water-holding capacity, and negatively charged surface aiding in the removal of stormwater pollutants. Thus, it is critical to test whether ESCS can be a better alternative to sand

to meet the design and performance criteria of roadside stormwater infrastructures. To test this hypothesis, model biofilters were packed with a compacted and uncompacted mixture of roadside soil, biochar as a reactive amendment, and one of the bulking agents: sand or ESCS. Comparing biofilter's hydraulic and pollutant removal behavior during simulated heavy rainfall and drought, we show that ESCS could have the potential to increase the resilience of roadside biofilters during changing climates.

10.2 Material and Methods

10.2.1 Stormwater preparation

For all experiments, natural stormwater was used, which was collected from Ballona Creek in Los Angeles, CA (34° 00′32″ N, 118° 23′3″ W). The creek receives dry-weather irrigation runoff from 318 km^2 of the urban area, with 82% developed and 61% impervious surface. The detailed characteristics of stormwater were reported elsewhere (Borthakur et al., 2022; Ghavanloughajar et al., 2021). Within 1 h of sample collection, the pH and conductivity of the stormwater were measured using a meter connected to an ion-selective electrode (Model #9107BN, Fisher Scientific) and conductivity probe (Two-Cell Accumet, Fisher Scientific), respectively. The stormwater sample was stored at 4 °C until its use in the experiment. We collected dry-weather flow because actual stormwater runoff is not available year-round. Since pollutant concentrations in dry-weather flow are often too low, we spiked the samples with metals or E. coli to reach levels more representative of roadway runoff. This approach allowed us to use a realistic background water matrix, rather than relying on synthetic stormwater, while still evaluating pollutant removal under conditions relevant to Caltrans.

The stormwater was spiked with pollutants to examine their removal in biofilters. We tested the capacity of different media mixtures in compacted roadside biofilters to remove *E. coli*

and heavy metals, as they are often the leading cause of total maximum daily load (TMDL) violations in urban areas (Vogel and Moore, 2016). As dissolved metal can be toxic to *E. coli* (Borthakur et al., 2022), stormwater spiked with *E. coli* was first used to estimate the *E. coli* removal capacity of media mixtures, before repeating the same procedure with stormwater spiked with heavy metals to estimate the metal removal capacity of the media mixture. The collected stormwater was first autoclaved to kill native microorganisms and spiked with a kanamycin-resistant strain of *Escherichia coli* K12 to make the final mean concentration of *E. coli* in influent to $3.4 \pm 0.4 \times 10^5$ CFU mL^{-1} (Valenca et al., 2020). To prepare the stormwater contaminated with metals, natural stormwater was spiked with the most common metals found in road runoff in Los Angeles, which included Pb, Zn, Ni, Cd, Co, Cu, and Cr so that the final concentration of each metal would be 100 µg L^{-1} (Ferreira et al., 2013). We did not include iron and aluminum in this study because these metals are easily precipitated at pH above 7 (typical pH of road runoff), and increase *E. coli* removal via coagulation with precipitated iron. The concentration is within the range found in highly polluted urban runoff (Grebel et al., 2013).

10.2.2 Preparation of biofilter media

A model biofilter without vegetation was designed for this study to limit the effect of confounding factors related to root growth on hydraulic and pollutant removal. In the roadside environment, a typical biofilter is designed by mixing native soil with sand as a bulking agent and occasionally with engineered media such as biochar to improve pollutant removal (Tirpak et al., 2021a). Sand is typically used in all biofilters to enhance the infiltration and alleviate the negative impact of compaction, but it doesn't offer additional capacity to remove most dissolved pollutants (Tirpak et al., 2021a). In contrast, ESCS aggregate can provide the function of the bulking agent while removing dissolved and particulate pollutants from contaminated runoff

(Borthakur et al., 2022). Here we tested ESCS aggregates (ARCOSA Lightweight, USA) as an alternative bulking agent for sand to improve the hydraulic performance of soil on the roadside. Commercially available biochar (Rogue biochar, Oregon Biochar, OR) and coarse sand (ASTM 20-30, Humboldt Mfg Co.) were used. The coarse sand (600–850 μm) was washed in de-ionized (DI) water to remove silica colloids and dried at 105 °C overnight. The biochar, which was produced by the gasification of softwood at 900–1000 °C, has been previously tested for its use in compacted biofilters (Ghavanloughajar et al., 2020). Biochar and ESCS were sieved (mesh #10) to remove particles larger than 2 mm to minimize the formation of preferential flow paths in the packed media. We mixed sand (75% by volume) with soil (25% by volume) to represent a conventional biofilter media (Tirpak et al., 2021a). As the contaminant removal capacity of sand is minimal (Tirpak et al., 2021a), 25% (by volume) of sand was replaced with biochar to enhance pollutant removal in the roadside biofilter. Thus, the final composite mixture contains sand (50%), soil (25%), and biochar (25%) by volume. To compare the utility of ESCS as an alternative bulking agent of sand, another composite mixture was created using ESCS (50%), soil (25%), and biochar (25%).

10.2.3 Model biofilter design

Model biofilters were designed following the method described in a previous study (Ghavanloughajar et al., 2020). Briefly, a transparent PVC tube (5.1 cm ID and 61.0 cm length) was glued with PVC fittings and connected to a control valve to regulate the effluent flow. Three types of media mixture were packed in a total of 18 columns with or without compaction, where triplicate columns with and without compaction were used per media mixture: (1) sand and soil; (2) sand, soil, and biochar; (3) ESCS, soil, and biochar. To simulate the compaction of roadside soil during road construction, the media mixture was added incrementally in layers and

compacted to a layer height of 3.8 cm using a standard Proctor hammer (2.5 kg). To ensure that comparable energy of a standard Proctor test was applied on the filter media, the hammer was dropped 7 times from 30.4 cm height per layer. The procedure was repeated for 4 layers so that the total height of the filter layer became 15.2 cm. The bulk density was calculated during each layer's compaction to ensure uniform filter media distribution. After packing, the filter media was characterized for porosity and saturated hydraulic conductivity following methods described in a previous study (Le et al., 2020). The mixture composition of the biofilter columns and their hydraulic characteristics are summarized in Table 10.1.

Table 10.1 Hydraulic characteristics and design parameters of laboratory compacted biofilters.

Media composition (v/v, %)	Bulk density (g cm^{-3})	Pore volume of filter layer (cm^3)	K_{sat} (mm h^{-1})	Porosity %
Sand (75%) Soil (25 %)	1.83±0.09	92.6±5.8	341±12	27.4±4.3
Sand (50%) Soil (25 %) Biochar (25%)	1.55±0.46	95.3±6.4	41±5	30.71±2.1
ESCS (50%) Soil (25 %) Biochar (25%)	1.08±0.02	122.6±3.6	131±30	38.6±1.2

Mean and standard deviation over mean for each parameter was estimated from measurements in triplicate columns.

10.2.4 Water retention behavior of compacted biofilter media during prolonged drying periods

We compared the water-holding capacity of media mixtures during the natural drying of filter media following the method outlined elsewhere (Trifunovic et al., 2018). Briefly, the media mixture was repacked in empty 250 cm^3 ring cores to match the same bulk density of the

compacted filter layer in the model biofilters, and the soil water retention curve and the unsaturated hydraulic conductivity of treatments were measured using the HYPROP device (METER Group, Inc., USA). The HYPROP measures the unsaturated hydraulic conductivity based on the evaporation method by simultaneously recording the sample weight and soil matric potential during the sample drying cycle from saturation to around pF 2.5, where pF = $\log_{10}$ h and h is the suction in cm below wilting point. We utilized the bimodal soil water retention model (Durner, 1994), which is ideal for describing changes in the physical properties of media having a heterogeneous pore structure. In this case, the water retention curve is expressed as a linear superposition of sub-curves of a homogeneous pore structure using a unimodal model (van Genuchten, 1980), and effective saturation was estimated using the equation below:

$$S_e = w_1 \left\{ \frac{1}{1 + (\alpha_1 h)^{n_1}} \right\}^{m_1} + (1 - w_1) \left\{ \frac{1}{1 + (\alpha_2 h)^{n_2}} \right\}^{m_2}$$

where S_e is effective saturation; w_1 is the weighing factor for the first sub curve subject to $0 < w_i < 1$; α is a scaling factor that determines the position of the pore size maximum; h is the suction (cm); n and m are empirical shape parameters and m =(1-1/n). S_e is related to volumetric water content as $\theta=\theta_r+(\theta_s-\theta_r) S_e$, where θ is the volumetric water content, θ_s is saturated water content, and θ_r is the residual water content ($cm^3\ cm^{-3}$). The model was implemented using a nonlinear fitting program (Seki, 2007), and the modeled water retention curve was fitted with experimental data using the derived parameters.

10.2.5 Testing pollutant removal capacity of biofilters

As dissolved metal can be toxic to *E. coli* (Borthakur et al., 2022), the experiments were conducted first by intermittently applying *E. coli*-spiked stormwater before applying heavy

metal-spiked stormwater. To simulate natural rainfall events, biofilters were subjected to intermittent infiltration of the contaminated stormwater followed by a drying event when the column was drained under gravity and left to dry at room temperature (22 ºC). During the application of *E. coli*-spiked stormwater, 3 PV of stormwater was applied at a flux of 1 mL min^{-1} on the top of the biofilters. This flux rate is lower than the minimum hydraulic conductivity of all media mixtures under compaction, ensuring stormwater would not pond on the top of the filter media during the injection. The effluent samples were collected in fractions from the bottom, but only the last 0.5 PV fraction of the samples were analyzed for *E. coli* concentration using a spread plate technique described elsewhere (Mohanty et al., 2013). The last 0.5 PV after injection of at least 3 PV of contaminated stormwater represents the steady-state concentration and has been used to estimate the removal capacity of the biofilters (Mohanty et al., 2013). The removal capacities of different media mixtures were compared by estimating the log removal as -log (C/C_0), where C is the effluent concentration (C), and C_0 is the influent concentration. The intermittent injection of *E. coli*-spiked stormwater was repeated 5 times to estimate each configuration's mean bacterial removal capacity.

Unlike bacteria that can break through within 3 PV of stormwater injection, metals can take a long time to appear in the effluent based on the metal adsorption capacity of filter media. To ensure the metal breakthrough in the effluent, we applied approximately 700 PV of contaminated stormwater over 60 days and measured effluent metal concentration at specific time intervals. For the analysis of dissolved metals, effluent samples were centrifuged at 6120 G-force for 15 min to settle any suspended particles larger than 0.04 μm. The supernatant was acidified (pH ~3) and analyzed for heavy metals using an Inductively Coupled Plasma-Mass

Spectroscopy. The metal removal capacity of biofilters was calculated by using the equation: $1 - (C_e/C_i)$; where C_e and C_i represent the concentration in the effluent and influent, respectively.

10.3 Results

10.3.1 ESCS-amended media have higher infiltration capacity than sand-amended media

Compaction reduced the hydraulic conductivity of all media mixtures (Figure 10.1). Under compaction, the hydraulic conductivity of ESCS-amended soil and biochar mixture was greater than sand-amended soil and biochar mixture indicating ESCS media is better than sand to alleviate the negative impact of compaction (Figure 10.2). The mean hydraulic conductivity of compacted sand-soil biofilter with 75% sand was 341 mm h^{-1} (Figure 10.2). Adding biochar to the sand and soil mixture reduced their hydraulic conductivity significantly to 41 mm h^{-1}, which is below the desired design infiltration rate of 50-127 mm h^{-1}. Replacing sand with ESCS as bulking media increased the hydraulic conductivity by 220% to 131 mm h^{-1} and met the design infiltration rate for stormwater biofilters.

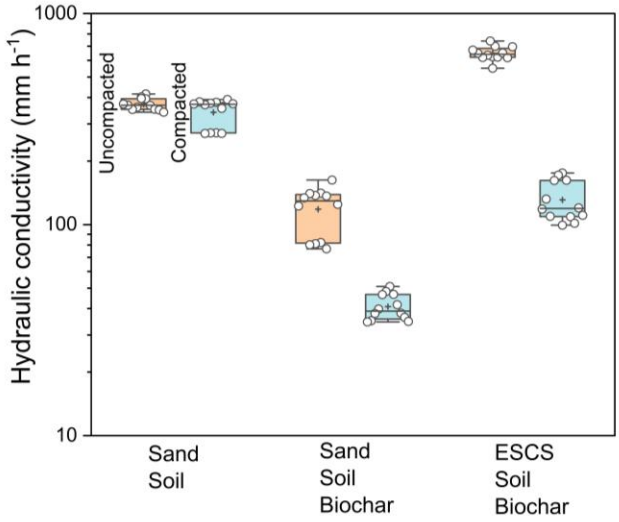

Figure 10.1 Comparison of hydraulic conductivity of three media mixtures with and without compaction: sand (75% by volume) and soil (25%); sand (50%), soil (25%), and biochar (25%); ESCS (50%), soil (25%), and biochar (25%). Plus (+) signs indicate the mean hydraulic conductivity of a total of 12 measurements in triplicate columns per media mixture type.

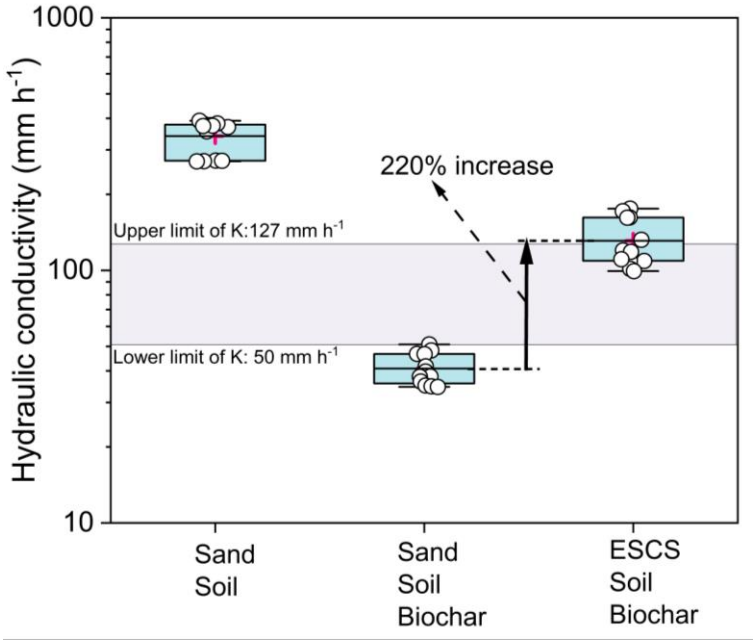

Figure 10.2 Comparison of hydraulic conductivity of three media mixtures under compaction: sand (75% by volume) and soil (25%); sand (50%), soil (25%), and biochar (25%); ESCS (50%), soil (25%), and biochar (25%). The shaded area indicates the design hydraulic conductivity of the biofilter. Plus (+) signs indicate the mean hydraulic conductivity of a total of 12 measurements in triplicate columns per media mixture type.

10.3.2 ESCS media retained more water than sand in between infiltration events

The plant-available water is a crucial parameter for vegetation performance under drought. An increase in drying duration increases water loss by evaporation from filter media pores, thereby increasing suction or negative pressure in the pores. At a given suction, corresponding to a specific drying duration, the ESCS-amended biofilter media retained more moisture than the sand-amended biofilters (**Error! Reference source not found.**). The water-holding capacity of the sand-soil mixture was the lowest, which increased with the addition of

biochar (**Error! Reference source not found.**). Replacing sand with ESCS further increased the

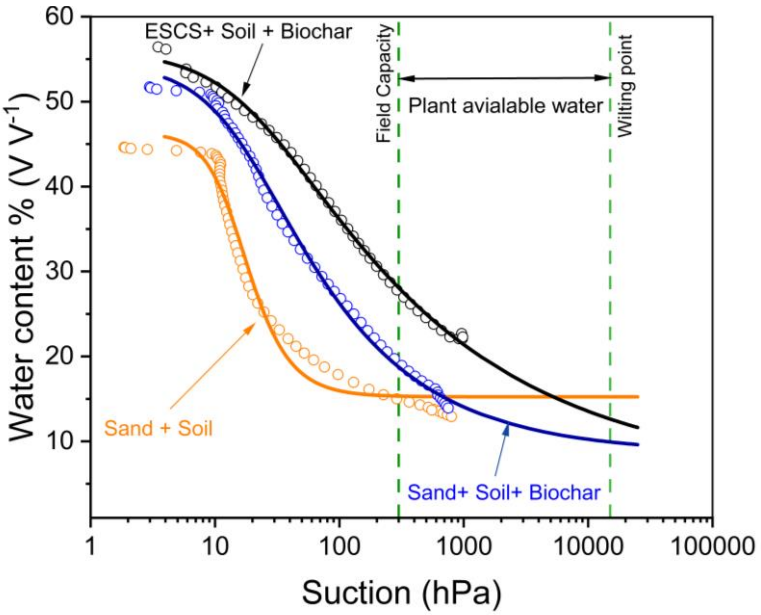

water-holding capacity by 58%.

Figure 10.3 Comparison of water retention behavior of three types of biofilter media mixtures. The solid lines indicate the van Genuchten (1980) unimodal fit for the experimental data. The plant-available water is the difference between the vertical dash lines of field capacity and the permanent wilting point. This measurement was taken from core samples with similar bulk density (a representation of compaction) in columns treated using HyProp instruments. The purpose of this measurement was to better understand pore size distribution and water retention behavior, rather than to evaluate treatment variability.

Table 10.2 Parameter of van Genuchten model from water retention curve

Media mixture	θ_s	θ_r	$\theta_{pF\ 2.5}$ (300 hPa)	$\theta_{pF\ 4.2}$ (15000 hPa)	PAW	α	n	K_s ($mm.h^{-1}$)
Sand + soil	46.28	15.24	15.32	14.30	1.02	0.066	2.967	341
Sand + Soil + biochar	54.46	8.60	18.57	9.01	9.56	0.059	1.519	41
ESCS + soil + biochar	55.95	5.51	27.86	12.48	15.38	0.048	1.296	131

θ_s: Saturated water content, θ_r Residual water content, $\theta_{pF\ 2.5}$ Field capacity, $\theta_{pF\ 4.2}$: Permanent wilting point, PAW: Plant available water, α: scaling factor, n: empirical shape parameter, K_s: saturated hydraulic conductivity.

10.3.3 Pore water in ESCS-amended media have higher DO than that in sand-amended media

Compaction decreased dissolved oxygen (DO) concentration in pore water (Figure 10.4). Under compaction, DO concentration in pore water in ESCS-amended filter media was higher than that in sand-amended filter media. Effluent pH and electrical conductivity from all columns remained consistent at 7.6 ± 0.1 and 1363 ± 24 µS cm^{-1}, respectively (Figure 10.4).

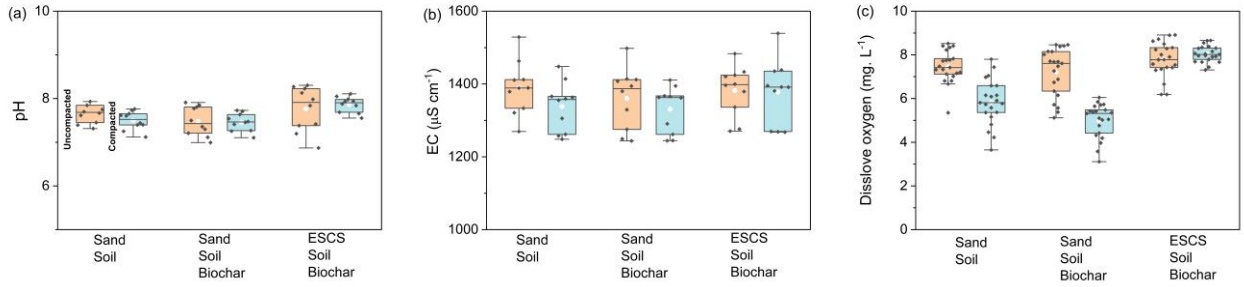

Figure 10.4 The effect of compaction on water quality parameter (a) pH (b) EC (c) Dissolve oxygen (mg. L^{-1}).

10.3.4 Replacing Sand with ESCS in uncompacted columns improved E-coli removal

In uncompacted conditions, ESCS-amended biofilter media removed more *E. coli* than sand-amended biofilter (Figure 10.5). Compaction appears to increase the average *E. coli* removal for both media mixtures, although the difference in removal between both media mixtures was insignificant. All media mixtures recorded > 2 log removal irrespective of compaction, potentially because the soil had an unusually high capacity to adsorb *E. coli*. The sand-only filter media had limited removal of 56%, but adding soil increased removal by 4 orders of magnitude, confirming the soil was either toxic to *E. coli* or had an unusually high capacity to adsorb *E. coli* (Figure 10.6).

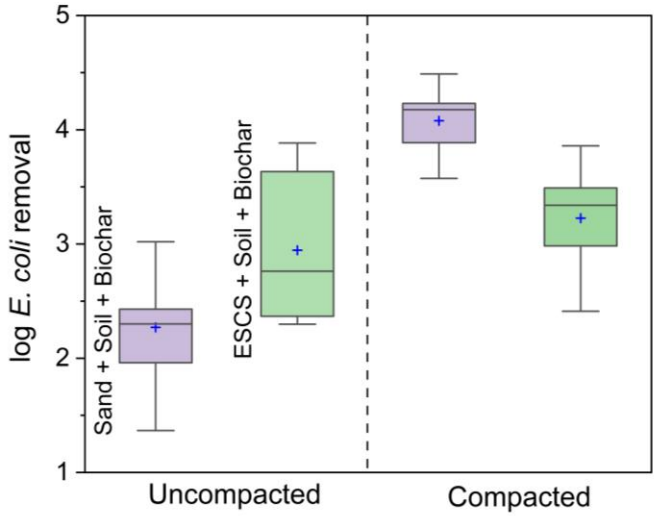

Figure 10.5 The removal of *E. coli* by compacted and uncompacted soil-biochar biofilters amended with sand or ESCS.

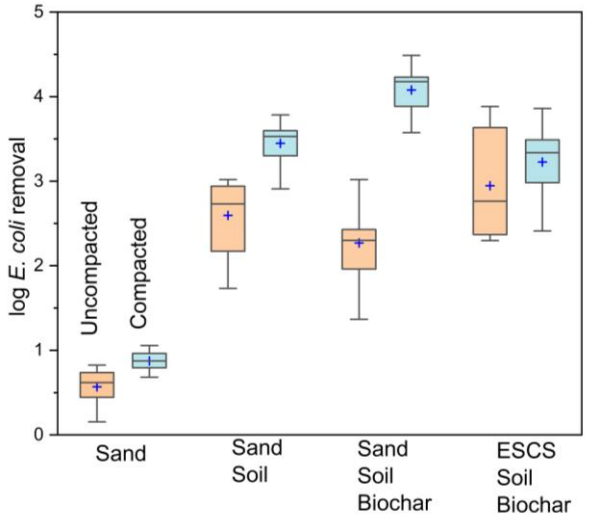

Figure 10.6 Effects of compaction on *E. coli* removal capacity in all media composition.

10.3.5 ESCS media improved metal removal in the long run

In general, the removal of metals decreased with increased exposure to metal-contaminated stormwater but the reduction was more prominent in the media mixture amended with sand than in the mixture amended with ESCS (Figure 10.7). After the passage of 700 PV of contaminated stormwater, the media mixture amended with ESCS consistently removed more metals than the mixture amended with sand (Figure 10.8). At that point, the average removal for all metals in the sand column was 62.9± 8.5 %, which increased to 83.5± 4.9 % when sand was replaced with ESCS. The extent to which ESCS improved metal removal depended on metal types. Replacement of sand with ESCS increases the removal of Pb, Co, Ni, Cu, Zn, Cd, and Cr by 30.7%, 23.5%, 27.8%, 22.7%, 8.8%, 11.0%, and 19.6%, respectively.

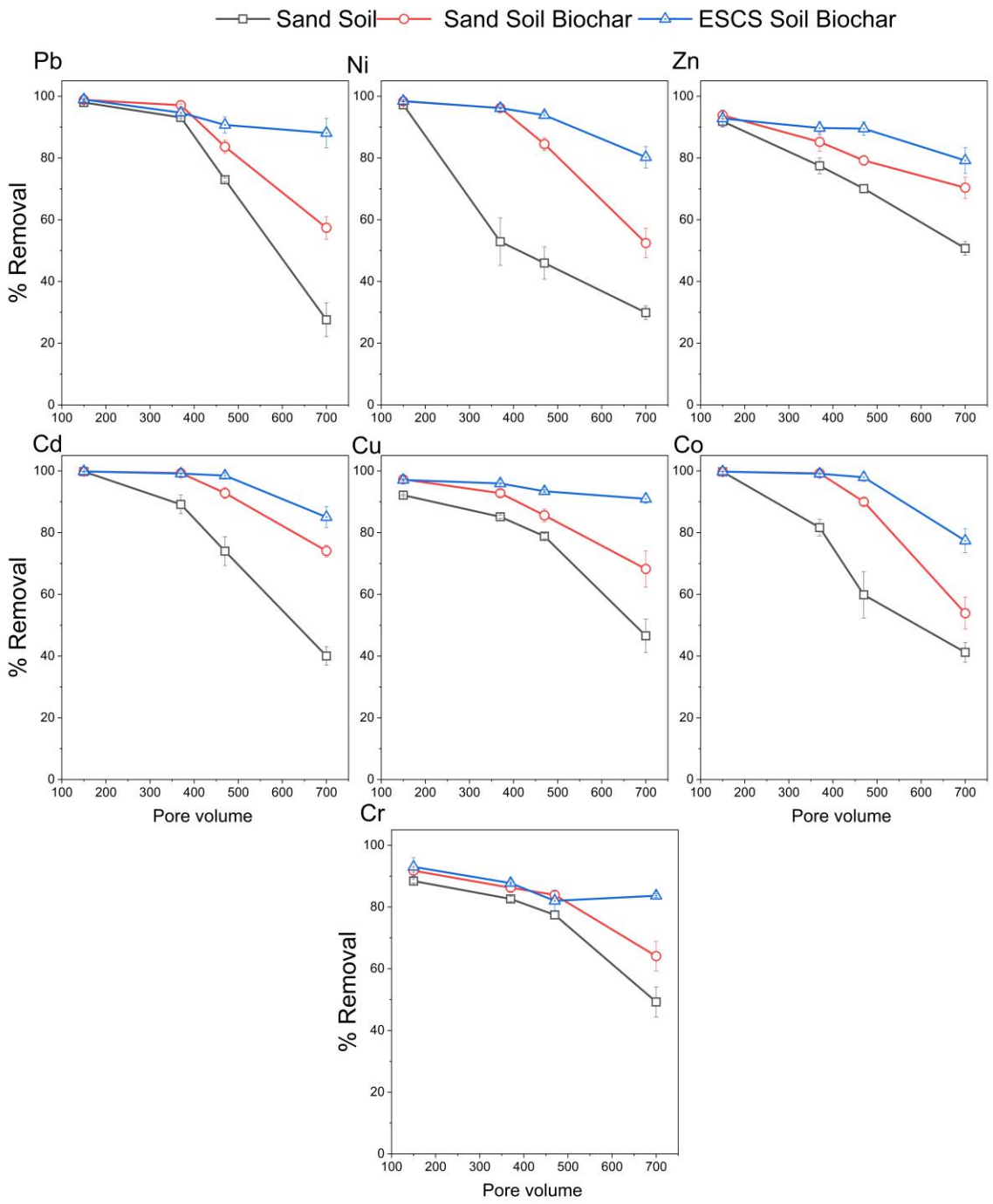

Figure 10.7 The metal removal performance of ESCS amended biofilter over extended exposure time. Error bars are one standard deviation over the mean based on results from triplicates columns.

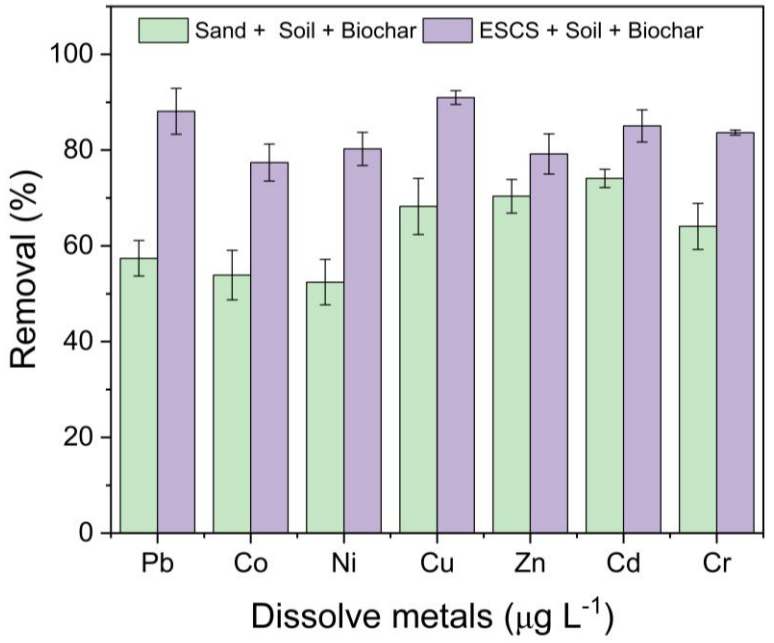

Figure 10.8 The metal removal performance of ESCS amended biofilter after exposure of 700 PV metal contaminated natural stormwater. Error bars indicate one standard deviation over the mean based on the results from triplicates columns.

10.4 Discussion

10.4.1 Cause of better hydraulic performance of ESCS than sand under compaction.

The compaction of roadside soil limits their natural infiltration capacity, and the addition of sand could improve the capacity to some extent but not to the desired limit (~250 cm h^{-1}) to handle high flow rates during extreme rainfall events. Our results (Figure 10.1) show that the addition of ESCS media could help the roadside soil mixture meet the desired infiltration threshold despite compaction. We attributed the results to the high aggregate size of ESCS. The ESCS has a larger grain size than sand, creating large macropores while packing columns (Chung et al., 2018). The macropore distribution creates a more connected flow path and enhances the infiltration rate in ESCS media (Chandel et al., 2022). Soil-water retention curves of all media mixtures in our study confirmed an increase in macro and mesoporosity of soil amended with ESCS (Figure 2). Unlike other amendments such as biochar that can break under compaction pressure (Le et al., 2020), ESCS media appears to remain mostly intact under

compaction due to its structural stability of aggregate created under high heat. Our results corroborated the results of other studies on ESCS without compaction that showed the addition of ESCS could increase the infiltration capacity of stormwater treatment systems (Funai and Kupec, 2019; Mechleb et al., 2014). Our study shows that the hydraulic conductivity of ESCS does not deteriorate as much as sand due to large aggregate and protected intraparticle pore space. As ESCS can be produced in any size, they can be tailored to specific aggregate sizes based on soil hydrological groups. The high infiltration capacity of ESCS-amended roadside soil is particularly beneficial to soak more water from high-speed runoff from the road surface. The enhanced infiltration could reduce flooding and increase groundwater recharge. Thus, adding ESCS amendments to thousands of square miles of unused space on roadside soil could transform them into multifunctional managed aquifer recharge facilities for water sustainability (Alam et al., 2021), which is otherwise not possible in the space-constraint urban landscape.

10.4.2 Cause of higher plant-available water in ESCS-amended soil than in sand-amended roadside soil

Most green infrastructures contain plants by design, which often require irrigation, thereby adding overall maintenance costs. The maintenance cost would be higher in dry climates. Furthermore, irrigation is often impractical in remote roadside soil. Thus, adding an amendment that could retain water for a longer period after rainfall without limiting the infiltration capacity could solve the issue. Our result shows that ESCS could serve that function. ESCS retained more water than sand during the drying period. ESCS exhibited higher water content at field capacity and higher plant available water than sand (Figure 10.2 and Table 10.1). We attribute the result to the formation of mesopore during compaction. The pore space geometry and dimensions and packing density affect water retention behavior in porous media (Zhai et al.,

2020). Unlike solid sand, ESCS aggregates have internal micro and mesopores that stay intact despite compaction and contribute to water retention. During packing, ESCS likely created more inter particles of mesopores and macropores than the smaller sand particles. This could be one reason why ESCS has a more significant impact on water retention at field capacity (Liu et al., 2017). Moisture retained within the internal pore of ESCS can become available to the surrounding soil matrix as the roadside soil dries and supplies water to the plant (Wang et al., 2019). Our result also explained why incorporating ESCS as a replacement for high sand content increased plant life survival rates during dry spells in rain gardens (Funai and Kupec, 2019). As climate change has increased extreme hydrological events such as prolonged drought, improving the water retention capacity of roadside soil or filter media in stormwater control measures by adding ESCS could support healthy vegetation establishment and microbial community and increase their climate resilience.

10.4.3 Cause of high E. coli removal in ESCS amended soil

E. coli is one of the most difficult pollutants to remove in stormwater control measures because of the low capacity of sand unless other amendments, such as biochar and iron filing, are added to improve the *E. coli* removal (Ghavanloughajar et al., 2021; Valenca et al., 2021). This study shows that replacing sand with alternative bulking agents such as ESCS would improve *E. coli* removal in both uncompacted and compacted soil, but the benefit of ESCS is particularly more prominent in uncompacted amended soil. Unlike solid sand grain, porous ESCS media has a higher surface area with more reactive sites. ESCS could also adsorb metals and other chemicals that could inactivate *E. coli* after their initial attachment (Borthakur et al., 2022). This result is particularly important because the hydraulic retention time of stormwater in ESCS-amended media was lower than that of sand-amended media in the uncompacted column.

Compacted sand-amended soil and biochar mixture removed more *E. coli* than compacted ESCS-amended soil-biochar mixture, possibly because of extra removal of *E. coli* by staining. The hydraulic conductivity of sand-amended soil and biochar mixture decreased drastically after compaction due to pore blockage by broken biochar particles (Le et al., 2020). Thus, extra removal came at the cost of a net reduction in the water treatment volume. It should be noted that the *E. coli* removal in our study was unusually high, possibly because the soil either adsorbed more *E. coli* or was toxic to *E. coli*. This explains why the sand and soil mixture removed more than one log *E. coli* (Figure S4). Thus, the benefit of ESCS media might have been more apparent in soils with low *E. coli* adsorption capacity. Such soil can be identified by measuring metal contamination. However, if resources permit, performing small-scale column tests with E. coli directly would yield more precise and dependable results.

10.4.4 Cause of improved metal removal in ESCS-amended soil

In road runoff, metal concentration can be high, and sand has little capacity to remove dissolved metal. Our results show that an addition of ESCS to the soil mix can improve their capacity to remove metals. The metal removal decreased in both sand and ESCS with an increase in exposure to metal-contaminated runoff, indicating exhaustion of their adsorption capacity. However, the exhaustion rate was slower in ESCS than in sand, indicating the performance life of ESCS-amended media would last longer than sand-amended media. The result is consistent with other studies (Kalhori et al., 2013; Shojaeimehr et al., 2014). ESCS media could remove metals via adsorption and complexation due to their high cation exchange capacity (Borthakur et al., 2022). Some clay or shale exhibits high metal removal capacity. As ESCS media is composed of expanded clay and shale, ESCS removed more metals than silica sand.

10.4.5 Conceptual understanding of why ESCS can be a better bulking agent than sand

Our results proved that ESCS could provide many benefits over sand if used as a bulking agent in green infrastructures. ESCS can simultaneously increase the hydraulic conductivity of soil to quickly handle large volume runoff without diminishing water retention during a long drying period between rainfall events. ESCS enables high infiltration by virtue of their large aggregate size, which can be controlled based on design specifications. ESCS has intraparticle pores that are preserved despite compaction and retain water. In contrast, sand grains do not have any internal pores, and water retention in sand arises from interparticle pore space, which is determined by packing density and soil pore size. If the sand and soil mixture is heavily compacted, then the macro and mesopores are converted to micropores, thereby decreasing the water availability for plants. Thus, a combination of large aggregate size, their ability to withstand compaction, and preserved mesopores and micropores in intraparticle spaces enable ESCS to provide better hydraulic functions than sand in green infrastructures (Figure 10.5). ESCS also exhibited a much higher capacity to remove metals and *E. coli* than sand. Sand is made out of silicate, which has limited surface areas and reactive sites to adsorb any pollutants (Tirpak et al., 2021a). In contrast, ESCS aggregates are made of shale, clay, and slates, which are stabilized at high heat. This creates a reactive surface that can absorb pollutants. Previous studies provided a mechanistic explanation of why ECSC could remove more metals and *E. coli* (Borthakur et al., 2022), and our study corroborated that evidence under compaction and in the presence of soil.

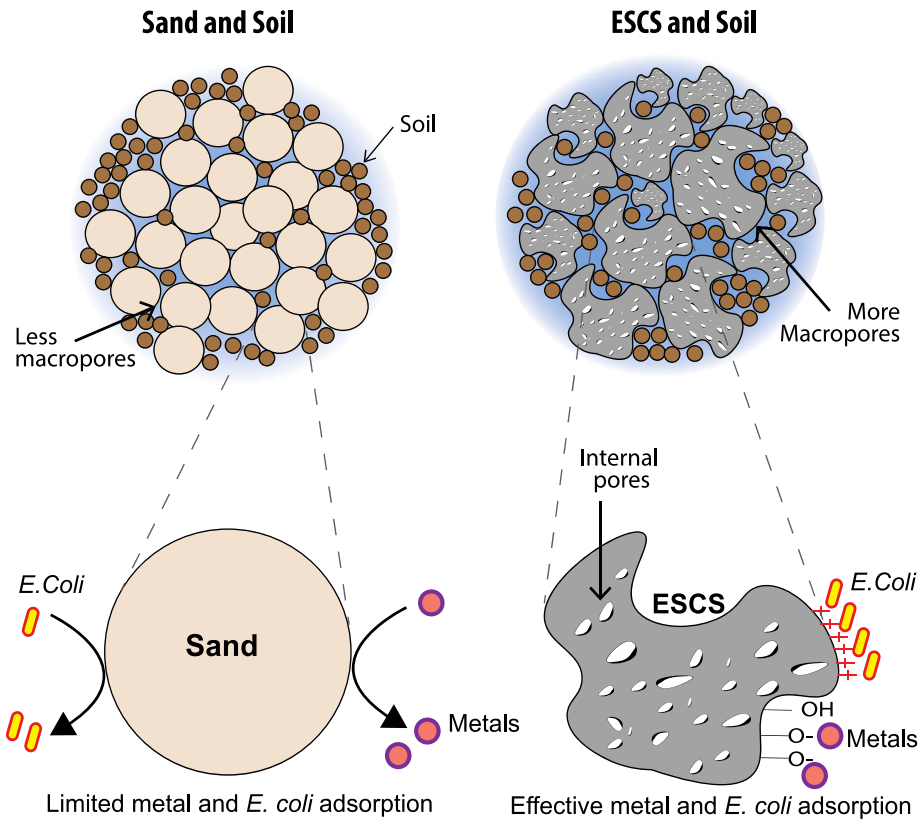

Figure 10.9 Conceptual illustration showing ESCS could have many advantages over sand due to their shape, internal pores, and reactive surfaces.

10.4.6 Environmental Implications

The results have far-reaching implications for designing climate-resilient green infrastructures in the roadside environment. An increase in infiltration capacity would help infiltrate high-flowing road runoff. The use of ESCS in other locations without compaction could help the distributed green infrastructures to soak more water from runoff during high-intensity rainfall events, which are projected to become more frequent during climate change. Increasing the water-holding capacity of the filter layer in the green infrastructure could make the plants survive longer during long drying periods and reduce the overall maintenance cost for irrigation. This is particularly beneficial in the remote roadside environment, where providing irrigation can be expensive. The high pollutant removal capacity of ESCS compared to sand can also lower the

burden of using a separate amendment other than a bulking agent to meet the pollutant removal goal. As road runoffs are often polluted with metals, ESCS provides a better alternative to meet the TMDL requirement. However, ESCS is more expensive than sand, although most of the cost is related to shipping a large quantity of media for long distances. Fortunately, ESCS is a lightweight material with a mean density of 1.25-1.65 g cm^{-3}, compared to the sand density of 2.65 g cm^{-3}. Thus, this would reduce the shipping cost to specific locations. The overall cost could be comparable by adding the life cycle benefits of the increased treatment volume via enhanced infiltration and better pollutant removal capacity. Thus, ECSC has the potential to be used as an alternative bulking agent in all green infrastructures to increase their climate resilience.

10.5 Conclusions

Roadside soils in space-constraint urban areas provide an opportunity to install stormwater biofilters and increase groundwater recharge, but the required compaction of roadside soils makes it unfeasible to design biofilters following the design specification of using conventional filter media that include 70% or more sand. Our study examined whether replacing sand with ESCS could increase infiltration despite compaction and provide other intended functions during extreme hydrological conditions such as high-intensity rainfall and drought. Replacing sand with ESCS not only increased infiltration capacity despite compaction but also increased water holding capacity, thereby increasing plant available water. This could potentially lower irrigation frequency to maintain the vegetation and increase the resilience of biofilters to remain functional during long drying periods between rainfall events. ESCS also provided additional benefits of increasing biofilter capacity to remove pollutants such as *E. coli* and heavy metals. The results indicate that ESCS media possess a unique characteristic as a bulking agent

that, despite having a larger aggregate size, increase both infiltration capacity and water retention. Replacing sand with ESCS in stormwater control measures could improve their ability to withstand extreme hydrological conditions such as high-intensity rainfall by quickly infiltrating water and long drying period by retaining more water near the root zones. Thus, including ESCS in biofilter media specification in roadside soil could turn the transportation infrastructures from a source of pollution to a network of sustainable water solutions in water-stressed space-constrained urban areas.

10.6 References

Ahmadi, M.S., Sušnik, J., Veerbeek, W., Zevenbergen, C., 2020. Towards a global day zero? Assessment of current and future water supply and demand in 12 rapidly developing megacities. Sustainable Cities and Society 61, 102295. https://doi.org/10.1016/j.scs.2020.102295

Alam, S., Borthakur, A., Ravi, S., Gebremichael, M., Mohanty, S.K., 2021. Managed aquifer recharge implementation criteria to achieve water sustainability. Science of The Total Environment 768, 144992. https://doi.org/10.1016/j.scitotenv.2021.144992

Borthakur, A., Chhour, K.L., Gayle, H.L., Prehn, S.R., Stenstrom, M.K., Mohanty, S.K., 2022. Natural aging of expanded shale, clay, and slate (ESCS) amendment with heavy metals in stormwater increases its antibacterial properties: Implications on biofilter design. Journal of Hazardous Materials 429, 128309. https://doi.org/10.1016/j.jhazmat.2022.128309

Chandel, A., Sharma, S., Shankar, V., 2022. Prediction of hydraulic conductivity of porous media using a statistical grain-size model. Water Supply 22, 4176–4192. https://doi.org/10.2166/ws.2022.043

Chung, C.-K., Kim, J.-H., Kim, J., Kim, T., 2018. Hydraulic Conductivity Variation of Coarse-Fine Soil Mixture upon Mixing Ratio. Advances in Civil Engineering 2018, 1–11. https://doi.org/10.1155/2018/6846584

Das, T.K., Kabir, A., Zhao, W., Stenstrom, M.K., Dittrich, T.M., Mohanty, S.K., 2023. A review of compaction effect on subsurface processes in soil: Implications on stormwater treatment in roadside compacted soil. Science of The Total Environment 858, 160121. https://doi.org/10.1016/j.scitotenv.2022.160121

Dordio, A., Carvalho, A.J.P., 2013. Constructed wetlands with light expanded clay aggregates for agricultural wastewater treatment. Science of The Total Environment 463–464, 454–461. https://doi.org/10.1016/j.scitotenv.2013.06.052

Durner, W., 1994. Hydraulic conductivity estimation for soils with heterogeneous pore structure. Water Resour. Res. 30, 211–223. https://doi.org/10.1029/93WR02676

Epps, T.H., Hathaway, J.M., 2021. Inter-Event Water Quality Variability and Intra-Event Pollutant Dynamics in Context of Effective Impervious Area. J. Sustainable Water Built Environ. 7, 04021013. https://doi.org/10.1061/JSWBAY.0000953

Ferreira, M., Lau, S.-L., Stenstrom, M.K., 2013. Size Fractionation of Metals Present in Highway Runoff: Beyond the Six Commonly Reported Species. Water Environment Research 85, 793–805. https://doi.org/10.2175/106143013X13736496908870

Fry, T.J., Maxwell, R.M., 2017. Evaluation of distributed BMP s in an urban watershed—High resolution modeling for stormwater management. Hydrol. Process. 31, 2700–2712. https://doi.org/10.1002/hyp.11177

Funai, J.T., Kupec, P., 2019. Evaluation of Three Soil Blends to Improve Ornamental Plant Performance and Maintain Engineering Metrics in Bioremediating Rain Gardens. Water Air Soil Pollut 230, 3. https://doi.org/10.1007/s11270-018-4049-x

Ghavanloughajar, M., Borthakur, A., Valenca, R., McAdam, M., Khor, C.M., Dittrich, T.M., Stenstrom, M.K., Mohanty, S.K., 2021. Iron amendments minimize the first-flush release of pathogens from stormwater biofilters. Environmental Pollution 281, 116989. https://doi.org/10.1016/j.envpol.2021.116989

Ghavanloughajar, M., Valenca, R., Le, H., Rahman, M., Borthakur, A., Ravi, S., Stenstrom, M.K., Mohanty, S.K., 2020. Compaction conditions affect the capacity of biochar-amended sand filters to treat road runoff. Science of The Total Environment 735, 139180. https://doi.org/10.1016/j.scitotenv.2020.139180

Grant, S.B., Fletcher, T.D., Feldman, D., Saphores, J.-D., Cook, P.L.M., Stewardson, M., Low, K., Burry, K., Hamilton, A.J., 2013. Adapting Urban Water Systems to a Changing Climate: Lessons from the Millennium Drought in Southeast Australia. Environ. Sci. Technol. 47, 10727–10734. https://doi.org/10.1021/es400618z

Grebel, J.E., Mohanty, S.K., Torkelson, A.A., Boehm, A.B., Higgins, C.P., Maxwell, R.M., Nelson, K.L., Sedlak, D.L., 2013. Engineered Infiltration Systems for Urban Stormwater Reclamation. Environmental Engineering Science 30, 437–454. https://doi.org/10.1089/ees.2012.0312

Han, Y., Lau, S.-L., Kayhanian, M., Stenstrom, M.K., 2006. Characteristics of Highway Stormwater Runoff. Water Environment Research 78, 2377–2388. https://doi.org/10.2175/106143006X95447

He, C., Liu, Z., Wu, J., Pan, X., Fang, Z., Li, J., Bryan, B.A., 2021. Future global urban water scarcity and potential solutions. Nat Commun 12, 4667. https://doi.org/10.1038/s41467-021-25026-3

Kalhori, E.M., Yetilmezsoy, K., Uygur, N., Zarrabi, M., Shmeis, R.M.A., 2013a. Modeling of adsorption of toxic chromium on natural and surface modified lightweight expanded clay aggregate (LECA). Applied Surface Science 287, 428–442. https://doi.org/10.1016/j.apsusc.2013.09.175

Kalhori, E.M., Yetilmezsoy, K., Uygur, N., Zarrabi, M., Shmeis, R.M.A., 2013b. Modeling of adsorption of toxic chromium on natural and surface modified lightweight expanded clay aggregate (LECA). Applied Surface Science 287, 428–442. https://doi.org/10.1016/j.apsusc.2013.09.175

Le, H., Valenca, R., Ravi, S., Stenstrom, M.K., Mohanty, S.K., 2020. Size-dependent biochar breaking under compaction: Implications on clogging and pathogen removal in biofilters. Environmental Pollution 266, 115195. https://doi.org/10.1016/j.envpol.2020.115195

Liu, Z., Dugan, B., Masiello, C.A., Gonnermann, H.M., 2017. Biochar particle size, shape, and porosity act together to influence soil water properties. PLoS ONE 12, e0179079. https://doi.org/10.1371/journal.pone.0179079

Luthy, R.G., Wolfand, J.M., Bradshaw, J.L., 2020. Urban Water Revolution: Sustainable Water Futures for California Cities. J. Environ. Eng. 146, 04020065. https://doi.org/10.1061/(ASCE)EE.1943-7870.0001715

Malakootian, M., Nouri, J., Hossaini, H., 2009. Removal of heavy metals from paint industry's wastewater using Leca as an available adsorbent. Int. J. Environ. Sci. Technol. 6, 183–190. https://doi.org/10.1007/BF03327620

McGrane, S.J., 2016. Impacts of urbanisation on hydrological and water quality dynamics, and urban water management: a review. Hydrological Sciences Journal 61, 2295–2311. https://doi.org/10.1080/02626667.2015.1128084

Mechleb, G., Gilbert, R., Christman, M., Gupta, R., Gross, B., 2014. Use of Expanded Shale Amendment to Enhance Drainage Properties of Clays, in: Geo-Congress 2014 Technical Papers. Presented at the Geo-Congress 2014, American Society of Civil Engineers, Atlanta, Georgia, pp. 3444–3454. https://doi.org/10.1061/9780784413272.334

Mohanty, S.K., Torkelson, A.A., Dodd, H., Nelson, K.L., Boehm, A.B., 2013. Engineering Solutions to Improve the Removal of Fecal Indicator Bacteria by Bioinfiltration Systems during Intermittent Flow of Stormwater. Environ. Sci. Technol. 47, 10791–10798. https://doi.org/10.1021/es305136b

Mohanty, S.K., Valenca, R., Berger, A.W., Yu, I.K.M., Xiong, X., Saunders, T.M., Tsang, D.C.W., 2018. Plenty of room for carbon on the ground: Potential applications of biochar for stormwater treatment. Science of The Total Environment 625, 1644–1658. https://doi.org/10.1016/j.scitotenv.2018.01.037

Nkansah, M.A., Christy, A.A., Barth, T., Francis, G.W., 2012. The use of lightweight expanded clay aggregate (LECA) as sorbent for PAHs removal from water. Journal of Hazardous Materials 217–218, 360–365. https://doi.org/10.1016/j.jhazmat.2012.03.038

Schaller, J., Cramer, A., Carminati, A., Zarebanadkouki, M., 2020. Biogenic amorphous silica as main driver for plant available water in soils. Sci Rep 10, 2424. https://doi.org/10.1038/s41598-020-59437-x

Seki, K., 2007. SWRC fit – a nonlinear fitting program with a water retention curve for soils having unimodal and bimodal pore structure (preprint). https://doi.org/10.5194/hessd-4-407-2007

Shojaeimehr, T., Rahimpour, F., Khadivi, M.A., Sadeghi, M., 2014. A modeling study by response surface methodology (RSM) and artificial neural network (ANN) on Cu2+ adsorption optimization using light expended clay aggregate (LECA). Journal of Industrial and Engineering Chemistry 20, 870–880. https://doi.org/10.1016/j.jiec.2013.06.017

Tirpak, R.A., Afrooz, A.N., Winston, R.J., Valenca, R., Schiff, K., Mohanty, S.K., 2021a. Conventional and amended bioretention soil media for targeted pollutant treatment: A critical review to guide the state of the practice. Water Research 189, 116648. https://doi.org/10.1016/j.watres.2020.116648

Tirpak, R.A., Hathaway, J.M., Khojandi, A., Weathers, M., Epps, T.H., 2021b. Building resiliency to climate change uncertainty through bioretention design modifications. Journal of Environmental Management 287, 112300. https://doi.org/10.1016/j.jenvman.2021.112300

Trifunovic, B., Gonzales, H.B., Ravi, S., Sharratt, B.S., Mohanty, S.K., 2018. Dynamic effects of biochar concentration and particle size on hydraulic properties of sand. Land Degrad Dev 29, 884–893. https://doi.org/10.1002/ldr.2906

Valenca, R., Borthakur, A., Zu, Y., Matthiesen, E.A., Stenstrom, M.K., Mohanty, S.K., 2021. Biochar Selection for *Escherichia coli* Removal in Stormwater Biofilters. J. Environ. Eng. 147, 06020005. https://doi.org/10.1061/(ASCE)EE.1943-7870.0001843

Valenca, R., Ramnath, K., Dittrich, T.M., Taylor, R.E., Mohanty, S.K., 2020. Microbial quality of surface water and subsurface soil after wildfire. Water Research 175, 115672. https://doi.org/10.1016/j.watres.2020.115672

van Genuchten, M.Th., 1980. A Closed-form Equation for Predicting the Hydraulic Conductivity of Unsaturated Soils. Soil Science Society of America Journal 44, 892–898. https://doi.org/10.2136/sssaj1980.03615995004400050002x

Vogel, J.R., Moore, T.L., 2016. Urban Stormwater Characterization, Control, and Treatment. water environ res 88, 1918–1950. https://doi.org/10.2175/106143016X14696400495938

Vogel, J.R., Moore, T.L., Coffman, R.R., Rodie, S.N., Hutchinson, S.L., McDonough, K.R., McLemore, A.J., McMaine, J.T., 2015. Critical Review of Technical Questions Facing Low Impact Development and Green Infrastructure: A Perspective from the Great Plains. water environ res 87, 849–862. https://doi.org/10.2175/106143015X14362865226392

Wang, D., Li, C., Parikh, S.J., Scow, K.M., 2019. Impact of biochar on water retention of two agricultural soils – A multi-scale analysis. Geoderma 340, 185–191. https://doi.org/10.1016/j.geoderma.2019.01.012

Weathers, M., Hathaway, J.M., Tirpak, R.A., Khojandi, A., 2023. Evaluating the impact of climate change on future bioretention performance across the contiguous United States. Journal of Hydrology 616, 128771. https://doi.org/10.1016/j.jhydrol.2022.128771

Wu, W.-Y., Lo, M.-H., Wada, Y., Famiglietti, J.S., Reager, J.T., Yeh, P.J.-F., Ducharne, A., Yang, Z.-L., 2020. Divergent effects of climate change on future groundwater availability in key mid-latitude aquifers. Nat Commun 11, 3710. https://doi.org/10.1038/s41467-020-17581-y

Zhai, Q., Rahardjo, H., Satyanaga, A., Dai, G., 2020. Estimation of the soil-water characteristic curve from the grain size distribution of coarse-grained soils. Engineering Geology 267, 105502. https://doi.org/10.1016/j.enggeo.2020.105502

11 Task 4: Empirical models to quantify infiltration capacity of compacted filter media mixture.

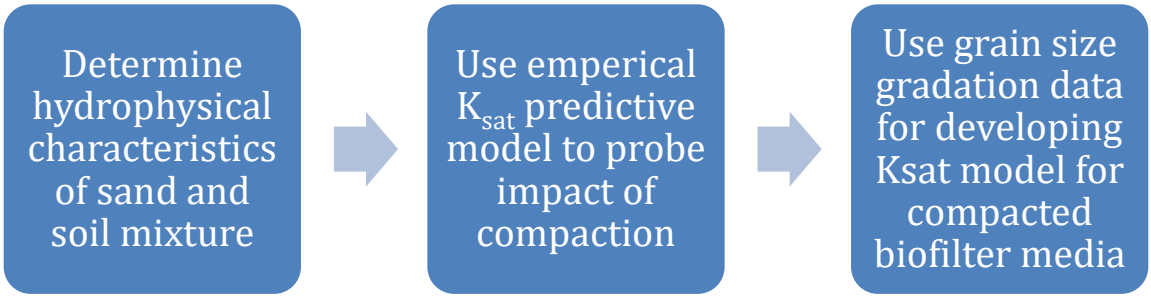

11.1 Motivation

Hydraulic properties of stormwater biofilter mixture varied widely based on amendments type, amounts, and native soil properties (Pearson et al., 2013; Pitt et al., 2002; Sileshi et al., 2015). In general, compaction reduces the infiltration of biofilter media by reducing porosity, but to what extent compaction would reduce infiltration capacity of the biofilter media is challenging, thereby making it difficult for the stormwater manager to predict the amount of bulking agent needed to alleviate the compaction impacts. This task aims to collect enough experimental data on hydraulic conductivity of sand and soil mixtures under compaction and predict the amount of sand needed to achieve the desired hydraulic conductivity at a site by developing empirical models. The developed model would provide critical information the biofilter design guidance in roadside environment.

11.1.1 Objective

Establish a relationship between compaction and soil hydraulic conductivity of filter media based on soil types, amendment fractions, moisture content, particle size distribution, and chemical properties of amendments and use a regression model to quantify the compaction impact.

11.1.2 Hypothesis

The existing empirical models would not be able to predict hydraulic conductivity of compacted soil and sand mixture without accounting for changes in porosity and other properties in the compacted media.

11.2 Methods

The grain size distribution curve was used to calculate the individual D_x values (D_{10}, D_{50}, and D_{90}) of with different ratios of the sand-soil mixture four soil hydrologic groups (SHG A, B, C, D). D_x expresses the grain diameter (μm) where x is the weight percentage of the total mixture finer or smaller that the size D. Grain size analysis was used to calculate the amount of coarse (sand) and fine fractions (silt and clay) present in the mixture. Hydraulic conductivity and bulk density of all mixtures were determined as described in Task 3a.

Pearson correlations were used to verify the link between physical properties of mixture with their infiltration rate under compaction. To select predictive models, existing K_{sat} prediction models were first considered. Most prediction models available in the literature for granular soils use one or more characteristic properties of media mixture. Only a few predictive models consider other parameters such as the soil porosity (η) or void ratio (e), which changes during compaction. K_{sat} prediction methods should consider porosity or void ratio, as the density of the soil matrix (i.e., whether the soil is in a loose or dense state) can significantly affect the saturated hydraulic conductivity of the soil. Here we evaluated our data in four empirical models: Hazen

(1892), Slichter (1898), Terzaghi (1925), and Chapuis (2004). The details of empirical models are given in a later section.

Results and discussion

11.2.1 Relationship of hydraulic conductivity with hydro-physical characteristics of media

The compacted soil and sand mixture was characterized by grain size gradation, sand-silt-clay content, bulk density, and saturated hydraulic conductivity (k_{sat}). The details are summarized in Table 11.1. A correlation matrix was developed using the parameters listed above to comprehend which parameter can explain the variability of k_{sat} under compaction (Figure 11.1). The k_{sat} was positively correlated with D_{10} and the sand fraction and negatively correlated with silt and clay fraction. The bulk density showed a non-significant correlation with K_{sat}.

The D_{10} was found to be the most important parameter for K_{sat} prediction. The hydraulic conductivity of the sand-soil mixture linearly increased with an increase in the D_{10} (Figure 11.2). Higher D_{10} provided more void space for the fluid to move through the interconnected voids, thereby increasing the K_{sat} value (Pliakas and Petalas; 2011). Empirically, the D_{10} size has been a critical soil gradation parameter for k_{sat} prediction (Chandel et al., 2022; Boadu, 2000). Our study concludes that under compaction, D_{10} also plays a significant role in predicting media k_{sat} capacity. In a soil, bulk density is used to measure the degree of compaction, which could quantify hydraulic conductivity. However, our analysis showed that the bulk density of various ratios of compacted soil/sand media mixture did not explain the variability of k_{sat} data. Large values of k_{sat} were recorded in a high bulk density media mixture due to the higher bulk density of pure sand media compared to soil. Compacted media bulk density did not reflect the hydraulic function. Our data concludes that the relative size of the bulking material compared to soil grain size determines the hydraulic conductivity of the mixture under compaction.

Table 11.1. Hydro-physical characteristics of soil and sand samples

Biofilter media		Size distribution (µm)			Texture (%)			Physical properties	
Soil group	Mixing ratio (w/w%) Sand: Soil	D_{10}	D_{50}	D_{90}	Sand	Silt	Clay	Bulk density (g cm^{-3})	K_{sat} (inch.h^{-1})
Soil A1	0 : 100	2.82	49.03	307.05	45.4	47.3	7.3	1.54	0.13
	70 : 30	19.51	799.15	1181.42	83.6	14.2	2.2	2.01	2.87
	80 : 20	49.03	844.05	1204.31	89.1	9.5	1.5	1.95	5.06
	90 : 10	552.01	880.23	1222.57	94.5	4.7	0.7	1.90	18.67
Soil A4	0 : 100	5.48	193.83	959.27	67.5	28.1	4.4	1.92	0.29
	70 : 30	67.15	825.37	1208.83	90.2	8.4	1.3	2.10	4.57
	80 : 20	193.83	859.12	1220.09	93.5	5.6	0.9	2.05	5.47
	85 : 15	409.07	873.48	1225.00	95.1	4.2	0.7	1.95	7.79
Soil B1	0 : 100	1.44	17.68	123.96	23.7	63	13.2	1.60	0.10
	70 : 30	7.52	794.92	1180.32	77.1	18.9	4	2.25	0.02
	80 : 20	17.68	841.84	1203.80	84.7	12.6	2.6	2.21	1.65
	85 : 15	40.14	861.96	1213.61	88.6	9.5	2	2.08	5.44
	90 : 10	516.92	879.39	1222.39	92.4	6.3	1.3	1.99	18.91
Soil B2	0 : 100	1.73	23.85	139.29	26.9	61.9	11.2	1.69	0.07
	70 : 30	9.52	794.93	1180.32	78.1	18.6	3.4	2.14	0.54
	80 : 20	23.85	841.85	1203.80	85.4	12.4	2.2	2.13	0.62
	85 : 15	48.50	861.96	1213.61	89	9.3	1.7	2.18	2.23
	90 : 10	513.54	879.39	1222.39	92.7	6.2	1.1	2.10	15.50
Soil B3	0 : 100	3.80	86.29	288.75	56.9	37.1	6	1.76	0.14
	70 : 30	36.28	797.92	1181.21	87.1	11.1	1.8	2.18	1.93
	90 : 10	548.19	879.99	1222.55	95.7	3.7	0.6	1.93	4.82
	95 : 5	637.64	895.46	1230.37	97.8	1.9	0.3	1.93	34.93
Soil B4	0 : 100	3.44	84.43	817.10	54.6	39.7	5.7	1.48	0.20
	50 : 50	9.44	704.78	1138.45	77.3	19.8	2.9	1.77	1.18
	60 : 40	14.31	770.37	1166.13	81.8	15.9	2.3	1.93	1.72
	65 : 35	19.07	796.07	1178.43	84.1	13.9	2	1.93	4.86
	70 : 30	27.83	817.10	1189.47	86.4	11.9	1.7	1.96	11.11
	80 : 20	84.43	854.01	1208.46	90.9	7.9	1.1	2.00	20.27

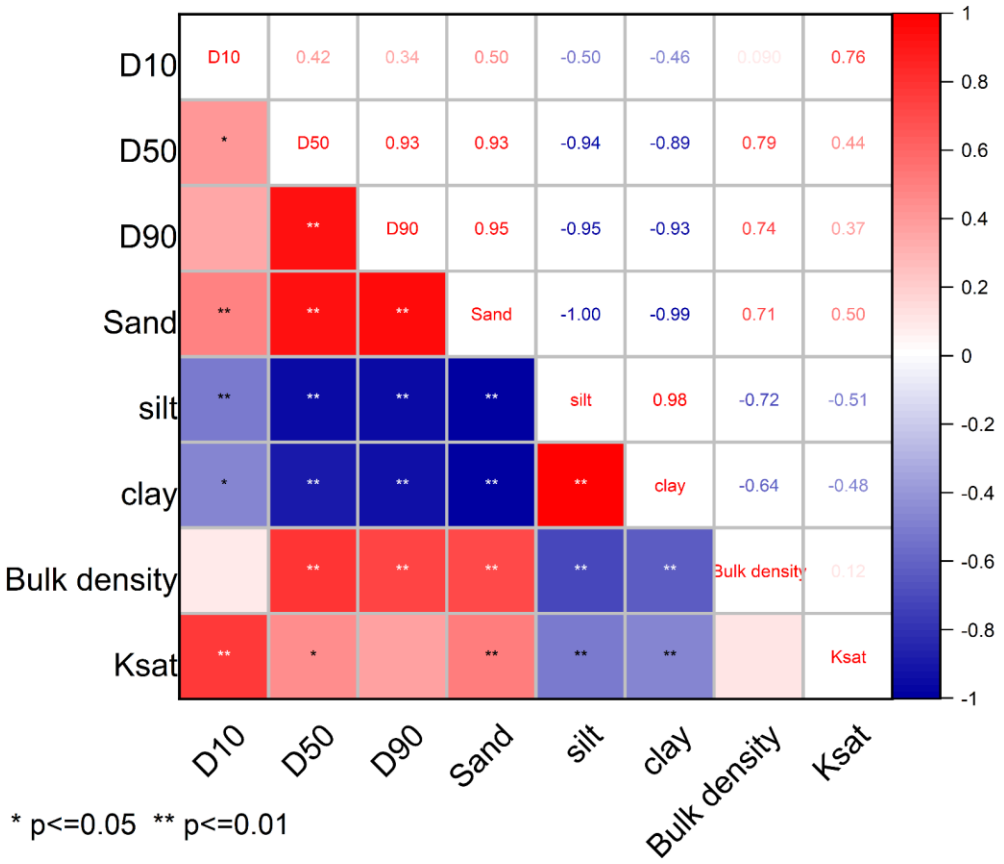

Figure 11.1. Correlation matrix of media's hydro-physical properties. The red color is positively correlated, and blue is negatively correlated. The upper right half shows the Pearson correlation coefficient values (r). D_{10} is positively correlated, and silt and clay negatively correlate with K_{sat} value. Bulk density shows an insignificant correlation with the k_{sat} values.

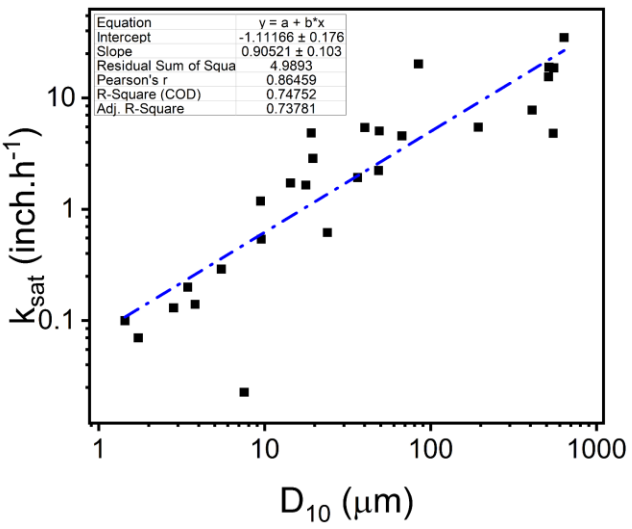

Figure 11.2. Measured hydraulic conductivity values as a function of the sand-soil mixture effective grain size, i.e., D_{10}.

11.2.2 Analysis of empirical K_{sat} predictive equations

We evaluated our data in four empirical models such as The Hazen (1892), Slichter (1898), Terzaghi (1925), and Chapuis (2004).

Hazen Model: Hazen (1892) recommended the following empirical relationship (Eq. 10.1) for loose, uniform sands:

$$K_{sat} = CD_{10}^2 \qquad \text{(Eq. 10.1)}$$

The prediction performance of the Hazen Equation was calculated assuming C = 1.0. The coefficient of 1.0 has been identified as being applicable to loose (i.e., uncompacted or normally consolidated) clean sands with a D_{10} value between 0.1 mm and 3 mm.

Slichter Model: The form of Slichter's equation (Eq. 10.2) is similar to Hazen, but with the addition of a porosity term (as simplified and reported in Vukovic and Soro 1992, but corrected for the units provided below):

$K_{sat} = 10.2\ \eta^{3.287}\ D_{10}^2$ (Eq. 10.2)

where η = porosity, ksat is in cm/s, and D_{10} is in mm.

Terzaghi Model: Terzaghi (1925) also used porosity as a critical property in a K_{sat} prediction method, enabling the prediction to include the effect of soil density. The Terzaghi equation is as follows:

$$k_{sat} = c_0 \frac{\mu_{10}}{\mu_t} \left(\frac{n-0.13}{\sqrt[3]{1-\eta}} \right)^2 D_{10}^2 \quad \text{(Eq. 10.3)}$$

where, C_0 = 8 for smooth grains and 4.6 for grains of irregular shape, μ_{10} = water viscosity at 10 ^oC μ_t = water viscosity at the soil temperature "t" (usually 20 ^oC), η = porosity. For laboratory conditions, the ratio μ_{10}/μ_t can usually be taken as 1.30.

Chapuis Model: Chapuis (2004) developed a method using the same void ratio scalar but simplified the approach using D_{10} (Eq. 10.4). Since this method includes the void ratio, it provides a potentially helpful approach to dealing with the compaction effect on Ksat, providing a relationship between K_{sat}, D_{10}, and void ratio. This method was based on 100 rigid wall permeameter hydraulic conductivity tests on sands with void ratios that varied from 0.4 to 1.5, with an effective grain size diameter, d_{10}, of 0.13 to 1.98 mm. Based on this work, Chapuis (2004) provided the following equation to estimate K_{sat}:

$$k = 2.4622 \left[D_{10}^2 \frac{e^3}{1+e} \right]^{0.7825} \quad \text{(Eq. 10.4)}$$

where "e" is the void ratio, and other variables are as defined previously.

The experimental k_{sat} data is plotted against the model predicted k_{sat} data to evaluate the suitability of the empirical model (Figure 11.3). A one-to-one correspondence line is drawn for

all four models. The models underestimate the k_{sat} values than the experimental k_{sat}. This suggests that the empirical model could not capture the compaction impact fully, which will need further optimization of model parameters or the development of a new model for compacted biofilter.

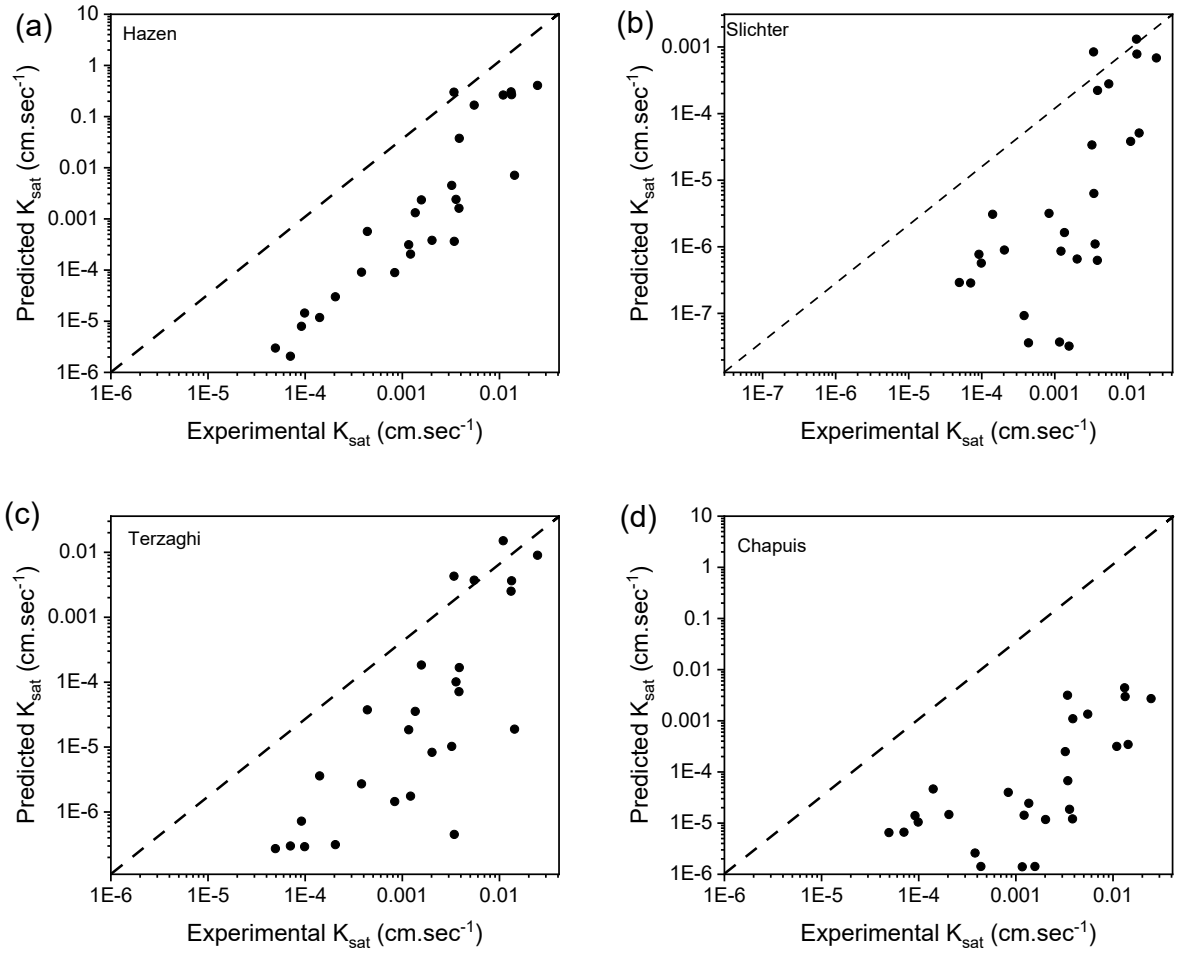

Figure 11.3. K_{sat} prediction using four empirical model (a) Hazen, (b) Slichter (c) Terzaghi (d) Chapuis

11.3 Summary and implication

We analyzed the hydraulic data of different sand-soil mixtures under compaction to develop a predictive model for infiltration rate. The infiltration rate of sand-soil filters was positively correlated with the effective grain size (D_{10}) and negatively correlated with the finer fraction of the mixture, i.e., silt and clay. The empirical predictive models for infiltration underestimated the infiltration capacity of compacted biofilters. This indicates that optimization of empirical models is needed to predict the compaction impact. A well-calibrated infiltration predictive model for compacted biofilter systems would provide stormwater managers a guidance for designing biofilters based on hydraulic properties of native soil and media mixture.

11.4 References

Boadu, F.K., 2000. Hydraulic conductivity of soils from grain-size distribution: new models. Journal of Geotechnical and Geoenvironmental Engineering, 126(8), pp.739-746.

Chandel, A., Sharma, S. and Shankar, V., 2022. Prediction of hydraulic conductivity of porous media using a statistical grain-size model. Water Supply, 22(4), pp.4176-4192.

Pitt, R., Chen, S.-E., Clark, S., 2002. Compacted Urban Soils Effects on Infiltration and Bioretention Stormwater Control Designs, in: Global Solutions for Urban Drainage. Presented at the Ninth International Conference on Urban Drainage (9ICUD), American Society of Civil Engineers, Lloyd Center Doubletree Hotel, Portland, Oregon, United States, pp. 1–21.

Pearson, B., Beeson, R., Reinhart-Adams, C., Olexa, M., Shober, A., 2013. Determining Variability in Characteristics of Residential Landscape Soils that Influences Infiltration Rates. AUF 39.

Pliakas, F. and Petalas, C. 2011 Determination of hydraulic conductivity of unconsolidated river alluvium from permeameter tests, empirical formulas and statistical parameters effect analysis. Water Resources Management 25 (11), 2877–2899.

Hazen, A. 1892. Some Physical Properties of Sands and Gravels, with Special Reference to their Use in Filtration. 24th Annual Report, Massachusetts State Board of Health, Pub.Doc. No.34, 539-556

Kozeny, J. 1927. Uber Kapillare Leitung Des Wassers in Boden. Sitzungsber Akad. Wiss.Wien Math.Naturwiss.Kl., Abt.2a, 136,271-306 (In German)

Slichter C.S.. Theoretical investigations of the motions of groundwater. USGS, pages 295–384, 1898.

Sileshi, R., Pitt, R., Clark, S., 2015. Impacts of Soil Texture, Structure, and Compaction on Bioinfiltration Device Performance: Results of Lab and Field Investigations, in: Low Impact Development Technology: Design Methods and Case Studies. Presented at the 2011 Low Impact Development Conference, American Society of Civil Engineers, Philadelphia, Pennsylvania, pp. 4–15.

Terzaghi, K., and Peck, R. B. 1964. Soil Mechanics in Engineering Practice. Wiley, New York.

12 Task 5. Interim guidance for the construction of BMPs

This interim guidance summarizes the key parameters for designing and implementing infiltration-type Best Management Practices (BMPs) for stormwater treatment along Caltrans' right-of-way. It is based on laboratory studies and field site evaluations conducted by the University of California, Los Angeles (UCLA).

12.1 Soil Types

- Identify the native soil group at the site (Hydrologic Soil Groups A, B, C, or D).
- Measure hydraulic properties to confirm the actual HSG of soil as HSG noted in USGS catalog could differ significantly.
- Assess key soil properties: hydraulic conductivity, particle size distribution, soil mineral such as organic carbon, and compaction level.
- All Caltrans roadside soils evaluated require amendments to achieve adequate infiltration when compacted to 90% compaction level. Addition of ESCS or sand can improve infiltration capacity despite compaction.
- The contaminant removal capacity can be further improved by addition of amendments such as biochar when infiltration rate is high.

12.2 Bulking Agents and Amendments

In BMP filter media design, it is critical to distinguish between bulking agents and amendments, as they fulfill different engineering and treatment objectives.

Bulking agents are incorporated to enhance infiltration rates within the filter bed. They typically have larger granule sizes, which increase pore spaces, improving water movement through the media, especially under field compaction. In our studies, sand has served as the

standard bulking agent due to its consistent performance across all soil types and its ability to achieve moderate to high permeability. Additionally, Expanded Shale, Clay, and Slate (ESCS) was evaluated as a new bulking agent. ESCS not only improves infiltration rates but also offers enhanced water retention and heavy metal removal capabilities, making it a versatile choice for both infiltration and treatment-focused BMPs.

Other candidate bulking agents, such as vermiculite and perlite, were found to be unsuitable; when subjected to compaction, these materials were easily compressed, resulting in reduced pore space and clogged flow paths. Our results showed that only sand and ESCS reliably maintained required infiltration rates in compacted conditions, while other agents impeded hydraulic performance.

Amendments are added to filter media primarily to boost pollutant removal and support the establishment of vegetation. In our conventional media design, compost is blended with sand and soil, while in our engineered media, we used biochar with ESCS and soil. Of these, biochar demonstrated superior performance, particularly in the removal of organic contaminants and pathogens (such as E. coli), when compared to compost, especially under compacted conditions. Large-sized biochar particles (1.2–2.0 mm) were especially effective at minimizing compaction-induced reductions in infiltration and at reducing clogging in biofilters.

While compost can provide some pollutant removal and support nutrient cycling, it has notable drawbacks: it tends to release nutrients and dissolved organic carbon, which may actually decrease overall pollutant removal efficiency. Biochar, in contrast, does not have these negative side effects and is less prone to performance losses under compaction.

Summary:
Use sand or ESCS as bulking agents to ensure high infiltration rates under field compaction; ESCS is also preferred where enhanced water retention and heavy metal removal are needed.

Prefer biochar over compost as an amendment, particularly for sites subject to heavy compaction and where E. coli or organics are target pollutants. Select large particle size biochar for best hydraulic and treatment performance.

12.3 Blending Ratio

Compaction significantly reduces the infiltration capacity of biofilter media; however, the addition of suitable bulking agents, particularly sand or ESCS, can effectively mitigate this negative impact. The optimal proportion of sand or ESCS needed to restore infiltration rates depends on the soil hydrologic group and the native soil's physical properties.

12.3.1 Bulking Agents (Sand/ESCS)

To achieve the target infiltration rate of 1–3 inches per hour, a minimum of 50% bulking agent (by volume) is necessary. Blending ratios below this threshold result in suboptimal infiltration. Depending on the permeability of the native soil, the proportion of bulking agent may be increased up to 80% by volume. The final ratio should be determined based on laboratory or pilot-scale testing, with special consideration given to the mixture's D10 value (the particle size at which 10% of the soil mass is finer), which influences hydraulic performance.

12.3.2 Amendments (Biochar/Compost)

Amendments should comprise 10–25% of the total mix by volume. For example, a mixture of 25% biochar and 25% soil can achieve the desired infiltration rate while enhancing pollutant removal. Compost can also be included within this range, but site-specific testing is recommended to ensure hydraulic and treatment objectives are met.

12.3.3 Recommended Blending Ratios

- Sand/ESCS: 50–80% (by volume)

- Biochar/Compost: 10–25% (by volume)
- Native Soil: Remainder to balance media composition

The specific blending ratio should always be optimized for site conditions through laboratory or field-scale pilot testing, with adjustments based on observed soil behavior and performance criteria.

12.4 Depth of Amended Soil Layer

For roadside biofilter applications, the recommended depth of amended filter media is 6 to 12 inches. Depths greater than this are generally not advised, as they may compromise the structural stability of the roadside and increase the risk of ground instability.

12.5 Compaction Energy

To simulate actual field conditions, all amended filter media should be compacted to achieve 85-90% of the maximum dry density as determined by the California Compaction Test. This level of compaction reflects typical roadside construction practices and ensures that laboratory and pilot tests accurately represent real-world scenarios.

12.6 Underdrain Location (for Effluent Sample Collection)

An underdrain pipe should be installed at the base of the amended soil layer, with the outlet positioned for efficient collection of effluent samples. In typical roadside installations, however, direct access to subsurface drains for sampling is often impractical due to site constraints and limited accessibility. To address this challenge, performance testing and effluent monitoring are conducted in dedicated test beds constructed outside the main roadside area. This allows for controlled conditions and collection of infiltrated water samples for actual roadside applications.

13 Task 6: Select field sites for the pilot study and evaluate the construction of BMPs

13.1 Motivation

Urban road infrastructures can serve multiple functions beyond transportation, including runoff treatment and groundwater recharge. However, compaction of roadside soils impedes both infiltration and contaminant removal. The overarching goal of this study is to develop soil-based roadside BMPs that maintain high infiltration and contaminant removal even under typical compaction conditions.

13.1.1 Objective

The central objective of Task 6 is to move from laboratory-scale findings to real-world validation by constructing and evaluating pilot-scale, soil-based Best Management Practices (BMPs) that retain high infiltration and contaminant removal capacities even under compaction typical of Caltrans rights-of-way.

13.2 Site Selection Process

13.2.1 Desktop and Virtual Screening

The initial phase of site selection involved a comprehensive review using Google Maps and Caltrans Right of Way (ROW) data to locate candidate field sites within Los Angeles County. The team utilized the USDA NRCS Web Soil Survey to identify soil hydrologic groups (A, B, C, D) at each location, which facilitated a pre-screening of sites based on soil infiltration potential. six preliminary sites were selected from this mapping and virtual inspection,

concentrating on the presence of drainage infrastructure, visible stormwater flow paths, and vehicular accessibility.

Site 1 Site 2 Site 3

Site 4 Site 5 Site 6

Figure 13.1 All selected field sites from virtual inspection.

13.2.2 Criteria for Site Selection

Sites were selected based on the following criteria:

- **Soil Type:** One site with high infiltration (Hydrologic Soil Group A/B), one with low infiltration (Group C/D).
- **Proximity to Existing Drainage Infrastructure:** Presence of a culvert or drainage system capable of directing runoff to the BMP.
- **Accessibility:** Sites accessible by vehicle for regular monitoring and sample collection.
- **Slope:** Less than 10% slope to ensure both BMP effectiveness and construction safety.
- **Approval:** All sites subject to review and approval by Caltrans.

Table 13.1 Information of the different sites near Los Angeles, California.

Site	Location Description	Latitude / Longitude	Distance from UCLA (miles)	Hydrologic Soil Group	Key Features	Google Maps Link
1	CA-60/Pomona Freeway, Exit 19	34.033271 / -118.026728	24.5	C (Low Infiltration)	Selected site; drainage, accessible, <10% slope	Link
2	I-605 Freeway, Exit 14A	33.974639 / -118.080448	33	B (High Infiltration)	Selected site; drainage, accessible, <10% slope	Link
3	I-210, Sunland Blvd, Exit 210	34.260184 / -118.331342	26	B	Alternate; drainage, accessible	Link
4	I-605 Freeway, Exit 14A (Alternate entry)	33.974639 / -118.080448	33	B	Alternate; similar to selected Site 2	Link
5	I-5, Western Avenue, Exit 145A	34.163769 / -118.296431	18	B	Alternate; drainage, accessible	Link
6	I-5, Alameda Ave, Exit 145B	34.170293 / -118.303443	19	B	Alternate; drainage, accessible	Link

13.2.3 Field Verification

Following desktop screening, the team conducted multiple site visits to all shortlisted locations. Each site was carefully evaluated for stormwater flow, existing culverts or drainage features, topographic suitability (targeting slopes less than 10%), and ease of access for equipment and personnel. These field assessments led to the identification of two potential field

sites, both meeting the hydrologic and infrastructural criteria necessary for effective pilot BMP installation.

Figure 13.2 Field site inspections by the project team.

13.2.4 Final Site Selection and Regulatory Review

During more detailed site assessments, one of the two shortlisted locations was excluded due to significant access constraints and the absence of a natural slope, which would have prevented reliable stormwater inflow, outflow, and representative sample collection. The remaining site, referred to as Site 1 (locations 1), was finalized based on locations, established drainage system, safe and consistent vehicular access, and suitable topography. Subsequent meetings with Caltrans construction and environmental compliance staff confirmed that the planned pilot installation would not require additional environmental permitting, as there would be no major ground disturbance or alteration of natural flow.

	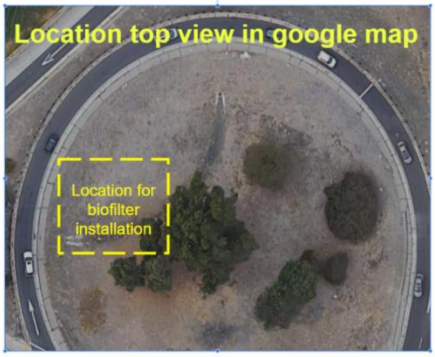
Location 1	Location 2
34.03327, -118.0267	33.974639 , -118.080448
exit 19 for CA-60/Pomona Fwy	Highway 605, Exit 14 A
Hydrologic soil group: C	Hydrologic soil group: B
Existing drainage system can capture stormwater and divert it to installed BMP. Soil is capable of infiltration. Accessible by car to enter area for monitoring and collecting samples Slope of the designated sites (<10% slope)	Existing drainage system can capture stormwater and divert it to installed BMP. Accessible by car to enter area for monitoring and collecting samples Slope of the designated sites (<10% slope)

Figure 13.3 Finalized two field locations for pilot study.

13.3 Soil Testing and Laboratory Characterization

Upon selection of the final field site, representative soil samples were collected for laboratory characterization. Tests included particle size distribution, hydraulic conductivity under standard Proctor compaction, organic matter content, and pollutant removal potential, following established ASTM and Caltrans protocols. This laboratory work (as conducted in project Tasks 3d and 4) provided key data to inform the selection of appropriate soil amendments and to determine the optimal blending ratios, compaction levels, and expected performance of the amended BMP media.

13.4 BMP Placement and Site Preparation

A field survey done by the UCLA research team and reviewed by Caltrans engineering staff was undertaken to determine the optimal position for the BMP structures within the selected site. Key considerations included proximity to stormwater inflow points, minimal disruption to existing drainage, safety, and practicality for equipment placement and future maintenance.

Figure 13.4 Field site 1, inspection for pilot system installation.

13.5 Technical Design of Pilot BMPs

13.5.1 Stormwater Management Approach

The BMP system is designed to intercept stormwater at an inflow outlet, provide temporary storage without restricting the original pipe flow, and divert water to dedicated test beds for performance assessment. The system layout ensures ease of sample collection and clear separation between inflow and outflow.

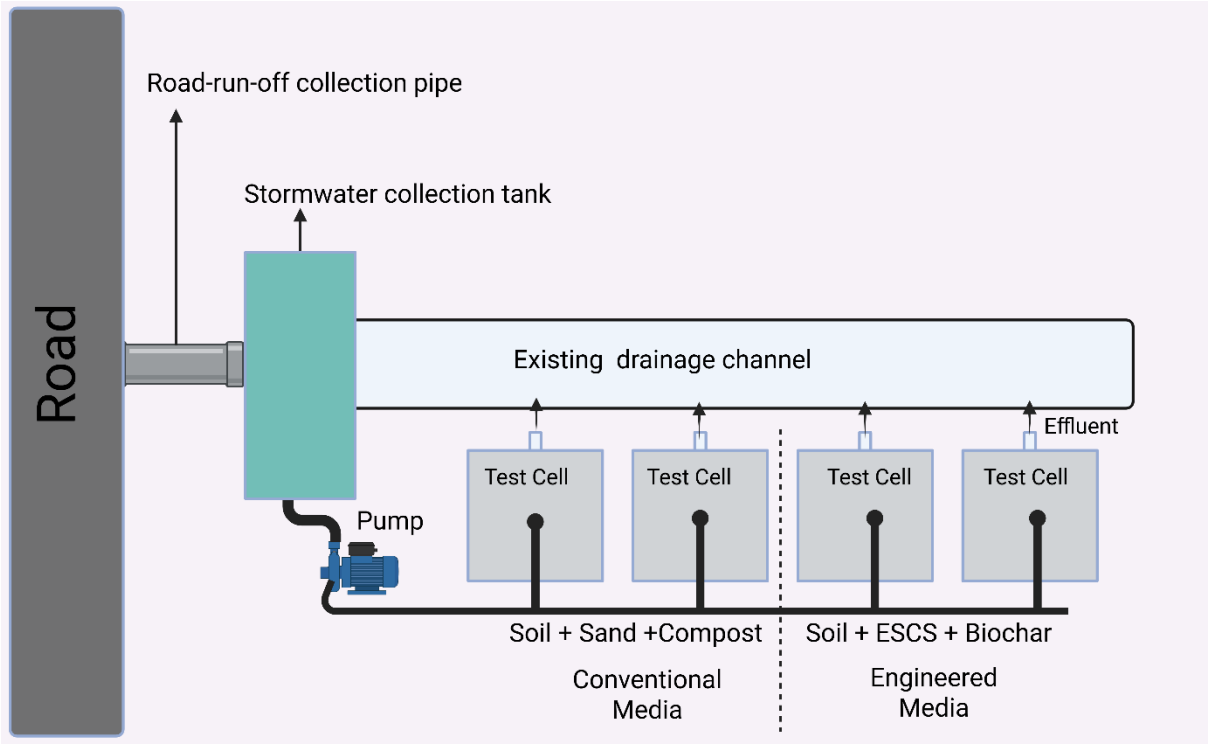

Figure 13.5 Schematic for pilot test bed showing the configuration of field setup.

13.5.2 Test Bed Specifications

The test beds are constructed of high-strength fiberglass, with internal dimensions of 3 feet by 3 feet and a depth of 2 feet, and a wall thickness of 0.5 inches. This provides a mechanically robust structure that resists deformation under compaction and field use. Each test

bed is custom-fabricated based on predetermined design specifications and is fitted with a 6-inch diameter outlet at the base for efficient effluent collection and monitoring.

13.5.3 Underdrain and Sampling Infrastructure

A 6-inch perforated PVC underdrain is installed at the base of each test bed, surrounded by a 6-inch pea gravel drainage layer to facilitate unobstructed collection of infiltrated water. One of the criteria for the underdrain is that the outflow should be above the ground level to collect samples. This configuration enables systematic sampling of effluent for chemical analysis, thereby tracking both hydraulic performance and pollutant removal efficiency under actual field conditions.

13.6 Conclusions

The site selection and design process described in this report has ensured that the chosen field site provides the necessary characteristics for a robust evaluation of pilot-scale, soil-based BMPs for stormwater management. By integrating laboratory findings with practical, field-ready construction and monitoring protocols, this project is positioned to provide meaningful insights into the performance of amended roadside soils under real-world compaction and hydrologic conditions. The experience and data gained through this pilot will directly inform the design and implementation of future Caltrans BMPs, contributing to improved stormwater management and water quality protection statewide.

With the site selected and designs ready, the next step is test bed installation. The test beds and underdrains were installed, amended soils will be blended and compacted, and monitoring equipment set up. Once installed, the BMPs will be ready for performance monitoring during rain events.

14 Task 7: Field Pilot Testing

14.1 Introduction

The global urban population increased from 29.6% (0.8 billion) in 1950 to 56.2% (4.4 billion) by 2020, driving a more than 50% rise in water demand and intensifying urban water scarcity (He et al., 2021). This rapid urbanization has also significantly expanded impervious surfaces, resulting in up to a fivefold increase in stormwater runoff compared to pre-development conditions (Rahman et al., 2023). Moreover, the compaction of roadside soils due to vehicular traffic and infrastructure development further reduces infiltration capacity by 60–80%, while also impairing pollutant removal efficiency (Li et al., 2021). Urban roadway runoff presents a major environmental concern, as it transports hazardous contaminants such as heavy metals (Pb, Cu, Zn, Cd) and suspended solids into downstream water bodies, threatening aquatic ecosystems and public health (Tirpak et al., 2021). In response, the U.S. Clean Water Act's National Pollutant Discharge Elimination System (NPDES) program, specifically through its Municipal Separate Storm Sewer System (MS4) permit requirements under 40 CFR §122.34, mandates post-construction stormwater controls that enhance infiltration and aim to maintain pre-development hydrologic conditions to the maximum extent practicable (MEP), often through green infrastructure and low-impact development (LID) strategies (Simpson et al., 2023). Improving stormwater infiltration and treatment is thus essential to addressing both urban water scarcity and water quality degradation.

One potential solution to address urban runoff and water quality issues is the implementation of biofiltration systems within the roadside clear zones of urban roads. These systems can significantly enhance infiltration, reduce surface runoff, and improve stormwater quality. However, to ensure roadway stability, these clear zones are typically compacted to

approximately 90% of their maximum dry density, which significantly reduces infiltration capacity. The compaction process collapses macropore spaces into micropores, resulting in decreased hydraulic conductivity and compromised water infiltration (Das et al., 2023). Conventional stormwater biofilters employing sand–compost media frequently fail under these compacted conditions due to rapid clogging and insufficient permeability, limiting their long-term functionality. This highlights the necessity of developing engineered biofilter media capable of sustaining high infiltration rates under compacted conditions, while also ensuring effective removal of contaminants from urban stormwater.

Biofilters employing mixtures of sand, compost, and soil are commonly utilized in urban stormwater management due to their cost-effectiveness and pollutant removal capacity. However, standard media blends such as the 4:2:2 sand:compost:soil ratio face critical performance limitations under the compacted conditions typical of roadside applications (Le Coustumer et al., 2012). Elevated compost content, while enhancing microbial activity and nutrient cycling, contributes to long-term degradation of hydraulic performance through organic matter decomposition and downward migration of fines, which reduce pore connectivity and promote surface sealing and anaerobic zone formation during storm events, particularly in sandy matrices (Hatt et al., 2007; Le Coustumer et al., 2012). Moreover, the high organic load can compromise metal retention, as leachates from decomposing compost form soluble complexes with trace metals such as Zn and Cu, increasing their mobility and reducing filtration effectiveness (Blecken et al., 2009; Sun et al., 2019). Sand, a key structural component, is critical for maintaining porosity and facilitating drainage, yet its permeability is highly susceptible to compaction-induced reductions, especially when combined with fine particulates from compost and soil, leading to clogging and diminished infiltration capacity over time (Lucas & Greenway,

2011). Furthermore, while sand supports physical filtration, its limited cation exchange capacity constraints its ability to immobilize dissolved heavy metals (Bratieres et al., 2008; Trowsdale & Simcock, 2011). These challenges underscore the need to optimize filtration media composition by adjusting the sand-to-compost ratio and incorporating amendments that enhance both physical stability and chemical reactivity (Payne et al., 2014). Such optimization is essential to ensure sustained infiltration rates, resistance to clogging, and effective removal of heavy metals in stormwater runoff, particularly in high-compaction settings where long-term performance is critical.

Replacing the conventional 4:2:2 sand:compost:soil blend with a 4:2:2 combination of Expanded Shale, Clay, and Slate (ESCS) aggregates, biochar, and soil may significantly enhance the hydraulic and pollutant removal functions of bioretention media used in compacted roadside environments. ESCS is a thermally expanded, porous ceramic aggregate that retains high permeability and resists compaction, offering superior water infiltration compared to sand under high-pressure conditions (Zhao et al., 2021). This structural stability is critical in clear zones where soil is often compacted to engineering specifications. ESCS particles also exhibit large internal surface areas and interconnected pore networks that support both water retention and microbial colonization traits beneficial for extended pollutant treatment cycles and vegetation health (Funai and Kupec, 2019). Biochar, when added as a reactive amendment, further enhances the media's adsorption capacity for heavy metals and pathogens, owing to its microporosity and surface chemistry (Mohanty et al., 2018; Moustakas et al., 2021). Studies have demonstrated that biochar-ESCS blends retain significantly more dissolved metals like Cu, Pb, and Zn, and show increased resilience against clogging and leachate formation compared to compost-rich systems, which may degrade over time and facilitate metal mobility (Borthakur et al., 2022; Zhang et al.,

2024). Moreover, the combined use of biochar and ESCS improves soil water availability during drought, reduces anaerobic zone formation, and promotes stable infiltration rates key parameters for the long-term functionality of urban green infrastructure. These findings highlight the promise of ESCS-biochar media as a chemically robust and hydraulically stable alternative to conventional sand-compost blends in sustainable stormwater management.

To address the limitations of stormwater biofilters under compacted roadside conditions, this study compares the performance of engineered and conventional media in sustaining infiltration, resisting clogging, and removing heavy metals. The E. coli in stormwater was below detection limit and not used in this study. Specifically, a 4:2:2 mixture of Expanded Shale, Clay, and Slate (ESCS), biochar, and soil is evaluated against the standard 4:2:2 sand:compost:soil blend. The objective is to determine whether engineered media can provide superior hydraulic conductivity and contaminant attenuation while maintaining long-term functionality under compaction. By focusing on these critical parameters, the study aims to guide the design of more effective stormwater filtration systems for high-compaction urban environments.

14.2 Methods

14.2.1 Site description

The pilot-scale stormwater biofilter was installed at Exit 19 of CA-60/Pomona Freeway (34.034087°N, -118.028326°W), approximately 35 miles from UCLA. This urban location was selected for its significant stormwater runoff generation from highway surfaces and surrounding impervious areas. Key selection criteria included: (1) existing drainage infrastructure capable of directing runoff to the treatment system, (2) Group C (moderately infiltrative) soils suitable for stormwater filtration, (3) gentle slopes (<10%) ensuring stable implementation, and (4) proximity to UCLA facilitating monitoring and maintenance. The site's adjacency to this major transportation corridor provides representative urban runoff conditions while enabling accessible

sampling and performance evaluation. Geographic location of stormwater filter installation site is shown in Figure1.

Figure 14.1 Pilot-scale stormwater biofilter installation site location: (a) location on google maps (b) aerial site view.

14.2.2 Site Inspection

Prior to system installation, comprehensive site investigations were conducted to inform the design of the integrated stormwater treatment system. Field measurements confirmed the road runoff outlet pipe had a 31.8 cm (12.5 in) diameter with a 30.5 cm (1 ft) burial depth from pipe center to surface, establishing critical design parameters for the water collection tank. The treatment system was strategically configured with filtration units positioned 4.6 m (15 ft) downstream of the outlet pipe on level terrain (<3% slope) to facilitate uniform flow distribution. The pump station was planned to setup at the center point of all the four stormwater filters to maintain proper hydraulic operation. All the proposed designs were shown in the Figure 2.

Figure 14.2. Site investigation (a-f) and proposed pilot stormwater filtration plan (g).

14.2.3 Materials amendments

The study evaluated two distinct stormwater filter media configurations to assess their performance in treating urban runoff: conventional and engineered stormwater filters. The conventional filter media consisted of a carefully proportioned blend of 4 parts sand, 2 parts

compost, and 2 parts topsoil, following the composition established by Tripak et al. (2021). The sand component was sourced from Vulcan Materials Company in Irwindale, California, and complied with the California Department of Transportation (Caltrans) Standard Specifications Section 90-1.02C(4)(d), featuring a maximum 3/8-inch combined aggregate gradation to ensure proper hydraulic conductivity. The compost was obtained from the Capistrano Greenery composting facility at the Prima Deshecha Landfill in San Juan Capistrano, California, and met all requirements of Section 21-2.01C(2). The topsoil was characterized by 60-90% sand content (dry weight), with less than 20% passing the No. 200 sieve, less than 5% clay, and no gravel, ensuring optimal filtration characteristics while preventing clogging.

The engineered filter media was designed to enhance both hydraulic performance and contaminant removal capabilities. This innovative configuration replaced traditional components with advanced materials, consisting of 4 parts expanded shale, clay, and slate (ESCS) as the primary aggregate, 2 parts biochar for improved adsorption of pollutants, and 2 parts topsoil meeting the same specifications as in the conventional system. The ESCS lightweight aggregate was specifically selected for its superior permeability and water retention properties, while the Rogue Biochar, purchased from Oregon Biochar Solutions in White City, Oregon, provided exceptional cation exchange capacity for heavy metal removal. The ESCS with size between 0.4 to 2.8 mm was selected for this study. This systematic approach to material selection and validation ensured consistent, reproducible experimental conditions for accurate performance comparison between the two filter types.

The filtration systems incorporated a multi-layer design to optimize treatment performance. A 0.5 cubic foot layer of bagged pea gravel (Vigoro Premium Pea Gravel Pebble Landscape Rock, sourced from Home Depot) served as the base material, providing structural

support and initial coarse filtration. Above this gravel layer, an ASTM C33-compliant 20-30 grade sand liner (purchased from Humboldt Manufacturing Company) was installed to ensure proper filtration and structural stability. This carefully engineered substrate created an ideal foundation for the overlying filter media, promoting uniform flow distribution while preventing preferential pathways that could compromise treatment efficiency. The complete system design reflected current best practices in stormwater management while incorporating innovative materials to address emerging water quality challenges.

14.2.4 Design of the planter box

The custom-fabricated stormwater filter bed and collection tank were constructed from glass fiber-reinforced material procured from Hood Manufacturing Inc. Glass fiber was selected as the primary construction material due to its exceptional chemical resistance, high structural strength (capable of withstanding compaction forces), and lightweight properties. The stormwater filter bed was designed with dimensions of 36" × 36" × 24" (L × W × H), representing a scaled-down bioretention cell capable of effectively managing stormwater runoff, as demonstrated in previous studies (Szalaj et al., 2007).

The filter bed was equipped with a 4-inch diameter outlet pipe positioned 6 inches above the bottom surface (measured from the center of the hole to the base). This design feature was implemented to prevent clogging of the underdrain system while simultaneously optimizing infiltration rates and pollutant removal efficiency, consistent with established stormwater treatment principles (Mangarella et al., 2002). The elevated outlet configuration promotes the formation of a saturated zone within the lower portion of the filter media, enhancing denitrification processes and heavy metal precipitation.

The stormwater collection tank was fabricated with dimensions of 72" × 48" × 18" (L × W × H) and a wall thickness of 0.375 inches. Two rectangular overflow notches (14" W × 4" H) were incorporated into the upper section of the tank to safely discharge excess water during high-flow conditions. The total storage volume of the water tank is 28 cubic ft. which is equivalent to storing 210 US gallons of water. All components were precision-engineered to ensure compatibility with standardized stormwater testing protocols while maintaining structural integrity under field-relevant hydraulic loading conditions.

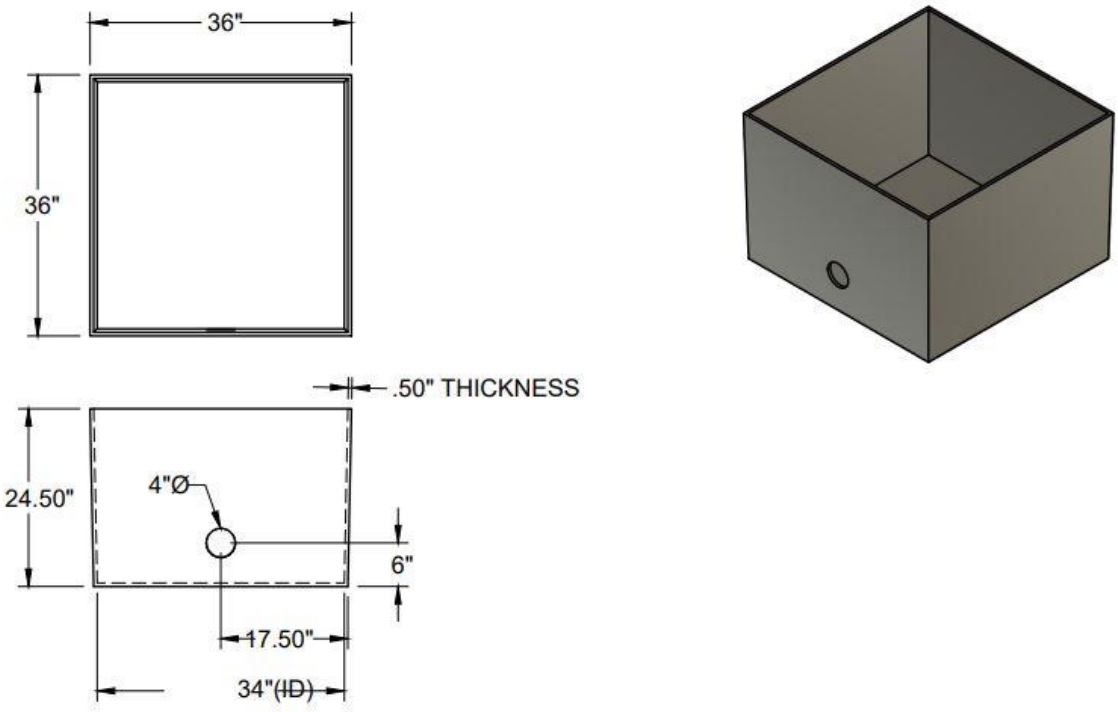

Figure 14.3 AutoCAD design schematic of planter box stormwater filtration units showing cross-sectional dimensions (L × W × H = 36” × 36” × 24.5”).

14.2.5 Preliminary test before installation

Prior to field installation, the filter bed underwent rigorous testing at UCLA to evaluate its structural integrity and performance under compaction stresses. A hand compactor (Husky 51

in. Steel Handle 8 in. × 8 in.) was employed to simulate compaction forces on the media layers, ensuring the bed walls could withstand yielding without failure. Preliminary assessments, illustrated in Figure 4, documented the stormwater filter's construction phase, highlighting the compaction process and layer stratification. Preliminary, waterflow measurements were done. These pre-installation tests ensured the filter bed's robustness and functionality before deployment in real-world stormwater management applications.

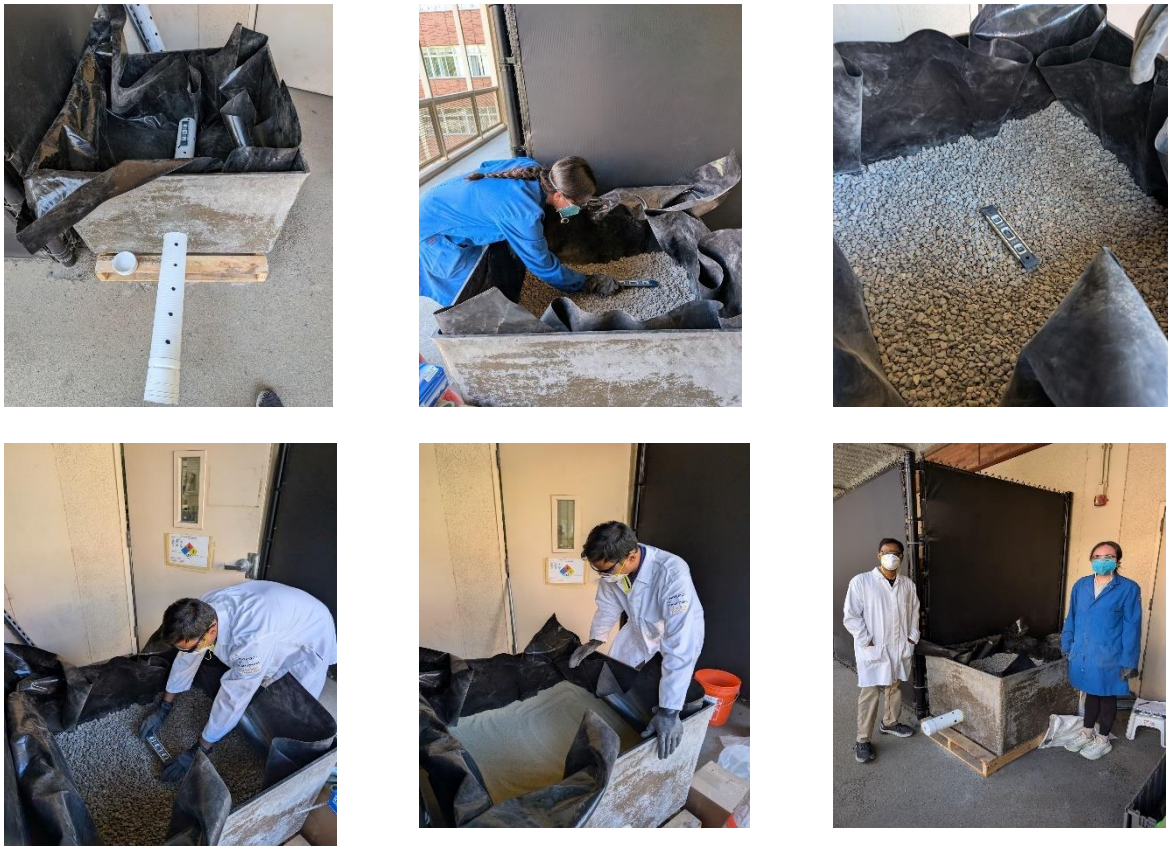

Figure 14.4 Preliminary compaction and packing tests of the stormwater filter media layers prior to field installation at the pilot site.

14.2.6 Pilot scale installation

14.2.6.1 Stormwater collection tank installation

The installation process began with thorough site preparation, including the removal of weeds and debris to facilitate proper excavation. The ground was excavated to establish a consistent elevation, maintaining a 21-inch vertical clearance from the centerline of the stormwater runoff outlet pipe to the surface. A 26 ft² collection area downstream of the pipe outlet was precisely leveled using a bubble level to ensure uniform placement of the water collection tank. The tank was positioned to align the stormwater discharge with a custom-designed rectangular notch, optimizing inflow efficiency. To mitigate potential displacement during high-flow conditions, the perimeter of the tank was reinforced with strategically placed rocks, enhancing structural stability. Before and after installation pictures were shown in figure 5.

Figure 14.5 Water collection tank installation at pilot site: (a) pre-installation conditions and (b) post installation water collection tank.

14.2.6.2 Installation of the stormwater filters

The stormwater filtration system comprised four downstream filter units, with the first unit positioned 15 ft from the initial collection point and subsequent units spaced 1 ft apart. Prior to installation, the mulch layer was removed from each designated site, and the upper 2 inches of soil was excavated and stored for later use. The excavated soil was sieved to comply with Caltrans topsoil specifications (as detailed in the Materials Amendments section) and reapplied after leveling the substrate using a bubble level to ensure uniform compaction.

Each filtration unit was constructed with a 4 inch base layer of expanded shale, clay, and slate (ESCS) aggregate. To optimize hydraulic performance, additional ESCS material was graded to establish a 0.3% slope toward the center of each unit, promoting efficient drainage. A 20-mil thick LLDPE geomembrane liner (Vevor) was installed to encapsulate the ESCS layer and filter box edges, preventing intermixing with the overlying biofilter media. A 4 inch diameter outlet was integrated near the base of each unit, fitted with a 5 ft-long perforated triple-wall drainage pipe (Advanced Drainage Systems). The pipe was positioned such that 3 ft extended into the filtration chamber, while the remaining section discharged externally. Epoxy sealant (Gorilla) was applied at the pipe-liner interface and along the outlet perimeter to ensure a watertight seal.

14.2.6.3 Compaction and packing the stormwater filters

Table 14.1 Installation steps for stormwater treatment filters.

S. No	Process	Pictures
1	Filter bed installation	 
2	Adding drainage layer	 
3	Mixing of Conventional filter media	 
4	Mixing of engineered filter media	 

5 Adding media layers


6 Packed planter box


Pea gravel (14 in total depth) was layered atop the geomembrane liner, with thorough compaction using a hand compactor after every 2 inches increment (15–20 min per layer). A 2 inches sand layer was subsequently added and compacted to enhance structural stability. For conventional filter media, a mixture of sand, compost, and native soil (4:2:2 ratio) was prepared with 10% water (v/v) and homogenized using a standardized garden spade (Anvil). The mixture was applied in 6 layers, with 25 min compaction intervals after every 2 inches addition. A final 2 inches pea gravel layer was distributed across the surface to minimize erosion.

For engineered filter media, ESCS, biochar, and native soil (4:2:2 ratio) were blended with 10% water (v/v) and similarly homogenized. The mixture was layered and compacted following the same protocol as the conventional media. A pilot study was conducted using two conventional and two engineered filter units to evaluate comparative performance in contaminant retention and hydraulic efficiency.

14.2.6.4 Pump and Distribution Setup

The water delivery system was constructed using a 12V diaphragm pump (Model 6-9206, Chapin International) with a capacity of 1.0 GPM. The pump inlet was connected to a 3/8" ID PVC tubing (Masterkleer, McMaster-Carr), with the intake end fitted with a protective mesh

screen to prevent coarse particle intrusion. A 250 g counterweight was attached to ensure stable submersion during operation. The pump outlet was similarly connected to 3/8" ID PVC tubing, which conveyed water to the distribution manifold.

A rectangular aluminum manifold (McMaster-Carr) with one 3/8" NPT inlet and four 1/4" NPT outlets served as the central distribution hub. The connection between the pump outlet and manifold inlet was secured using a 3/8" aluminum barbed hose fitting (McMaster-Carr). Four 1/4" aluminum barbed fittings were installed at the manifold outlets to facilitate flow division to the filtration units.

The distribution network consisted of four 1/2" diameter PVC riser pipes (Orbit), each capped at one end and perforated along its length with 5/64" diameter holes to ensure uniform water distribution across the filter media. The open ends of the risers were connected to 90° elbow adapters (1/4" hose ID to 1/2" NPT female, McMaster-Carr) and positioned vertically within each filter unit. Flexible 1/4" ID PVC tubing (Masterkleer) connected each riser to the corresponding manifold outlet, completing the distribution circuit.

Power was supplied by a 12V 16Ah LiFePO4 deep-cycle battery through a 16AWG wiring harness equipped with an inline switch and alligator clips. This configuration allowed for controlled activation of the pumping system during experimental runs. The complete pilot-scale setup, illustrating all components and connections, is presented in Figure 6.

Figure 14.6 Pilot scale experimental setup of the stormwater filtration units.

14.2.7 Stormwater quality monitoring

Stormwater collected from the storage tank was systematically pumped with an effective loading rate of 0.63 cm h^{-1} through each filtration unit, with paired influent and effluent samples collected for comprehensive water quality analysis. The loading rate is much smaller than the 85th percentile 24-rainfall depth, because most of the water would result in an overflow on compacted media with net infiltration capacity below 1. . Samples were evaluated for key physicochemical parameters including turbidity (NTU), pH, and dissolved heavy metal concentrations (Pb, Co, Ni, Zn, Cu, and Cd) using standardized analytical methods (SM 2130B for turbidity, and EPA 200.8 for metals via ICP-MS). Continuous flow rate monitoring was conducted to assess hydraulic performance, with particular attention to infiltration capacity and potential clogging phenomena.

14.2.8 Quantification of metals

Samples for measuring metals were collected in 250 mL polypropylene bottles.To begin the metal analysis of water samples following EPA Method 200.8, first prepare a 35% nitric acid solution by adding 10 mL of concentrated nitric acid (trace metal grade) to 8 mL of distilled water, then diluting to a final volume of 20 mL with additional distilled water. Store this solution in a sealed container for later use. For each sample, transfer 9.95 mL of unfiltered water into a 15 mL centrifuge tube and add 0.05 mL of the 35% nitric acid solution to adjust the pH to below 2, verifying with pH paper. If the pH remains above 2 due to alkalinity, add additional acid dropwise until the target pH is reached. Allow the samples to sit for at least 16 hours to ensure complete acid digestion and metal dissolution. After incubation, centrifuge the samples at 3000 rpm for 15 minutes to separate suspended solids. Finally, transfer the clear supernatant into 5 mL vials, avoiding any settled precipitate, before analysis via ICP-MS to determine total recoverable metal concentrations.

14.2.9 Measuring the microplastics in the influent and effluent samples

Microplastic particles present in stormwater were analyzed using a protocol adapted from Leonard et al. (2022). To isolate the particles, samples were filtered under vacuum using 24-mm G4 glass fiber filters with a nominal pore size of 1.2 μm (Thermo Fisher Scientific, Cat. No. 09–804–24C). After filtration, the filters were treated with 0.17 mL of a Nile Red staining solution (0.5 μg mL^{-1} in chloroform) by dispensing the dye onto each filter within a clean glass Petri dish. The filters were then placed in a fume hood and left to dry at room temperature for 24 hours to ensure complete solvent evaporation. This drying period was critical to eliminate excess dye and reduce the risk of nonspecific fluorescence, which could otherwise interfere with image-based detection.

Once dried, the filters were transferred onto standard microscope slides for imaging. A portable fluorescence microscope, assembled using a smartphone-based imaging system (Figure 1A), was employed to capture high-resolution images (5360 × 7152 pixels). Images were initially saved in Digital Negative (DNG) format and subsequently converted to Tagged Image File Format (TIFF) using the dcraw.exe utility to facilitate processing.

Image analysis was performed using MATLAB software, incorporating routines from the Image Processing Toolbox. The analysis pipeline extracted the red fluorescence channel corresponding to Nile Red emission and identified individual particles based on their fluorescence signature.

14.3 Results and discussion

14.3.1 Effect on the Infiltration

Field monitoring across five rainfall events (January–March 2025) revealed that replacing conventional compost/sand media with biochar/engineered soil composite (ESCS) significantly enhanced infiltration capacity, with median effluent fluxes increasing from 1.8 cm/h to 5.9 cm/h (a 3.3-fold improvement). Results are shown in Figure 7. This aligns with laboratory studies demonstrating that biochar's high porosity (200–300 μm) resists compaction-induced pore collapse, while ESCS promotes hierarchical pore networks that sustain permeability under dynamic flow conditions (Mohanty et al., 2023).

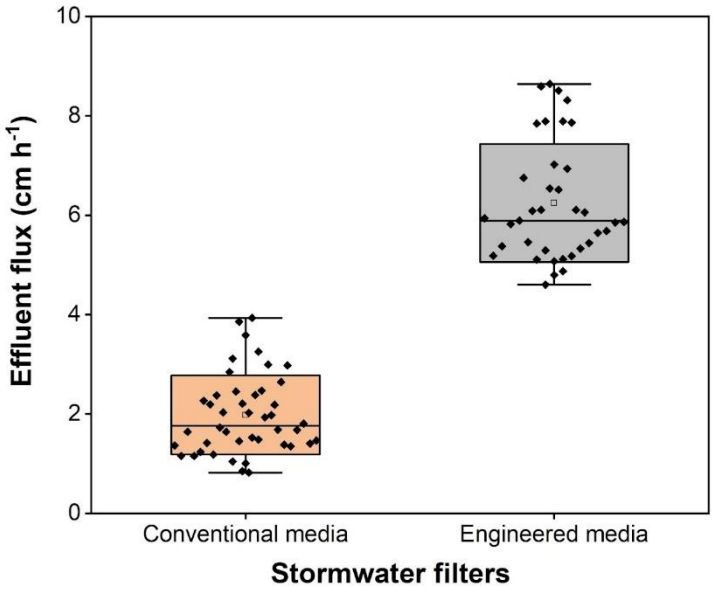

Figure 14.7 Comparison of the effluent flux of conventional media filters (50% Sand, 25% compost, 25% soil) and engineered media filters (50% ESCS, 25% biochar, 25% soil).

14.3.2 Effect of Ponding potential

The study revealed significant differences in ponding behavior between conventional and engineered stormwater filters. The conventional filter exhibited poor drainage performance, with an effluent-to-influent discharge ratio (Q_{eff}/Q_{in}) of only **~0.3**, leading to frequent water accumulation and eventual flooding during storm events. In contrast, the engineered filter demonstrated superior hydraulic efficiency (Q_{eff}/Q_{in} **~0.8**) with no observable ponding, even under continuous inflow conditions (as shown in figure 8). This enhanced performance is attributed to the engineered media's optimized pore structure biochar's high porosity (200–300 μm) and ESCS's stable granular matrix mitigate clogging and maintain consistent permeability, whereas the conventional media's organic-rich compost fraction likely contributed to pore blockage and reduced infiltration over time (Le et al., 2020). These findings underscore the limitations of compost-based filters in high-flow applications and highlight the engineered

system's reliability for urban stormwater management, where ponding poses operational and safety risks (Boehm et al., 2020).

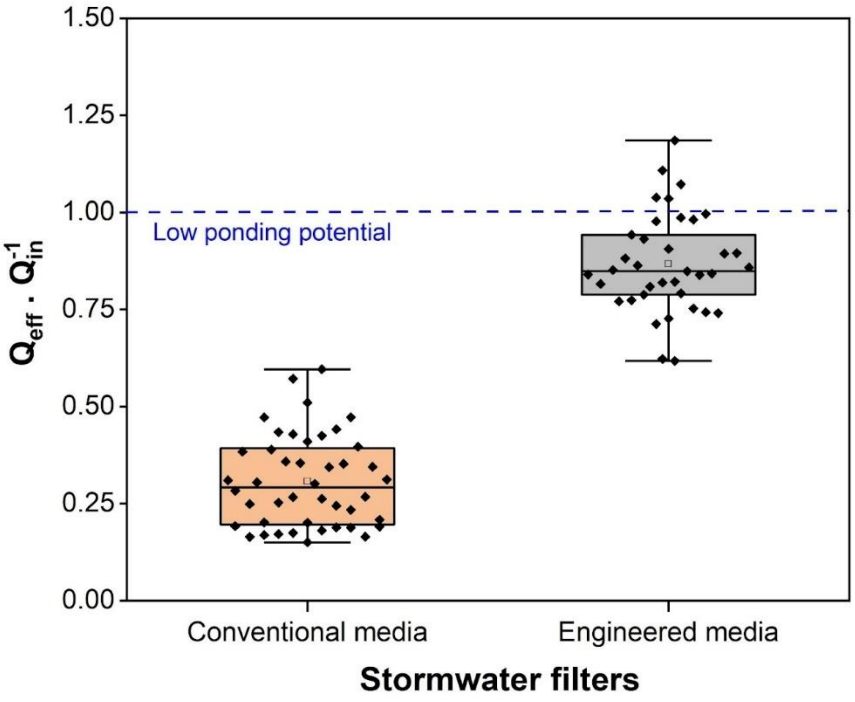

Figure 14.8 Comparison of ponding potential of conventional media filters (50% Sand, 25% compost, 25% soil) and engineered media filters (50% ESCS, 25% biochar, 15% soil). Blue dotted lines indicate low ponding potential.

14.3.3 Metal concentration in the stormwater

The stormwater influent exhibited significant variability in total metal concentrations, with distinct patterns observed across different metals. Lead (Pb), copper (Cu), and cadmium (Cd) demonstrated relatively low variability (0.1–0.5 log-scale range), reflecting more consistent input sources such as brake wear (Pb) and corrosion of plumbing materials (Cu) (Das et al., 2023). In contrast, cobalt (Co), nickel (Ni), and zinc (Zn) showed higher variability (0.5–1 log), likely due to intermittent contributions from galvanized structures (Zn) and industrial runoff (Co,

Ni) (Brown & Peake (2006)). Median concentrations followed the order: Zn (102 µg/L) > Cu (19.3 µg/L) > Pb (2.3 µg/L) > Ni (1.5 µg/L) > Co (0.5 µg/L) > Cd (0.06 µg/L) (shown in figure 9). This results are aligning with typical urban runoff profiles reported in similar climates (Le Coustumer et al., 2010). The pronounced fluctuations in Co, Ni, and Zn suggest these metals are more sensitive to short-term environmental factors (e.g., antecedent dry days, traffic volume) compared to Pb and Cd, which may accumulate steadily on road surfaces (Liu et al., 2021). These findings highlight the need for stormwater treatment systems capable of handling both consistent low-level metal inputs and episodic high-load events.

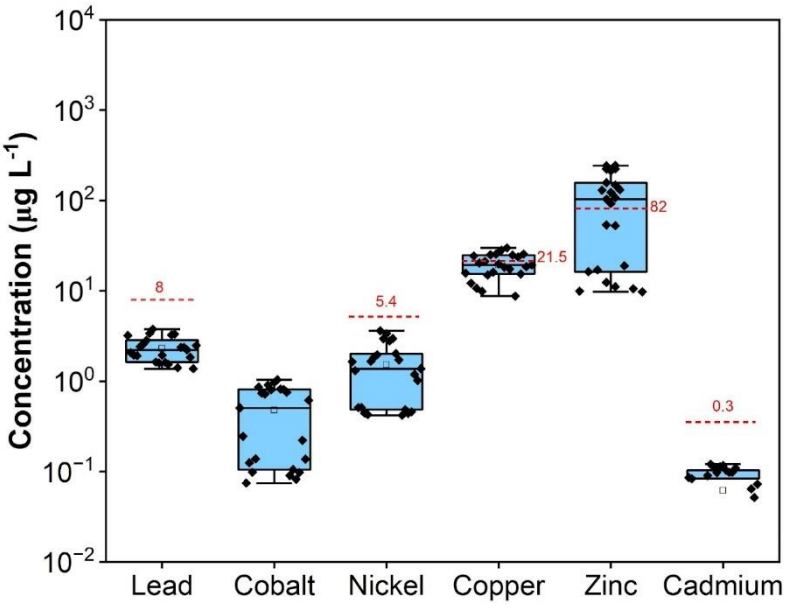

Figure 14.9. Metals concentration found in the stormwater runoff. Short red dashed lines indicate the median metal concentrations in urban stormwater runoff, based on data from the international BMP database (https://bmpdatabase.org/get-data).

14.3.4 Effect on the metal concentration due to the media type

The engineered media filters demonstrated superior metal removal performance compared to conventional filters, with significantly lower median effluent concentrations across all monitored metals. While influent metal concentrations varied substantially between sampling events due to differing antecedent conditions, the engineered media consistently achieved higher removal efficiencies: 55% for Pb, 47% for Co, 59% for Ni, 61% for Cu, 27% for Zn, and 54% for Cd (shown in Figure 10). In contrast, the conventional filter media showed limited retention capacity and even exhibited metal leaching in some cases, particularly for soluble species like Zn and Cd. While compost could be a potential source of nutrients and metals, it has to be widely used in bioretention cells. Compost is used extensively in bioretention cells because it provides an ideal soil medium that filters pollutants and supports healthy plant growth. This performance disparity highlights two critical mechanisms: (1) biochar's high-affinity binding sites in the engineered media effectively immobilized metals through surface complexation and cation exchange (Rajapaksha et al., 2016), while (2) the organic matter in conventional media likely facilitated metal mobilization via dissolved organic carbon complexation (Mohanty et al., 2023). It's noteworthy to mention that we did not do any prewashing of media in this study. So, potential residual amounts can remain in the media. The relatively lower Zn removal (27%) in both systems reflects the dominance of colloidal fractions that bypass physical filtration (Li et al., 2021), though the engineered media still reduced total Zn concentration by >25%. These results align with column studies showing biochar-amended filters achieve 50-70% metal retention under dynamic flow conditions (Tirpak et al., 2021), confirming their field applicability for urban stormwater treatment where metal variability is high.

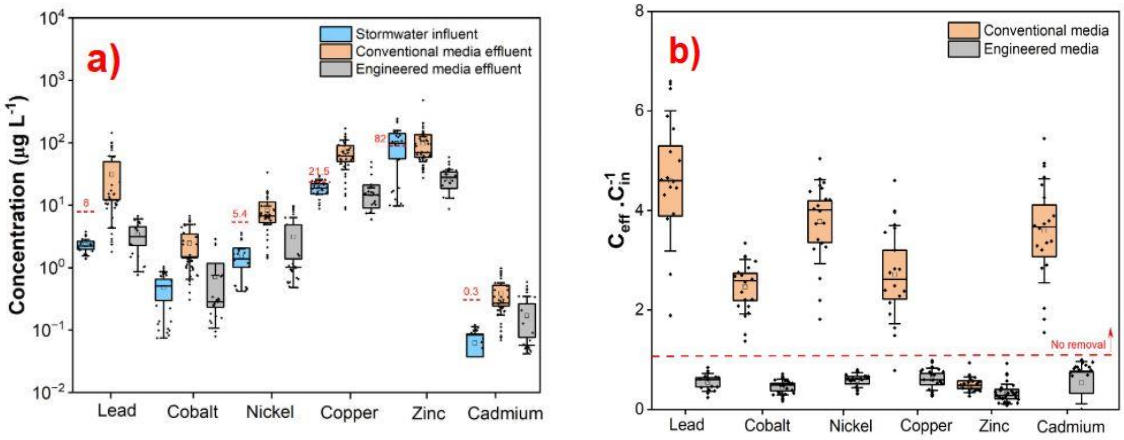

Figure 14.10 (a) Comparison of metal concentrations in stormwater influent, conventional media filter effluent, and engineered media filter effluent. Red dashed lines indicate median metal concentrations in urban stormwater runoff, based on data from the International BMP Database (https://bmpdatabase.org/get-data); (b) Comparison of metal removal efficiencies for conventional and engineered stormwater filter media. The red dotted line indicates zero removal efficiency.

14.4 Conclusion

The results demonstrate that engineered biochar-amended filters significantly outperform conventional stormwater filtration systems across all evaluated metrics. Although it is noteworthy to mention that this monitoring is for a very short period of time (5 storm events). Some of the leaching outcomes could come from normal leaching of new soil and compost. The engineered media exhibited 3.3 times greater infiltration capacity (5.9 cm/h vs. 1.8 cm/h) and superior drainage performance (Qeff/Qin ~0.8 vs. ~0.3), completely eliminating ponding issues observed in conventional systems. Most notably, the biochar-based filters achieved substantially higher metal removal efficiencies (47-61% for Pb, Co, Ni, Cu, and Cd) compared to conventional media, which showed tendencies for metal leaching. While zinc removal remained comparatively lower (27%) due to its predominant colloidal fractions, the overall treatment performance confirms engineered filters as a robust solution for urban stormwater management, particularly in high-traffic areas where metal contamination and compaction challenges are prevalent.

14.5 Future Work Recommendations

To build upon these findings, several critical investigations are proposed:

- Controlled challenge testing using Ballona Creek stormwater spiked with metals and co-pollutants (tire wear particles, microplastics) to evaluate system performance under worst-case contamination scenarios
- Comprehensive analysis of additional pollutant classes including emerging contaminants like tire wear chemicals and microplastics
- Long-term (multi-year) in situ performance monitoring at the current test location, which offers the unique advantage of:
- Real-world aging assessment under actual climatic and usage conditions

  This extended evaluation would provide vital data on system durability, maintenance requirements, and long-term treatment efficacy for informed stormwater management decisions.

14.6 References

Blecken, G. T., Zinger, Y., Deletic, A., Fletcher, T. D., Hedström, A., & Viklander, M. (2009). Laboratory study on stormwater biofiltration: Nutrient and metal removal. Water Science and Technology, 59(7), 1277-1286.

Boehm, A. B., Bell, C. D., Fitzgerald, N. J., Gallo, E., Higgins, C. P., Hogue, T. S., ... & Wolfand, J. M. (2020). Biochar-augmented biofilters to improve pollutant removal from stormwater–can they improve receiving water quality?. Environmental Science: Water Research & Technology, 6(6), 1520-1537.

Borthakur, A., Das, T.K., Mohanty, S.K. (2022). Natural aging of expanded shale, clay, and slate (ESCS) amendment enhances stormwater treatment by increasing E. coli removal and metal retention. Environmental Pollution, 314, 120165.

Bratieres, K., Fletcher, T. D., Deletic, A., & Zinger, Y. (2008). Nutrient and sediment removal by stormwater biofilters: A large-scale design optimisation study. Water Research, 42(14), 3930–3940.

Brown, J. N., & Peake, B. M. (2006). Sources of heavy metals and polycyclic aromatic hydrocarbons in urban stormwater runoff. Science of the total environment, 359(1-3), 145-155.

Bui, V. K. H., Nguyen, T. P., Tran, T. P., Nguyen, T. N., Duong, T. N., Nguyen, V. T., ... & Nguyen, X. C. (2024). Biochar-based fixed filter columns for water treatment: A comprehensive review. Science of The Total Environment, 176199.

Das, T. K., Kabir, A., Zhao, W., Stenstrom, M. K., Dittrich, T. M., & Mohanty, S. K. (2023). A review of compaction effect on subsurface processes in soil: Implications on stormwater treatment in roadside compacted soil. Science of the Total Environment, 858, 160121.

Das, T. K., Raoelison, O. D., Rehman, H., Zhang, Y., Chau, W., Thamiz, L., ... & Mohanty, S. K. (2023). Use of expanded shale, clay, and slate aggregates and biochar in the clear zone of road infrastructures for sustainable treatment of stormwater. Journal of Cleaner Production, 428, 139443.

Funai, B., Kupec, K. (2019). Plant survivability in rain gardens amended with lightweight aggregate (ESCS). Water Environment Research, 91(6), 464–472.

Hatt, B. E., Fletcher, T. D., & Deletic, A. (2008). Hydraulic and pollutant removal performance of fine media stormwater filtration systems. Environmental Science & Technology, 42(7), 2535–2541.

He, C., Liu, Z., Wu, J., Pan, X., Fang, Z., Li, J., & Bryan, B. A. (2021). Future global urban water scarcity and potential solutions. Nature communications, 12(1), 4667.

J. Li, W. Zhang, P. Kumar, Compaction effects on infiltration capacity of roadside soils: Mechanisms and modeling, J. Environ. Manage. 301 (2021) 113888. https://doi.org/10.1016/j.jenvman.2021.113888

J. Liu, Y. Wang, D. Li, Road-derived microplastics and associated contaminants in urban stormwater: Abundance, fate, and treatment challenges, Environ. Sci. Technol. 56 (2022) 3001-3011. https://doi.org/10.1021/acs.est.1c07333.

Le Coustumer, S., Fletcher, T. D., Deletic, A., Barraud, S., & Lewis, J. F. (2009). Hydraulic performance of biofilter systems for stormwater management: Influences of design and operation. Journal of hydrology, 376(1-2), 16-23.

Le Coustumer, S., Fletcher, T. D., Deletic, A., Barraud, S., & Poelsma, P. (2012). The influence of design parameters on clogging of stormwater biofilters: A large-scale column study. Water Research, 46(20), 6743-6752.

Le, H., Valenca, R., Ravi, S., Stenstrom, M. K., & Mohanty, S. K. (2020). Size-dependent biochar breaking under compaction: implications on clogging and pathogen removal in biofilters. Environmental Pollution, 266, 115195.

Lucas, W. C., & Greenway, M. (2011). Hydraulic response and nitrogen retention in bioretention mesocosms with regulated outlets: Part I–Hydraulic response. Water Environment Research, 83(8), 692–702.

Mangarella, P., & Palhegyi, G. (2002). Santa Clara Valley Urban Runoff Pollution Prevention Program: Hydromodification Management Plan Literature Review. GeoSyntec Consultants, Walnut Creek, CA.

Mohanty, S.K., Boehm, A.B., Cantwell, M.G., Fulthorpe, R.R., Deletic, A. (2018). Biochar as a stormwater control measure for nutrients, metals, and pathogens. Water Research, 141, 1–17.

Moustakas, K., Fatta-Kassinos, D., Malamis, D., et al. (2021). Biochar and its potential for wastewater treatment applications. Environmental Science and Pollution Research, 28, 24484–24504.

Payne, E. G. I., Pham, T., Cook, P. L. M., Fletcher, T. D., Hatt, B. E., & Deletic, A. (2014). Biofilter design for effective nitrogen removal from stormwater – Influence of plant species, inflow hydrology and use of a saturated zone. Water Science and Technology, 69(6), 1312–1319.

Premarathna, K. S. D., Biswas, J. K., Kumar, M., Varjani, S., Mickan, B., Show, P. L., ... & Vithanage, M. (2023). Biofilters and bioretention systems: the role of biochar in the blue-green city concept for stormwater management. Environmental Science: Water Research & Technology, 9(12), 3103-3119.

Rajapaksha, A. U., Chen, S. S., Tsang, D. C., Zhang, M., Vithanage, M., Mandal, S., ... & Ok, Y. S. (2016). Engineered/designer biochar for contaminant removal/immobilization from soil and water: potential and implication of biochar modification. Chemosphere, 148, 276-291.

Simpson, I. M., Schwartz, J. S., Hathaway, J. M., & Winston, R. J. (2023). Environmental regulations in the United States lead to improvements in untreated stormwater quality over four decades. Water Research, 243, 120386.

Sun, X., Davis, A. P., & Seagren, E. A. (2019). Modeling long-term metal accumulation and breakthrough in bioretention systems. Water Research, 157, 53–64.

Szalaj, W. L. (2007). Stormwater Management Rule Implementation Process.

Tirpak, R. A., Afrooz, A. N., Winston, R. J., Valenca, R., Schiff, K., & Mohanty, S. K. (2021). Conventional and amended bioretention soil media for targeted pollutant treatment: A critical review to guide the state of the practice. Water Research, 189, 116648.

Trowsdale, S. A., & Simcock, R. (2011). Urban stormwater treatment using bioretention. Journal of Hydrology, 397(3–4), 167–174.

Ulrich, B. A., Weelborg, K., Haile, T. M., Singh, U. B., & Magner, J. (2024). Field evaluation of a biochar-amended stormwater filtration system for retention of nutrients, metals, and Escherichia coli. Environmental Science: Water Research & Technology, 10(10), 2546-2558.

Zhang, L., Zhou, J., Chen, W., Li, L., Liu, J. (2024). Improving stormwater infiltration and retention in compacted urban soils using ESCS amendments. Journal of Environmental Management, 345, 118327.

Zhao, Z., Wang, X., Liu, L., Wu, X., Cao, J. (2021). Biochar-assisted immobilization of heavy metals in contaminated soils: A review. Journal of Hazardous Materials, 409, 124935.

Leonard, J., Koydemir, H. C., Koutnik, V. S., Tseng, D., Ozcan, A., & Mohanty, S. K. (2022). Smartphone-enabled rapid quantification of microplastics. *Journal of Hazardous Materials Letters*, *3*, 100052.

15 Task 8: Final Guidance and Life Cycle Cost Analysis.

15.1 Objective

The objective of this work is to do the cost benefit analysis of the media materials that are used in the construction of the roadside stormwater filters.

15.2 Introduction

The construction of roadside stormwater filters involves selecting filter media that balance performance, durability, and cost-effectiveness. With growing emphasis on sustainable infrastructure, understanding the long-term economic implications of conventional versus engineered media is essential. This task aims to perform the cost benefit analysis of materials used in the filter media. Specifically comparing traditional filters (sand, compost, and soil) to engineered alternatives (ESCS, biochar, and soil) filters. The goal is to guide future design decisions by evaluating both capital costs over a projected system lifespan.

15.3 Methods

15.3.1 Filtration Media Composition in Pilot-Scale Biofilter Units

Two pilot-scale biofilter units were constructed using planter boxes (dimensions: 36″ × 36″ × 24″). The first unit contained conventional filter media, comprising a 4:2:2 (v/v/v) mixture of sand, compost, and native soil. The second unit utilized engineered filter media, consisting of a 4:2:2 (v/v/v) blend of expanded shale, clay, and slate (ESCS), biochar, and native soil. All media components were homogenized with 10% (v/v) water to ensure uniform mixing and compacted to approximately 90% of their maximum bulk density. The filtration media layer was maintained at a 6-inch thickness, yielding a total media volume of 45 cubic feet per unit.

15.3.2 Cost and Quantity Analysis of Filter Media Materials

The compost was sourced from the Capistrano Greenery composting facility (Prima Deshecha Landfill, San Juan Capistrano, California) at no cost. However, for bulk procurement, a reference cost of $50 per cubic yard was applied (source: HomeGuide). The sand component, obtained from Vulcan Materials Company (Irwindale, California), complied with the California Department of Transportation (Caltrans) Standard Specifications (Section 90-1.02C(4)(d)), featuring a maximum 3/8-inch combined aggregate gradation to ensure optimal hydraulic conductivity.

The native topsoil (no cost incurred) exhibited 60–90% sand content (dry weight), with <20% passing the No. 200 sieve, <5% clay content, and no gravel, ensuring effective filtration without clogging. The ESCS lightweight aggregate was procured from Acrosa Lightweight Aggregates, while Rogue Biochar was sourced from Oregon Biochar Solutions (White City, Oregon), selected for its high cation exchange capacity to enhance heavy metal removal.

A detailed cost breakdown for all filtration media materials is provided in Table 15.1.

Table 15.1 Cost of the filtration media materials.

S. No	Materials	Traditional filter	Engineered filter
1	Compost (source: https://homeguide.com/costs/compost-cost)	$ 1.85 /ft^3	-
2	Soil (site soil)	-	-
3	Sand (Vulcan materials)	$1.85/$ft^3$	-
4	Rogue Biochar (Oreagon biochar)	-	$4/ ft^3
5	ESCS (Acrosa)	-	$ 5.6 / ft^3

15.4 Results and Discussion

15.4.1 Cost Comparison and Hydraulic Performance

The cost analysis of biofiltration media revealed a notable disparity between traditional and engineered filter systems. The traditional filter, comprising sand, compost, and native soil, was significantly more economical at \$1.4/ft³, while the engineered filter incorporating expanded shale, clay, and slate (ESCS) and biochar cost \$5.7/ft³, primarily due to the expense of ESCS (\$4.2/ft³) and biochar (\$1.48/ft³). Despite this cost difference, the engineered media demonstrated a three times higher infiltration capacity, suggesting superior hydraulic performance. This enhancement can be attributed to the porous structure of ESCS and biochar, which reduces clogging and maintains long-term permeability.

Table 15.2 Cost Analysis of Filter Media Materials for Packing the filtration Layer.

S. No	**Materials used to pack volume of 4.5 ft^3**	**Traditional filter**	**Engineered filter**
1	Compost (volume of compost used 1.67 ft^3)	\$ 0.7 /ft^3	-
2	Soil (volume of soil used 1.67 ft^3)	-	-
3	Sand (volume of sand used 3.34 ft^3)	\$0.7/ft^3	-
4	Rogue Biochar (volume of soil used 1.67 ft^3)	-	\$1.48/ft^3
5	ESCS (volume of sand used 3.34 ft^3)	-	\$ 4.2/ft^3
	Total cost for packing	**\$1.4/ ft^3**	**\$5.7/ ft^3**

15.4.2 Pollutant Removal Efficiency and Long-Term Benefits

Beyond improved hydraulic function, the engineered filter exhibited greater pollutant removal efficiency, particularly for heavy metals and organic contaminants. Biochar's high cation exchange capacity and ESCS's adsorptive properties contributed to enhanced contaminant retention compared to conventional media. Although the initial investment is higher, the engineered system's extended lifespan, reduced maintenance needs, and consistent treatment performance may offset costs over time. These findings highlight the potential of engineered biofiltration for applications requiring high-efficiency stormwater or wastewater treatment, where long-term operational benefits outweigh upfront expenses. Furthermore, biochar can provide carbon sequestration benefits compared to compost or other amendments because biochar is made up of waste biomass trapping carbon for more than 50 years.

15.5 Conclusions and Recommendations

The comparative analysis of traditional and engineered biofiltration media reveals a distinct trade-off between cost and performance. Traditional filter media composed of sand, compost, and native soil incurs a relatively low material cost of $\$1.4/ft^3$; however, engineered media incorporating expanded shale, clay, and slate (ESCS) and biochar demonstrates superior hydraulic and contaminant removal performance, albeit at a higher cost of $\$5.7/ft^3$. Engineered media exhibited a three times increase in infiltration capacity and improved pollutant retention, attributed to the due greater porosity, higher cation exchange capacity, and increased structural stability. Despite the elevated initial investment, engineered biofiltration media represent a more sustainable and robust long-term solution for stormwater quality management. The higher upfront cost may be justified by reductions in maintenance frequency, extended media lifespan, and improved compliance with water quality standards.